Moshen M. Baligh
Vitoon Vivatrat
Charles C. Ladd

Exploration and Evaluation of Engineering Properties for Foundation Design of Offshore Structures

MIT-T-79-001   C. 2

Exploration and Evaluation
of Engineering Properties for
Foundation Design of
Offshore Structures

by

Mohsen M. Baligh
Vitoon Vivatrat
Charles C. Ladd

Sea Grant College Program
Massachusetts Institute of Technology
Cambridge, Massachusetts 02139

AUTHORS

Mohsen M. Baligh is Associate Professor in the MIT Department of
Civil Engineering.

Vitoon Vivatrat contributed to this project while a Research Assistant
at MIT.

Charles C. Ladd is Professor of Civil Engineering in the MIT Department
of Civil Engineering.

.

ABSTRACT

This report investigates the in situ evaluation of clay properties by means of cone penetrometers and pore pressure probes.

A review of existing theories of cone penetration indicates an almost complete neglect of the fact that continuous deep penetration is a steady-state problem where the deformations and strains in the soil can be estimated with far less uncertainty than the stresses. A logical approach to penetration problems consists of combining the strain-path of soil elements with appropriate constitutive laws to determine penetration resistance.

A semi-empirical theory is developed to predict the undrained shear strength of clays from measurements of cone resistance and pore pressures during cone penetration. The theory accounts for the tip angle, tip enlargement and clay anisotropy.

Extensive penetration testing is conducted in three clay deposits to identify important parameters affecting cone penetration and to evaluate the proposed theory. The continuity of the cone penetration records permits a detailed study of soil variability. Results indicate that cone resistance and field vane data detect approximately the same inherent soil variability which depends on the soil type. Additional results show that: (1) The cone resistance q_c measured with the FUGRO electrical cone is repeatable. In agreement with the theory, q_c increases as the cone angle decreases, and tends to decrease by tip enlargement depending on soil type and stress-history. Moderate variation in penetration velocity does not change q_c significantly. (2) Measurements of sleeve friction are not consistent in soft to medium clays. (3) Pore pressure u during steady penetration is repeatable, and varies with soil type, stress-history and the location of the porous stone on the cone or the shaft behind it. u is generally high and can exceed the initial total vertical stress. (4) The ratio u/q_c correlates well with the soil type (clay vs. sand) and the stress-history of clays. u/q_c is thus a promising parameter for detecting stratigraphy, soil identification and variability, and possibly for evaluating the stress history of clays.

An evaluation of theoretical predictions is made by comparing the predicted undrained shear strength s_u (cone), to s_u (reference) based on actual embankment performance after strain-rate effects are empirically accounted for. Results obtained with enlarged cones at two sites show excellent agreement. For the "standard" cone shape (FUGRO), the theory predicts reasonable upper and lower bounds of the strength but predictions can be improved if pore pressure measurements and/or more sophisticated analyses are conducted.

Empirical correlations between q_c and the undrained shear strength obtained by the field vane test are presented for the three sites tested in this program and six additional Scandinavian sites. These correlations depend on the soil type, stress-history and depth.

FOREWORD

A two year research program entitled "Exploration and Evaluation of Engineering Properties of Marine Soils for Foundation Design of Offshore Structures", sponsored primarily by the National Oceanic and Atmospheric Administration through its M.I.T. Sea Grant Program, was initiated in July 1976 by the Constructed Facilities Division at M.I.T. The final objective of the program was to improve the present capabilities of the geotechnical profession in the area of offshore site investigation through evaluating existing in situ tests and, whenever possible, to develop new more reliable methods and devices to determine the necessary soil parameters for foundation design.

The electrical (Dutch) cone penetrometer and the pore pressure probe represent a new generation of in situ testing devices which are particularly valuable offshore, and combine simplicity, consistency and economy. For applications in medium to soft clays they lack a solid evaluated experience by the profession and a well-defined common basis for analysis, especially in the U.S. Hence, the research consisted of three components:

1. Develop improved theoretical methods for relating Dutch cone penetration resistance and pore pressure measurements data to the actual in situ undrained strength characteristics of marine clays.

2. Perform Dutch cone and pore pressure probe tests on several representative soil types for which there already exists extensive information about in situ undrained stress-strain-strength behavior.

3. Interpret the results of the measured cone penetration and pore pressure data with the improved theoretical models in light of the known undrained stress-strain-strength behavior of the soils and prepare guidelines for the use and interpretation of Dutch cone test data.

ACKNOWLEDGEMENTS

TABLE OF CONTENTS

LIST OF TABLES

LIST OF FIGURES

NOTATION

Symbols and abbreviations may be found under the following subject headings:

ANALYSIS OF DEFORMATION AND STRAINS

MEASUREMENTS, PREDICTIONS AND IN-SITU STRESSES

SLIPLINE THEORY

SOIL PARAMETER AND EMPIRICAL FACTORS

STATISTICAL ANALYSIS

ANALYSIS OF DEFORMATION AND STRAINS

x,y,z	Rectilinear coordinates.
r,z,ϕ	Circular cylindrical coordinates.
R,Θ,ϕ	Spherical coordinates.
v_x, v_y, v_z	Components of the velocity vector.
$\dot{\varepsilon}_{xx}, \dot{\varepsilon}_{yy}, \dot{\varepsilon}_{xy}$..	Components of the strain-rate tensor.

a	Scale factor.
B	Half the base width of a wedge.
c_i	Scalar value of stream function.
D_{ij}	Component of the rate-of-deformation tensor.
r_c	Radius of a penetrating cone.
r_o	Initial r coordinate of a streamline.
t	Time.
v	Eulerian velocity vector.
V	Velocity of the indenter in the initial problem or incident velocity of the conjugate problem.
x	Position vector.
x_o	Initial x coordinate of a streamline.
y_o	Coordinate parallel to the major direction of motion of an undefined element.
γ	Half the apex angle of the cavity behind a steady advancing wedge.
δ	Half the apex angle of a wedge.

ε_{ij} Components of the natural strain tensor.

$\varepsilon_1, \varepsilon_2, \varepsilon_3$ Principal strain components.

ε_{max} Maximum shear strain in an element.

$\dot{\varepsilon}_{ij}$ Component of the strain-rate tensor.

λ An arbitrary constant.

ψ Stream function.

MEASUREMENTS, PREDICTIONS, AND IN-SITU STRESSES

p_L Limit pressure from pressuremeter test or expansion pressure for a long cylindrical cavity.

p_o Initial isotropic stress in the soil.

p_S Expansion pressure for a spherical cavity

q_c Cone penetration resistance.

q_u Ultimate bearing capacity of footing.

q_w Wedge penetration resistance.

u Pore pressure.

u_o Initial static pore pressure.

σ_h Horizontal total stress.

σ_{ho} Initial horizontal total stress.

$\sigma_{vo}, \bar{\sigma}_{vo}$ Initial vertical total and effective stresses.

SLIPLINE THEORY AND YIELD CONTOUR

x, y Plane cartesian frame of reference.

$\sigma_x, \sigma_y, \tau_{xy}$ Stress components in frame xy.

$1/2(\sigma_y - \sigma_x), \tau_{xy}$ Deviatoric stress components in frame xy.

α, β Plane rectilinear coordinates inclined at θ to xy.

$\sigma_\alpha, \sigma_\beta, \tau_{\alpha\beta}$ Stress components in frame $\alpha\beta$.

$1/2(\sigma_\beta - \sigma_\alpha), \tau_{\alpha\beta}$ Deviatoric stress components in frame $\alpha\beta$.

$1,3$ Subscripts denoting principal directions.

o, f Subscripts denoting initial and failure conditions.

a,b	Axes of an elliptic yield contour.
A,B	Skempton's pore pressure parameters.
A_f	Pore pressure parameter A at failure.
B	Half the width of a wedge.
c	Cohesive strength ($\phi = 0$).
$\overline{c}$	Cohesion intercept in Mohr-Coulomb failure envelope based on effective stresses.
$\overline{CK_oU}$	K_o-consolidated undrained shear test.
d	$1 - b^2/a^2$.
f	$1/2(1 - K_o)$.
g	$2A_f - 1$.
G	Shear modulus.
i	Angle between σ_1 and the vertical at failure
k	$1/2(1 + K_o)$.
ℓ	Arc length along yield contour.
N_w	Wedge resistance factor.
$N_w(\omega)$	Wedge resistance factor for different friction level.
O_p	Origin of planes.
p	$1/2(\sigma_1 + \sigma_3)$.
p_b	Pressure acting on the gap behind the wedge.
P	An arbitrary material point in plastic state.
P^*	A point on the yield contour representing stresses at point P.
q	$1/2(\sigma_1 - \sigma_3)$.
q_f	$1/2(\sigma_1 - \sigma_3)$ at failure.
q_u	Ultimate bearing capacity of a strip footing.
q_w	Penetration resistance of a wedge (stress).
V	Velocity of a wedge.
W	Point representing the wedge on a hodograph.
$\overline{\alpha}$	Slope of the failure envelop on a p-q diagram.
γ	Half the apex angle of the cavity behind a steady advancing wedge.
δ	Half the apex angle of a wedge.
$\dot{\varepsilon}_\alpha, \dot{\varepsilon}_\beta, \dot{\gamma}_{\alpha\beta}$	Normal and shear strain-rate components in frame $\alpha\beta$.

θ Inclination between two rectilinear coordinate systems xy and $\alpha\beta$.

λ A scale factor.

μ Coefficient of fraction = $\tau/\overline{\sigma}_n$.

$\sigma_1,\sigma_2,\sigma_3$ Principal stresses.

$\overline{\sigma}_n$ Effective normal stress acting on wedge face.

τ Shear stress acting on wedge face.

ϕ 2ϕ = inclination of the tangent to yield contour.

ψ angle related to the slip-line field for pseudosteady wedge penetration.

ω Angle defining the uniform stress zone in front of wedge face = $1/2 \cos^{-1}(\tau/c)$.

SOIL PARAMETERS AND EMPIRICAL FACTORS

a,b   Axes of an elliptic yield contour.

A,B   Skempton's pore pressure parameters.

$\overline{c}$ Intercept of Mohr Coulomb envelope.

$\overline{CK_oU}$ K_o-consolidated undrained shear test.

d $1- (b/a)^2$

E   Young's modulus.

G   Shear modulus.

K_o Coefficient of earth pressure at rest.

K_s Anisotropic strength ratio = $s_u(H)/s_u(V)$.

m $(1 - K_s)(1 + K_s)$.

OCR   Overconsolidation ratio = $\overline{\sigma}_{vm}/\overline{\sigma}_{vo}$, $\overline{\sigma}_{vm}/\overline{\sigma}_{vc}$.

$p,\overline{p}$ $1/2(\sigma_v + \sigma_h)$, $1/2(\overline{\sigma}_v + \overline{\sigma}_h)$.

q $1/2(\sigma_v - \sigma_h)$.

q_f $0.5(\sigma_1 - \sigma_3)_f$.

S_t Sensitivity = s_u(undisturbed)/s_u(remolded).

s_u Undrained shear strength = q_f or $\tau_{ff} = q_f \cos \overline{\phi}$.

s_u(AVE)   Average s_u for a combination of failure modes.

s_u(field) s_u for embankment design or bearing capacity analyses.

s_u(REF)   Reference s_u for cone penetration theory.

$s_u(x)$ s_u from a particular mode of failure or test x.

       V: in-situ plane strain compression.

       H: in-situ plane strain extension

     45°:   in-situ simple shear.

      FV: field vane test.

    PSC: $\overline{CK_oU}$ plane strain compression test.

    PSE: $\overline{CK_oU}$ plane strain extension test.

    DSS: $\overline{CK_oU}$ direct simple shear test.

     TC: $\overline{CK_oU}$ triaxial compression test.

     TE: $\overline{CK_oU}$ triaxial extension test.

     u   pore water pressure.

   u_f pore water pressure at failure.

   w_ℓ liquid limit.

   w_n natural water content.

   w_p plastic limit.

   α $s_u(AVE) = \alpha[s_u(V) + s_u(H)]$.

   γ_t Total unit weight of soil.

   Δx An increment of quantity x.

   μ Field vane correction factor.

   μ_R Field vane correction factor for strain-rate effect.

   $\overline{\sigma}_{vc}$ Vertical consolidation stress.

   $\overline{\sigma}_{vo}$ Initial vertical stress.

   $\overline{\sigma}_{vm}$ Maximum past pressure.

   ϕ Angle of internal friction.

   $\overline{\phi}$ Effective angle of internal friction.

STATISTICAL ANALYSIS

   a   Input parameter in filtering procedure.

   d   Depth.

   i   Arbitrary layer designation.

   M   Median value of data points in a prescribed region.

V   Coefficient of variation (mean/standard deviation).

x   A normalized variable (Eq. (6.3)).

Δ Input parameter (depth increment) in filtering procedure.

σ Standard deviation.

σ_{q_c} Standard deviation of q_c.

CHAPTER 1

INTRODUCTION

The prediction of foundation performance for engineering structures represents an essential part of geotechnical engineering (Lambe, 1973). In many cases, the accuracy and reliability of predictions depend primarily on an adequate knowledge of foundation soil conditions and soil properties. In situ measurements have recently attracted considerable attention as a means of determining soil conditions and properties during site investigation and for design purposes. The stimuli for this increased interest are:

(1) A concern over the time and the escalating cost required by traditional exploration techniques which rely on boring, sampling, and laboratory tests, and the reliability of the results of such procedures.

(2) The increasingly difficult environments in which engineering structures are founded and where foundation exploration is required, as typified by offshore locations or frozen soils.

(3) Attempts to better define in situ stresses and soil properties, such as deformability and permeability, which are not readily evaluated by laboratory tests to complement the advances in analytic capabilities of the geotechnical profession.

(4) The necessity to assess the spatial and inherent variability of soil properties for design and reliability studies of more important or complex structures.

The cone penetrometers and the pore pressure probes studied herein represent a new generation of in situ testing devices which have no mechanically moving parts and are readily amenable to remote control and automated data recording and processing. These instruments combine simplicity, consistency, and economy, and are rapidly gaining world-wide acceptance especially in offshore soil exploration work. They can define soil stratigraphy and type, assess soil variability, and infer in situ soil properties, e.g. strength, deformability properties (cone) and permeability (pore pressure probe), (Schmertmann, 1975; Mitchell and Gardner, 1975; Torstensson, 1975; and Wissa et al., 1975.) For application in medium to soft clays, cone penetration lacks the necessary evaluated experience by the profession, especially in the U.S., (Ladd et al., 1977) and a common basis for analysis (Baligh, 1975).

This report attempts to develop a better understanding of the cone penetration mechanism in clays, through theoretical and experimental studies, in order to provide reliable interpretation methods for cone penetration testing.

Chapters 2, 3, and 4 comprise theoretical and analytical developments. Chapter 2 discusses deformations and strains in the soil during cone penetration, reviews existing theories for cone penetration and considers different theoretical approaches to continuous deep cone penetration. In view of the complex stress-strain-pore pressure behavior of clays, a new approach to cone penetration is introduced, the strain-path method. Chapter 3 extends the steady state wedge penetration theory (Baligh, 1972) to anisotropic soils. Results of this theory represent the basis for the proposed cone penetration theory. Chapter 4 presents an approximate and

more practical theory of cone penetration for immediate use.

Chapters 5, 6 and 7 describe the experimental part of this study which is conducted to determine the effect of different factors on cone resistance, evaluate theoretical predictions and hence provide improved interpretation methods, develop new applications of existing instruments, and identify possible improvements of these instruments. Chapter 5 outlines the experimental program which was designed on the basis of extensive soil behavior studies at M.I.T. in the past 15 years on three clay deposits. Chapter 6 presents a new method for studying the variability characteristics of a clay deposit based on in situ measurements, and applies this method to records of cone resistance and field vane tests. Chapter 7 presents results from extensive cone and pore pressure probe testing which involves a number of special instruments and more than 6,000 ft of penetration. The experimental results are compared to theoretical predictions and to results reported by other in situ devices.

Chapter 8 synthesizes the theoretical and experimental work regarding the undrained shear strength of clays, and checks the validity of the proposed cone penetration theory. For practical purposes, Chapter 9 presents empirical correlations between cone resistance and the undrained shear strength of clays obtained by field vane tests. Chapter 10 summarizes the major findings and conclusions of this research.

CHAPTER 2

EXISTING THEORIES AND APPROACHES TO CONE PENETRATION

The cone penetration test basically consists of pushing a cone into the soil at a constant rate (1 to 2 cm/sec) while measuring the soil resistance. The test is simpler and faster to perform than other in situ tests (e.g. the field vane and the pressuremeter) and provides a continuous record with depth. The cone test is, therefore, well suited for offshore work when the environmental conditions are very severe and the field work is limited with high operating costs. The value of any in situ test depends primarily on its repeatability and the reliability of the method used in interpreting its results. When sufficient evaluated experience is available, empirical correlations provide one method of interpretation, e.g., Bjerrum's approach to use the field vane test in embankment design, 1972. Another method of interpretation consists of understanding the mechanism of the test and then relating measurements to the particular aspect of soil behavior to be determined by the test. This can only be achieved by means of rational theories.

The development of a rational theory for cone penetration is more complicated than, say, the pressuremeter test. The added difficulties are caused by the two-dimensional nature of the cone test compared to the one-dimensional (plane strain) conditions imposed by the pressuremeter.

2.1 The Cone Penetration Process

The continuous deep penetration of a cone (or pile) in a homogeneous soil mass represents a steady state problem, i.e., to an observer moving with the cone (or pile), the deformation pattern, the strain and stress fields in the soil do not change with time. This is different from other important

problems in soil mechanics such as the bearing capacity of a footing or the expansion of a cavity, where deformations, stresses and strains vary with time.

The <u>steady state</u> condition severely restricts the acceptable modes of deformation (i.e., the velocity fields). Experimental observations by Rourk (1961), Vesic (1963), Robinsky and Morrison (1964), Szechy (1968), and others indicate that the deformation pattern due to penetration by a rigid indenter is similar in different soils even though the penetration resistance can be drastically different. This suggests that the penetration by rigid indenters is closer to a <u>strain-controlled problem</u> than a stress-controlled problem, and that rational approaches to the penetration process should give primary consideration to deformations and strains, Baligh (1972). It is, therefore, surprising that most of the existing theories for cone penetration totally neglect soil deformations and consider soil stresses only.

2.2 Existing Theories of Cone Penetration in Clays

A complete theory of cone penetration should determine stresses, strains and displacements in the soil to satisfy the boundary conditions corresponding to steady quasi-static motion of the cone and the field equations based on the actual soil behavior. However, because soil behavior is very complicated and cone penetration involves large deformations, simplifications are necessary. Different simplifications lead to different theories. Existing theories for cone penetration (and bearing capacity of pile tips) are based on one of two approaches: plane-strain slip-line solutions or expansion of cavities. Both approaches rely on modifications of more rigorous solutions to simplified problems. The simplifications are made with respect to

problem geometry, the stress-strain behavior of the soil, and the mode of

deformation. Table 2.1 summarizes the predicted cone penetration resis-

tance, q_c, in clays[*] according to the different theories discussed below.

(1) The plane-strain bearing capacity solution approach. This

approach treats cone penetration as an incipient failure problem and is pri-

marily based on Prandtl's fundamental solution for a strip footing on the

surface of a rigid-plastic half-space, Fig. 2.1, (Terzaghi, 1943; Meyerhof,

1951; etc.). Modifications of Prandtl's solution are made by introducing a

shape factor to account for the difference in geometry between the plane

strain strip footing and the axisymmetric cone, and a factor to account for

embedment below the surface. The point resistance q_c of a cone (or pile) is

then written as:

$$q_c = N_c \, s_u + \sigma_{vo};$$ (2.1)

$$N_c = (\text{shape factor}) \times (\text{depth factor}) \times (5.14),$$

where N_c = the cone resistance factor;

s_u = undrained shear strength of clay,

and σ_{vo} = initial vertical total stress in the soil.

The shape factor is generally assumed to be 1.2 to 1.3 (Terzaghi, 1943;

Skempton, 1951), whereas the depth factor is assumed to be 1.5 to 1.6 for

deep foundations (Skempton, 1951; Brinch Hansen, 1961 and 1970). Because

Prandtl's solution applies to incipient failures, theories based on this

---

[*] q_c is the force per unit projected area of the tip.

approach cannot predict deformations or strains associated with steady cone penetration. In fact, these theories cannot distinguish between bearing capacity and steady cone penetration.

To account for the effect of cone angle, Mitchell and Dorgunoglu (1973) use Meyerhof's solution for incipient (rough) wedge penetration at the surface instead of Prandtl's solution. Thus for a cone with an apex angle 2 δ, q_c is given by:

$$q_c = N_c \, s_u + \sigma_{vo} \tag{2.2}$$

N_c = (shape factor) × (depth factor) × (2.57 + 2 δ + cot δ),
where δ is in radians and is equal to or less than $\pi/4$.

Meyerhof (1961) presents another approximate solution to the point resistance of a cone at depth. He assumes that the circumferential stress is the minor principal stress and that the slip line field on a meridian plane in the axisymmetric cone problem is identical to that for the plane-strain wedge penetration. With these assumptions, he obtains the bearing capacity factor numerically, and finds that the bearing capacity of a cone is slightly larger than that of a wedge and is given by:

$$q_c = N_c \, s_u + \sigma_{vo} \tag{2.3}$$

$N_c \simeq$ (1.09 to 1.15) × (6.28 + 2 δ + cot δ)

(the shape factor is introduced herein to provide a uniform presentation of different theories).

(2) The cavity expansion approach. This approach is based on the expansion of cylindrical or spherical cavities in an infinite medium, starting

from zero radius. Because of the simplicity of these one-dimensional prob-
lems, solutions based on more realistic and complex soil properties
(e.g., strain-hardening and strain-softening) can be obtained (Bishop et al.
1945; Chadwick et al., 1963; Ladanyi, 1967 and 1972; Baguelin et al., 1972;
Palmer, 1972; Prevost and Hoeg, 1975a and 1975b; etc). For an incompres-
sible elastic-perfectly plastic soil with a shear modulus G, the solution
has a very simple form:

$$p_L = p_o + s_u (1 + \ln G/s_u) \text{ for a cylindrical cavity;}$$

$$\tag{2.4}$$

$$p_S = p_o + 1.33 s_u (1 + \ln G/s_u) \text{ for a spherical cavity.}$$

For a cylindrical cavity, p_o is the total horizontal stress and
for a spherical cavity, p_o is the isotropic initial stress in the soil (Bis-
hop et al.,1945).

Bishop et al (1945) recognize that the difference between p_L and p_S
is not large and propose that, during deep penetration of a smooth cone,
q_c lies between p_L and p_S. They also indicate that q_c approaches p_L for
sharp cones and approaches p_S for blunt cones, i.e., q_c for smooth cones
decreases as the cone angle, 2 δ, decreases. Measurements in metals using
40° to 120° lubricated cones seem to support this approximation. However,
deformation measurements due to blunt cone penetration discussed subse-
quently do not support the axially symmetric patterns predicted by spherical
cavity expansion.

Gibson (1950) extends the above theory to bearing capacity in
clays by making the additional assumption that the shear stress on the cone
surface equals the undrained shear strength of the clay, s_u. Thus for a cone

with an apex angle 2δ, he proposed that q_c is given by:

$$q_c = N_c \, s_u + \sigma_{vo} \; ; \qquad\qquad (2.5)$$

$$N_c = 1.33 \, (1 + \ln G/s_u) + \cot \delta \; ;$$

where the term $\cot \delta$ is the friction contribution, and σ_{vo} indicates the influence of the initial stresses (assumed isotropic) in the soil.

Vesic (1975 and 1977) proposes the stress field around the cone tip illustrated by Fig. 2.1. The pressure on a cylindrical surface beneath the cone tip is assumed to equal p_S, and the stresses increase towards the cone face in the same manner as in a radial-fan shear zone of the slip-line theory for rigid plastic material in plane strain deformation. Vesic also suggests that p_o in Eq. 2.4 represents the in situ octahedral normal stress $\sigma_{oct} = 1/3(\sigma_{vo} + 2 \, \sigma_{ho})$ instead of σ_{vo}. Thus q_c for a blunt cone with $\delta = 90°$ is given by:

$$q_c = N_c \, s_u + \sigma_{oct} \; ; \qquad\qquad (2.6)$$

$$N_c = 1.33 \, (1 + \ln G/s_u) + 2.57,$$

where the factor 2.57 represents the stress increment in the radial shear fan under the cone tip.

The modifications made by Gibson and Vesic to the cavity expansion solutions derived by Bishop et al. have no solid theoretical basis, but rely mostly on engineering judgement. Therefore, their accuracy and validity can only be judged on the basis of experimental verification.

Working with Vesic, Al Awkati (1975) related q_c to p_L using an empirical factor determined from experiments. For the undrained shearing of

clays, he proposed that:

$$q_c = N_c \, s_u + \sigma_{oct} \; ; \qquad\qquad (2.7)$$

$$N_c = \lambda(1 + \ln G/s_u).$$

Experiments in sands show that λ is approximately 1.9 for a 60° cone, and 1.85 for $2 \, \delta \geq 83°$. Experiments in clays are still needed. This method is purely empirical and cannot determine deformations and strains.

(3) <u>Steady penetration approach</u>. To account for the continuous nature of cone penetration, Baligh (1975) bases his approach on the slip-line solution for <u>steady penetration</u> of a rigid wedge in a rigid perfectly plastic material developed by Baligh (1972) and Baligh and Scott (1976). The axisymmetric counterpart of this problem is that of a cone with no rigid boundary behind it to constrain soil deformation. He proposes that the work, q_c, required to push a conventional cone a unit distance, Fig. 2.2a, is the sum of the work required to push the cone in Fig. 2.2b and the work required to keep the cavity open, Fig. 2.2c. The first component is estimated as 1.2 times the penetration resistance of a wedge (i.e., using a shape factor = 1.2), while the second component is the expansion pressure for a cylindrical cavity, p_L (Eq. 2.4). According to this theory, q_c is given by:

$$q_c = N_c \, s_u + \sigma_{ho} \; ; \qquad\qquad (2.8)$$

$$N_c = 1.2(5.71 + 3.33 \, \delta + \cot \delta) + (1 + \ln G/s_u).$$

Subsequently, Baligh et al (1977) used the q_c in Eq. 2.8 as an upper bound for cone resistance. They also proposed a lower bound on q_c for conventional (unenlarged) cones and provided solutions for enlarged cones.

Chapter 4 of this report describes these developments in detail and predictions of this theory are later compared to in situ measurements.

2.3 Discussion of Approaches to Cone Penetration Theories

(1) Strain-path approach. The stress path method (Lambe, 1967) provides a method for systematically simplifying and solving a number of problems in soil mechanics. First the initial and incremental stresses are estimated at selected locations in the soil mass. Laboratory tests are then conducted on soil samples obtained from these locations in order to subject the samples to the same stress paths expected in the actual problem. Strains obtained from those tests are then integrated to predict displacements (settlements). The success of the stress path approach in predicting field performance relies on the accuracy in estimating stress and stress increments, the number of soil elements investigated, and the ability of laboratory tests to minimize the effects of sample disturbance (in the sampling process) and to duplicate the estimated stress paths. However, even under ideal conditions involving an infinite number of samples, the stress path approach fails to satisfy compatibility of displacements (or strains)[*] and therefore, provides approximate answers. A more complete stress path approach requires a number of iterations of the type described above to account for soil nonlinearity.

In many shallow foundation problems involving surface loading (or unloading), the stress path method proved satisfactory. One basic reason

---

[*] Deformations will, in general, cause some elements to overlap and develop gaps between others.

for this success is that the estimated stresses in these problems are sufficiently accurate, and do not depend significantly on soil nonlinearities. On the other hand, in deep penetration problems (and deep foundations), stresses in the soil are much more difficult to estimate than strains because these problems are closer to being strain-controlled. Research is currently underway at M.I.T. to implement a new approach for the solution of these problems: the strain path approach. In this approach, outlined by Baligh (1975), the strain path of selected soil elements are estimated from a deformation pattern (velocity field) chosen on the basis of kinematic requirements. Laboratory tests are then conducted, or alternatively appropriate constitutive laws used, to determine the stresses in these elements when subjected to the estimated strain. These stresses are then combined to determine a stress field satisfying the equilibrium conditions.[*]

As an illustration of the strain path approach, Fig. 2.3 shows the deformation pattern due to penetration of a flat-end circular model pile in bentonite. A hemispherical "dead" zone of clay forms ahead of the pile tip and moves with it. Below this "dead" zone, the soil is pushed downward and outward. Intense shearing takes place near the pile in a zone roughly equal to its radius. At some distance behind the pile tip, the soil deformation becomes constant with respect to further penetration. This permanent distortion is very large near the pile but decreases significantly at some distance from the pile centerline. A blunt cone with a tip located within

---

[*]Hill (1963) presents a rigorous theoretical basis for this approach, both for steady and unsteady deformations. For steady deformation problems, the deformation pattern and the strain field do not change with time.

the hemispherical dead zone (i.e., with apex angle $2 \delta > 90°$) causes a similar deformation pattern in the soil.

The strain field in this problem can be computed from the measured displacements in Fig. 2.3 by numerical differentiation. This approach, was pursued by researchers at Cambridge University, England (especially with regard to retaining wall problems, Roscoe (1970) and others). The approach has one major disadvantage: unless deformations are measured very accurately (difficult in clay and non plane-strain problems), the computed strains will be in error because of the highly sensitive process of numerical differentiation. This is particularly true in regions of intense shearing or where irregularities due to testing imperfections are present. An alternative approach is to use analytical (or numerical) expressions for the velocity field that lead to a deformation pattern similar to the one observed. From the velocity field, the displacements, strains, and strain-history of soil elements can be obtained with any degree of accuracy. The velocity field also provides useful insights into the deformation mechanisms.

For a given velocity field, Vivatrat (1978) developed the necessary programs to compute the strain-rates, the strains and the deformations in the soil during steady penetration. Using the velocity field recommended by Baligh (1975) which consists of a spherical source superimposed on a uniform velocity, Vivatrat determined the distorted grid shown in Fig. 2.4. The predicted soil deformations are reasonably close to the measurements made by Rourk during penetration of a flat model pile in clay (Figs. 2.3 and 2.4), except in the immediate vicinity of the pile. Figure 2.5 shows the corresponding shear strain history of the two elements A and B, initially located at $0.7 \, r_c$ and $2 \, r_c$, respectively, from the pile axis, where r_c denotes the

radius of the pile. The minor principal strain, ε_3 is in the circumferential direction and is tensile. The major principal strain ε_1, lies on a vertical (meridian) plane and, initially, is in the vertical direction (along the axis of the pile). As the pile approaches the soil element, ε_1 rotates towards the horizontal direction. The degree of shearing due to penetration is described by the maximum shear strain, $\frac{1}{2}(\varepsilon_1 - \varepsilon_3)$, and the maximum shear strain on vertical planes, $\frac{1}{2}(\varepsilon_1 - \varepsilon_2)$. Figure 2.5 indicates that, ahead of the pile, significant shearing occurs and that $\frac{1}{2}(\varepsilon_1 - \varepsilon_2)$ is practically equal to $\frac{1}{2}(\varepsilon_1 - \varepsilon_3)$. As the pile tip reaches the location of the soil elements, the magnitude of the circumferential strain increases rapidly, and $\frac{1}{2}(\varepsilon_1 - \varepsilon_3)$ becomes predominant. Behind the pile tip, $\frac{1}{2}(\varepsilon_1 - \varepsilon_2)$ tends to decrease while $\frac{1}{2}(\varepsilon_1 - \varepsilon_3)$ asymptotically approaches a limiting value. For soil elements located between 5 r_c and 50 r_c behind the tip, $\frac{1}{2}(\varepsilon_1 - \varepsilon_2)$ is approximately half the value of $\frac{1}{2}(\varepsilon_1 - \varepsilon_3)$.

The rate of shearing depends on the slope of the curves in Fig. 2.5 and the penetration velocity, V. For standard cones with a diameter = 3.57 cm and V = 2 cm/sec, the shear rate ahead of the tip is approximately 50% per second for element A close to the cone (or pile) and 5% per second for element B some distance away from the cone (or pile). Such rates of shearing are much higher than the rates commonly used in laboratory tests and may significantly affect the measured strength in rate-sensitive soils.

The determination of a stress field based on the strains described above is complicated and requires additional effort. Work is currently conducted at M.I.T. to extend this approach to its logical conclusion and determine the penetration resistance. The major difficulties encountered are:

(a) the approach requires extensive sophisticated laboratory tests (e.g.,

true triaxial) on different soils or, alternatively, the availablity of good

soil behavior models and the appropriate parameters for any particular

soil; and (b) the procedure for obtaining a statically acceptable stress

field is complicated.[*]

Presently, reasonable estimates of strain paths are available for

blunt cones (2 $\delta \geq$ 90°) at some distance from the cone. Velocity fields for

sharp cones based on numerical solutions have been obtained and work is pre-

sently underway at M.I.T. to determine the corresponding stress fields.

(2) <u>Numerical solutions</u>. A second promising approach to develop

improved interpretation methods for cone resistance consists of using numeri-

cal solutions, e.g., finite elements. However, this approach faces major

difficulties: (1) Steady cone penetration involves very large displacements

and strains (Fig. 2.3); (2) the steady state requires velocity boundary

conditions (similar to fluid flow problems) rather than the more common stress

or displacement boundary conditions; and (3) realistic soil behavior models

are very complicated.

Existing numerical solutions are simplified. Baligh (1972)

presents finite element analyses of progressive (hence unsteady) wedge and

cone penetration at depth in a bilinear material.[**] His results show that:

(1) the penetration resistance increases with the displacement; (2) the

resistance on the cone is about 25% to 35% larger than that on the wedge;

(3) compressibility of the material (as reflected by Poisson's ratio)

---

[*]In an incompressible material, only the deviatoric stresses can be
determined from the estimated strain paths. The hydrostatic (isotropic)
stress field must be calculated on the basis of equilibrium requirements.

[**]Analysis of progressive cone penetration at surface is presented
by Chung and Lee (1974).

affects the penetration resistance, but has little influence on the displacement field; (4) the displacement patterns are similar in both cases, but in the case of a cone, the displacements are generally smaller and decay faster with distance from the indenter; and (5) the region ahead of the cone, or the wedge is heavily distorted and the displacements are predominantly in the radial direction. Behind the cone and the wedge, the displacement is mainly in the direction of penetration.

(3) <u>Analytic plasticity solutions</u>. Analytic plasticity solutions to cone penetration can provide very useful results. Most of the existing analytic plasticity solutions are obtained after simplifying the soil behavior by treating a rigid-perfectly plastic model. Axisymmetric problems, as in the case of cone penetration, require an additional assumption concerning the stress state in the plastic zone. Harr and von Karman (1909) assume that the circumferential (principal) stress is equal to one of the principal stresses in the meridian plane during plastic deformation. This simplification introduces errors of unknown magnitude according to Hill (1950).

In the case of footings, Shield (1955) presents the complete solution to the incipient penetration of a rigid circular footing on the surface of a half-space. His solution indicates that: (1) the plastic zone beneath a circular footing is shallower and narrower than beneath a strip footing (Hill, 1950); (2) the deformation pattern is very similar in both cases; (3) the contact pressure on the circular footing is non-uniform and increases from 5.14 c near the edge to 7.2 c near the center of the footing, where c is the shear strength of the material; (4) the bearing capacity determined by the average value of the contact pressure is approximately

- 39 -

10% higher for a circular footing than for a strip footing. Lockett (1963) presents solutions for progressive (hence unsteady) penetration of rigid lubricated cones, with apex angle $2 \delta \geq 105°$, at the surface of a half-space (starting from zero penetration).

Analytic plasticity solutions for steady deep cone penetration are complicated by the additional steady state requirement. If available, they would represent a valuable contribution to the interpretation of the cone penetration test.

2.4 Summary

Continuous and deep cone penetration represents a difficult steady state deformation problem where deformations and strains should be given primary consideration. Existing theories of cone penetration rely on modifications of rigorous solutions to simplified problems. Most theories are based on incipient plane strain solutions or expansion o f cavity solutions and do not consider deformations or strains. Baligh (1975) offers a more rational theory based on the steady penetration of a wedge. This theory is discussed in more detail in Chapter 4 since its predictions are later compared to field measurements.

A discussion of different approaches to cone penetration indicates that the strain path method presently pursued at M.I.T. is promising. This method is illustrated by the deep penetration of a flat ended pile (or blunt cones). Deformations, strains and strain-rates are estimated (approximately) using a relatively simple velocity field and the procedure developed by Vivatrat (1978). The analysis indicates that significant shearing occurs in the soil ahead of the cone tip, and that the maximum shear strain, $\frac{1}{2}(\varepsilon_1 - \varepsilon_3)$, takes place in horizontal (circumferential)

planes. The maximum shear strain on vertical (meridian) planes, $\frac{1}{2}(\epsilon_1 - \epsilon_2)$, is very close to $\frac{1}{2}(\epsilon_1 - \epsilon_3)$ ahead of the cone tip but decreases to about 50% of $\frac{1}{2}(\epsilon_1 - \epsilon_3)$ far behind the tip. The strain rates in the soil due to penetration are not uniform and, for typical cone sizes and penetration velocities, are several orders of magnitudes higher than typical laboratory tests.

Type of Approach	Reference	$q_c = N_c s_u + p_o$ Expression for N_c	N_c for $2\delta = 60°$		p_o
			$G/s_u = 100$	$G/s_u = 400$	
Bearing Capacity	Terzaghi (1943) Meyerhof (1951)	(shape factor)(depth factor) x 5.14	9.25	same	σ_{vo}
Bearing Capacity	Mitchell and Dorgunoglu (1973)	(shape factor)(depth factor) x $(2.57 + 2\delta + \cot\delta)$	9.63	same	σ_{vo}
Bearing Capacity	Meyerhof (1961)	(1.09 to 1.15) x $(6.28 + 2\delta + \cot\delta)$	10.2	same	σ_{vo}
Cavity Expansion	Bishop et al (1945)	$1.33(1 + \ln G/s_u)$	7.47	9.30	unspecified
Cavity Expansion	Gibson (1950)	$1.33(1 + \ln G/s_u) + \cot\delta$	9.21	11.03	σ_{vo}
Cavity Expansion	Vesic (1975,1977)	$1.33(1 + \ln G/s_u) + 2.57$	10.04	11.87	σ_{oct}
Cavity Expansion	Al Awkati (1975)	(correction factor) x $(1 + \ln G/s_u)$	10.65	13.28	σ_{oct}
Steady Penetration	Baligh (1975)	$1.2(5.71 + 3.33\delta + \cot\delta) +$ $(1 + \ln G/s_u)$	11.02 + 5.61 =16.63	11.02 + 6.99 =18.01	σ_{ho}

Table 2.1 Summary of existing theories of Cone Penetration in clays
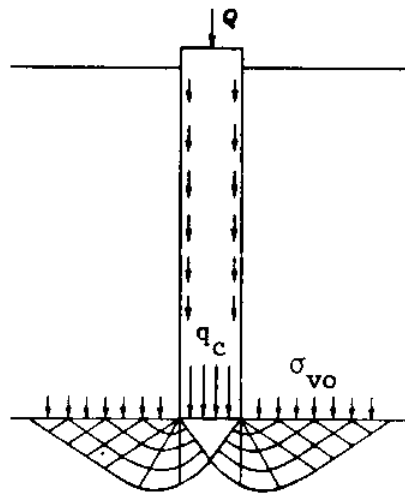
Prandtl (1920)
Reissner (1924)
Caquot (1934)
Buisman (1935)
Terzaghi (1943)
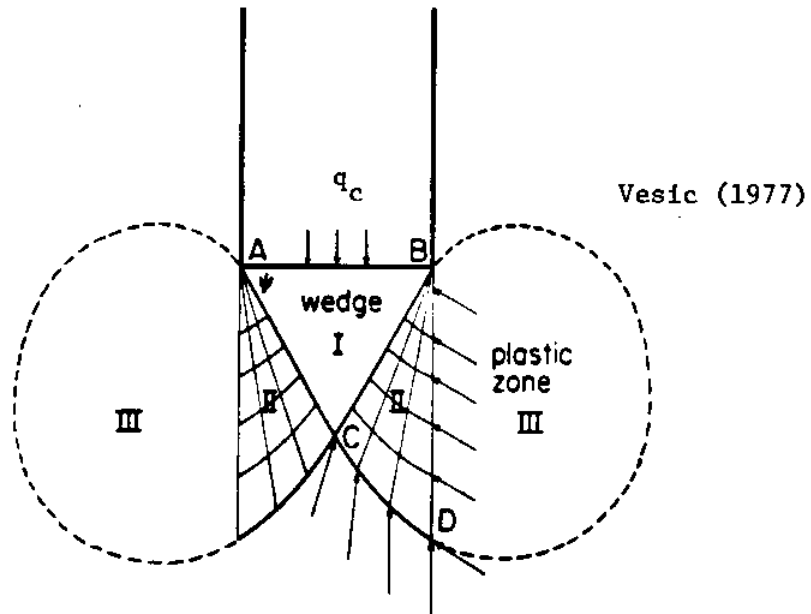
Vesic (1977)

Fig. 2.1 Assumed failure patterns for deep penetration.
(From Vesic, 1967; 1977.)
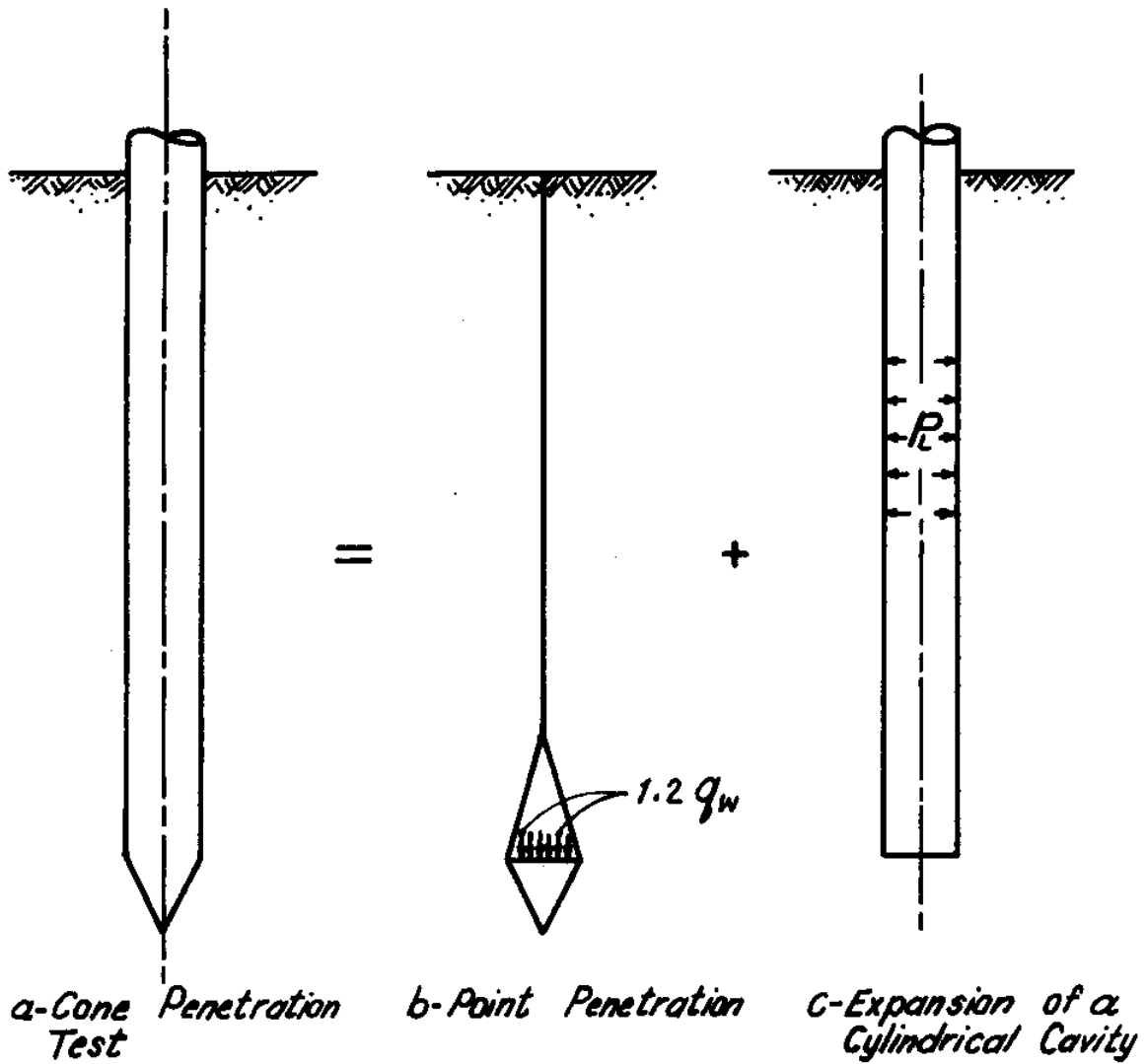
Fig. 2.2 Model for cone penetration mechanism according to Baligh (1975).
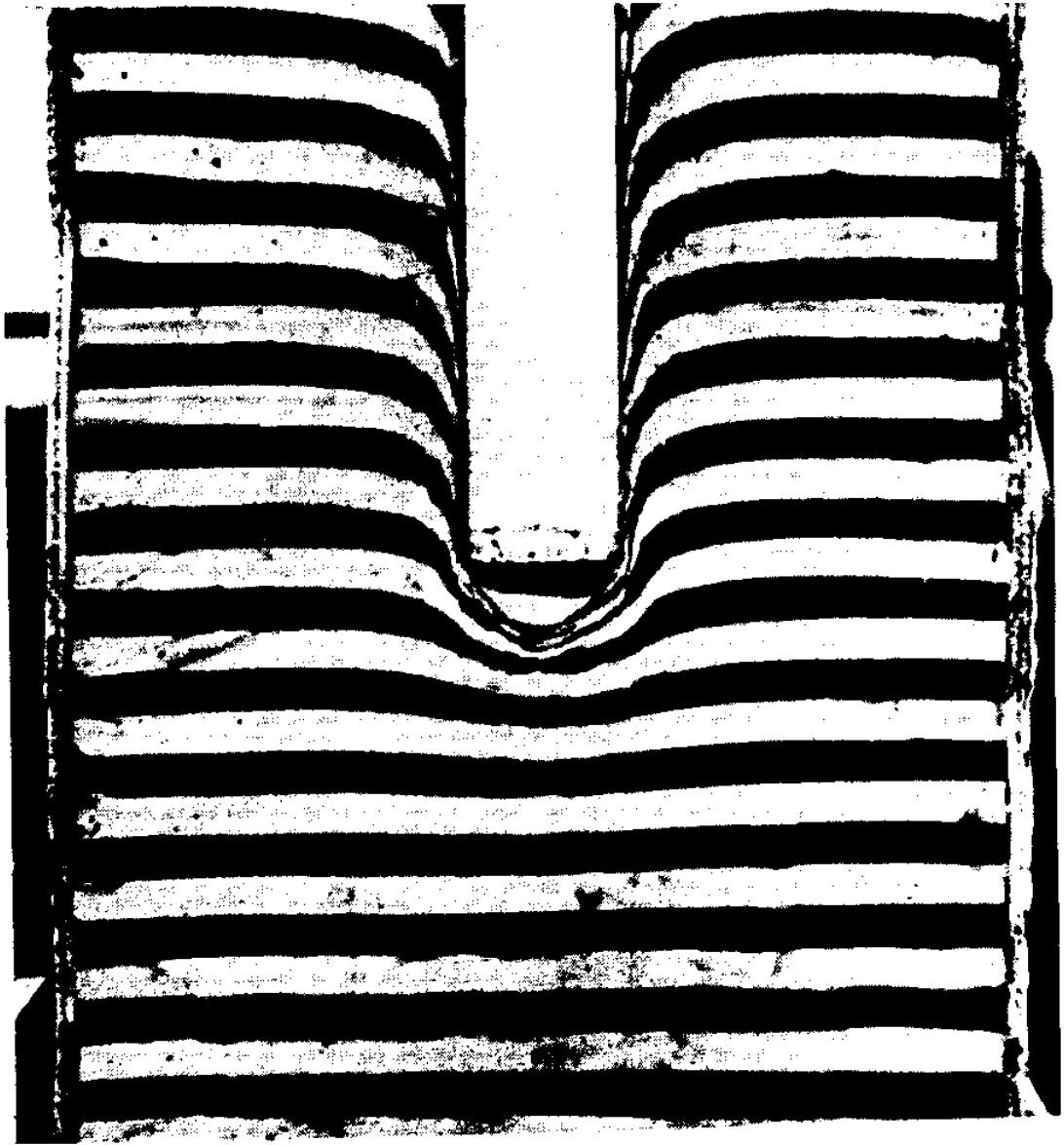
Fig. 2.3 Deformation pattern in bentonite due to cone penetration (from Rourk, 1961).
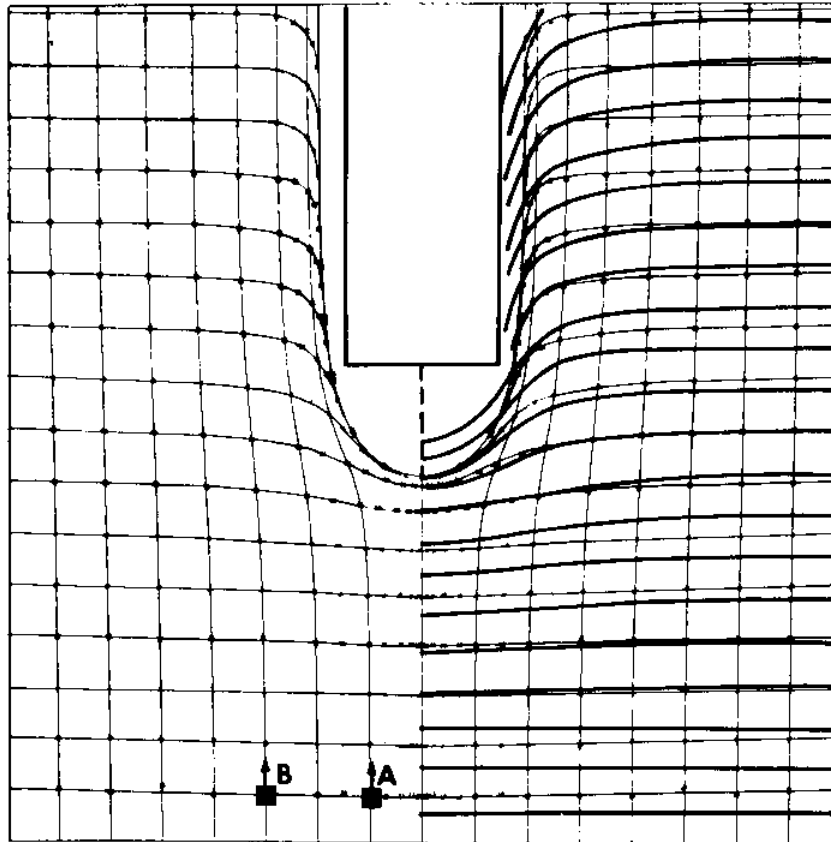
Fig. 2.4 Predicted and observed deformation patterns
due to flat pile penetration, Vivatrat (1978).

thin grid   = predicted deformation patterns,
heavy lines = observed deformation pattern
             (Rourk, 1961)
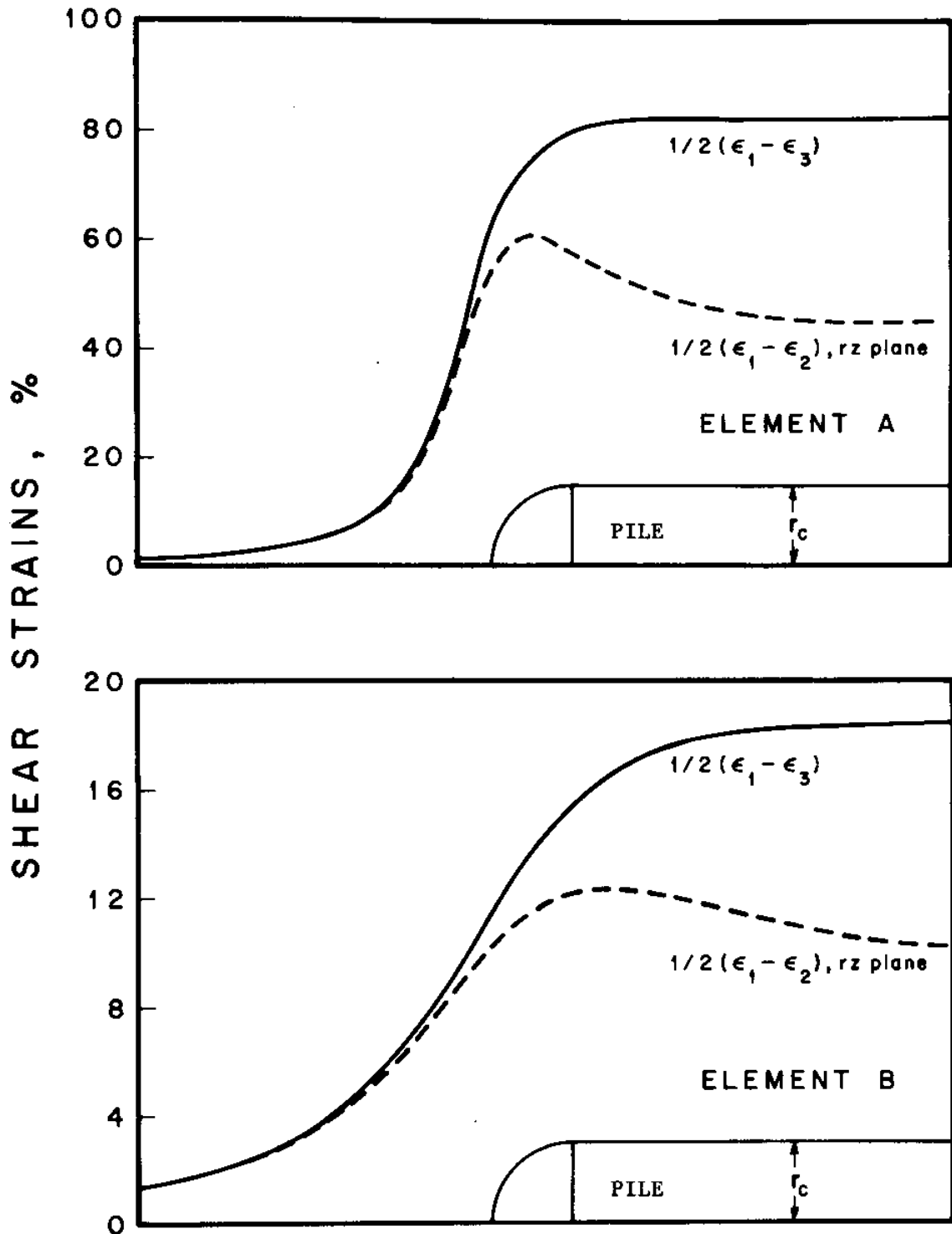
Fig. 2.5 Strain history on soil elements during flat pile penetration.

CHAPTER 3

STEADY WEDGE PENETRATION

Baligh (1975) proposes a theory for cone penetration based on solutions he obtained for steady wedge penetration in isotropic clays (Baligh, 1972 and Baligh and Scott, 1976). The cone penetration theory presented in Chapter 4 is based on the same approach and is later compared to field measurements. In this chapter we describe the wedge penetration theory for isotropic clays, present an extension of this theory to anisotropic clays developed by Vivatrat (1978), and then discuss the effect of factors neglected by these theories.

3.1 Theory of Steady Wedge Penetration in Isotropic Clays

A theory for plane-strain steady wedge penetration in an isotropic, rigid-plastic material was developed by Baligh (1972) and Baligh and Scott (1976) using slip-line fields. The basic features of this theory are:

(1) The wedge is rigid, has an infinite length (plane strain), and is sharp, i.e., an apex angle $2\delta \leq 90°$.

(2) The clay is homogeneous, <u>isotropic</u>, massless, rigid perfectly plastic, incompressible, with a shear strength s_u which is independent of the hydrostatic stress ($\phi = 0$) and the strain rate.

(3) The clay is initially subjected to an isotropic state of stress (i.e., $K_o = 1$).

(4) During steady penetration, the clay forms a "cavity" (or gap) behind the wedge. This cavity has straight surfaces and is subjected to an internal (pressure) stress, p_b.

(5) The geometry of the slip-line field is determined by the incom-
pressibility requirement as well as the magnitude of the shear
stress τ acting on the wedge faces. Baligh (1972) obtained solu-
tions for the two limiting cases of $\tau = 0$ and $\tau = s_u$. Vivatrat
(1978) extended these solutions for intermediate values of τ, and
showed that for most practical purposes, the solution for $\tau = s_u$
("rough" wedge) applies approximately.

Figures 3.1 through 3.4 illustrate the results of this theory including
stresses, wedge resistance, deformations and strains for a "rough" 60°
wedge (i.e., for $\tau = s_u$).

(1) Stress field. Figure 3.1 shows, in the upper left hand diagram,
the slip-line field, in the upper right hand diagram, the streamlines along
which soil elements move relative to the wedge. The lower part of
Fig. 3.1 shows a stress diagram which describes the stress field in the
plastic zone around the wedge. In this diagram, the stress state at any
point such as A, adjacent to the wedge face, is represented by a Mohr circle.
The cycloid in the stress diagram represents the trace of the origin of
planes along any circular arc from the face of the wedge to the triangular
region containing element E. From the stress diagram, the normal and the
shear stresses acting on the wedge faces are approximately given by
(Baligh, 1975):

$$p = p_b + (5.71 + 3.33\ \delta)\ s_u$$

$$(3.1)$$

and $\qquad \tau = s_u$ ("rough" wedge).

We note that any increment in the cavity pressure, p_b, results in an equal

increment in the normal stress on the wedge faces, and hence does not

affect the wedge penetration resistance q_w^*.

With the stress field and the streamlines, we can determine

the stress path that a soil element is subjected to as penetration progresses.

The upper right-hand side of Fig. 3.1 shows the major principal stress direc-

tions for a soil element as it moves past the wedge. These directions are

important in the subsequent discussion of anisotropic clays where the shear

strength depends on the principal stress directions.

(2) <u>Penetration resistance</u>. The theory predicts the penetration

resistance, q_w to be:

$$q_w + p_b = p + \tau/\tan \delta$$

(3.2)

or $$q_w = (p - p_b) + \tau/\tan \delta$$

combining equations 3.1 and 3.2, we can write q_w as:

$$q_w = N_w s_u ,$$ (3.3)

where the wedge factor, N_w, for a sharp rough wedge with an apex angle

$2 \delta < 90°$, is approximately given by:

$$N_w = 5.71 + 3.33 \delta + \cot \delta$$ (3.4)

The solid line in Fig. 3.2 represents N_w vs. 2δ according to

Eq. 3.4. The wedge resistance factor, N_w, equals 9.5 ± 0.3 for

---

   *q_w is the external force per unit projected area to push the wedge.
Alternatively, q_w is the work done per unit length of the wedge (perpendicular
to the drawing in Fig. 3.1) to push the wedge a unit distance into the
soil.

$40° \leq 2 \delta \leq 90°$, and increases rapidly for smaller wedge angles 2δ. For the particular values of $2 \delta = 18°$, $30°$ and $60°$ used in the experimental program, the $N_w = 12.6$, 10.3 and 9.2, respectively.

(3) Deformations and strains. Deformations and strains due to steady wedge penetration can be obtained by the procedure described by Vivatrat (1978). Figure 3.3 shows the soil deformation pattern around a 60° wedge. The wedge causes intense deformation in a zone of width $2B(1 + 1/\sin \delta)$, where 2B is the base width of the wedge. The assumption of soil rigidity prior to yielding requires that straining of the soil occurs only within the plastic zone enclosed by the slip-line field shown in Fig. 3.1. This causes a velocity discontinuity across the boundary of the plastic domain and results in sharp kinks in the deformed grid, Fig. 3.3. Baligh (1972) compares this deformation pattern (which he obtained by a graphical method) with experimental observations in modeling clay and found that the agreement is good for sharp wedges, but becomes less satisfactory for blunt wedges.

The strain-history due to wedge penetration is illustrated in Fig. 3.4 for the three soil elements A, B, and C, located as shown in Fig. 3.3. The maximum shear strain $\varepsilon_{max} = \frac{1}{2}(\varepsilon_1 - \varepsilon_3)$ is plotted vs. the relative vertical distance between the element and the wedge tip. For a 60° wedge, element C, which is the furthest from the wedge, is subjected to a 15% peak shear strain. This high level of straining, however, decreases significantly for sharper wedges (see Vivatrat, 1978). Elements A and B, which are closer to the wedge centerline than element C, undergo significant unloading once they move beyond the base of the wedge, but are left with a permanent or "residual" maximum shear strain of 7 to 13%. The rate of shearing is relatively uniform in the soil just in front of the wedge faces.

For a 60° wedge, with width 2B = 3.56 cm,[*] and a penetration velocity of 2 cm/sec, the maximum shear strain rate is on the order of 15% per sec.

3.2 Anisotropic and Nonlinear Behavior of Clays

Most natural clays exhibit a stress-strain-strength behavior which depends on the applied stress system (i.e., the direction of the major principal stress relative to, say, the vertical). This is a result of the inherent aniso- tropic structural arrangement of clay particles and/or the anisotropic stresses during consolidation. Figure 3.5 shows the stress-strain behavior of three clays where results of cone penetration tests will be presented subsequently. Figure 3.5a shows results of K_o-consolidated undrained plane strain compression (PSC), plane strain extension (PSE), and direct simple shear (DSS) tests on normally consolidated (OCR = 1)[**] Boston Blue Clay, BBC, which is a lean clay with medium sensitivity. The difference in soil behavior between the three types of tests is clear, especially the soil stiffness. The peak shear stress, often used as a measure of the shear strength, s_u, of the soil, is not the same in the three tests and does not take place at the same straining level. Furthermore, $s_u(PSC) > s_u(DSS) > s_u(PSE)$. Figure 3.5b shows the same results for BBC, but for an OCR = 4. Noting the difference in the vertical scale be- tween the two figures, overconsolidation tends to:

1. increase the shear strength of the clay;

2. decrease the degree of anisotropy as expressed by, say the ratio $s_u(PSE)/s_u(PSC)$; and

---

[*]
   "Standard" cone penetrometers have a cross-sectional area of 10 cm^2, or a diameter of 3.56 cm, and are pushed at a rate of 1 to 2 cm/sec.
[**] OCR = overconsolidation ratio
        $= \overline{\sigma}_{vm}/\overline{\sigma}_{vc}$
     $\overline{\sigma}_{vm}$ = maximum vertical effective pressure
     $\overline{\sigma}_{vc}$ = consolidation vertical effective pressure prior to undrained shearing

3.   decrease the strain softening tendency of PSC tests.

Figure 3.5c shows the same results on normally consolidated (OCR = 1)

Connecticut Valley Varved Clay (CVVC). Compared to the response of BBC

at the same OCR = 1 shown in Fig. 3.5a, CVVC indicates:

1.   similar qualitative trends ;

2.   a smaller initial shear (i.e., higher K_o value);

3.   smaller values of s_u(PSC) and s_u(DSS);

4.   larger values of s_u(PSE); and

5.   the value of s_u(DSS) is smaller than s_u(PSE)

Figure 3.5d shows results of tests on normally consolidated (OCR = 1)

Atchafalaya Basin Clay (EABPL). This plastic clay exhibits a less pronounced

anisotropy and less strain softening than the lean BBC.

In order to simplify the highly nonlinear and anisotropic stress-strain-

strength behavior of clays, we assume that the clay is rigid-perfectly plas-

tic and has an anisotropic shear strength described by the elliptic yield

contour developed by Davis and Christian (1971) and shown in Fig. 3.6.

This contour satisfactorily approximates the undrained strength behavior of

most natural clays and is described by the vertical strength, s_u(V), and the

two parameters K_s and b/a defined in Fig. 3.6. To determine these two

parameters, the horizontal strength s_u(H) obtained from PSE tests and the

s_u(45°) obtained from DSS (say) are required. Table 3.1 shows the normalized

peak shear resistance in different failure modes for six normally-consolidated

clays, and the corresponding values of K_s and b/a computed on the basis of

the peak shear resistance. Since the peak resistance takes place at dif-

ferent strain levels, the use of peak resistances may not represent appropriate

values for the strengths in analyses. This issue of strain compatibility will be discussed subsequently.

3.3 Effect of Different Factors on Wedge Resistance

The wedge penetration theory described above is used in Chapter 4 to develop a cone penetration theory for interpreting cone resistance. It is, therefore, important to discuss simplifications made in developing the wedge theory since they represent uncertainties in the shear strength estimated on the basis of cone resistance measurements. These simplifications are discussed below and summarized in Table 3.2.

(1) Effect of strength anisotropy. Vivatrat (1978) presented a slip-line solution to steady wedge penetration in clays having elliptic yield contours. Since the undrained shear strength of an anisotropic clay is not unique, the wedge resistance factor N_w relating q_c to say, $s_u(V) = s_u(PSC)$, is not unique, but depends on the shape of the yield contour of the soil as described by K_s and b/a. Results of this theory are shown in Fig. 3.2.

In practice, the inverse problem is usually of interest, i.e., given the wedge (or later the cone) resistance, q_w, what can we infer regarding the soil strength? The anisotropic theory developed by Vivatrat (1978) indicates that, within an error of $\pm$ 15%, an average strength of the clay, $s_u(AVE)$, can be estimated by the isotropic theory described earlier, Fig. 3.7, where:

$$s_u(AVE) = \alpha[s_u(PSC) + s_u(PSE)]$$

$$(3.5)$$

or $\qquad s_u(AVE) = \alpha(1 + K_s) \, s_u(PSC).$

The parameter α varies between 0.45 and 0.49 for most clays ($0.5 \leq K_s \leq 1.0$,

$0.65 \leq b/a \leq 1.0$) and, for all practical purposes, can be approximated as 0.47, Fig. 3.8.

(2) Effect of soil deformability prior to yield. The slip-line theory assumes that the soil is rigid until the shear stress reaches the yield value. Figure 3.5, however, shows that clays deform before the peak shear stress is reached. The major effects of soil flexibility prior to yield are: 1) to develop soil deformations outside the plastic domain assumed by the theory, especially ahead of blunt wedges (Baligh, 1972); and 2) to decrease q_w estimated by the theory.

A good measure of soil deformability prior to yield is given by the ratio G/s_u, where G is the shear modulus and s_u the shear strength. The higher the ratio G/s_u, the closer the clay behavior to the idealized rigid-plastic material. Ladd et al. (1977) present experimental data showing that, for slightly overconsolidated and normally consolidated clays (OCR $\leq$ 2) in undrained conditions, the ratio G/s_u (from direct simple shear, DSS, tests) exceeds about 100 when the applied shear stress is below 2/3 s_u, and is significantly higher at lower stress levels.

The effect of soil deformability was considered by Mulhern (1959), Marsh (1964) and Hirst and Howse (1969) by means of experimental and analytical studies on progressive (hence unsteady) penetration of wedges and cones at the surface of a half-space. Their results indicate that this effect is more significant in blunt wedges (and cones) because of the change in the mode of deformation from the cutting predicted by slip-line theory to one of radial compression. Marsh (1964) suggests that, for a given indenter shape, the penetration resistance increases as G/s_u increases and

approaches the slip-line solution for rigid-plastic material. The apex

angle, 2δ , at which the rigid-plastic mode applies, depends on the ratio

G/s_u and the problem geometry (i.e., wedge vs. cone). Hirst and Howse

(1969) predict that, for a wedge with $2\delta \leq 60°$, the rigid-plastic mode

applies when G/s_u exceeds about 80. They also suggest that the effect of

soil deformability is less important for a cone than for a wedge with the

same apex angle because the stresses ahead of the cone decay faster with

distance.

Finally we expect that the effect of clay deformability is less

important in continuous steady penetration than in the unsteady problems

mentioned above. Therefore, the shear strength determined from the

wedge resistance, q_w, on the basis of Eqs. 3.3 and 3.4 is expected to

slightly underestimate the actual strength. The error is more pronounced

for blunt wedges in overconsolidated clays (where G/s_u is low) but less

significant in the case of cones.

(3) Effect of strain-softening. Equations 3.3 and 3.4 apply to

clays exhibiting no strain-softening behavior. For strain softening soils

(see Fig. 3.5a), a reduction in wedge (or cone) resistance must be ex-

pected. The strain path approach discussed in Chapter 2 provides a sys-

tematic method for determining the effects of strain softening which are

presently difficult to estimate. However, the shear strength estimated from

penetration resistance and Eqs. 3.3 and 3.4 is expected to underestimate

the peak shear strength of the clay.

(4) Strain rate. The rates of shear straining during penetration

are several orders of magnitude higher than typical rates used in

laborabory tests. Since the shear strength of clays increases with the

rate of straining, Ladd et al., (1977), neglecting rate effects can seriously underestimate penetration resistance especially in plastic clays. This means that the strength based on penetration resistance and Eqs. 3.3 and 3.4 can significantly overestimate the strength required in analyses involving the slow loading of clays.

(5) Friction at wedge-soil interface. Solutions in Eqs. 3.3 and 3.4 apply to rough wedges where the interface shear strength, τ , is assumed to equal s_u. Vivatrat (1978) shows that smaller values of τ cause a reduction in penetration resistance such that the strength estimated by Eqs. 3.3 and 3.4 can underestimate the actual strength of the clay. This depends on the magnitude of the pore pressures developed during penetration which are high in soft sensitive clays.

(6) Initial stresses. The initial stresses in clay deposits are rarely isotropic as assumed by the theory. For surface footings, D'Appolonia et al., (1971b) show that anisotropic initial stresses influence the progress of yielding and hence the load-settlement behavior. The effect of initial stresses on steady penetration resistance are difficult to estimate and require more sophisticated analyses, e.g., the strain path method.

(7) Shear stress on failure planes. The shear strength of soils is governed by effective stresses in accordance with the Mohr-Coulomb yield criterion or variations thereof. However, the use of effective stresses in the analysis of short-term stability of saturated clays requires the difficult task of measuring or estimating the pore water pressure at failure. For convenience and simplicity, these problems can be analyzed on the basis of total stresses ($\phi = 0$), Skempton (1948). This is due to the fact that, when no drainage takes place, the strength of clays is independent

of the confining stress [see, for example, Lambe and Whitman (1969)],

Total and effective stress analyses imply different inclinations of the failure plane with respect to the principal stress directions. The total stress analysis requires that the angle θ between the failure plane and the major principal stress be 45°, whereas the effective stress analysis requires $\theta = 45 \pm \bar{\phi}/2$, where $\bar{\phi}$ = the effective friction angle of the clay (with no cohesion intercept, $\bar{c} = 0$).[*] When related to the principal stresses, the shearing stress acting on the failure plane (at failure) according to the two approaches is, therefore, different. The total stress approach used in developing the plasticity solutions requires this shear stress to be $q_f = 1/2 (\sigma_1 - \sigma_3)$, whereas the effective stress approach requires a shear stress $\tau_{ff} = q_f \cos \bar{\phi}$. For typical values of $\bar{\phi} = 30°$, τ_{ff} is about 15% smaller than q_f.

Ladd (1971) recommends the use of $s_u = q_f$ in undrained bearing capacity analyses, but $s_u = \tau_{ff}$ in "total stress" circular arc stability analyses. Bjerrum (1973) presents case studies of embankment and footing failures which imply no noticeable difference in the empirical correction factors to be applied to field vane data for these two types of problems. The two recommendations by Ladd and Bjerrum, however, do not necessarily contradict, since conventional two-dimensional stability analyses neglecting end effects generally underestimate the factor of safety by about 10% (Azzouz and Baligh, 1978).

---

[*]Lo (1965) reported laboratory test results on about 650 samples of two clay types, indicating that θ is about 34°. These results contradict the predictions of the total stress analysis, but also imply a relatively low effective friction angle ($\bar{\phi} = 22°$) from the effective stress analysis.

Following Ladd's approach, the shear strength obtained from Eq. 3.3
on the basis of $s_u = q_f$, needs a reduction by about 15% to be used in
total stress circular arc stability analyses.

Type of Soil	Index Properties			$s_u/\overline{\sigma}_{vc}$ (1)			$K_s =$ $\dfrac{(5)}{(3)}$	$b/a =$ $\dfrac{(4)}{\sqrt{(3) \times (5)}}$
	w_ℓ (%)	P.I. (%)	(2) L.I.	(3) PSC	**(4) DSS	(5) PSE		
Portsmouth Clay	35	15	1.8	0.350	0.200	0.155	0.44	0.86
Haney Sensitive Clay	44	18	0.75	0.296	—	0.211	0.71	—
Boston Blue Clay	41	21	0.81	0.340	0.200	0.190	0.56	0.79
AGS CH Clay	71	40	—	0.370	0.250	0.220	0.59	0.88
San Francisco Bay Mud	88	45	1.04	0.370	0.250	0.280	0.76	0.78
Connecticut Valley Varved Clay	35-65	12-39	1.00	0.280	0.165	0.255	0.91	0.62

* From $\overline{CK_o U}$ plane strain tests with $\overline{\sigma}_{vc} > (1.5$ to $2) \times \overline{\sigma}_{vm}$

(1) $s_u = q_f = 0.5(\sigma_1 - \sigma_3)_f$ except for DSS where $s_u = (\tau_h)_{max}$

(2) $L.I. = \dfrac{w_n - w_p}{w_\ell - w_p}$

(3) plane strain compression

(4) direct simple shear

(5) plane strain extension

** Assuming $s_u(DSS) = s_u(45°)$

Table 3.1 Normalized undrained shear strength of six normally consolidated clays in different modes of failure* (data from Ladd et al, 1977; table courtesy of A.S. Azzouz).

Factor	Important in case of	Effect on estimated strength[*]
1. Anisotropy	Lean clays	± 15%
2. Soil deformability prior to yielding	Blunt wedges (more than cones) OC clays (G/s_u low) Fat clays	- 0 to 10%
3. Strain softening	"Soft" clays Lean clays	- 5 to 20%
4. Strain rate	Fat clays	+ (30 ± 15)%
5. Friction at wedge (or cone) - soil interface	"Soft" clays Sensitive clays Sharp wedges (and cones)	- 0 to 20%
6. Anisotropic initial stresses	"Soft" clays (low K_o) Lean clays	Difficult to estimate
7. Shear stress on failure planes	High $\bar{\phi}$	- 0 to 20%

[*] Based on theoretical penetration resistance in Eq. 3.3; + means s_u is overestimated by theory

Table 3.2 Probable errors in wedge penetration theory

SLIP LINE FIELD

STREAM LINES
DIRECTIONS
OF σ_1

2γ

p_b

$q_w + p_b$

$\tau = c$

p

2δ

σ_1

$$q_w + p_b = p + c/\tan\delta$$

$$c = S_u$$

$$\gamma = \sin^{-1}(1/\sqrt{2} \cdot \sin\delta)$$

τ

O

σ

c

c

p_b — $c(\frac{\pi}{2} + 2\gamma + 1)$ — $c(\pi + 2\delta)$

$$p = p_b + c(5.71 + 3.33\delta)$$
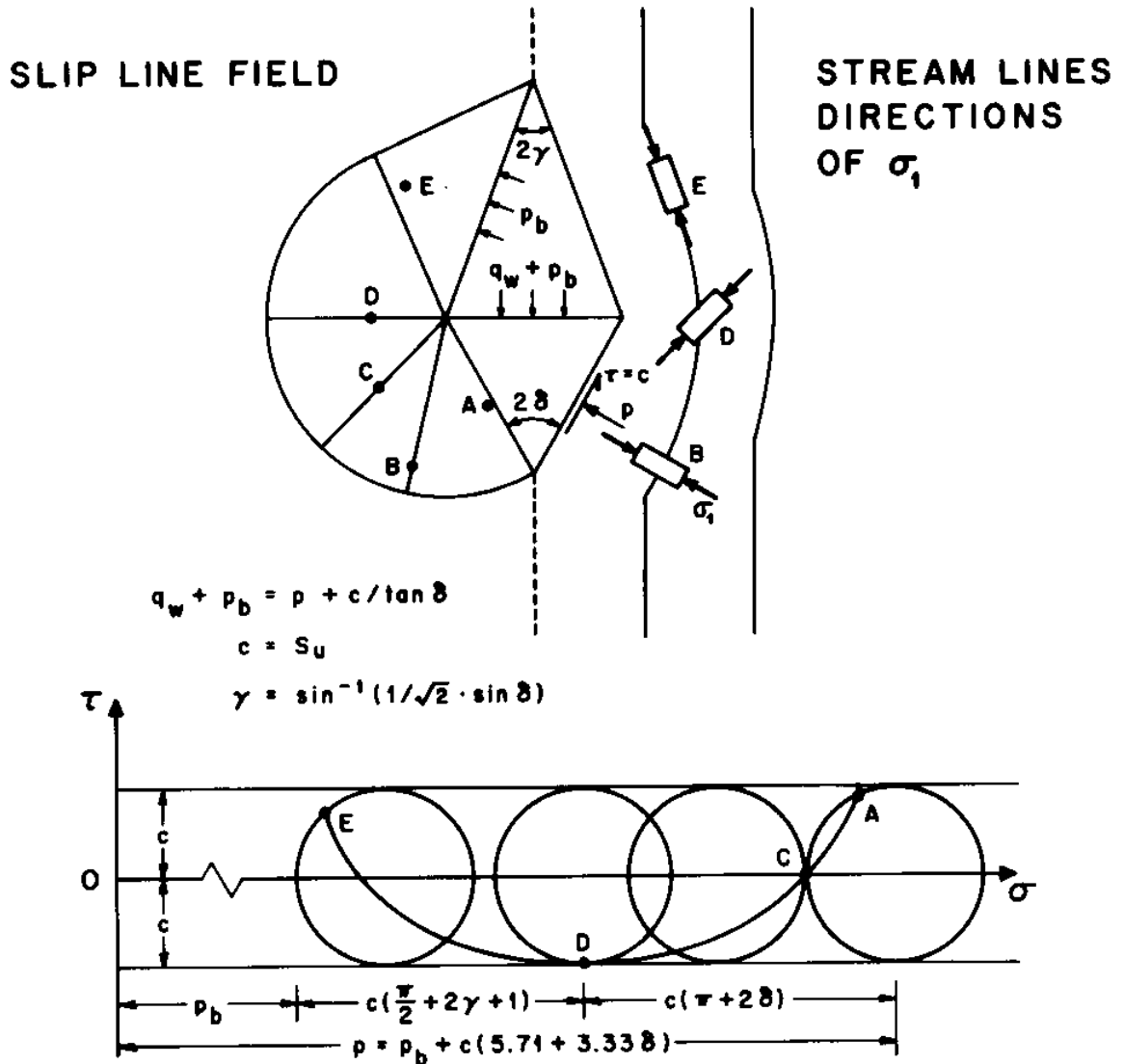
Fig. 3.1   Slip-line solution for steady wedge penetration
in isotropic clays.
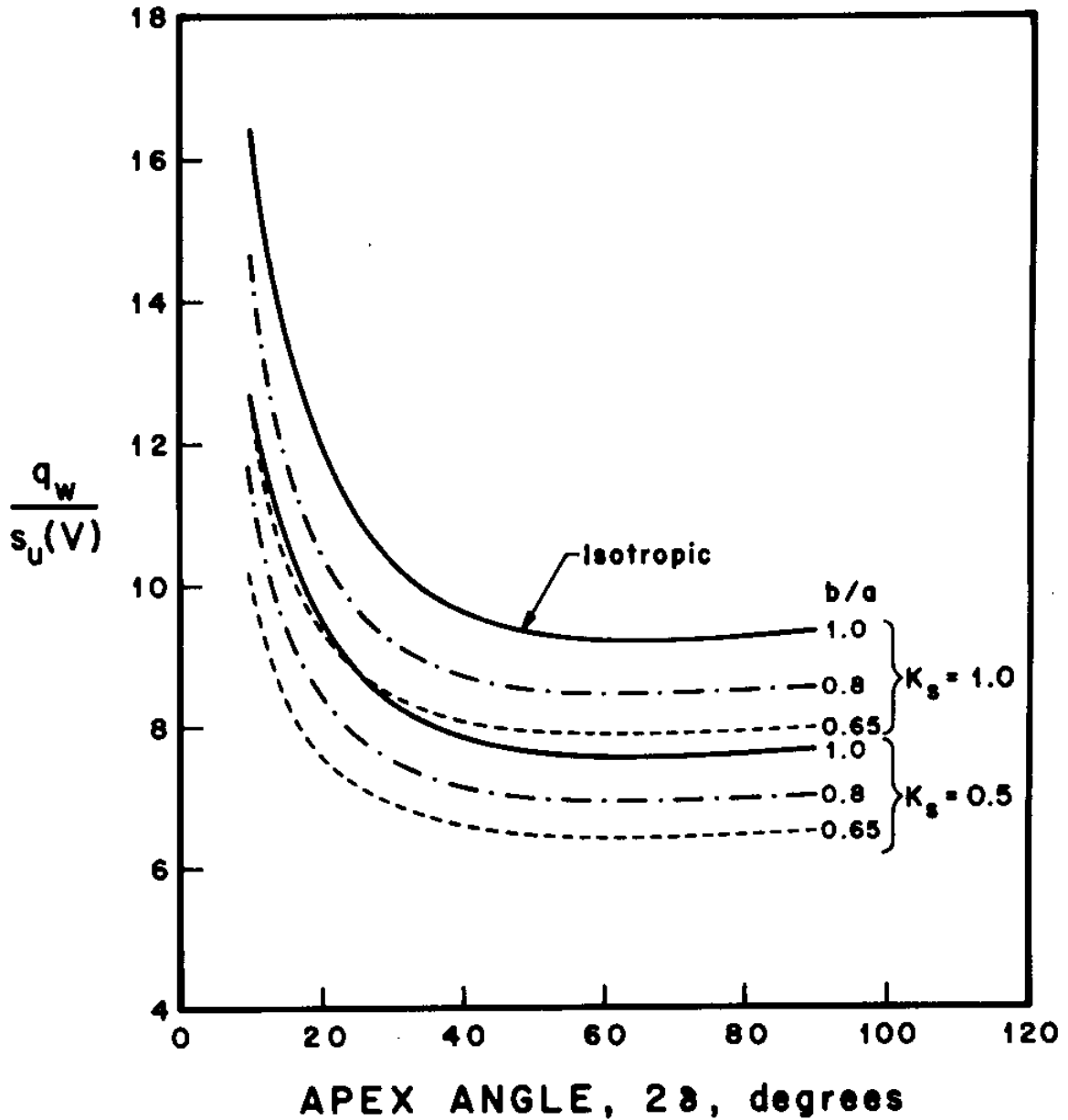
Fig. 3.2   Sharp rough wedge resistance factors for steady penetration in anisotropic clays.
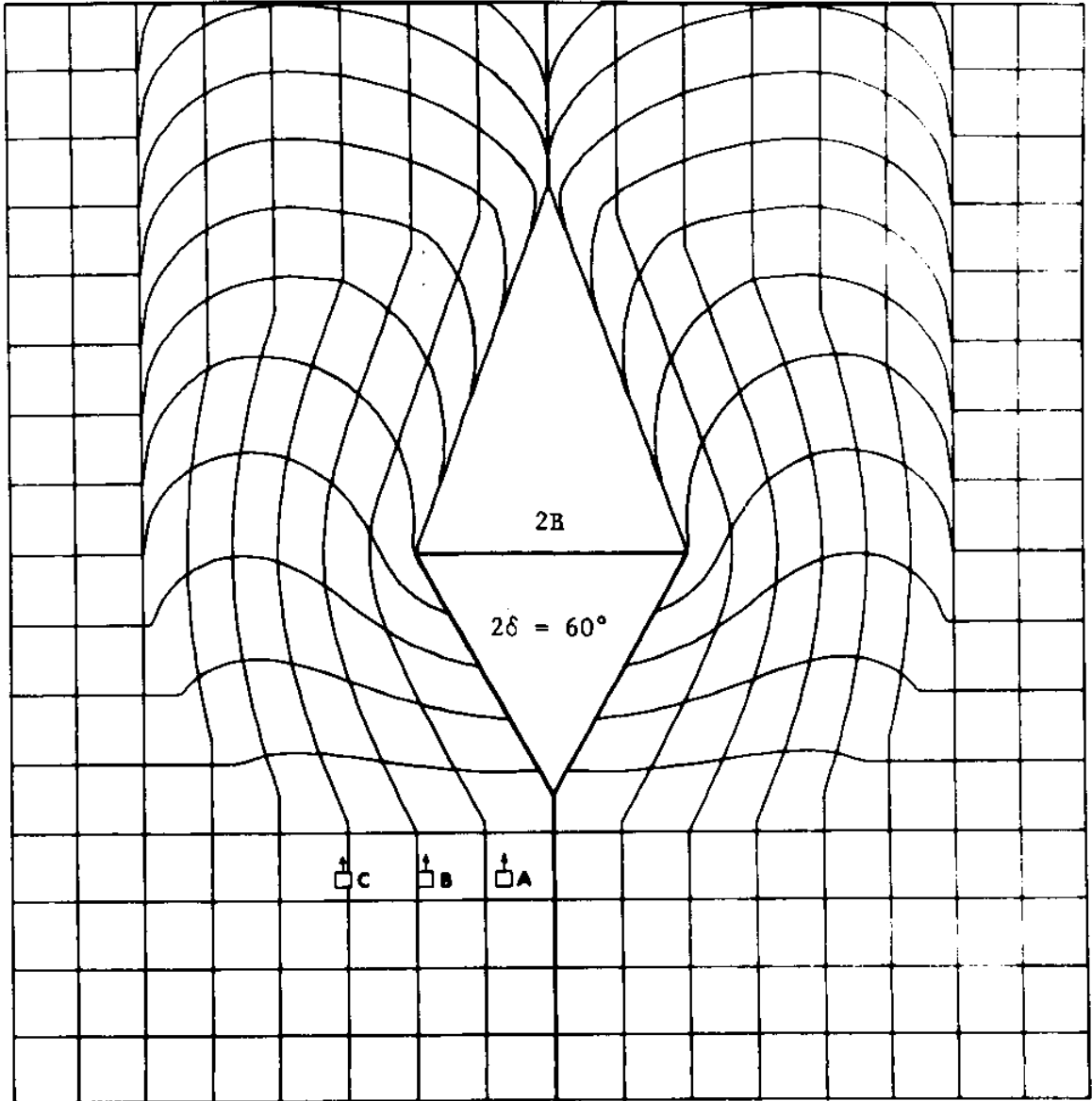
Fig. 3.3 Predicted deformation pattern around a 60° wedge (strain-history of soil elements A, B, and C is shown in Fig. 3.4).
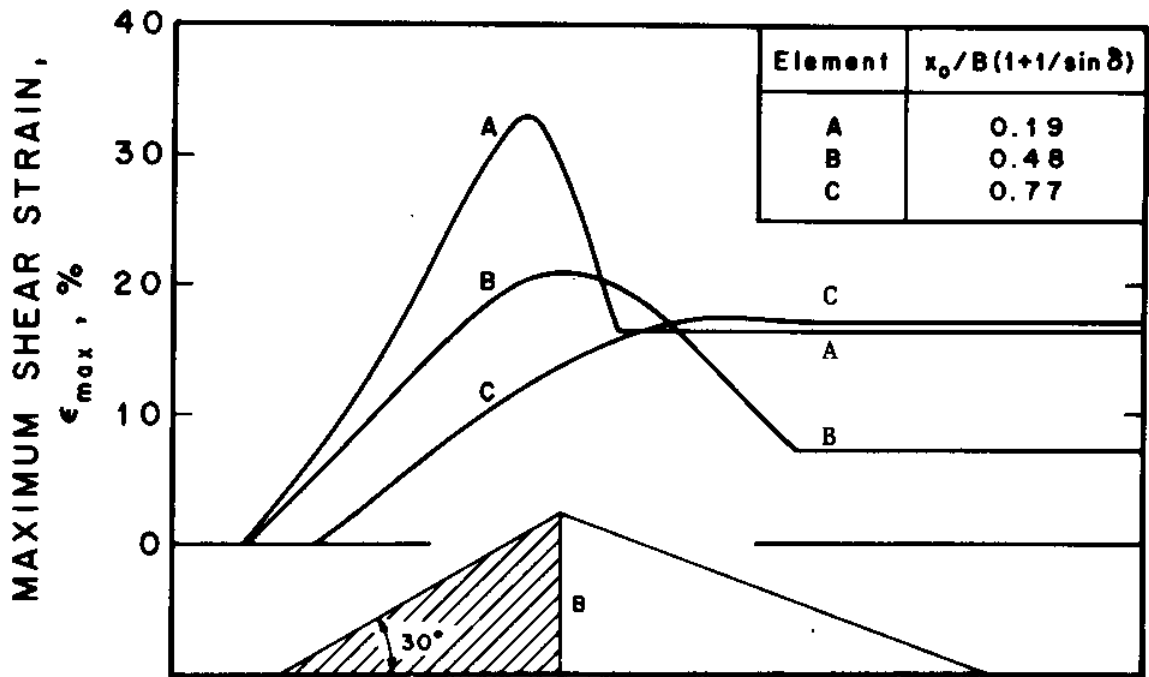
Fig. 3.4   Strain-history of soil elements
A, B, and C shown in Fig. 3.3.
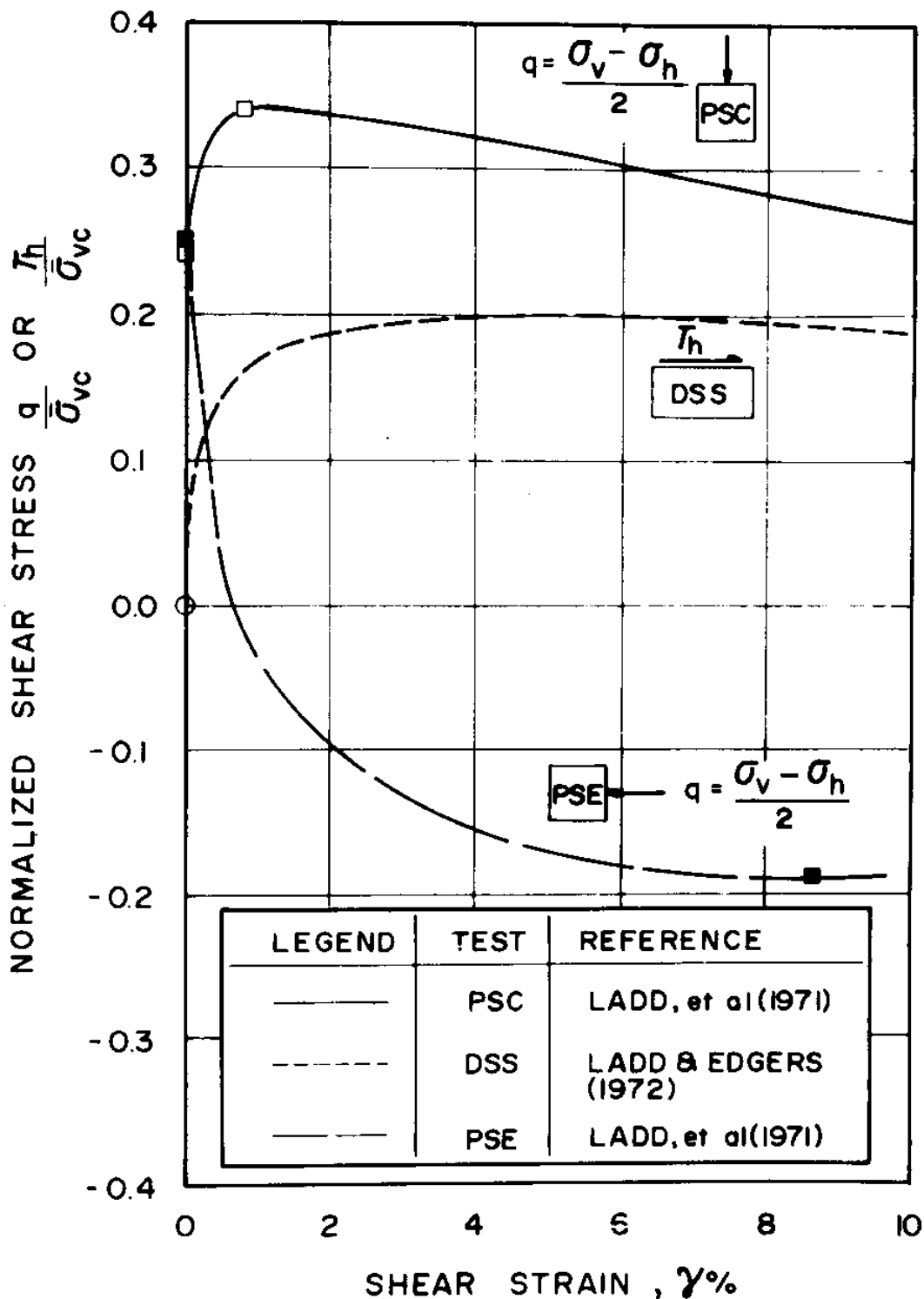
Fig. 3.5a Normalized stress-strain relations from $\overline{CK_0U}$ tests on normally consolidated Boston Blue Clay. (from Azzouz and Baligh, 1978)
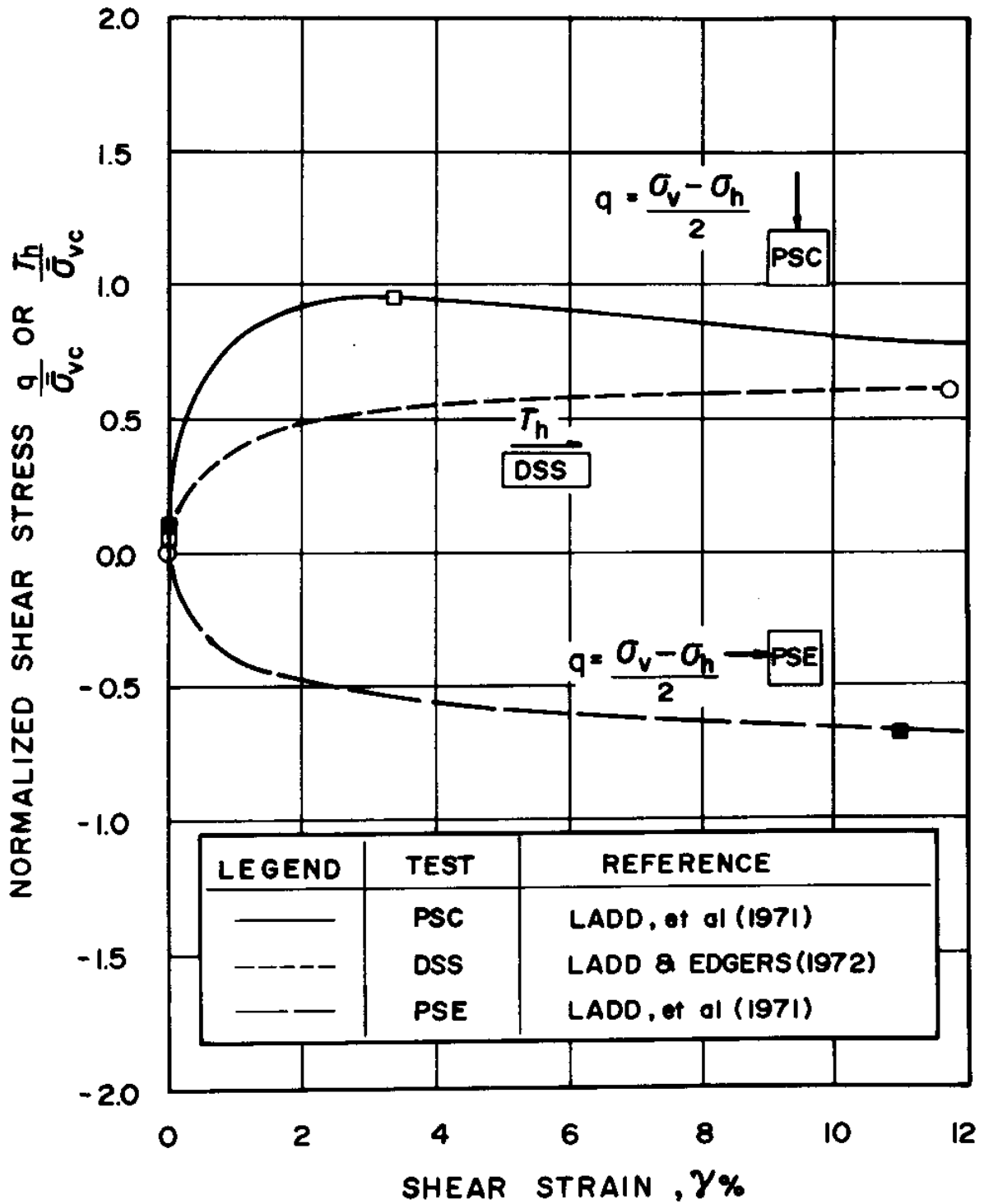
Fig. 3.5b Normalized stress-strain relations from $\overline{CK_o U}$ tests on Boston Blue Clay (OCR = 4) (from Azzouz and Baligh, 1978).
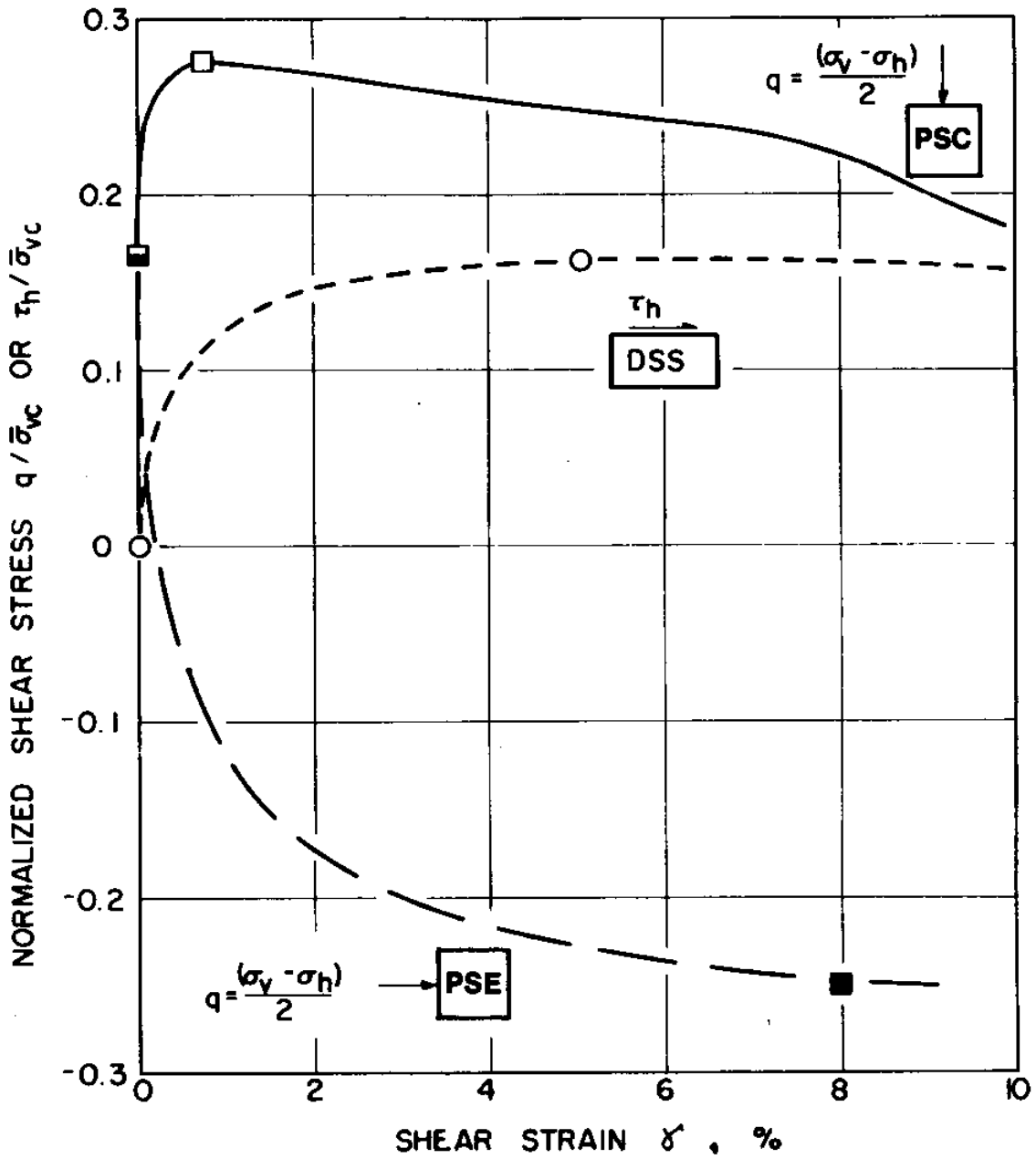
Fig. 3.5c Normalized stress-strain relations from $\overline{CK_oU}$ tests on normally consolidated Connecticut Valley Varved Clay (from Ladd, 1975).
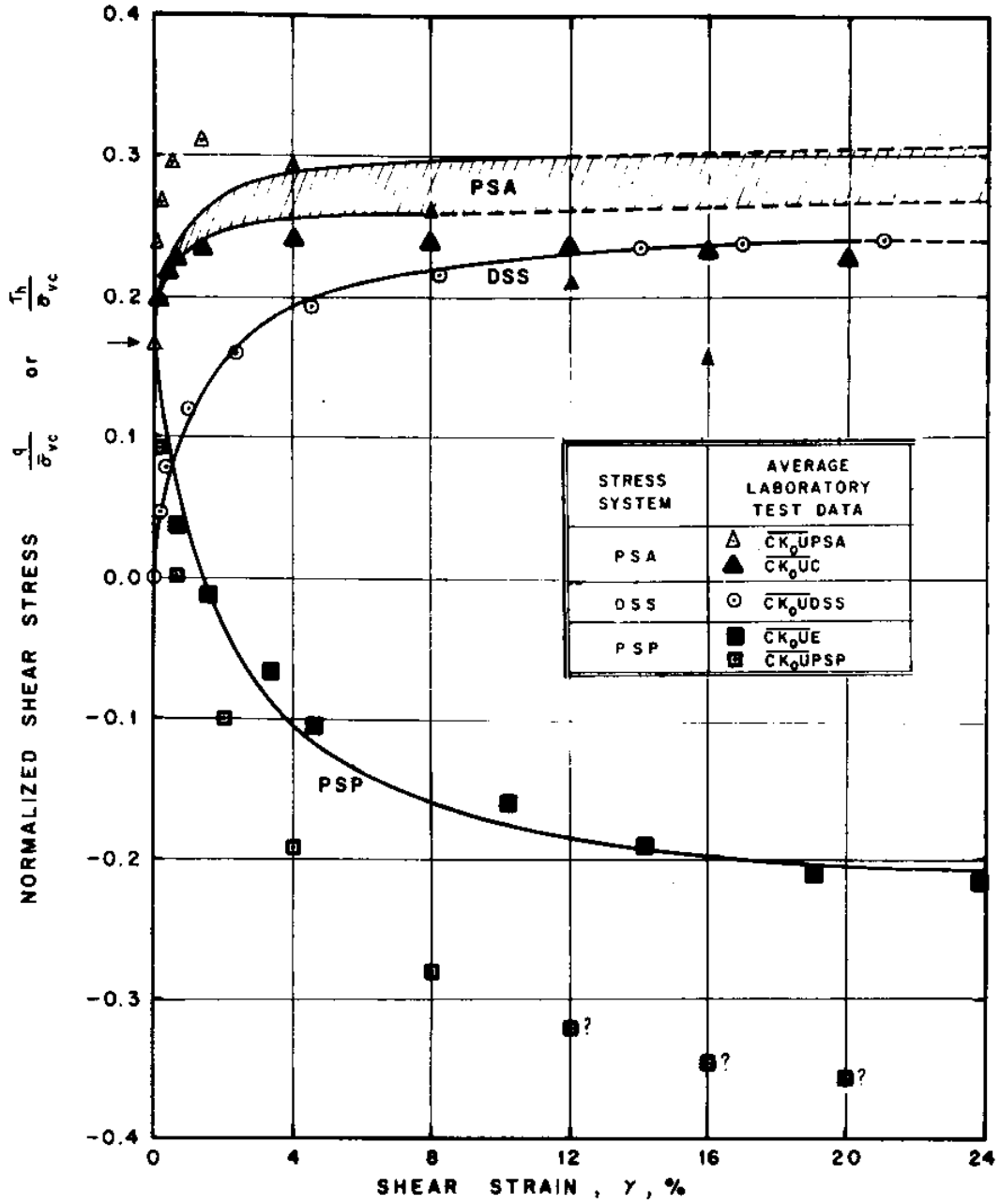
Fig. 3.5d   Normalized stress-strain relations from $\overline{CK_oU}$ tests
on normally consolidated EABPL Clays

(from Fuleihan and Ladd, 1976)

ELLIPTIC YIELD CONTOUR Davis and Christian (1972)
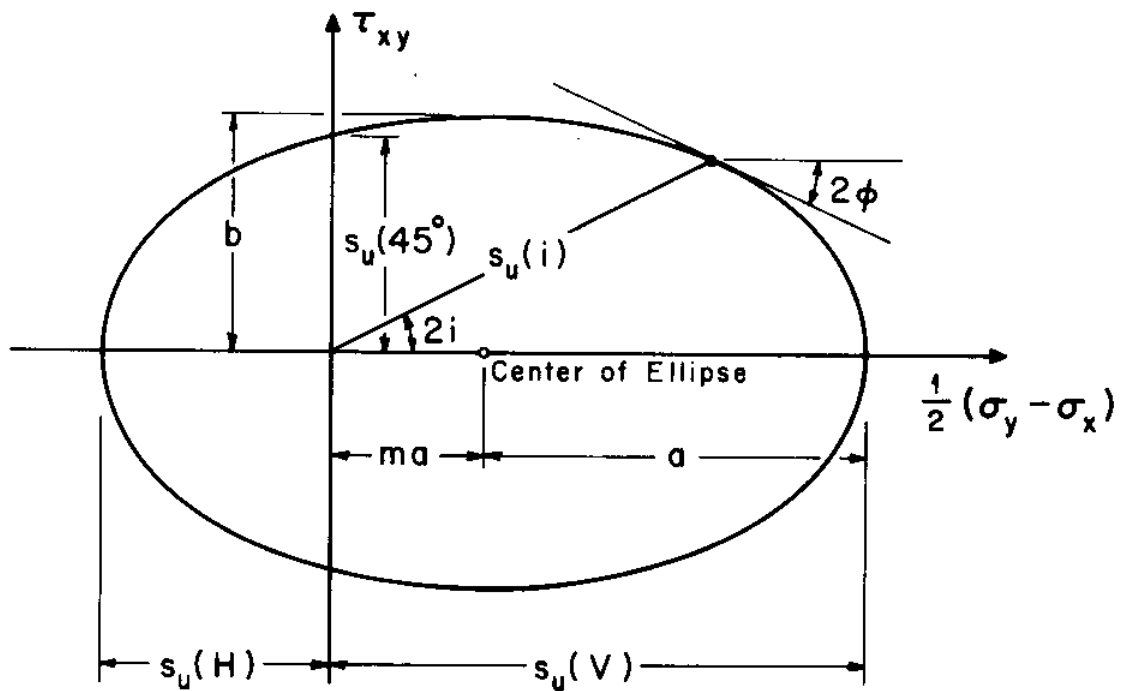
$$a = \frac{1}{2}\left[s_u(V) + s_u(H)\right] \quad ; \quad m = (1 - K_s)/(1 + K_s)$$

$$b = s_u(45°)/\sqrt{s_u(V)\,s_u(H)} \quad ; \quad K_s = s_u(H)/s_u(V)$$

Fig. 3.6 Elliptic yield contour

$$s_u(AVE) = \frac{2}{\pi} \int_{-\pi/4}^{+\pi/4} s_u(\phi, \; b/a, \; K_s) \; d\phi$$

= average shear strength on a
slip line consisting of a full
circle (or half a circle)

$\dfrac{q_w}{s_u(AVE)}$

Band for $0.50 \leq K_s \leq 1.0$

$0.65 \leq b/a \leq 1.0$

N_w (Isotropic)

APEX ANGLE, 2δ, degrees
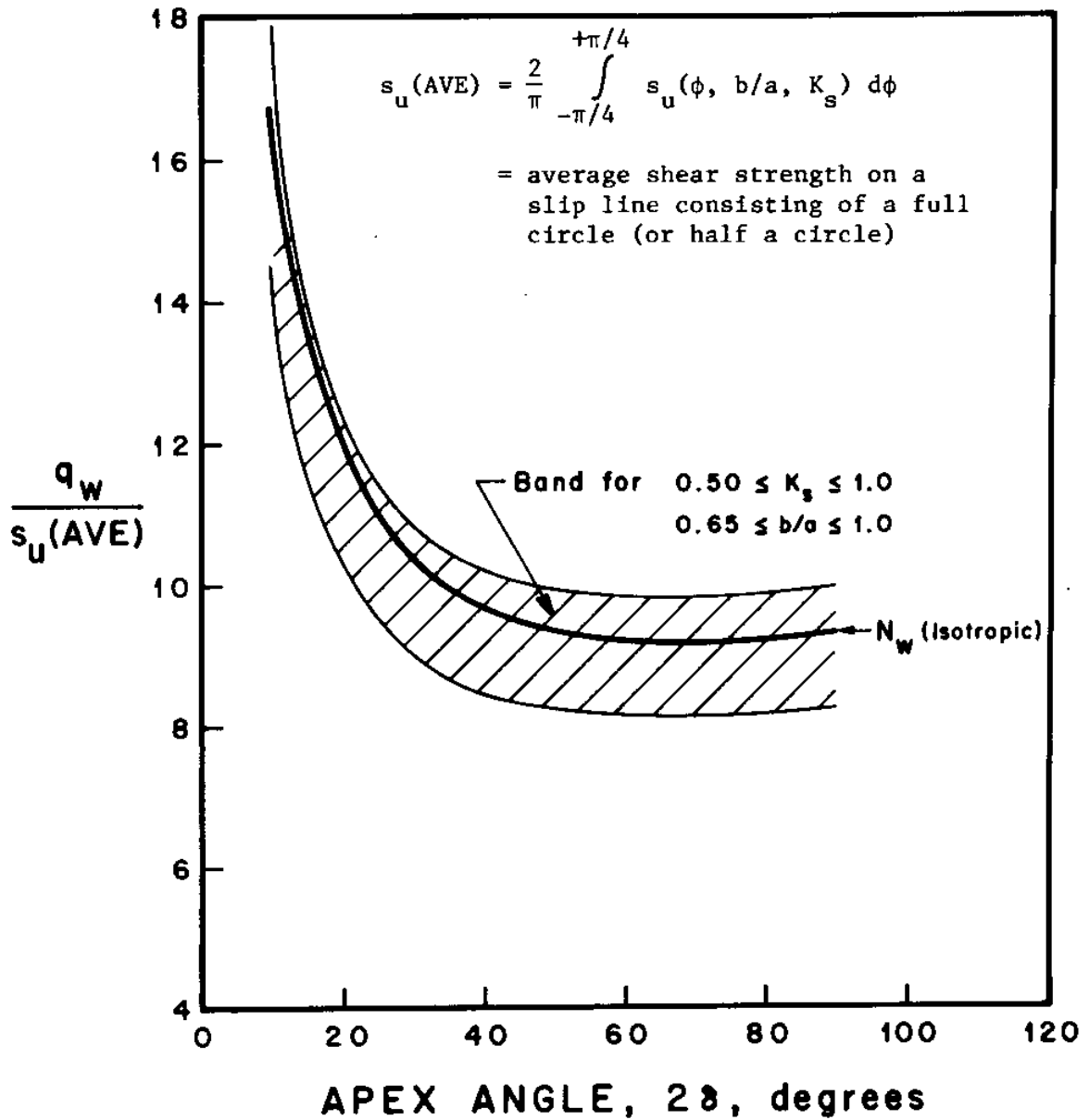
Fig. 3.7   Wedge resistance in terms of the "average"
strength, s_u (AVE)
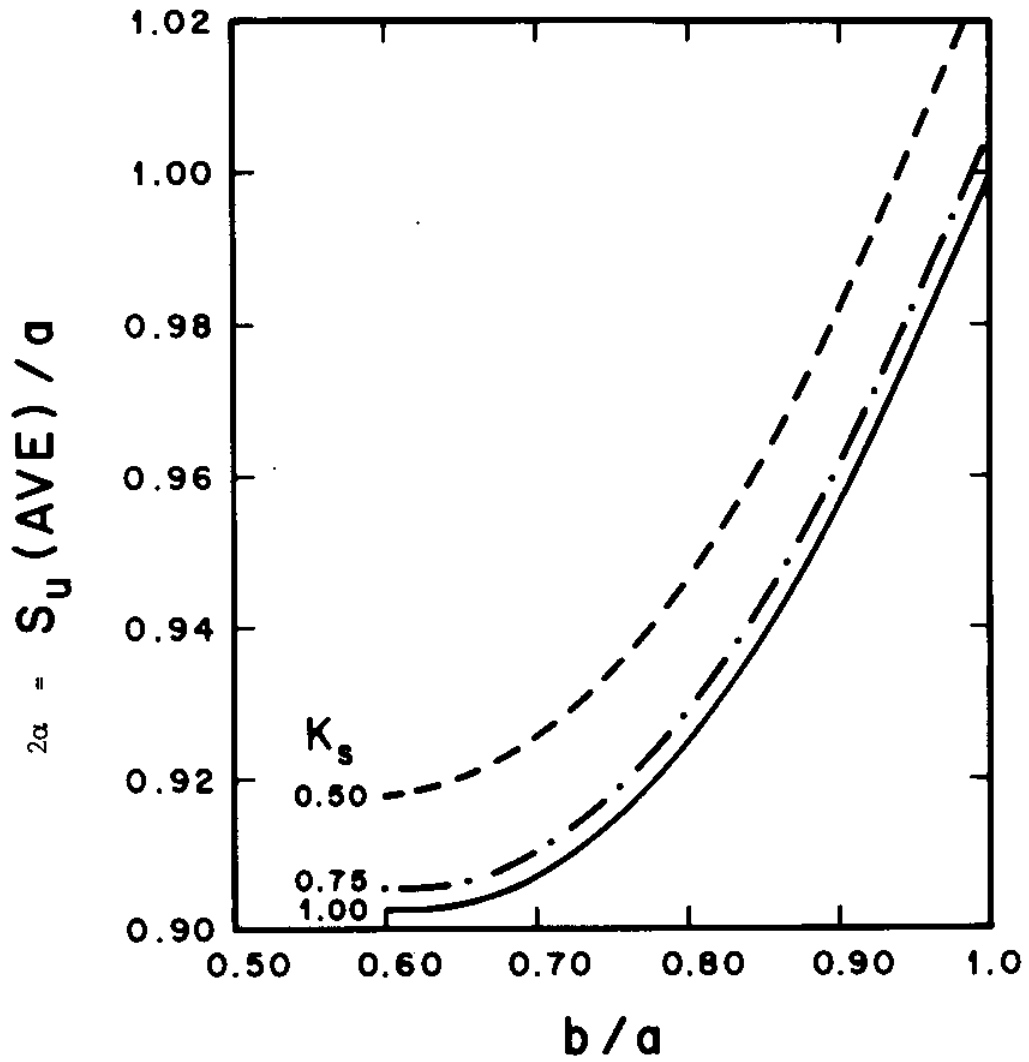
Fig. 3.8   The average strength, $s_u(AVE)$,

in terms of $a = 0.5[s_u(V) + s_u(H)]$

CHAPTER 4

A THEORY OF CONE PENETRATION IN CLAYS

4.1 Introduction

The continuous penetration of cones into deep soil layers represents a steady state problem. Chapter 2 estimates deformations and strains around a blunt cone (or pile) penetrating into clays and emphasizes the difference between steady state penetration and the more common bearing capacity theories based on incipient failure modes. Chapter 2 also discusses the difficulties encountered in obtaining rigorous solutions for the steady state cone penetration. This chapter presents an approximate semi-empirical theory of cone penetration in clays developed by Baligh et al (1977) which is based on wedge penetration solutions presented in Chapter 3.

4.2 Cone Resistance

The cone resistance, q_c, is the external force per unit area required to push the cone. Alternatively, q_c also represents the external work done per unit area of the cone per unit displacement during steady state penetration.

(1) Idealized cone. Chapter 3 presents an ideal plasticity theory for steady state wedge penetration in clays. According to this theory, the clay forms a "cavity" behind the wedge, Fig. 3.1, which is subjected to an isotropic state of stress, p_b. The wedge resistance, q_w, which is the external force per unit area required to push the wedge, depends on the wedge angle and the undrained shear strength of the clay, s_u, but is independent of p_b. The axisymmetric counterpart of the plane strain wedge problem is

that of a cone pushed by means of a shaft with a much smaller diameter, Fig. 4.1a. Based on a comparison of plane and axisymmetric deformation problems (Baligh, 1972) and the empirical shape factors often used in soil mechanics (Skempton, 1951; Brinch Hansen, 1970; Vesic, 1973), Baligh (1975) approximates q_c by :

$$q_c = 1.2 \ q_w \qquad (4.1)$$

where q_w is given by Eqs. 3.3 and 3.4.

Therefore, q_c is independent of the stress in the cavity, p_b, and in isotropic clays, q_c is given by:

$$q_c = N_c \cdot s_u; \qquad (4.2)$$

where N_c = cone resistance factor

$$= 1.2 \ (5.71 + 3.33 \ \delta + \cot \delta)$$

where 2δ is the apex angle in radians.

(2) <u>Enlarged cone</u>. In practice, a shaft with a finite diameter d is required to push a cone with base diameter D into the soil, Fig. 4.1b. Clay deformation due to penetration by "enlarged" cones (D/d > 1) is believed to be similar to the idealized case presented earlier (d → 0). The penetration resistance for enlarged cones can thus be obtained from Eq. 4.2 , provided that a correction is made to account for the presence of the shaft behind the cone, i.e.,

$$q_c + p_b (1 - d^2/D^2) = N_c \cdot s_u + p_b$$

or
$$q_c = N_c \cdot s_u + (d/D)^2 \ p_b \qquad (4.3)$$

where N_c is given by Eq. 4.2 .

Thus, the point resistance of "enlarged" cones depends on the pressure p_b in the cavity behind the cone which cannot, at present, be determined from the theory. For the ratio $D/d = 2$, used subsequently in our field tests to be described in Chapter 5 , the correction due to the shaft equals $2\,s_u$ when $p_b = 8\,s_u$ and equals s_u when $p_b = 4\,s_u$.

(3) <u>Regular (unenlarged) cone</u>. Recent developments in electric cone penetrometer technology lead to the adoption of the Fugro design (de Ruiter, 1971 and Chapter 5) as the "standard" geometry for future use. The Fugro cone has a 60° tip (2δ) and a straight cylindrical shaft behind the cone tip having the same 10 cm^2 cross-sectional area as the base of the cone tip, i.e., $D/d = 1$. This geometry is shown schematically in Fig. 4.1c and will hence forth be referred to as the "regular" or "unenlarged" cone.

The shaft behind an unenlarged cone imposes a rigid constraint on soil deformation and is most likely subjected to non-uniform stresses. Denoting the average normal stress on this shaft by p_b', and assuming that the stress increment in the soil between the cone face and the shaft behind the cone is the same as in an enlarged cone, we can write

$$q_c = N_c \cdot s_u + p_b' , \qquad (4.4)$$

where N_c is given by Eq. 4.2 .

Baligh (1975) presents an approximate theory for penetration of un-enlarged cones in isotropic clay (see Chapter 2). His theory is equivalent to assuming that p_b' equals the pressure required to expand an infinitely long cylindrical cavity in the clay mass. If the clay behavior is approximated by that of an elastic-perfectly plastic material, this expansion pressure is given by:

$$p_b' = \sigma_{ho} + (1 + \ell n\ G/s_u)\ s_u , \qquad (4.5)$$

where $\qquad\sigma_{ho}$ = initial horizontal total stress in the soil;

$$= u_o + K_o \bar{\sigma}_{vo}$$

G = undrained shear modulus of the clay.

Hence, for $D/d = 1$,

$$q_c = [N_c + (1 + \ln G/s_u)] \times s_u + \sigma_{ho} \qquad (4.6)$$

Figure 4.2 provides typical values of the at-rest-earth pressure coefficient, K_o, which is required in estimating σ_{ho}.

Baligh et al (1977) indicate that Eq. 4.6 assumes the work required to push an unenlarged cone equals the algebraic sum of work done in conducting two deformation processes: 1) pushing an enlarged cone with $D/d \rightarrow \infty$; and 2) expanding a cylindrical cavity. In reality, the two processes are not performed consecutively, but simultaneously. Hence, the actual work done is believed to be less than predicted by this approach, i.e., q_c in Eq. 4.6 is believed to represent an upper bound on the cone resistance of unenlarged cones ($D/d = 1$). On the other hand, a lower bound for q_c (of unenlarged cone) can be obtained by the cone resistance of the idealized enlarged cone ($D/d \rightarrow \infty$), i.e., Eq. 4.2.

In summary, Baligh et al (1977) recommend that, for regular cones ($D/d = 1$), the cone resistance q_c is in the range:

$$N_c \cdot s_u \leq q_c \leq N_c \cdot s_u + (1 + \ln G/s_u) \times s_u + \sigma_{ho} \qquad (4.7)$$

Figure 4.3 a shows the dependence of the cone resistance, q_c, on the cone angle 2δ. The solid curve (1), represents Eq. 4.2 which applies to the idealized cone where the diameter of the pushing rods, d, is very small compared to the cone diameter D (i.e., $D/d \rightarrow \infty$). This is also a lower bound

on q_c for all cones (with finite values of D/d). Curve (2) illustrates Eq. 4.6 and represents a typical upper bound for all cones in soft to medium clays.[*] Curve (2) is the same as curve (1) but shifted upwards because of:a) the effect of the initial horizontal stress, σ_{ho}, which, in this case, is about 7 s_u; and, b) the exterior work to expand a cylindrical cavity which, in this case, is about 6 s_u.

Figure 4.3b shows the effect of soil parameters on the predicted range of q_c. In typical "medium" to "soft" onshore clay deposits, the range of q_c for a 60° unenlarged cone is approximately given by:

$$11 \ s_u \leq q_c \leq (22 \ to \ 28) \ s_u \tag{4.8}$$

(γ_t/γ_w = 1.6 to 1.9; K_o = 0.55 ± 0.15; G/s_u = 150; $s_u/\bar{\sigma}_{vo}$ = 0.20 to 0.33).

---

[*]Assuming that K_o = 0.55, G/s_u = 150, $s_u/\bar{\sigma}_{vo}$ = 0.25, γ_t = 1.8 T/m^2 and the water table is located at ground surface.

a. IDEALIZATION

$$q_c + P_b = N_c \cdot s_u + P_b$$

$$N_c = 1.2[5.71 + 3.33\delta + 1/\tan \delta]$$

q_c = cone resistance

s_u = undrained shear strength of clay

P_b = isotropic pressure in the cavity behind the cone

2δ = cone angle
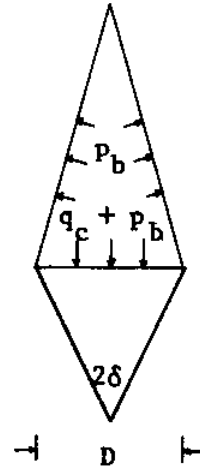
b. CONE WITH ENLARGED TIP   (D/d > 1)

$$q_c = N_c \cdot s_u + (d/D)^2 \cdot P_b$$

d = diameter of pushing rods

D = diameter of cone
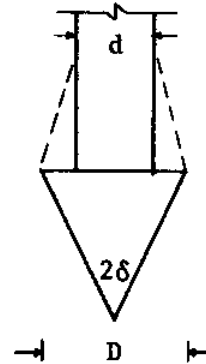
c. UNENLARGED CONE   (D/d = 1)

$$N_c \cdot s_u \leq q_c \leq N_c \cdot s_u +$$

$$[\sigma_{ho} + (1 + \ln G/s_u) \, s_u]$$
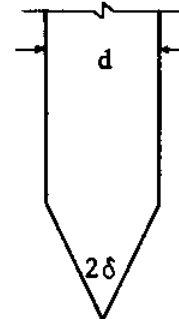
Fig. 4.1   Theoretical predictions of cone resistance in clays
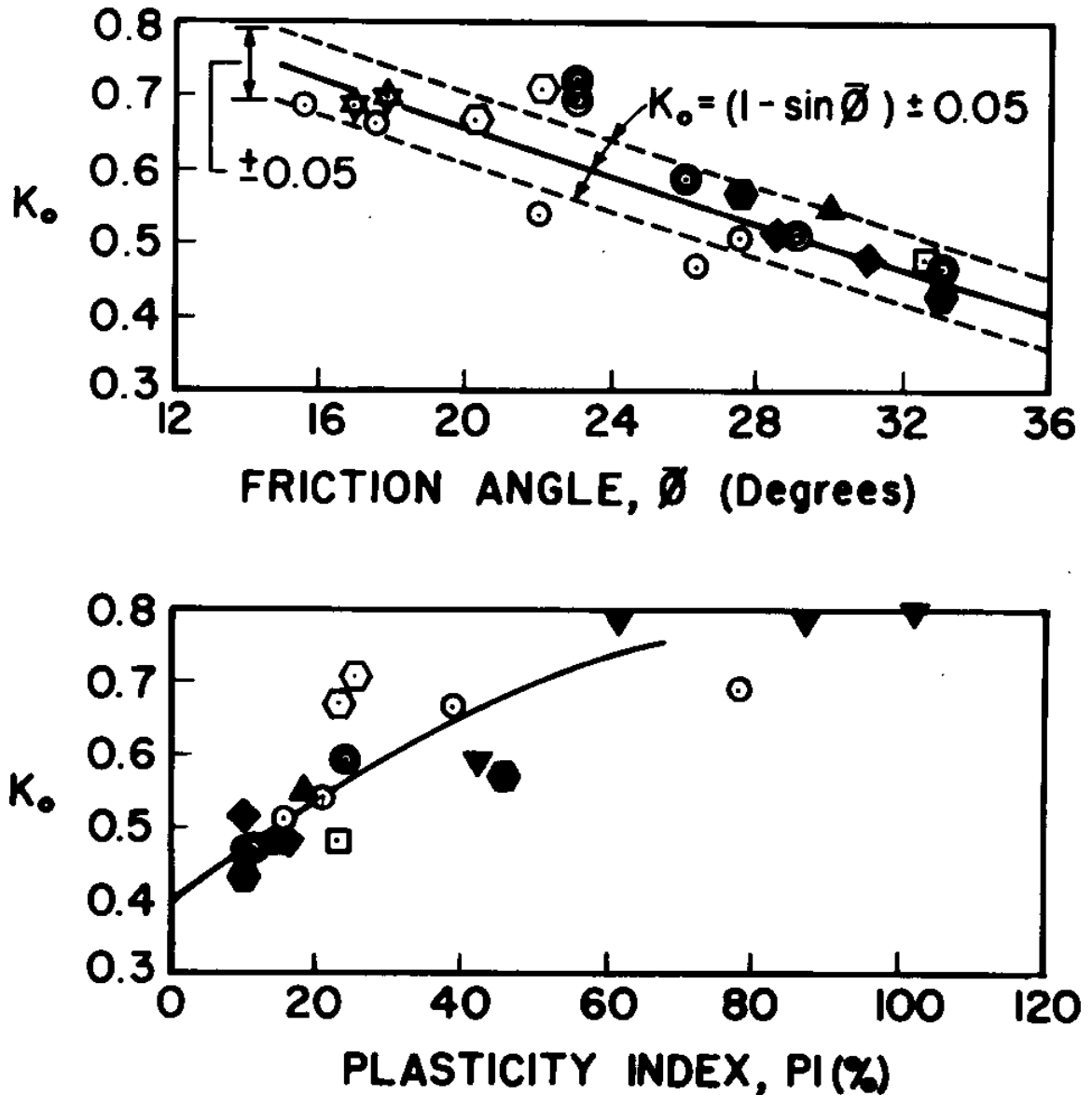
Fig. 4.2   Empirical correlations for K_o in normally consolidated clay deposit (from Ladd et al., 1977). For overconsolidated clays, K_o is approximately given by

$$K_o(OCR > 1) = K_o(OCR = 1) \cdot (OCR)^m$$

where $m \approx 0.35$ to 0.40 (unloading condition only).
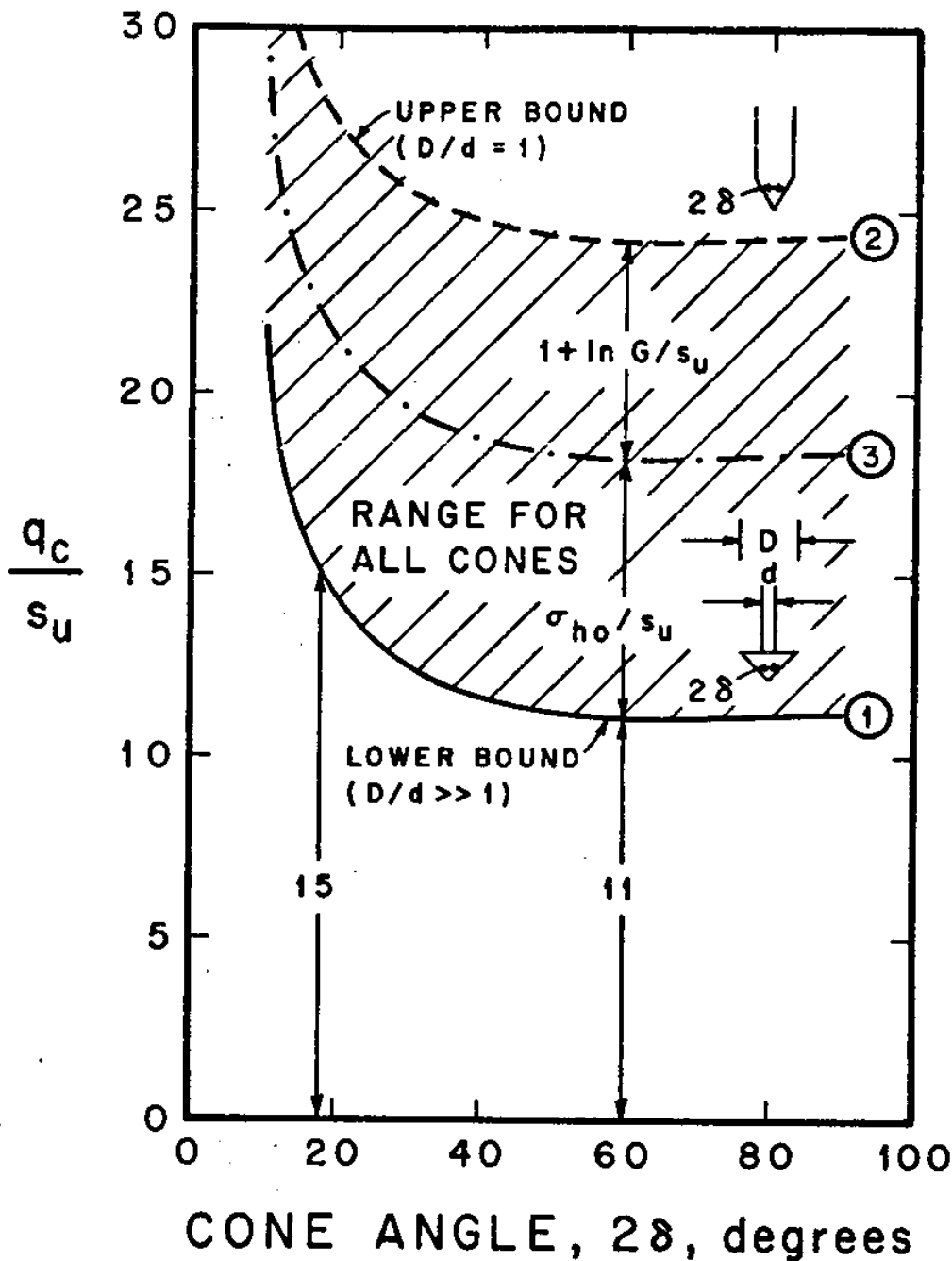
Fig. 4.3a Theoretical cone penetration resistance in clays.
(Upper bound computed for a total unit weight of
1.8 T/m^3, K_o=0.55, G/s_u=150, $s_u/\bar{\sigma}_{vo}$ = 0.25, and a
hydrostatic condition with water table at surface.)
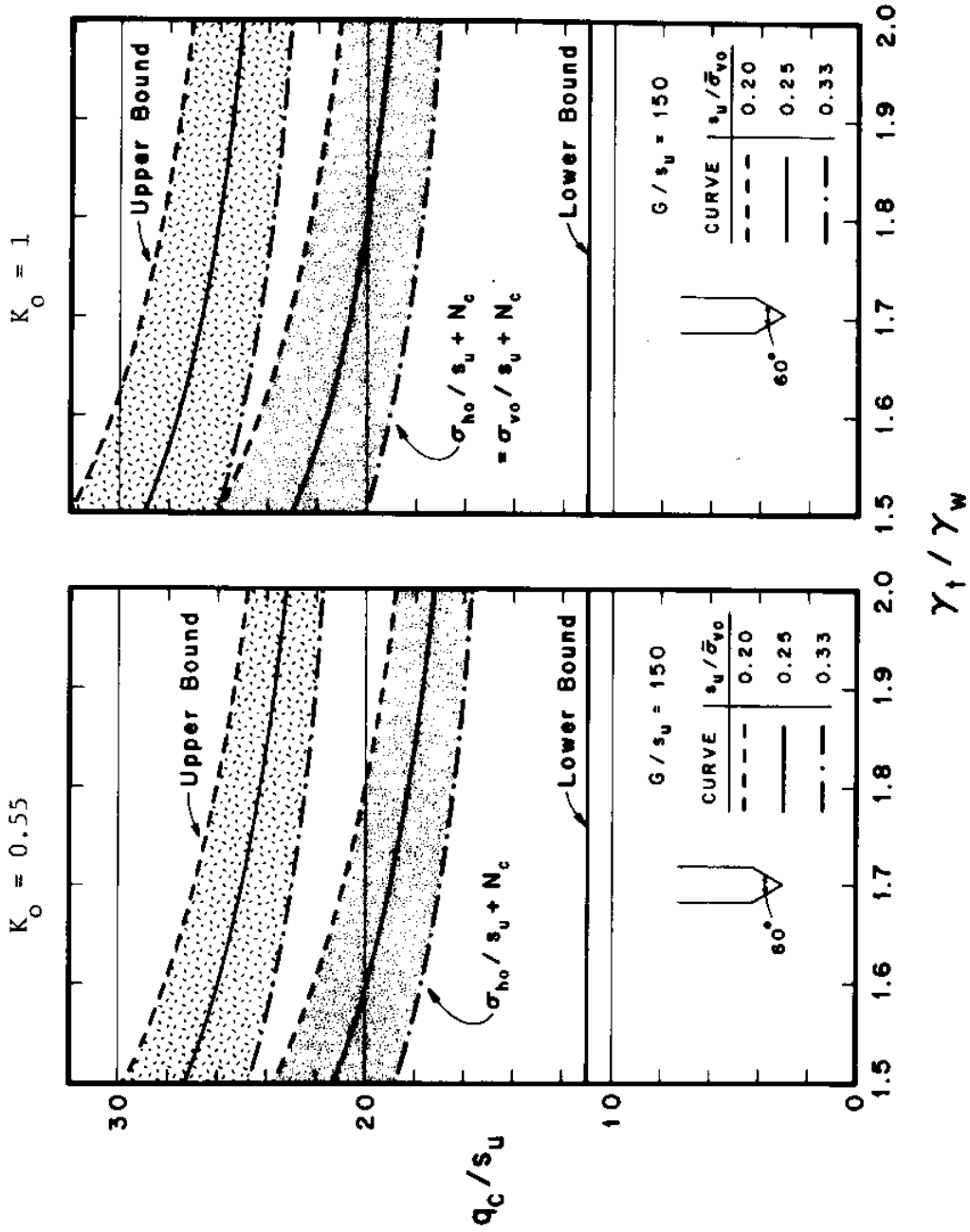
Fig. 4.3b Influences of soil parameters on predictions of cone resistance q_c (for a hydrostatic condition with ground water table at the surface, γ_t = average total unit weight of soil above level of cone penetration).

CHAPTER 5

FIELD TESTING PROGRAM

5.1 Objectives and Approaches

The primary objectives of the field testing program are to check the validity of the cone penetration theory presented in Chapter 4, provide a better understanding of the cone penetration process and hence lead to more reliable methods of interpreting cone penetration tests. The program consists of measurements of cone resistance and pore water pressures at different locations on the cone during quasi-static penetration. Factors of special interest in the experimental study are: the effects of cone angle, tip enlargement and the clay type and the repeatability of the tests and the variability of the soil.

Penetration tests were conducted in three clay deposits: Boston Blue Clay, Atchafalaya Basin Clay, and Connecticut Valley Varved Clay. These clays are post glacial clays having different depositional environments and characteristics and thus represent a wide spectrum of cohesive soils. M.I.T. studied the engineering properties of these deposits extensively in the last decade using various laboratory and field tests.

This chapter describes the equipment used in this study, the clay deposits tested, the testing program conducted at each site, and finally the similarities and differences among the deposits that may influence the cone penetration process.

5.2 Test Equipment

(1) Cone penetrometers. Most of the penetrometers and the

supporting equipment (signal recorder and pushing apparatus) used in this study are provided by Fugro, Inc. The Fugro cone, Fig. 5.1, uses electronic strain gages to measure the tip resistance and the friction on the friction sleeve. De Ruiter (1971) provides a thorough description of the apparatus. The "load cell" of this penetrometer is contained in a straight cylindrical shaft, 10 cm^2 in cross-section, behind the cone tip. The standard cone tip has the same 10 cm^2 base area (i.e., D/d = 1) and an apex angle (2δ) of 60°.

The penetrometer is pushed into the soils by a hydraulic system. During penetration, the electronic signal from the cone is transmitted to the surface by a cable strung through the pushing rods, and is recorded continuously on graph paper as a function of the penetrated depth (or time). This signal is adjusted electronically to produce a graph of cone tip resistance and sleeve friction at selected scales; the actual voltage of the signal from the load cell is not normally recorded.

In order to study the effect of cone angles (2δ) and tip enlargement (D/d), additional cone tips were constructed to test three different cone angles (2δ = 60°, 30° and 18°) and two values of D/d (= 1 and 2) using the Fugro equipment (d = 3.56 cm). Table 5.1 summarizes the size and shapes of the six different cone tips used in this study.

Very few tests were also conducted by means of a Begeman type mechanical cone provided by Fugro, Inc.

(2) The pore pressure probes. The pore pressure probe was developed at M.I.T. by Wissa et al. (1975). The original design is conical in shape (2δ = 18°) and measures pore pressure at the cone tip, Fig. 5.2a. Additional pore pressure probes were designed and constructed for this research

program following the same design concepts in order to measure the pore
pressures at the tip, along the cone face and at different locations on the
pushing rods (behind the cone) for $2\delta = 60°$ and $18°$. Figures 5.2b and c show
pictures of two of these probes, and Table 5.1 summarizes the different
probes used in this study. Each probe consists essentially of a porous stone
made of cintered steel connected hydraulically to an electro-mechanical pres-
sure transducer. The pushing and the signal-recording apparatus are simi-
lar to those used for cone resistance measurements with the exception that
the voltage output of the pressure transducer is always recorded.

5.3 Boston Blue Clay

Table 5.2 presents the sources of information on geology and
engineering properties of Boston Blue Clay on which the following summary
is based.

(1) Geology. The Boston Blue Clay was formed during the wane of the
of the late Pleistocene ice age (about 14,000 years ago) under a marine
environment in the Boston Basin, probably not very far from the ice margin.
The clay deposit overlaid a glacial till which covered the bedrock, and
had a typical thickness in excess of 50 to 125 ft depending on the topography
of the till. It included numerous lenses of fine sands, isolated sand
pockets and occasional stones or pebbles. Subsequent to clay deposition,
movements of the earth crust and of the sea level resulted in emergence
of the clay above the sea, followed by extensive weathering, desiccation,
and erosion of the upper part of the deposit. This was in turn followed by
at least two periods of submergence and deposition, of lesser significance,
in which outwash sand, and peat and silt were deposited above the clay.

(2) <u>Soil conditions at the test site</u>. The test site in Boston Blue

Clay is located in Saugus, Massachusetts, at Station 246, 160 to 200 ft offset

to the east from the centerline on the unfinished Interstate 95 embankment.

This and the adjoining section of the embankment has been studied extensively

by M.I.T. in the last 15 years; see for example, D'Appolonia et al (1971a)

on excess pore pressures during embankment construction; M.I.T. (1975)

on a planned embankment failure; Ladd et al (1979) on pressuremeter tests

and in-situ measurements of lateral earth pressures.

Figure 5.3 shows the soil conditions at the site; the clay is about

130 ft thick and underlies 20 ft of peat and sand. The top 50 ft of the clay

is heavily precompressed, probably due to desiccation, whereas the bottom

80 ft is only slightly overconsolidated. Figure 5.4 shows field vane mea-

surements at this and nearby locations; the "smoothed" and averaged profile

of four field vane tests[*] is shown in Fig. 5.5 (smoothing procedure to be

described in Chapter 6); Fig. 5.5 also shows the undrained shear strength pro-

files for different failure modes (plane strain compression, PSC, and plane

strain extension, PSE) based on the SHANSEP approach (Ladd and Foott, 1974),

computed using the stress history of the clay in Fig. 5.3 and the normalized un-

drained strength parameters determined from laboratory tests[**] (Fig. 5.6).

Table 5.3a summarizes the different penetration tests performed

at this site and Fig. 5.7 shows the layout of the test locations. The

detailed records of individual tests are given by Vivatrat, 1978.

---

[*]Two preconstruction tests and two tests relatively unaffected by
construction of the embankment fill.

[**]Selected stress-strain curves under different applied stress systems
are shown in Fig. 3.5.

5.4 EABPL Clays

Table 5.2 presents the sources of information in geology and engineering properties of the East Atchafalaya Basin Protective Levee (EABPL) Clay on which the following summary is based.

(1) Geology. The EABPL clays are backswamp deposits formed by floodwater in the Atchafalaya Basin of the Mississippi River Valley following the retreat of the last Pleistocene ice age when the sea level was considerably lower than the present level. As the sea level rose, a thick bed of sand and gravel was deposited in the valley followed by a layer of clay. The clay was deposited by floodwater in shallow ponded areas left behind natural levees, often in regular layers over an extended space. The earliest backswamp deposits in the Atchafalaya Basin were laid down about 15,000 years ago, but sedimentation continued to the present day. The thickness of the clay at the test site is over 120 ft.

(2) Soil conditions at the test site. The test site is located at station 1381 + 50 ft, 150 to 200 ft offset from the centerline to landside, along the East Atchafalaya Basin Protective Levee (EABPL),and about 35 miles south of Baton Rouge, La. Figure 5.8 presents the soil conditions at this site which indicates a zone of very high water content approximately between El.-10 and -25 ft (varying slightly among different test borings) containing peat, wood and plant roots. The bottom of this zone marks the transition of the depositional environment from one of swamp to one of shallow lake, perhaps associated with the formation of Atchafalaya River about 500 to 1000 years ago. For this research program, attention is concentrated on the lower, more uniform clay. Figure 5.9 shows the field vane strength which varies between 0.2 and 0.8 kg/cm^2 (TSF), and tends generally to increase with depth, but with a significant scatter. Figure 5.10 pre-

sents the profile of s_u(DSS) according to the SHANSEP approach together with the "smoothed" average of the field vane strength (smoothing procedure to be described in Chapter 6); the SHANSEP strength is computed based on the stress history of the clay in Fig. 5.8, and the normalized undrained strength parameters shown in Fig. 5.11. Because of the relatively isotropic behavior of this clay, s_u(DSS) approximately applies for all modes of failure and should govern the cone penetration resistance, if strain rate effects are neglected.[*] Between the depths of 40 and 120 ft, s_u(DSS) is approximately 20 to 40% smaller than s_u (field vane).

Table 5.3b summarizes the different penetration tests performed at this site, and Fig. 5.12 shows the layout of the test locations. The records of individual tests are presented by Vivatrat, 1978.

5.5 The Connecticut Valley Varved Clay

Table 5.2 presents the sources of information on the geology and engineering properties of this clay deposit on which the following summary is based.

(1) Geology. The Connecticut Valley Varved Clay (CVVC) is a glacial lake deposit formed during the retreat of the late-Pleistocene ice sheet from New England, approximately between 10,700 to 13,000 years ago. The soil contains alternate layers of different composition (high and low clay contents) as a result of the annual depositional sequences, and overlays a till layer which has a widely variable character ranging from fine silt to coarse gravel. The varved clay deposits had an original thickness consid-

---

[*]The effect of strain rate is important in this plastic clay and such an assumption is not justified.

erably in excess of 100 ft, but, in some locations, were extensively eroded

after the glacial lake drained (about 10,700 years ago). Present extent

of CVVC consists of a band, five to ten miles wide, along most of the

Connecticut River in Western Massachusetts, with a thickness ranging from

50 to over 150 ft. The surface is generally covered with a layer of sand,

typically 10 to 20 ft thick. The upper portion of the clays may also

have been desiccated.

(2) Soil conditions at the test site. The test site is adjacent to

the University of Massachusetts. campus in Amherst, Massachusetts, about two

miles east of the Connecticut River. The soil conditions at this site are pre-

sented in Fig. 5.13. The clay is highly precompressed above a depth of 35

ft, probably due to desiccation. Below this depth, the degree of precom-

pression is moderate, being about 0.6 kg/cm^2 (this could be caused by a

net erosion of 35 ft of overburden). The (Geonor) field vane strength,

Fig. 5.14, below the desiccated crust is almost constant at about

0.40 ± 0.50 kg/cm^2 with a sensitivity of 5 to 7. Figure 5.14 also shows the

SHANSEP strength profiles for the plane strain compression (PSC) and the

direct simple shear (DSS) modes of failure computed from the stress history of

the clay (Fig. 5.13) and the normalized undrained strength parameters shown

in Fig. 5.15. The plane strain extension strength, s_u(PSE), not shown here,

is only about 10% lower than s_u(PSC) for this varved material.

Table 5.3c summarizes the different penetration tests performed

at this site; the records of individual tests are presented by Vivatrat, 1978.

5.6 Comparison Between the Three Clay Deposits Tested

This section compares some important soil properties affecting cone

penetration in the three clays tested, namely: the strength of the clay

(including strength anisotropy), its stiffness, and the in situ state of stress.

The BBC and the CVVC deposits show similar patterns of overconsolidation, Figs. 5.16a and c. Both deposits have a heavily overconsolidated crust followed by a slightly overconsolidated (OCR $\leq$ 1.5) layer. The field vane strength is relatively uniform in both deposits (0.45 ± 0.1 kg/cm^2 in BBC, and 0.40 ± 0.05 kg/cm^2 in CVVC, Figs. 5.5 and 5.14, respectively).

The Atchafalaya Basin Clay (EABPL) exhibits a more complex stress history than the other two sites, with alternate zones of overconsolidated and normally consolidated clays. The field vane strength exhibits a larger scatter and a general increasing trend with depth (from about 0.2 to 0.7 kg/cm^2). The larger scatter is perhaps due to the more variable depositional conditions in a backswamp environment than in a lacustrine or marine environment. In addition, while the undrained shear strength of EABPL clay varies little with the mode of failure (e.g., vertical vs. inclined loading), the BBC and the CVVC possess pronounced strength anistropy as shown by the strength profiles in Figs. 5.5 and 5.14.

The effect of in-situ stresses on cone resistance can be described by the ratio of the initial vertical total stress, σ_{vo}, to the undrained shear strength, s_u, of the clay. Figure 5.16a, b, and c show the ratio σ_{vo}/s_u (field vane) for the three deposits tested. Clearly, this ratio decreases as OCR increases. In the slightly overconsolidated regions, σ_{vo}/s_u (field vane) varies between 7 and 12 in all three deposits, whereas it is less than 5 in the heavily overconsolidated regions.

The stiffness of clays as expressed by Young's modulus, E, or the shear modulus, G, is difficult to define and measure because of the non-linear stress-strain of behavior of clays, their anisotropic response, and

the effect of strain rate. Figure 5.17 shows the ratio E/s_u measured in K_o-consolidated undrained direct simple shear (DSS) tests for an applied shear stress (τ_h) equal to $1/3\ s_u$. For EABPL clay, the ratio E/s_u is only 200-250 at all OCR's, for normally consolidated and slightly overconsolidated BBC and CVVC, $E/s_u = 800 \pm 100$ and decreases significantly with increasing OCR. From Fig. 5.17 and the SHANSEP DSS strength profiles (Figs. 5.5, 5.10), Young's modulus E is estimated for the three clay deposits in a DSS mode of deformation when $\tau_h = 1/3\ s_u$ as shown in Figs. 5.18a to c. In all three deposits, E generally increases with depth. The EABPL clay has the lowest value of E, only about $100 \pm 50\ kg/cm^2$, whereas E in the BBC and CVVC deposits is generally 4 and 2 times higher, respectively.

	D/d	Cone Angle 2 δ	Remarks
Electrical Cone	1.0	60° 30° 18°	Fugro Apparatus with specially made tips; d = 3.56 cm
	2.0	60° 30° 18°	
Mechanical Cone	not applicable	60°	Begeman type (with friction mantle)
Pore Pressure Probe (porous stone at tip)	1.0	60° 18°	Wissa et al (1975)'s design, d = 3.81 cm
	1.9	18°	
Pore Pressure Probe (porous stone on cone face)	1.0	18°	Stone at mid-cone
	1.9	18°	Stone at ¼ x cone from tip
Pore Pressure Probe (porous stone behind cone)	1.0	60° 18°	Distance between porous stone and tip can be varied
	1.9	60° 18°	

Table 5.1   Summary of equipment characteristics

Type of Information \ Type of Deposit	Boston Blue Clay	EABPL Clay	Connecticut Valley Varved Clay
Type of Deposit	Marine illitic CL clay, medium sensitivity	Highly plastic deltaic clay, low sensitivity	Glacial lake clay, varved, medium sensitivity
Geology	Kenney (1964) Aldrich (1970)	Fisk et al (1952) Kolb and Shockley (1959) Krinitzsky and Smith (1969) Foott and Ladd (1973)	Ladd and Wissa (1970)
Engineering Properties (strength)	Ladd and Varallyay (1965) Kinner and Ladd (1973) Ladd et al. (1971a) Ladd and Edgers (1972)	Ladd and Edgers (1972) Ladd et al (1972) Fuleihan and Ladd (1976)	Ladd and Edgers (1972) Lacasse et al(1972) Ladd (1975) Sambhandharaska (1977)
Field Tests or Instrumentation	D'Appolonia et al. (1971a) Lambe et al (1972) Marr (1974) M.I.T. (1975)	Kaufman and Weaver (1967) USCE (1968) Foott and Ladd (1973)	Connell et al (1973)

Table 5.2 Sources of information on clay deposits tested

I 95 Embank-ment St 246 200 ft East	Test No.	Cone Angle 2δ	Diameter Ratio D/d	Rate Effect	Remarks
	1	60°	1	---	(St 263, 160 ft West)
	2	60°	1	---	(St 263, 160 ft West)
Cone	3	60°	1	---	
	4	60°	1	---	
(11 tests)	6	30°	1	---	
	7	18°	1	---	
	9	60°	2	yes	
	10	60°	1	yes	
	11	30°	2	yes	
	12	18°	2	yes	
	13	60°	N.A.	---	Begemann Mechanical Cone
	5	18°	1	---	stone at tip
	8	60°	1	---	stone at tip (Feb.'77)
Pore Pressure Probe	21*	18°	1	---	stone at tip
	22*	18°	1	---	stone at mid-cone
	23*	18°	1	---	stone just behind cone
	24*	18°	1	---	stone 3.2 d behind cone
(15 tests)	25*	18°	1	---	stone 4.7 d behind cone
	26*	18°	1	---	stone at mid-cone (St 263, 160 ft West) (June, '77)
	31*	18°	1	yes	stone 11 d behind cone
	32*	18°	1.9	yes	stone 11 d behind cone
	33*	18°	1.9	yes	stone 1.6 d behind cone
	34*	18°	1.9	yes	stone at tip
	35*	60°	1.9	yes	stone 0.84 d behind cone
	36*	60°	1	yes	stone 3.2 d behind cone
	37*	60°	1.9	yes	stone just behind cone (July, '77)

Note: *Pushed through predrilled hole filled with water

Table 5.3a   Penetration test programs at Saugus, MA

EABPL St 1381 +50 180 ft Landside	Test No.	Cone Angle 2 δ	Diameter Ratio, D/d	Rate Effect	R e m a r k s
.	1	60	1	--	---
	2	60	1	--	zero shift
	3	18	1	--	zero shift
	4	18	2	yes	---
	5	60	2	yes	---
Cone	7	30	2	yes	---
	8	60	1	yes	---
	10	30	1	yes	---
(13 tests)	12	18	1	--	---
	13	60	1	yes	---
	17*	18	2	--	wet hole
	18*	60	2	--	wet hole
	21	6C	1	--	ST 1385 + 50
Pore Pressure Probe	6	60	1	yes	stone at tip
	9	18	1.9	yes	stone close to tip
	11	18	1	yes	stone at mid cone
	14	18°	1	yes	stone lid behind cone
(8 tests)	15	60°	1.9	--	stone 1.6 d behind cone
	22	60°	1.9	--	stone 1.6 d behind cone
St 1385 +50	23	18°	1	--	stone at tip
	24	18°	1.9	--	stone 1.6 d behind cone

Note: There are 4 additional standard cone tests conducted by Fugro Gulf, Inc.
in 1976 in the same general area.

* Push through predrilled hole fill with water

Table 5.3b   Penetration test program at EABPL, LA, January, 1978

AMHERST, MA	Test No.	Cone Angle 2δ	Diameter Ratio, D/d	Rate Effect	Remarks
Cone (6 tests)	1	60°	1	--	performed at 200 ft
	2	60°	1	--	from main test site
	3	60°	1	yes	--
	4	30°	1	yes	--
	7	18°	2	yes	zero shift
	8	18°	1	--	--
Pore Pressure Probe (2 tests)	5	18°	1		stone at tip
	6	60°	1		stone at tip

Table 5.3c   Penetration test program at Amherst, Massachusetts, 1977.

cable

connection with rods

waterproof bushing

adjustment ring

strain gage
load cells

friction mantle

strain gage

load cells

conical tip (10 cm^2)

←—36 mm—→
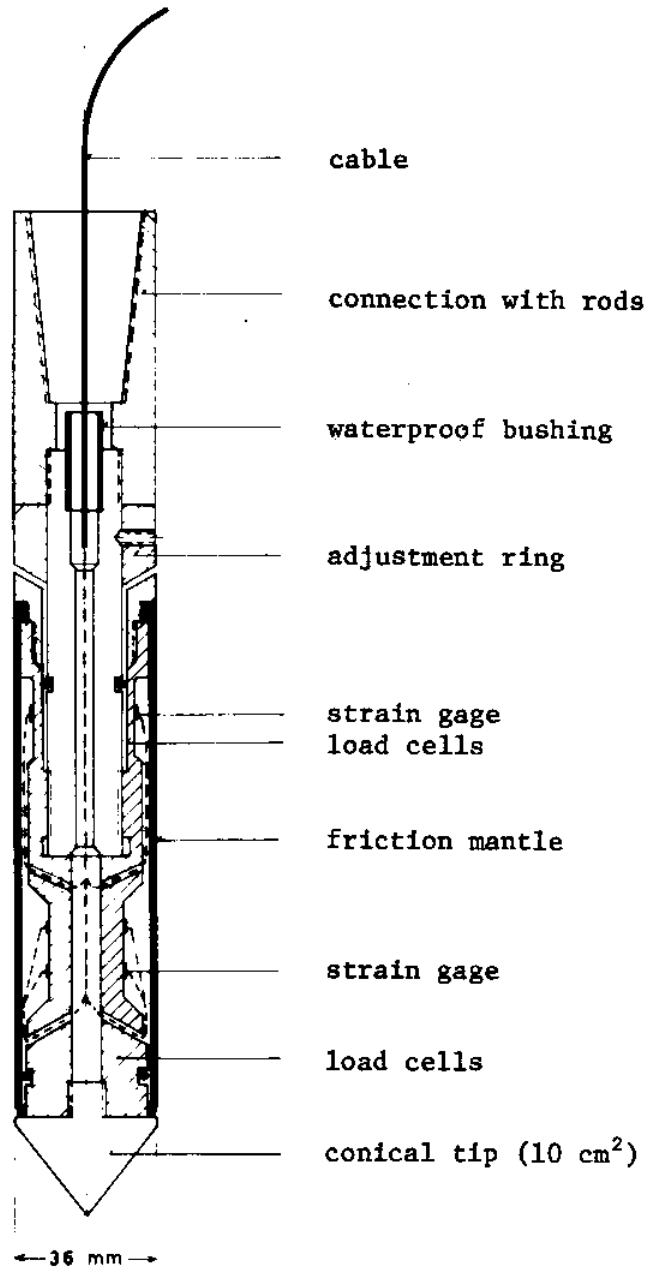
Fig. 5.1 Diagram of the Fugro electrical cone with
friction sleeve (from Sanglerat (1972))

SQUARE
A-ROD THREAD

WELD

PROTECTIVE TUBING

TUBE NUT

TRANSDUCER
ELECTRICAL
CABLE &
CONNECTOR

HOUSING

PRESSURE
TRANSDUCER

TRANSDUCER
LOCKNUT

TRANSDUCER O-RING

HOUSING
O-RING

CONE

O-RING
TIP BOLT

STAINLESS STEEL
POROUS TIP
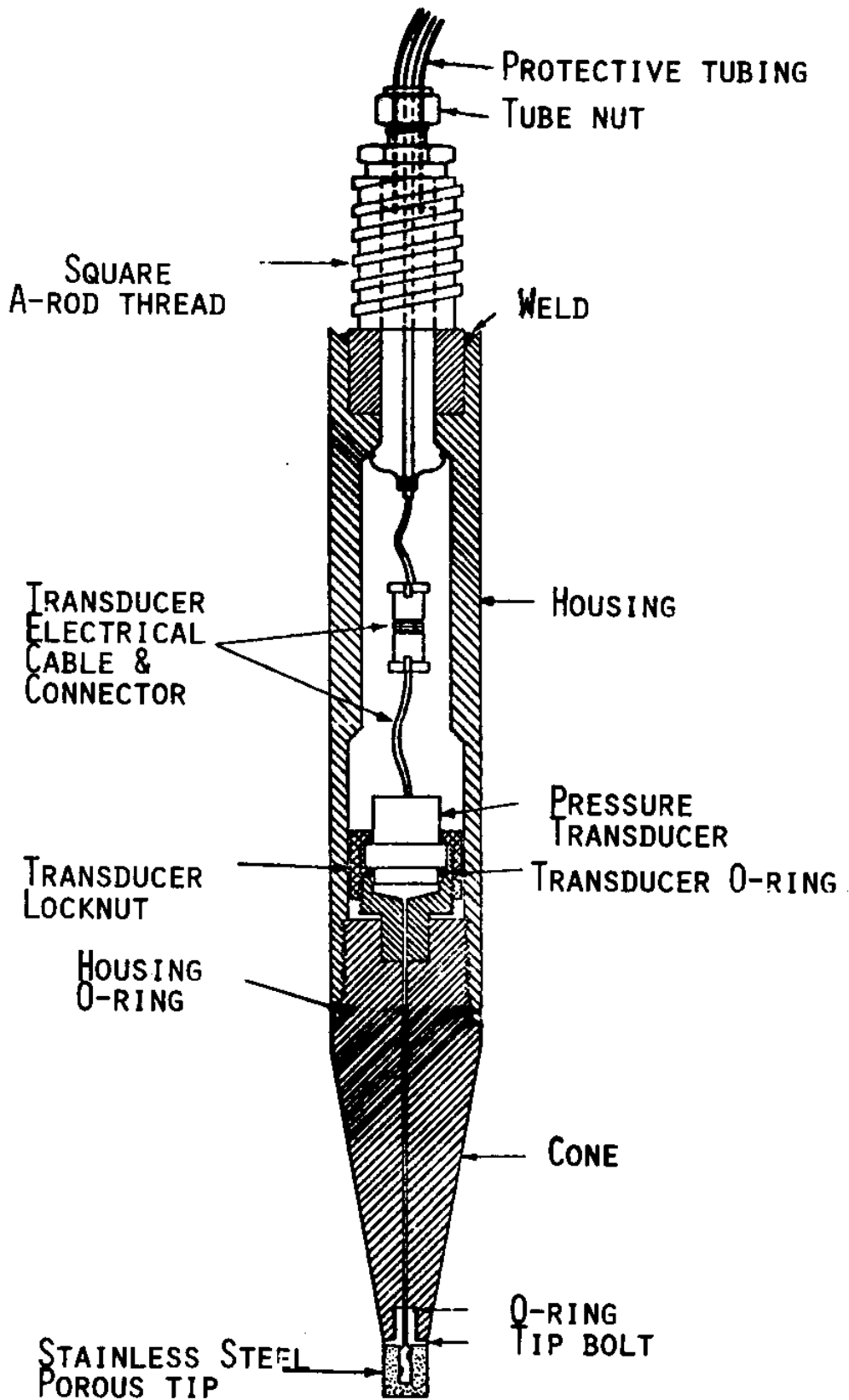
(a) Diagram of original design
(Wissa et al., 1975))

Fig. 5.2   The pore pressure probe
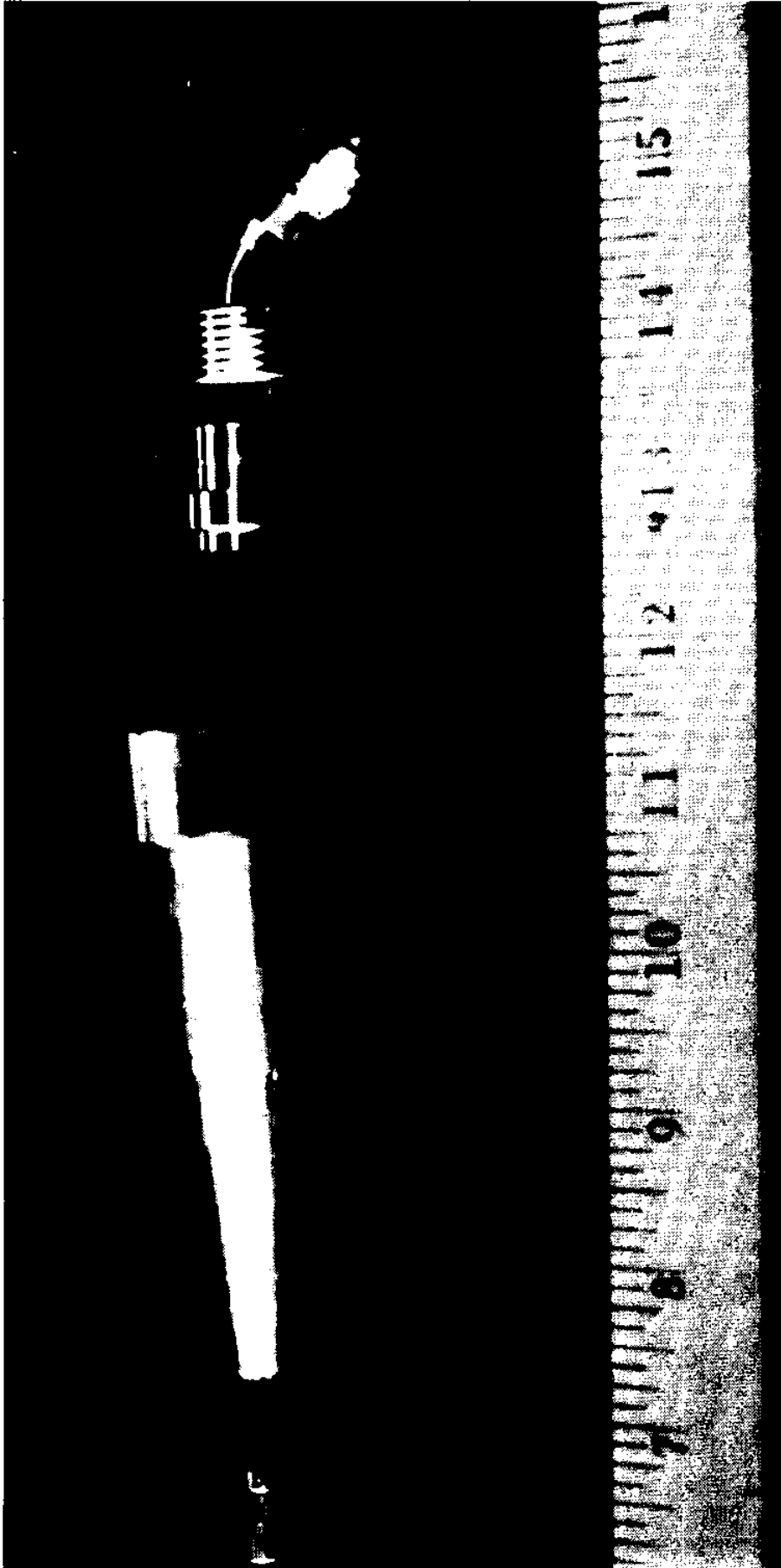
(b) 18° pore pressure probe with porous stone at tip.

Fig. 5.2   The pore pressure probe.
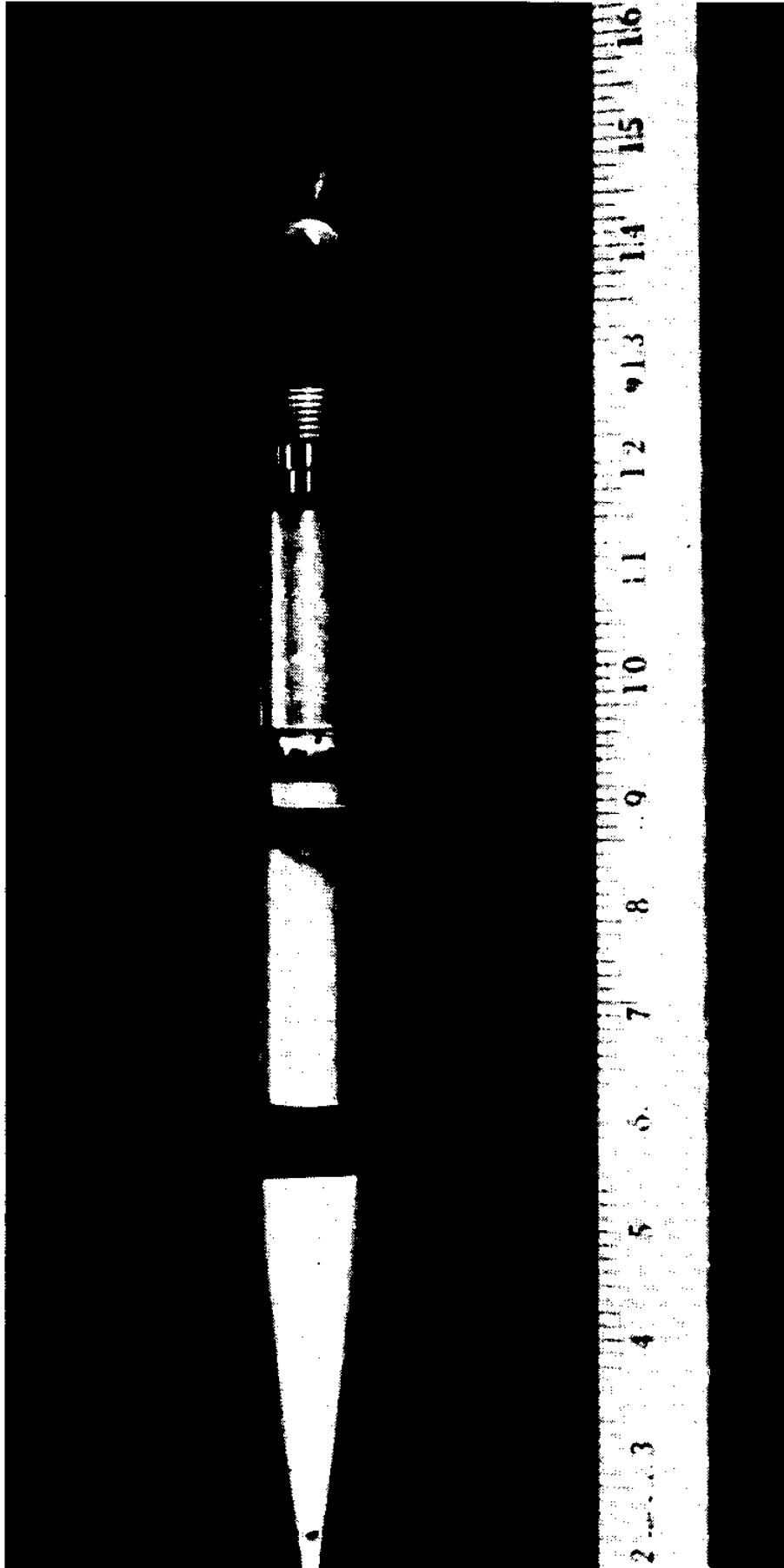
(c) Pore pressure probe with porous stone behind the conical tip.

Fig. 5.2   The pore pressure probe.
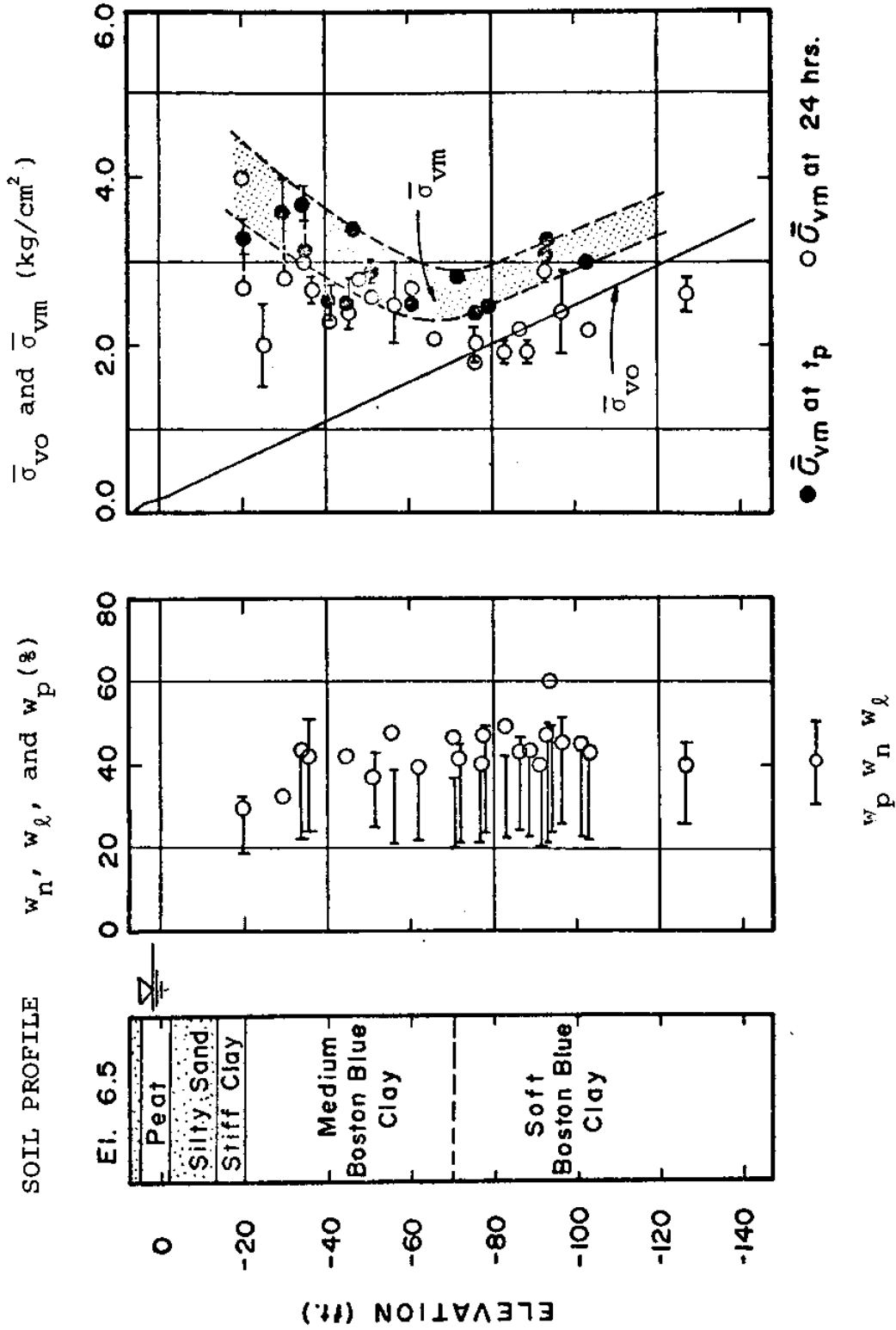
Fig. 5.3 Soil conditions at the Saugus, MA, test site (I95 embankment St. 246, 200 ft offset from centerline to the east; data from unpublished MIT reports; drawing courtesy of S. M. Lacasse).
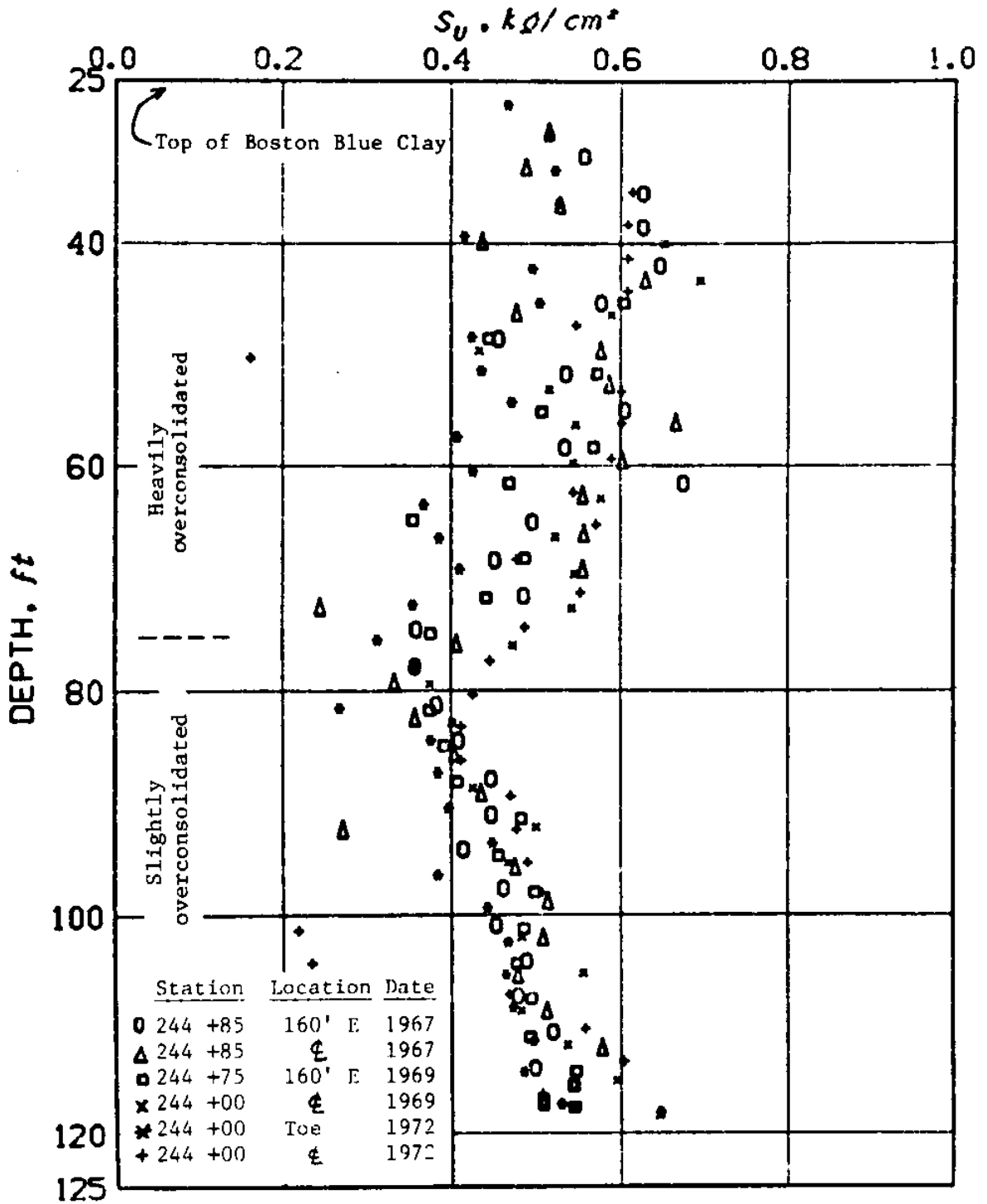
Fig. 5.4 Field vane test results at the Saugus, MA, test site (ground surface at El. 5 to 6 ft).
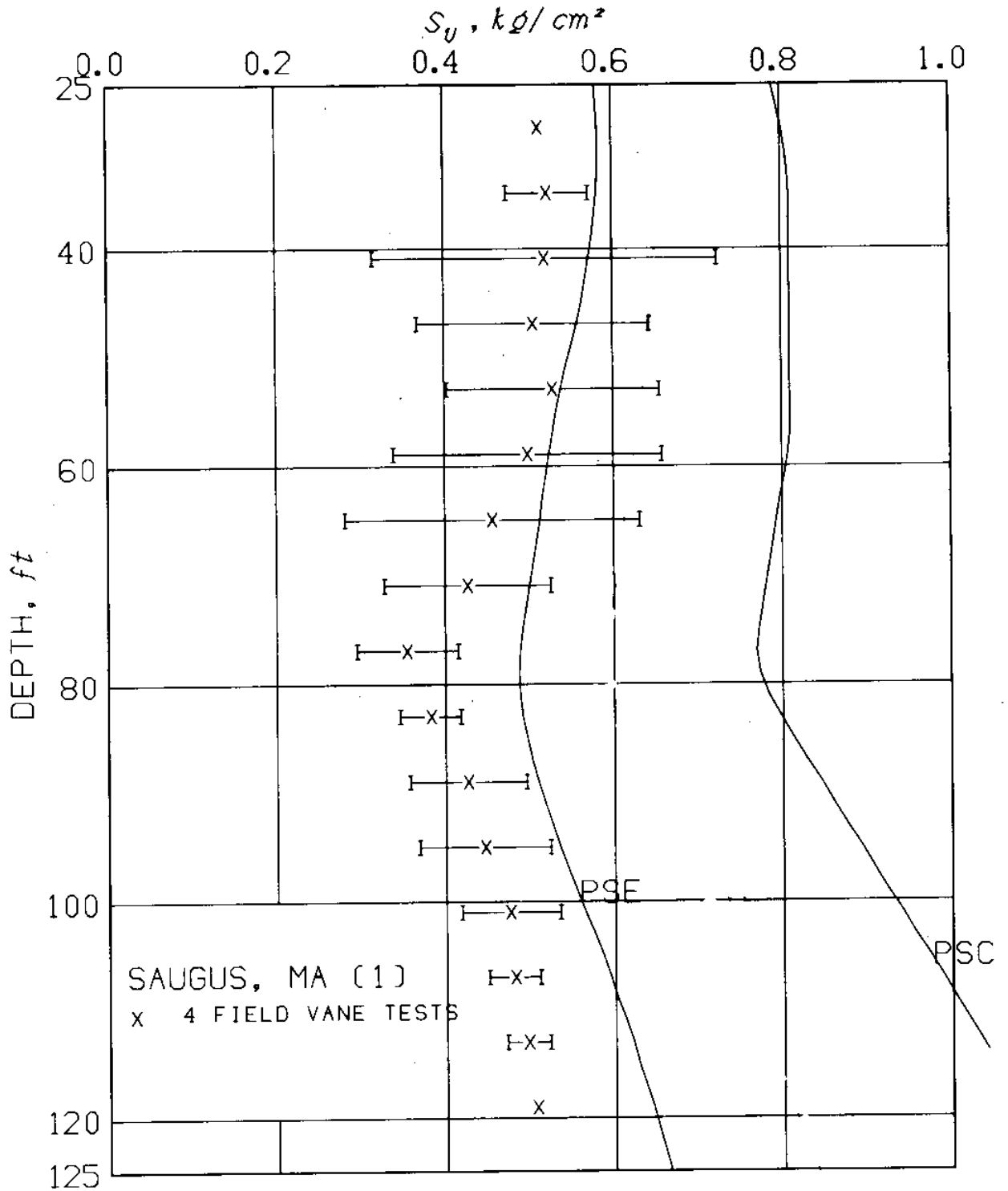
Fig. 5.5 SHANSEP and average field vane strength profiles at the
Saugus, MA, test site. (FV tests exclude tests at
centerline conducted in 1969 and 1972).
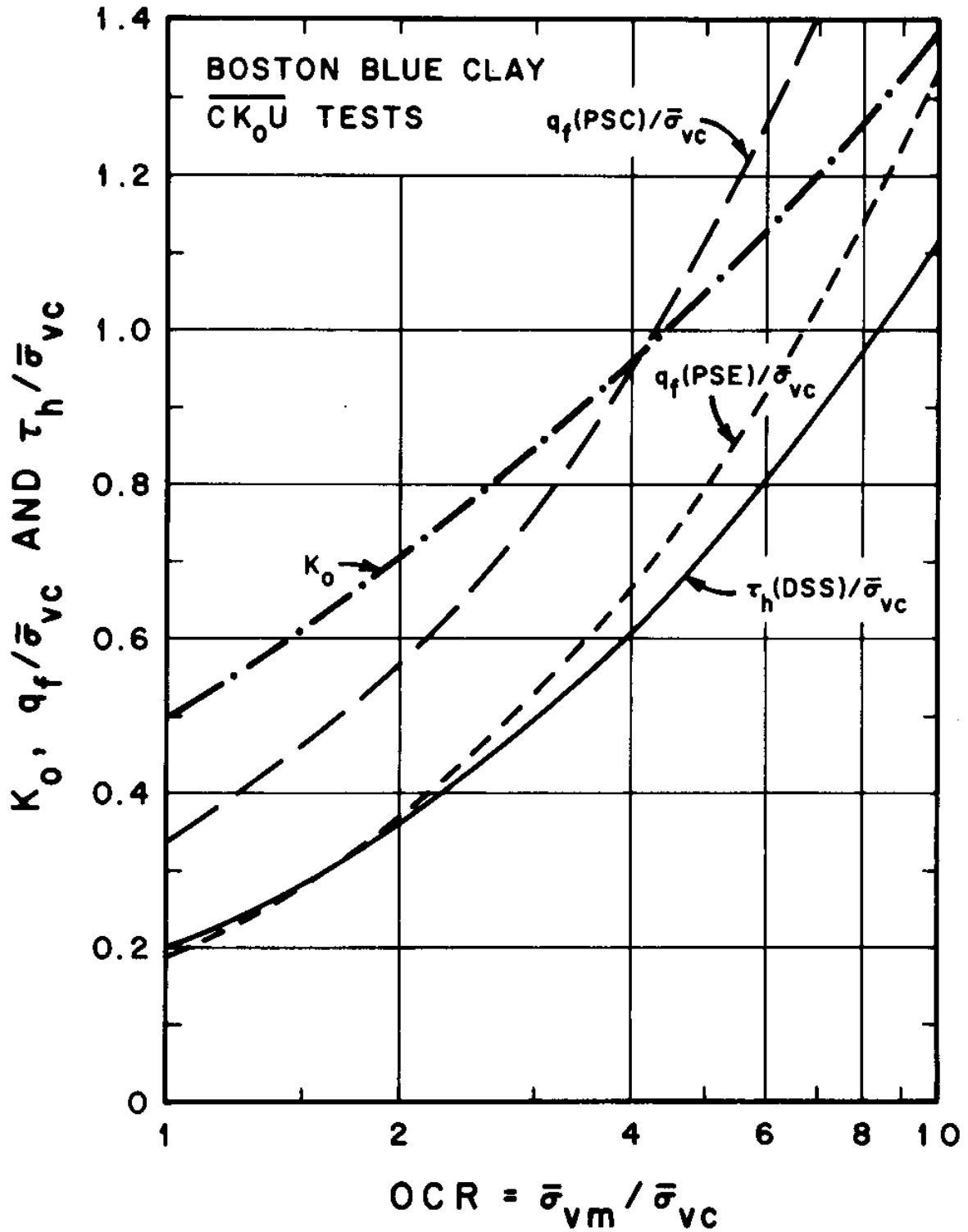
Fig. 5.6 SHANSEP undrained strength parameters and K_o for Boston Blue Clay.
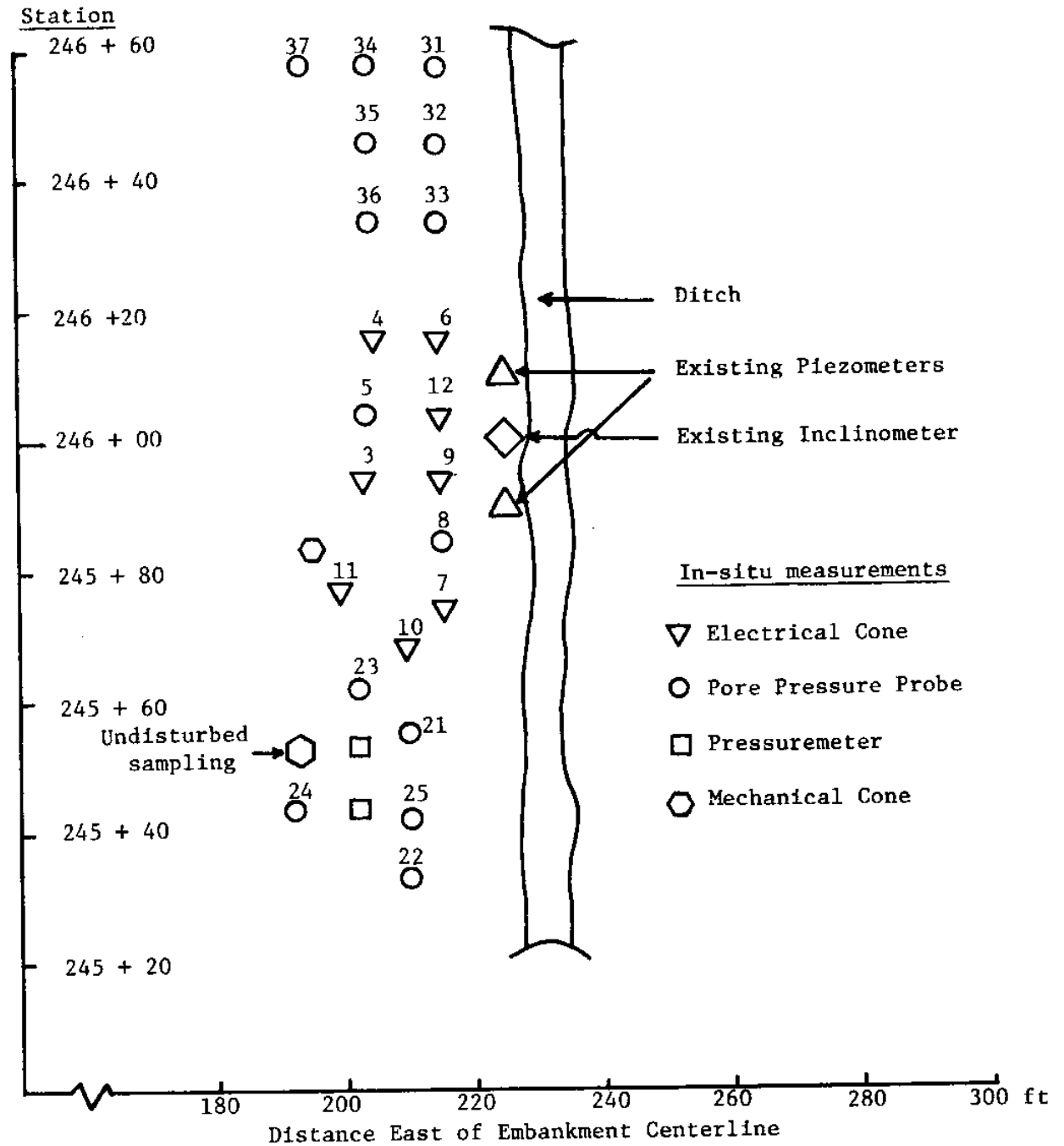
Fig. 5.7 Layout of penetration tests at the Saugus, MA, test site.
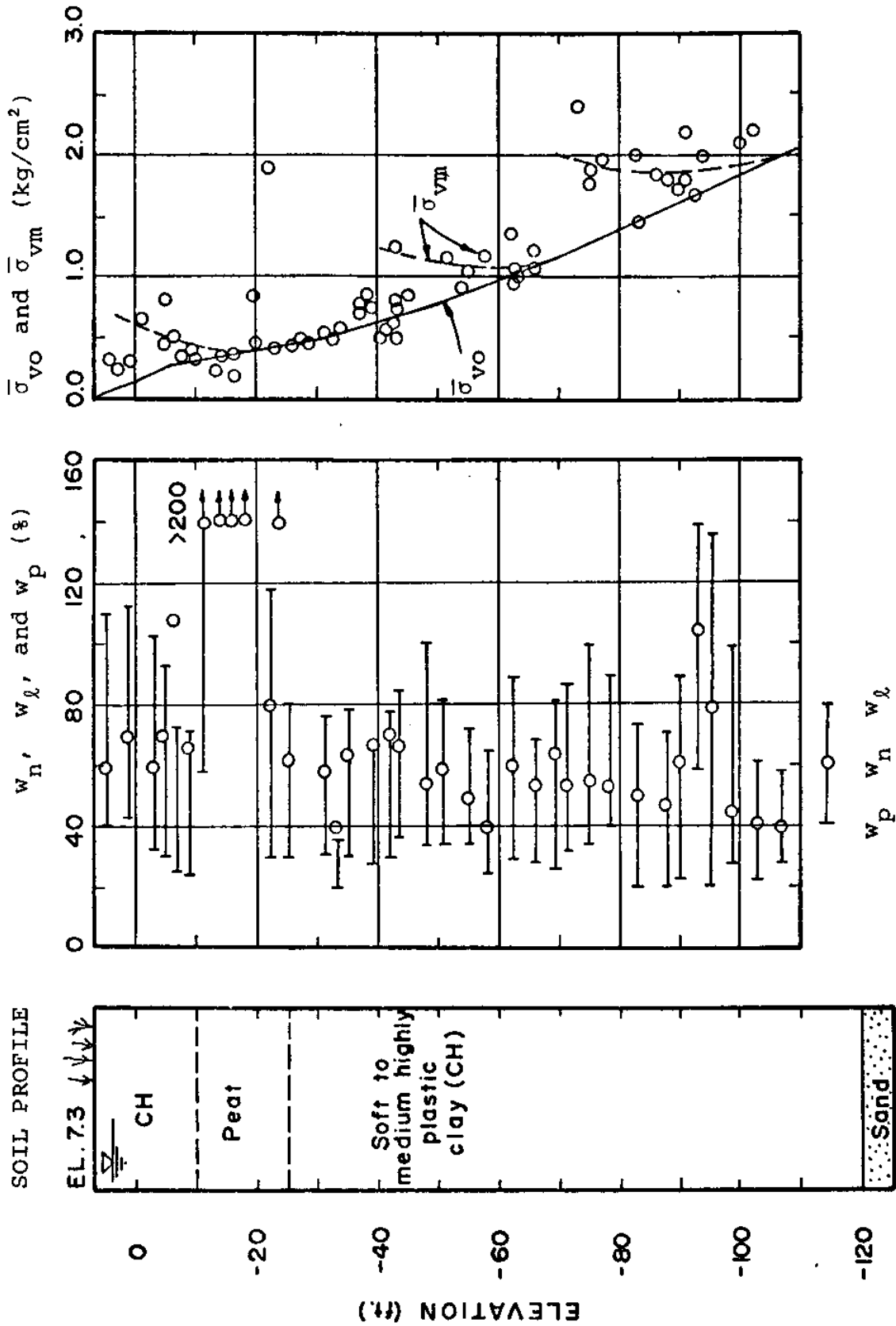
Fig. 5.8 Soil conditions at the East Atchafalaya Basin Protective Levee, LA, test site (Test section 2, 105 to 200 ft offset from centerline to land side; data from Foott and Ladd (1973), drawing courtesy of S. M. Lacasse).
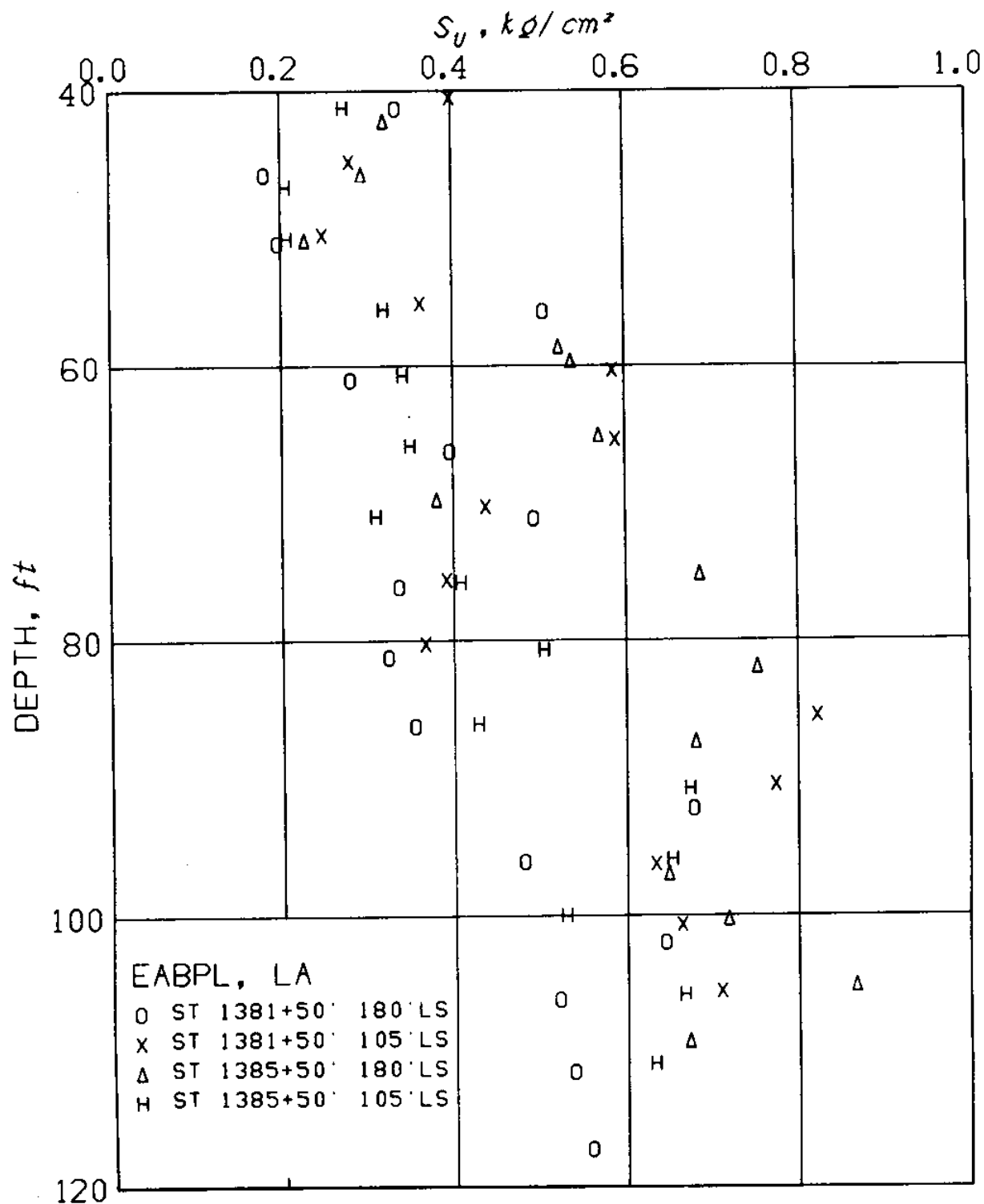
Fig. 5.9   Field vane strength measurements at the EABPL, La, test site
(data from USCE, 1968).
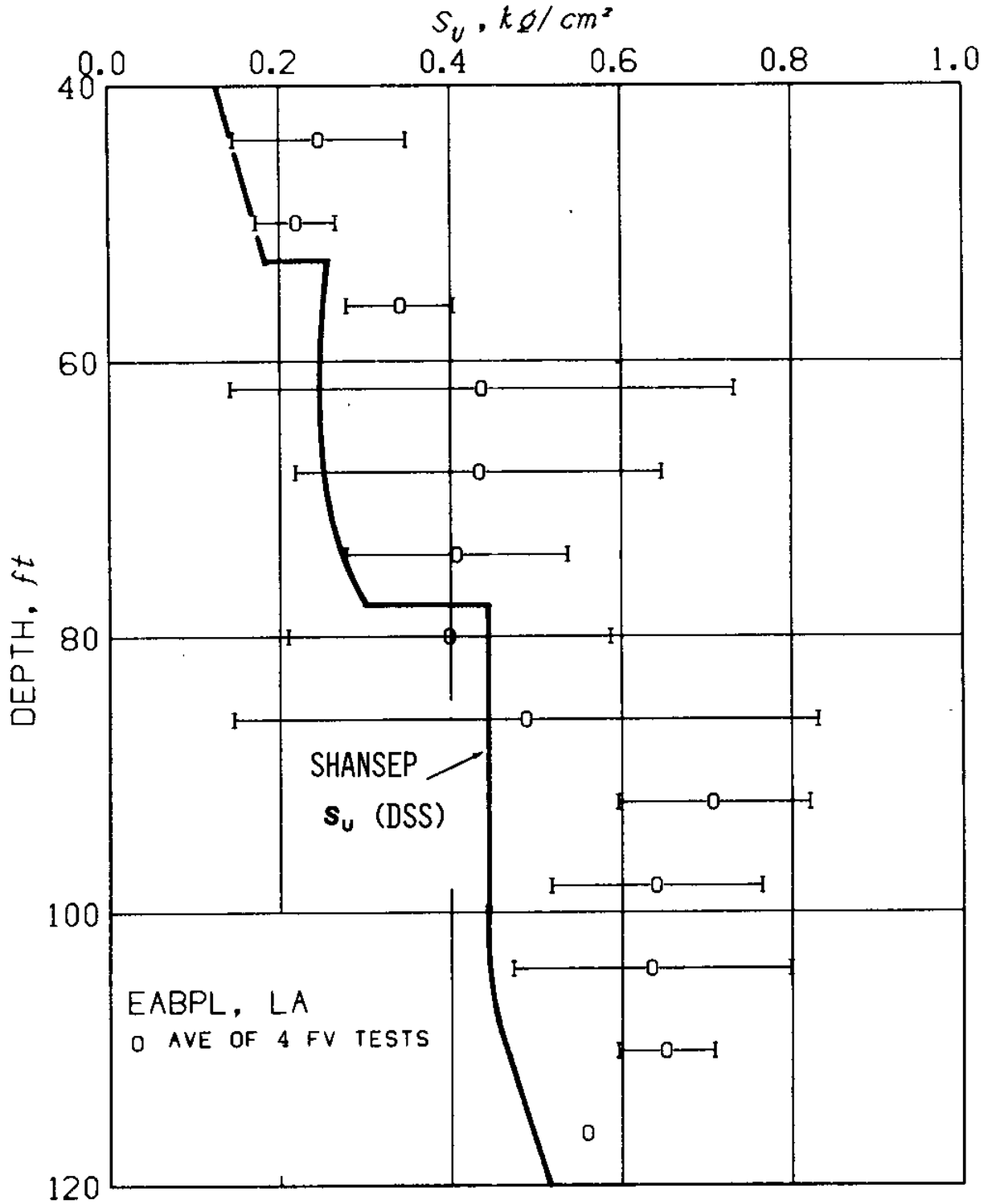
Fig. 5.10   SHANSEP and field vane strength profiles at the
EABPL, LA, test site (EABPL Clays).
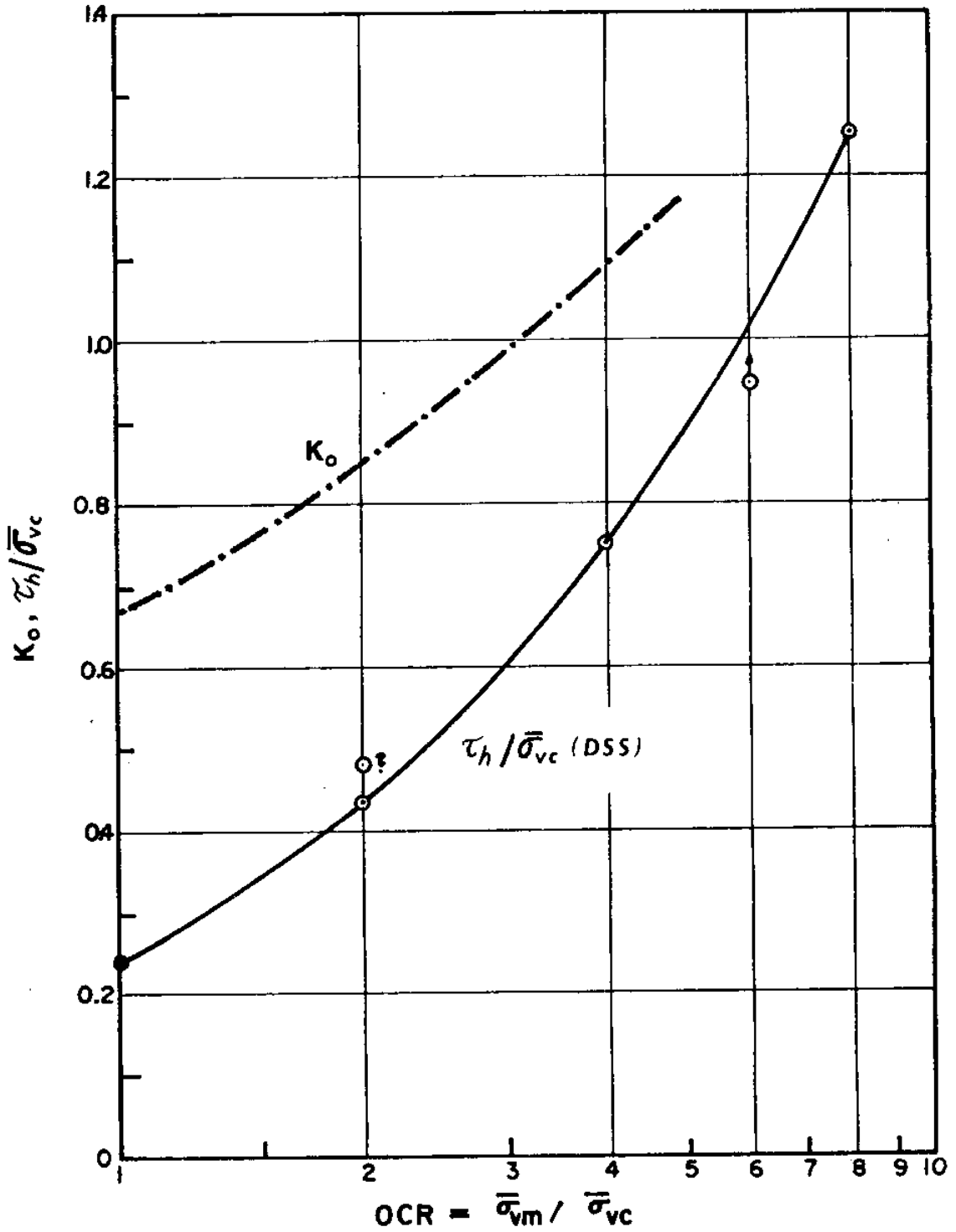
Fig. 5.11 SHANSEP undrained strength parameters and K_o for EABPL Clays (data from Ladd et al, 1972).
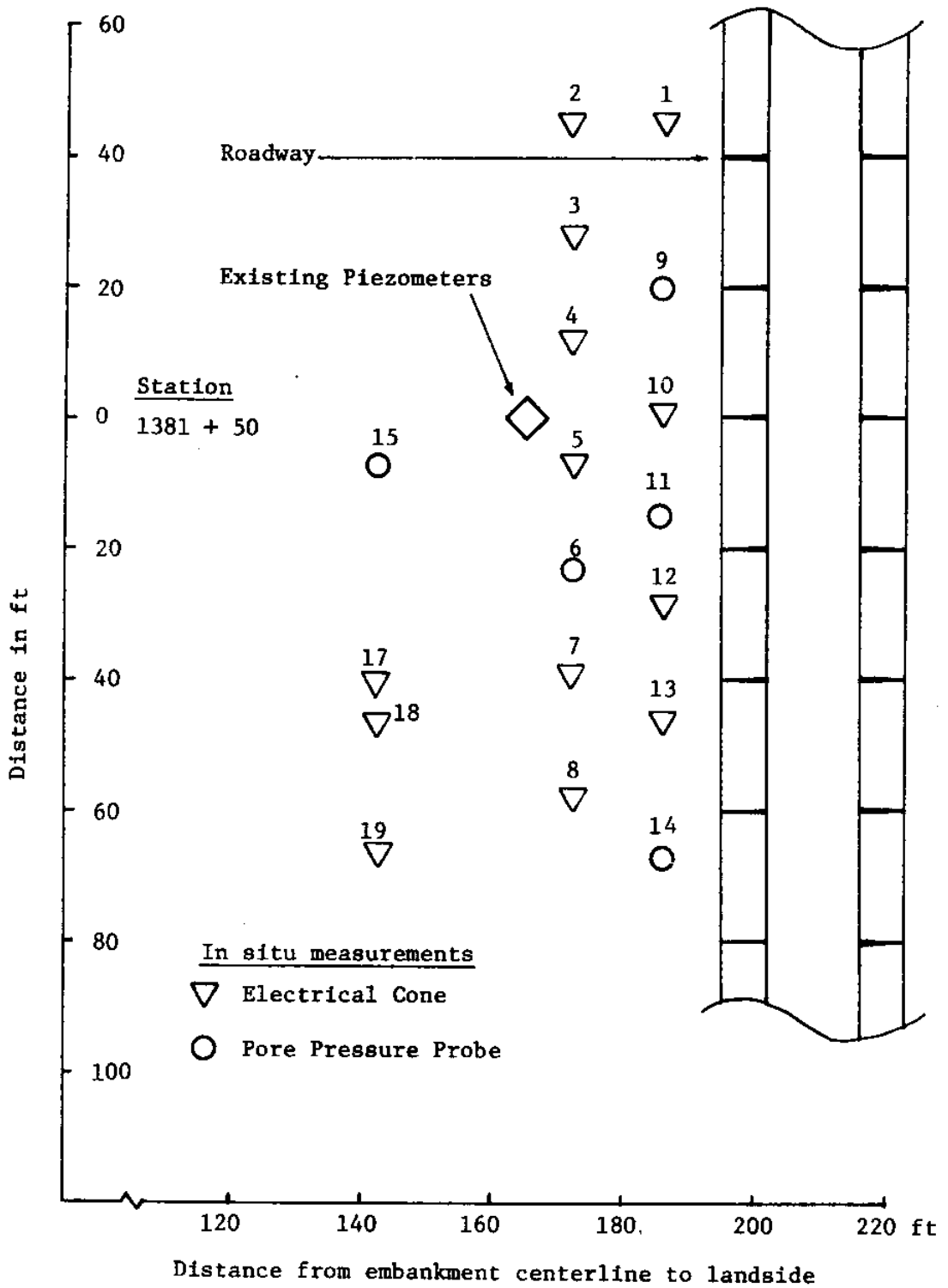
Fig. 5.12 Layout of penetration tests at the EABPL, LA, test site
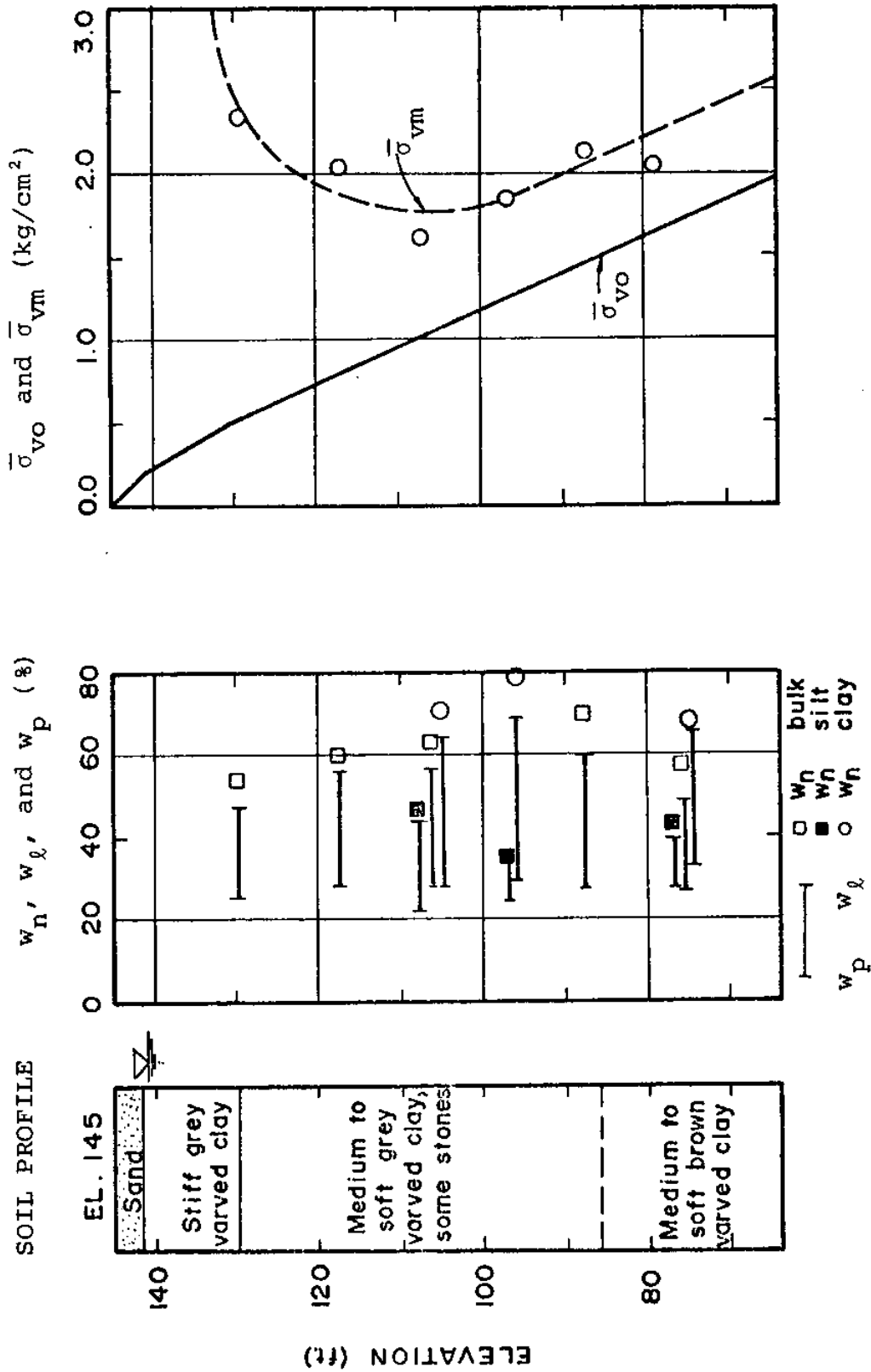
Fig. 5.13 Soil conditions at the Amherst, MA, test site. (Route 116 Bypass and North Hadley Road; data from Ladd (1975); drawing courtesy of S. M. Lacasse)
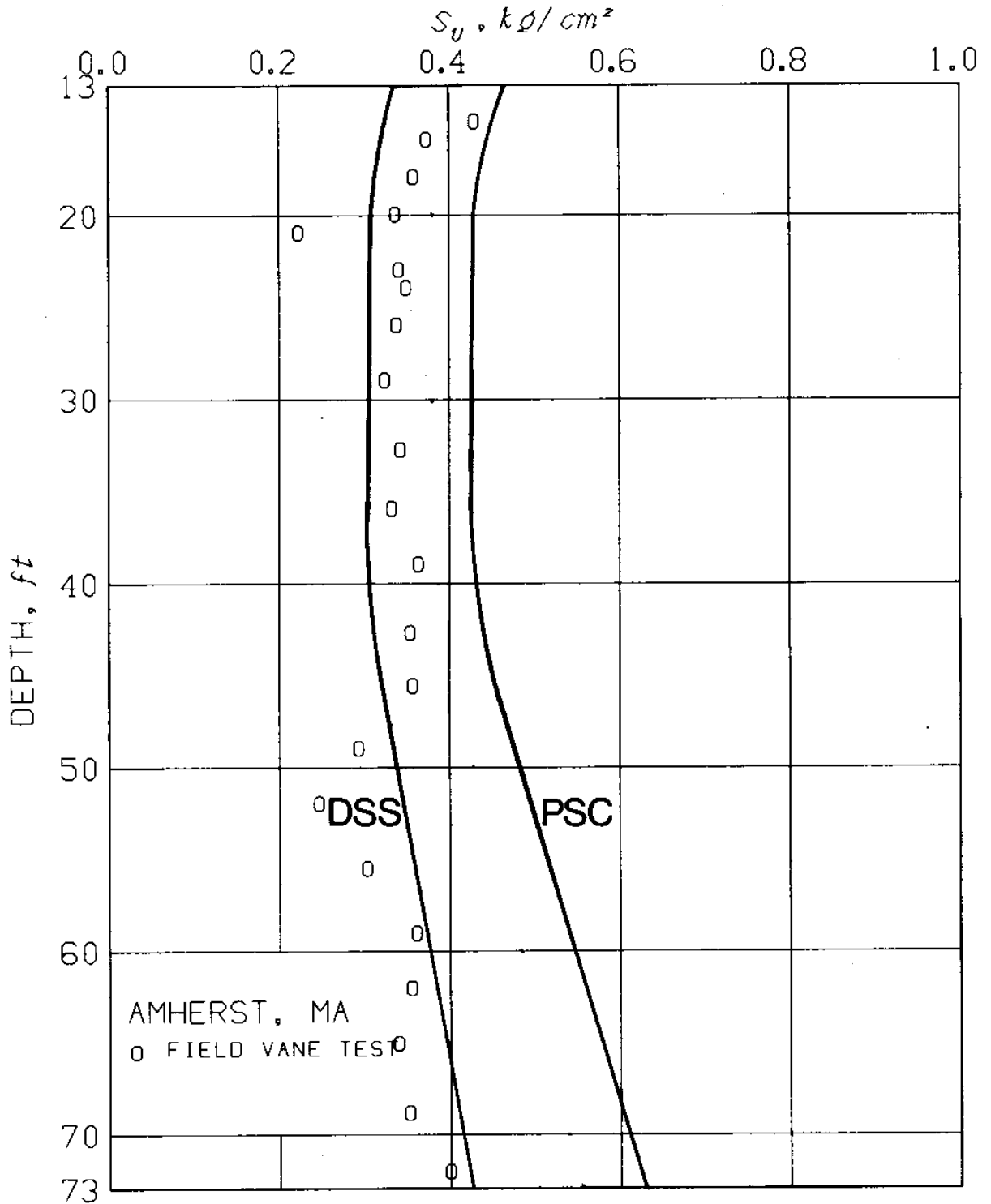
Fig. 5.14 SHANSEP and field vane strength profiles for the
Amherst, MA, test site (data from Ladd, 1975).

UNDRAINED STRENGTH RATIO $q_f/\bar{\sigma}_{vc}$ and $\tau_h/\bar{\sigma}_{vc}$

OCR = $\bar{\sigma}_{vm}/\bar{\sigma}_{vc}$

(1) All tests by MIT

(2) Average values plotted at OCR=1

TC

TE

DSS

All DSS Tests

	TC	DSS	TE	LOCATION
	◯	⊗	●	Amherst, MA.
	⬡	⊗		North ampton, MA.
	▢	⊠	■	E. Windsor, CONN.
	△	▲		Secaucus, N.J.
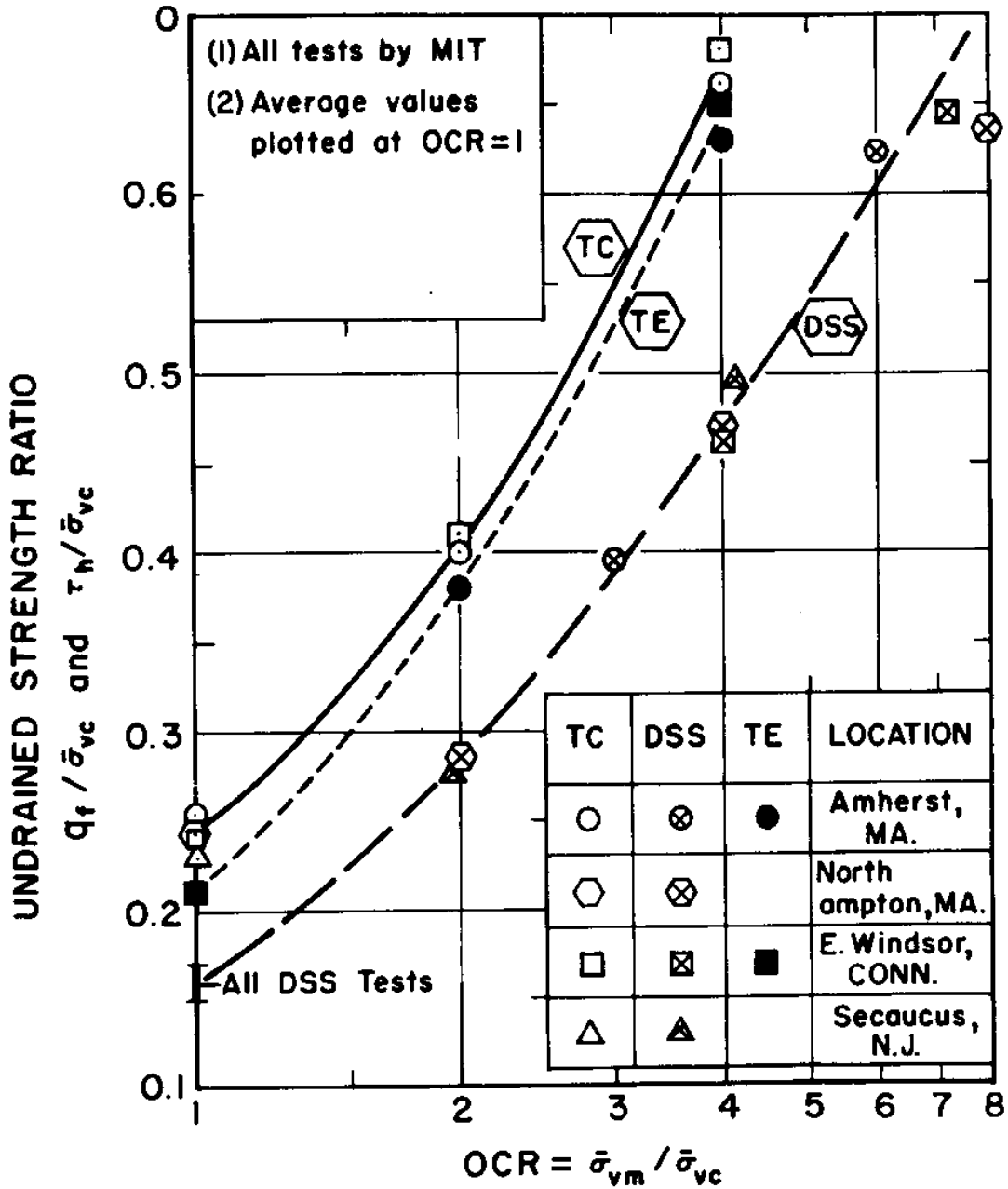
(a)   Undrained strength parameters

Fig. 5.15   SHANSEP undrained strength parameters and K_0 for Connecticut Valley Varved Clays (from Ladd and Foott, 1977).
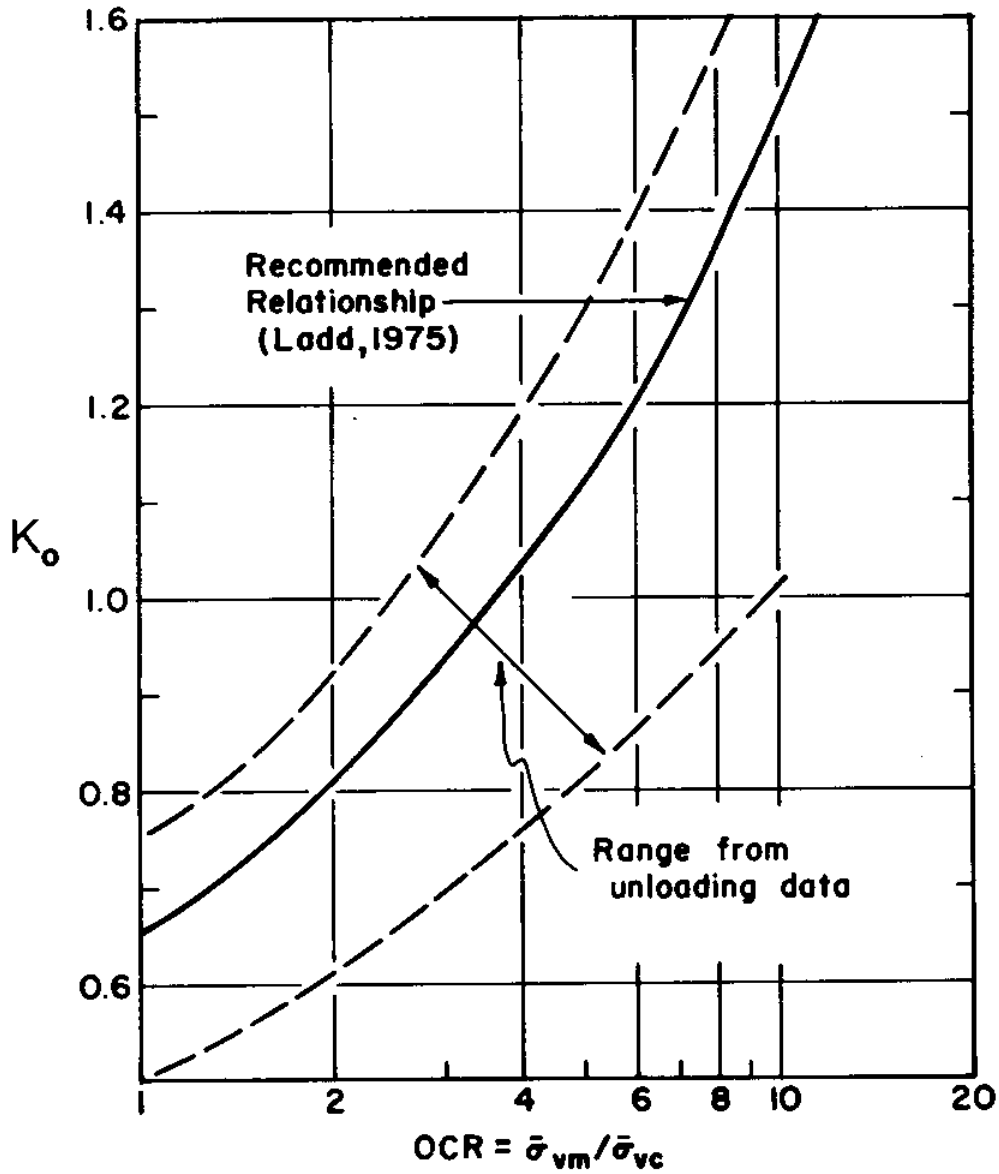
(b) Coefficient of earth pressure at rest, K_o

Fig. 5.15   SHANSEP undrained strength parameters and K_o for
con't   Connecticut Valley Varved Clay (from
          Ladd and Foott, 1977)
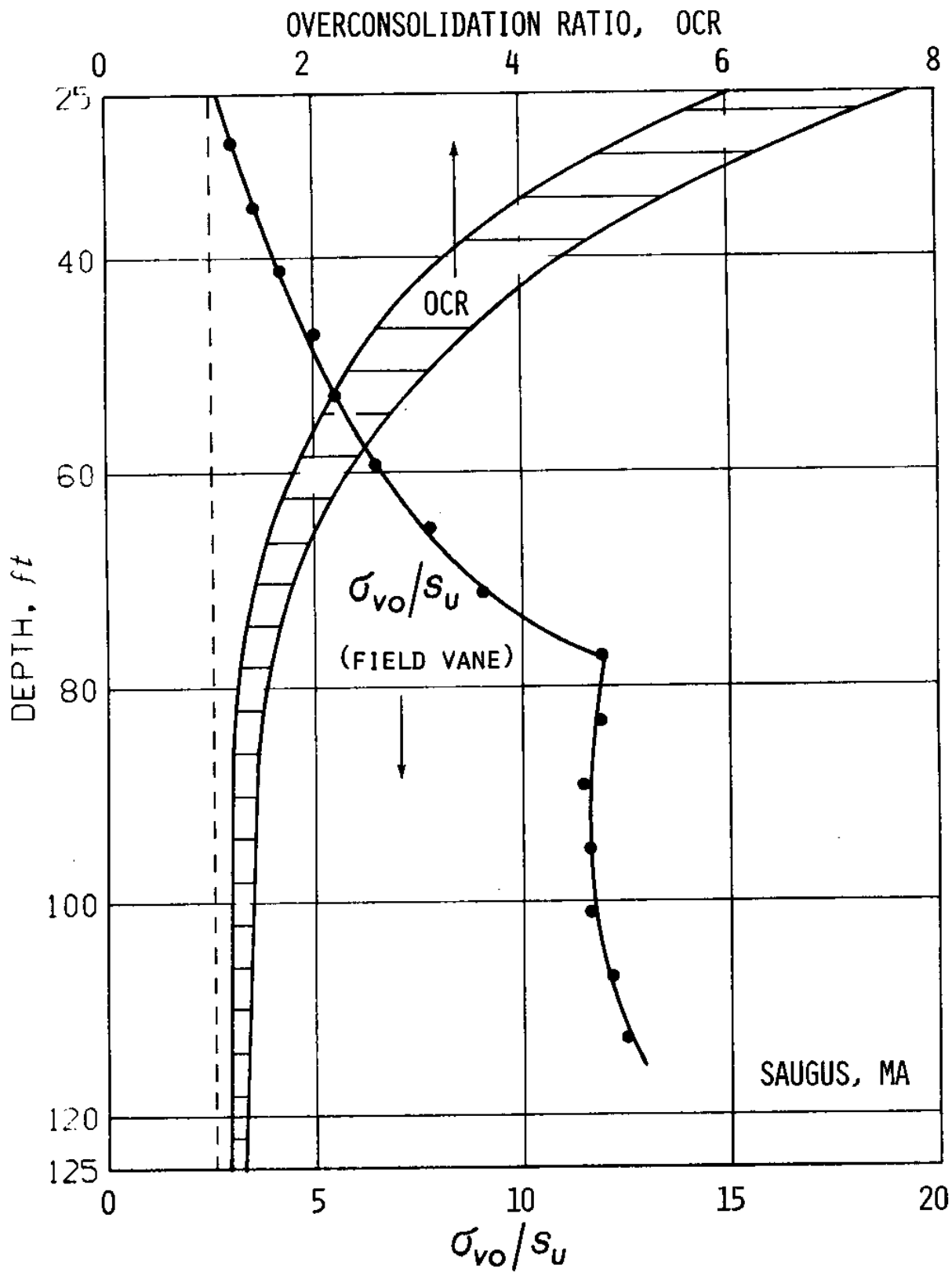
Fig. 5.16a Overconsolidation ratio and σ_{vo}/s_u (Field Vane) at the Saugus, MA, test site.
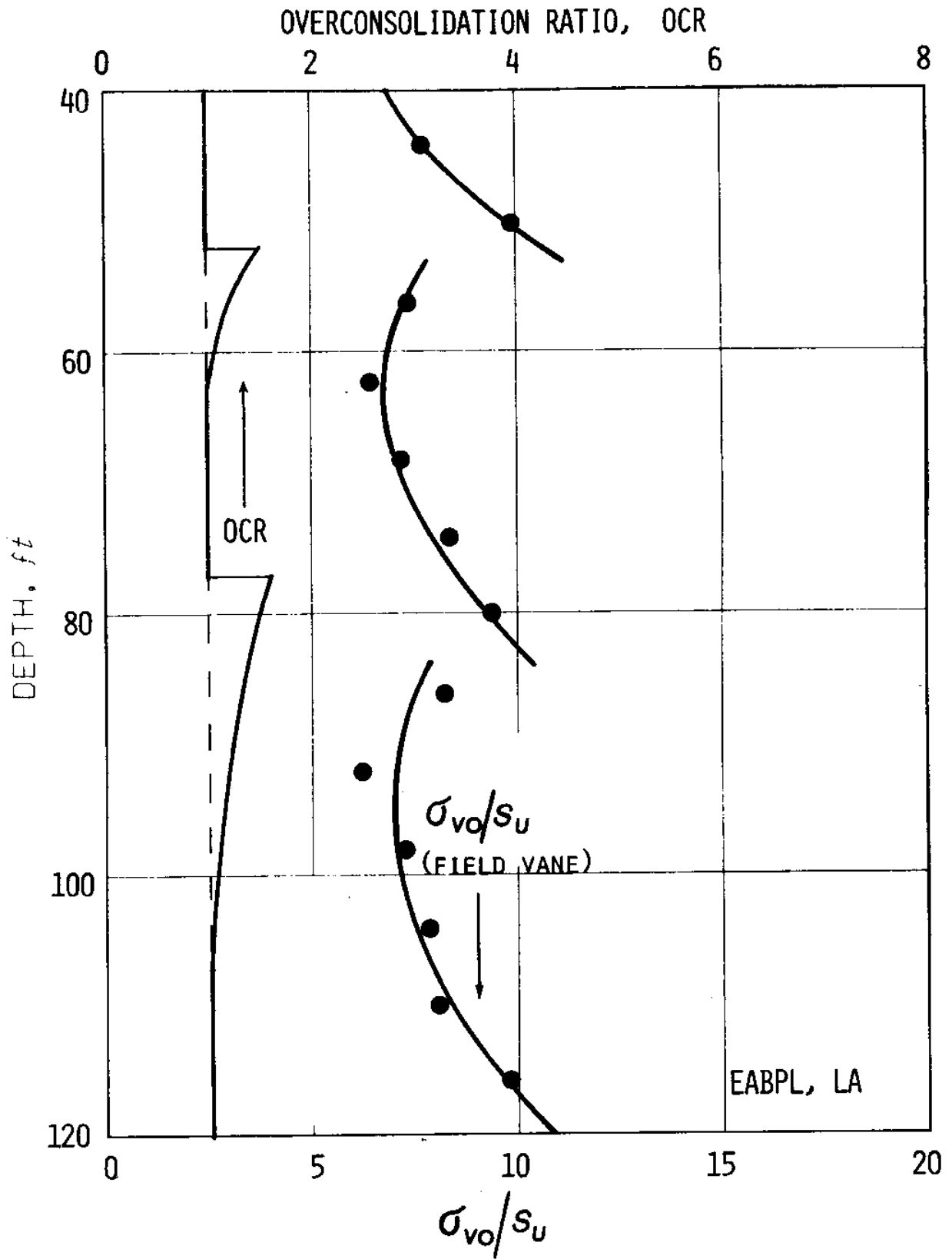
Fig. 5.16 b Overconsolidation ratio and σ_{vo}/s_u (Field Vane) at the
EABPL, LA test site
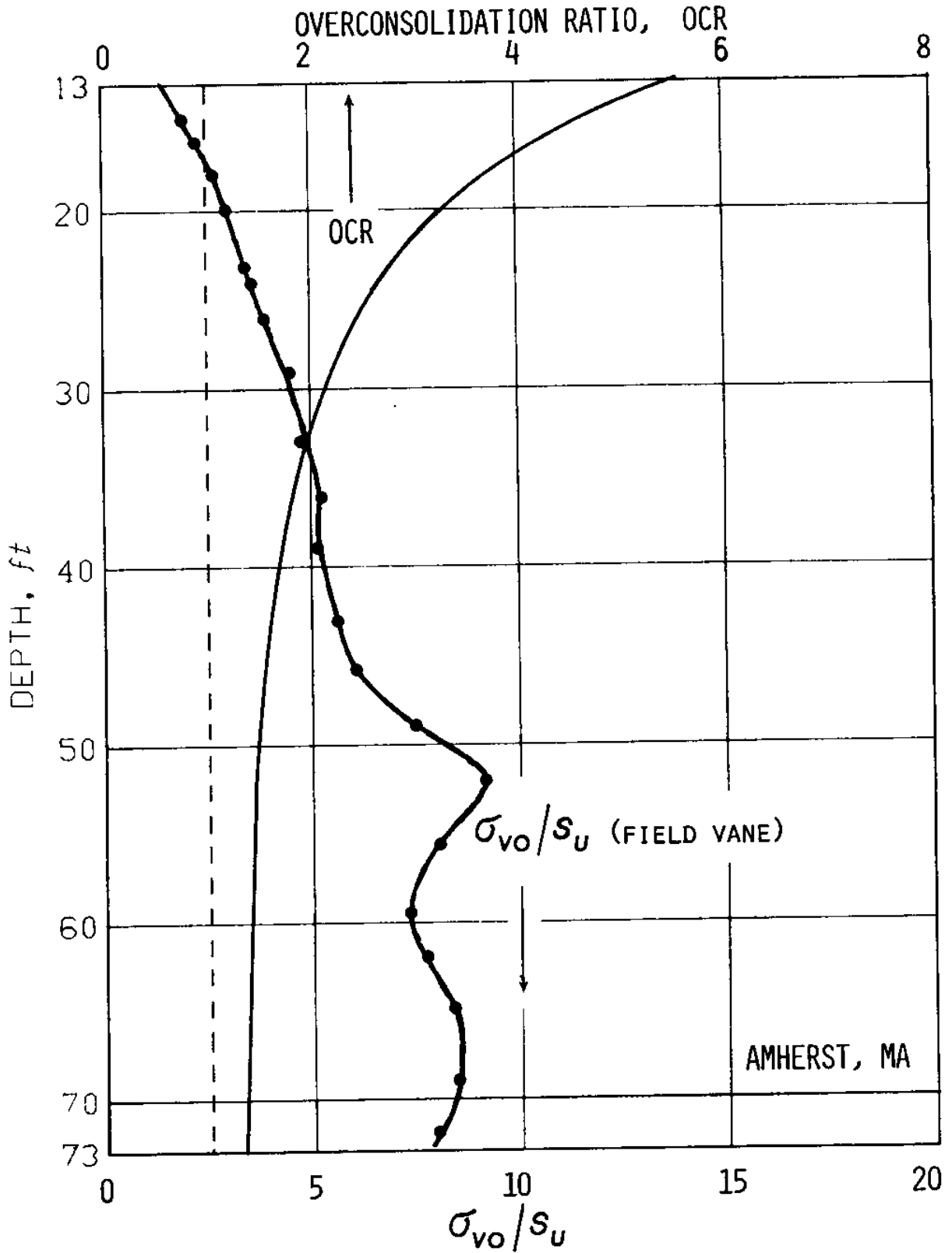
Fig. 5.16c Overconsolidation ratio and σ_{vo}/s_u (Field Vane) at the
Amherst, MA test site

$$\frac{E}{s_u} = \frac{3G}{s_u}$$

$$OCR = \bar{\sigma}_{vm}/\bar{\sigma}_{vc}$$
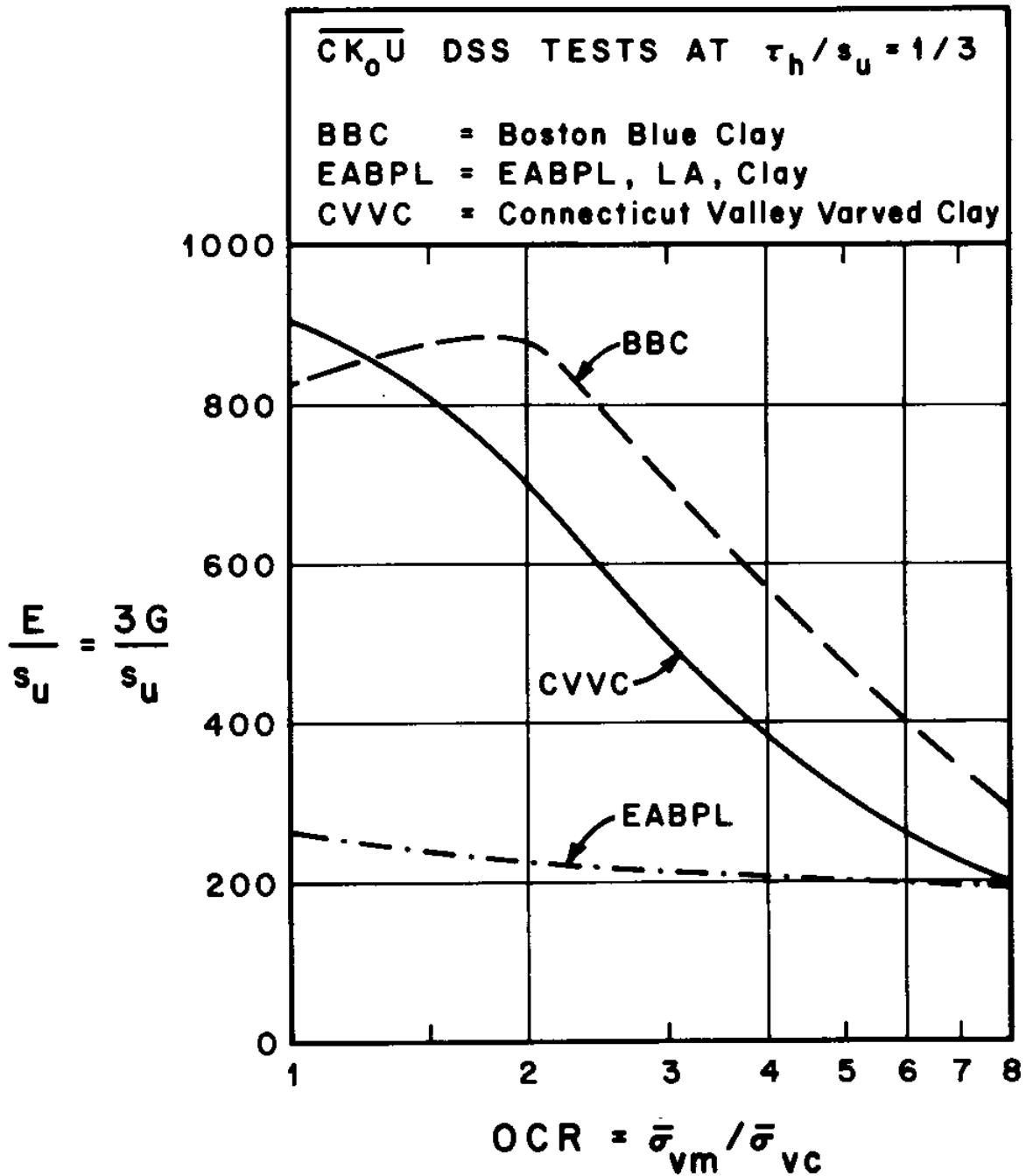
Fig. 5.17   The ratio E/s_u estimated from $\overline{CK_oU}$ DSS tests at $\tau_h = 1/3s_u$ for all three clay deposits   (data from Ladd et al, 1971a and Ladd and Edgers, 1972).
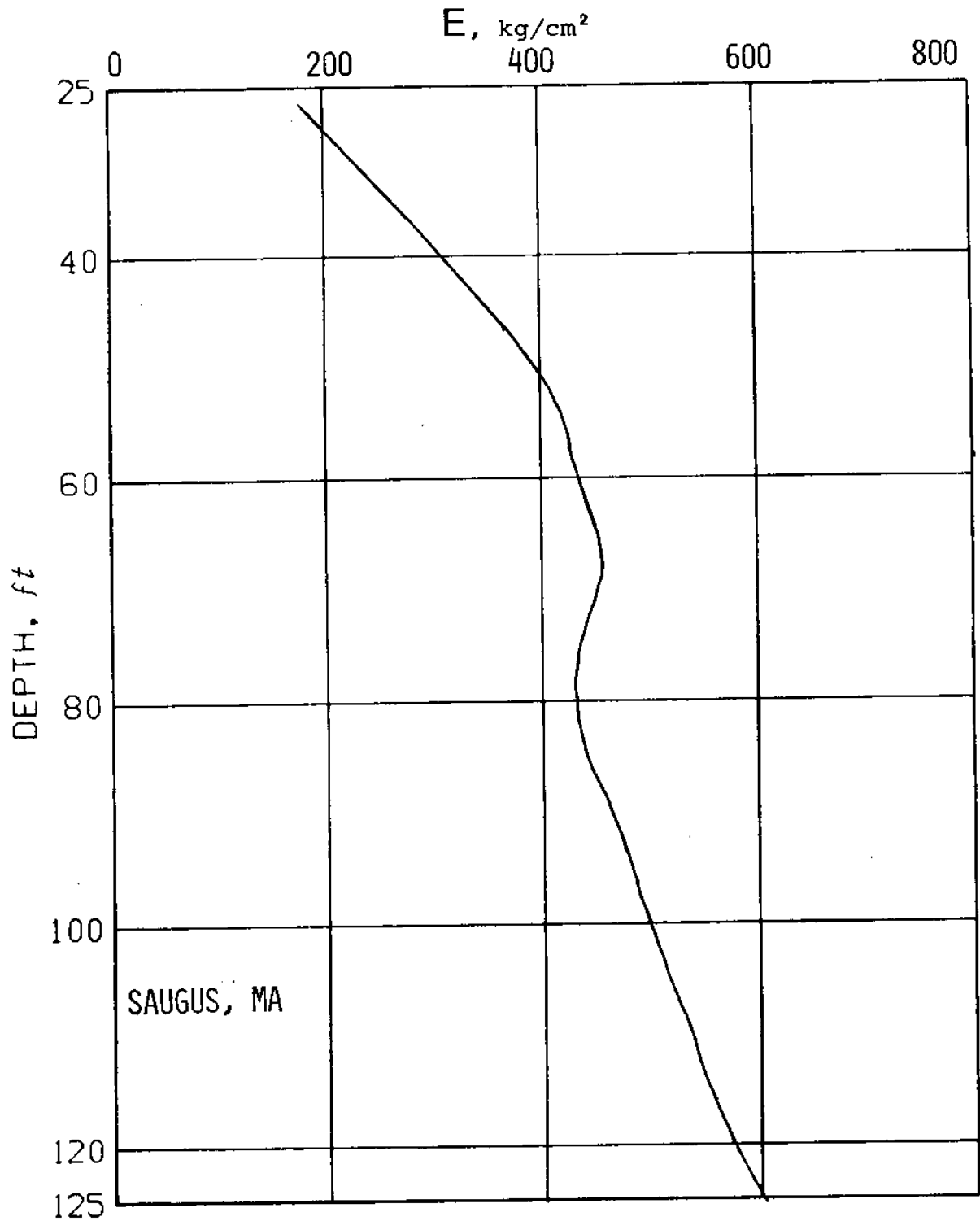
Fig. 5.18a Undrained Young's Modulus estimated from $\overline{CK_oU}$ DSS tests at $\tau = s_u/3$ for the Saugus, MA, test site.
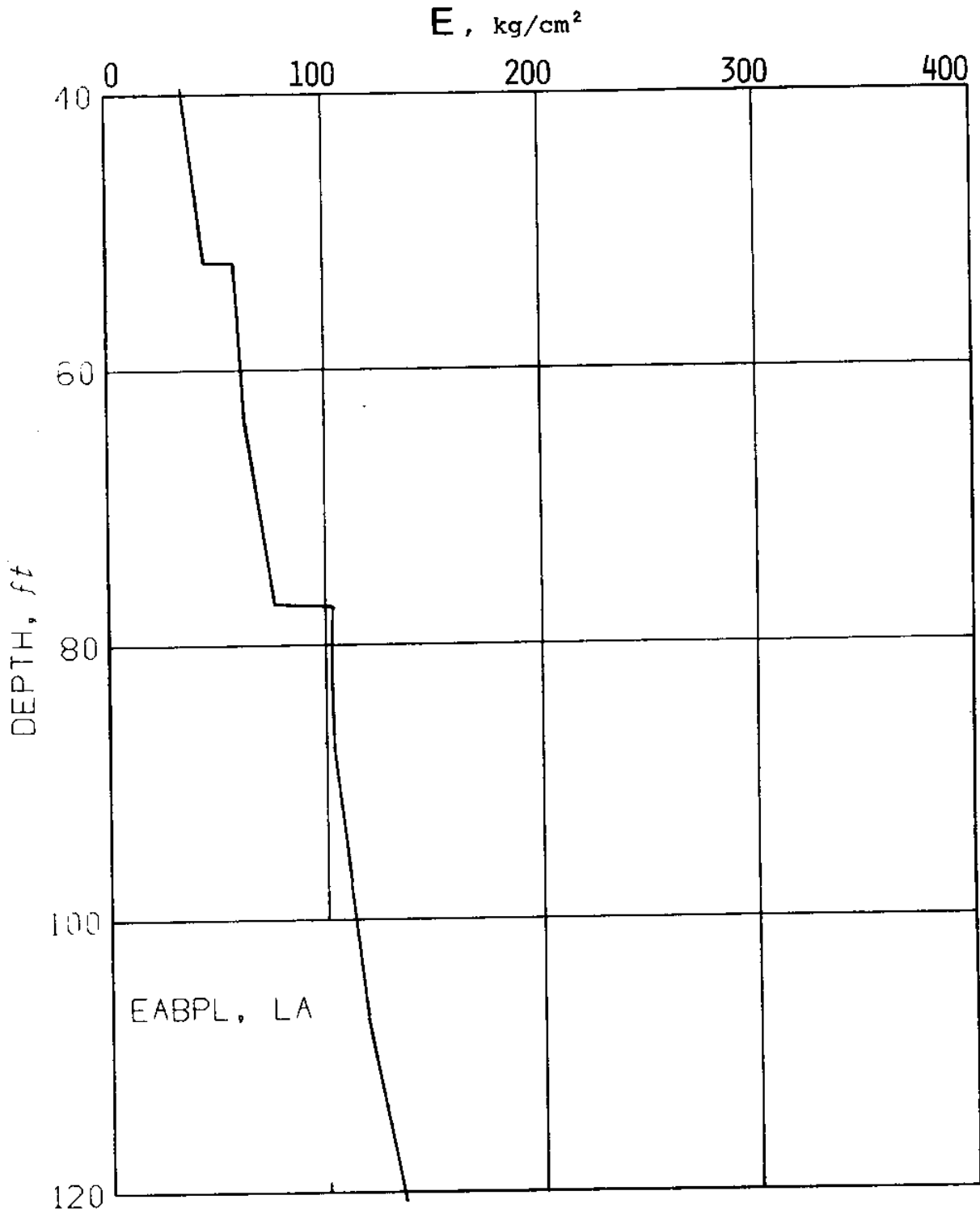
Fig. 5.18b Undrained Young's Modulus estimated from $\overline{CK_oU}$ DSS tests
at $\tau = s_u/3$ for the EABPL, LA, test site.
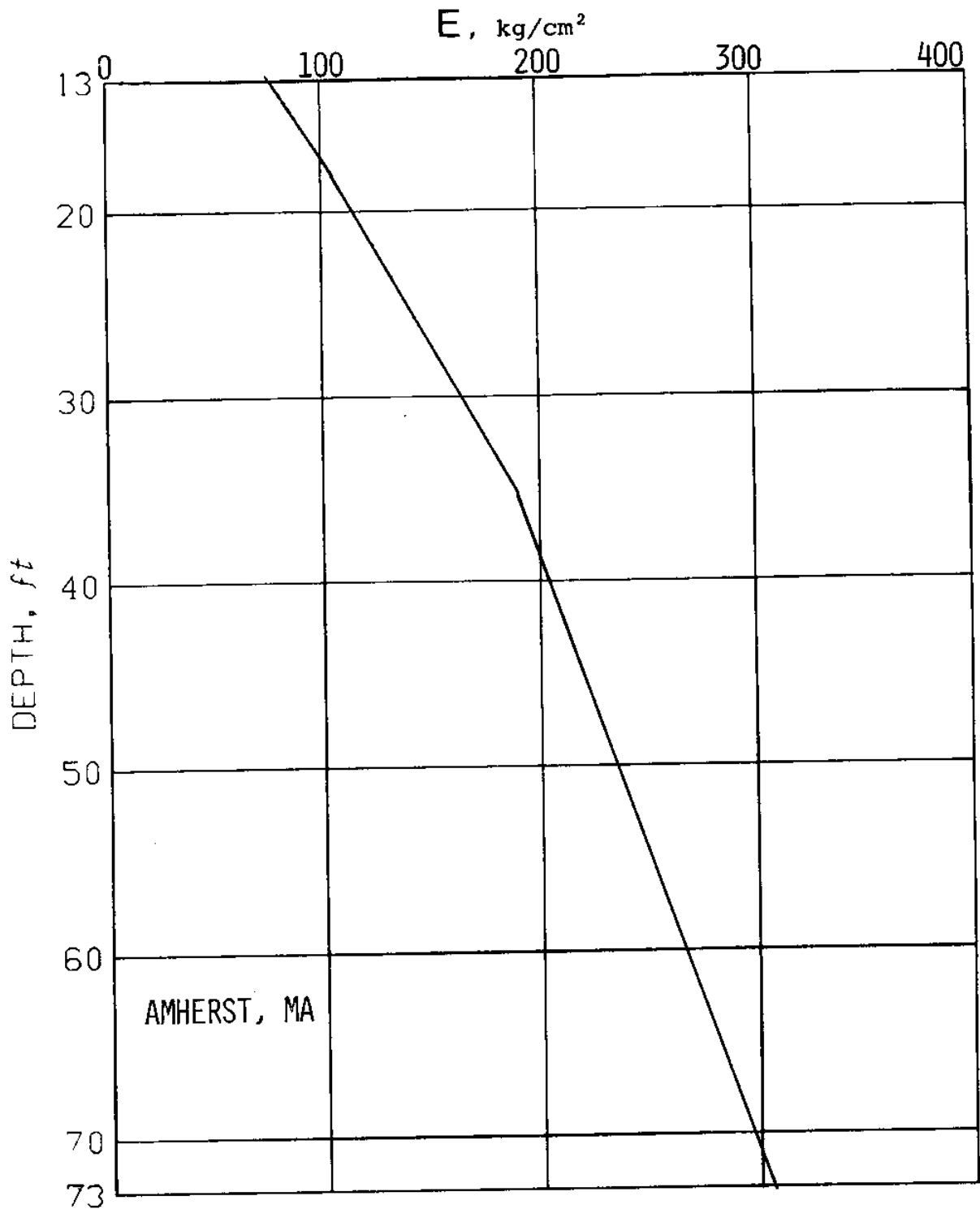
Fig. 5.18c Undrained Young's Modulus estimated from $\overline{CK_oU}$ DSS tests at $\tau = s_u/3$ for the Amherst, MA, test site.

CHAPTER 6

STATISTICAL ANALYSIS OF CONTINUOUS PENETRATION RECORDS

6.1 Introduction

Chapters 6 and 7 present the results of the field testing program

described in Chapter 5. In this chapter, the characteristics of the

measurements are described, and the variability of the standard cone

resistance ($2\delta = 60°$, $D/d = 1$) is analyzed. A procedure for filtering

penetration data is introduced in order to reduce the influence of local

soil variability on the data and allow easy comparison of test results.

This procedure is used extensively in Chapter 7 where measurements from

different cones and pore pressure probes are compared.

6.2 Continuous Penetration Records

The electrical cone and the pore pressure probe provide essentially

continuous data with depth, and hence can describe stratification and vari-

ability of a soil deposit more clearly than discrete measurements obtained

by other means such as the field vane test or laboratory tests on soil

samples. In many foundation designs, a good description of stratigraphy

at the site is more important than an accurate determination of

engineering properties, especially for erratic deposits and in cases when

weak thin layers are expected. Figures 6.1a and b show profiles of q_c mea-

sured with the standard cone ($2\delta = 60°$, $D/d = 1$) in the relatively uniform

Boston Blue Clay and the more variable EABPL Clay (see site descriptions in

Chapter 5). These plots are made from data points discretized at depth

intervals of 3 to 5 cm (constant in each test) with a computer-controlled

cathod-ray tube plotting device. For all clay deposits considered, these intervals reproduce the original continuous q_c record obtained from the strip chart recorder with sufficient accuracy. The dotted portions of the profile in Fig. 6.1a represent locations where the standard penetration rate (1 to 2 cm/sec) was changed. The cone resistance at a faster rate is denoted by F and at a slow rate by S in the figure.

During cone and pore pressure probe tests, penetration stops every 1 m (or 5 ft depending on rod length) for about one minute or less in order to add a new pushing rod. When penetration starts again, the cone resistance, q_c, and the pore pressure, u, goes through a transient period before reaching a steady state. This transient behavior is very brief in the case of q_c and can be neglected for all practical purposes. On the other hand, the pore pressure, u, typically does not reach a steady state until after about 4 to 15 cm of penetration (at a penetration rate of 1 to 2 cm/sec) depending on the characteristics of the soil and the probe.[*] Figure 6.2 shows a typical profile of pore pressure data obtained in Boston Blue Clay. By starting to push a new rod at a depth, say, of 50.5 ft, the steady state penetration is reached after half a foot or less and remains up to a depth of 53.5 ft, approximately. The installation of a new rod takes 33 seconds and pore pressures decay during this period. A detailed analysis of the pore pressure decay is underway at M.I.T. to estimate the consolidation behavior of the clay but,this is beyond the scope of this report.

In order to study the pore pressure, u, during steady penetration the

---

[*]If the response of the probe is slow due to improper deairing, the transient period will increase significantly.

transient records of u are deleted. An example of the steady penetration

u profile is shown in Fig. 6.3 for a 60° probe which is unenlarged (D/d = 1)

and where the porous stone is located at the cone tip.

Comparing Figs. 6.3 and 6.1b, representing the steady state pore

pressure, u, and the cone resistance, q_c, of the same cone in the same

deposit, we note the strong correlation betwen the high values ('peaks') of

q_c and the low values of u (depths 22 ft, 42 ft, 80 to 90 ft, 106 ft, etc),

in spite of the fact that the two measurements are carried out in separate

holes in this variable deposit. These peaks and troughs probably indicate

the presence of sand lenses, or perhaps highly over-consolidated clay. The

implications of the ratio u/q_c will be discussed further in Chapter 7.

6.3 Repeatability of Measurements and Data Filtering

Soil exploration data obtained from field and laboratory tests always

include some variability, which, in many cases, seriously affects major

design decisions. These variations are due to: (1) actual variability of

the deposit; (2) variability caused by the measuring device, e.g.,

strain-gage, pressure transducer, read-out equipment, etc., and (3) vari-

ability in the test procedures, e.g., soil disturbance, rate of testing,

etc.

In situ measurements obtained from the cone penetrometer and the pore

pressure probe involve very simple test procedures that minimize human

error and cause a consistent soil disturbance. Variability of measurements

in these tests is therefore due to either equipment problems or to the

actual soil variability.

In order to study the variability of q_c, repeated cone tests were performed in adjacent holes. Figures 6.4a, 6.5a and 6.6a show the cone penetration resistance q_c obtained in three clays: the relatively uniform deposits of Boston Blue Clay and Connecticut Valley Varved Clay, and the more variable EABPL Clay (Chapter 5). In each case, the (discretized) q_c measurements from two or three standard cone tests at close proximity (within a 40 ft radius of each other) are plotted together using different symbols. These figures indicate that q_c measurements generally form a well-defined band with a number of anomalies with small thickness which often do not appear in all tests. Many of these anomalies are less than 1 to 2 ft thick, and are probably due to local clay variability, inhomogeneities (e.g. sand lenses, stones, sea shells or pieces of wood). The existence of these anomalies in more than one hole suggests that they are not caused by equipment malfunction.

Inhomogeneities in soft clay deposits generally have a higher shear strength than the clay mass, and therefore are not as important in foundation design as low strength inhomogeneities in granular or rock deposits. However, a study of the basic strength properties of clays requires the elimination of these anomalies. The most common method of data smoothing is simply to eliminate "bad" points from the analysis on the basis of "engineering judgement." This procedure suffers from lack of repeatability, especially when different investigations are involved, and may lead to controversy and disagreement. For a field exploratory program where large amounts of data are obtained, a more systematic method of data smoothing is therefore essential.

Vivatrat (1978), developed a numerical procedure for systematically

filtering penetration data to eliminate anomalies and hence isolate clay behavior to be studied separately. The procedure is not based on sophisticated statistical and probabilistic concepts but is pragmatic and is believed to yield "reasonable" results. The soil is divided into sublayers of thickness Δ, where Δ is an input parameter, and the quantity of interest (q_c, u, etc) is assumed to be stationary within each sublayer in order to compute its statistical parameters. Anomalies within any sublayer i are filtered out as follows:[*]

1. Compute the median M and the standard deviation σ of data points contained in each of the three consecutive sublayers i-1, i, and i + 1.

2. Select a "representative" standard deviation S defined as:

$$S = \text{Minimum } \{1/2 \ [\sigma(i - 1) + \sigma(i)], \ 1/2 \ [\sigma(i) + \sigma(i + 1)],$$

$$1/2 \ [\sigma(i - 1) + \sigma(i + 1)]\} \qquad (6.1)$$

3. Remove all data points in layer i outside the range

$$M \pm aS, \qquad (6.2)$$

where a > 0 is a second input parameter.

This filtering process basically depends on the two parameters Δ and a. Small values of sublayer thickness, Δ, are necessary to satisfy the assumption of stationarity, and hence avoid errors due to the actual variation with depth in the quantity of interest. On the other hand,

---

[*]The computer software for the filtering and plotting results is given by Vivatrat (1978).

reliable statistics require each sublayer to contain a sufficient number
of data points (5 to 10 as a minimum). Also, Δ should not be less than the
thickness of the anomalies to be filtered from the data. The parameter a
influences the degree of filtering; small values of a (a < 1) retain only
data points which are close to the median of the data, whereas a large value
of a (a > 3) filters only extreme values of the data. Clearly, the pro-
cedure is not based on a rigorous statistical analysis but provides rea-
sonable results which, given Δ and a, can be exactly duplicated.

Using Δ = 2 ft and a = 2, Figs. 6.4b, 6.5b and 6.6b show the filtered
q_c measurements in the three clay deposits presented in Figs. 6.4a, 6.5a
and 6.6a, respectively. By comparing unfiltered and filtered q_c data
at the three sites, we note that, except for a few isolated regions, the
filter performs a reasonable smoothing of anomalies and gives results which
are probably similar to ones obtained on the basis of engineering judgement.
A major advantage of this procedure is the ability to assess soil vari-
ability after filtering. Figs. 6.4c, 6.5c and 6.6c show the mean and the
band of $\pm 2\sigma$, where σ is the standard deviation, of the filtered data.
Assuming a normal distribution about the mean, this band should contain
95% of the data points. The reader can easily check the filtering proce-
dure by comparing this band to one drawn based on his judgement to include
roughly 95% of the data points.

The influence of the parameters Δ and a on the filtering process
is illustrated for the highly variable EABPL clay in Figs. 6.7a to d by
comparing the mean and the standard deviation of: unfiltered data with
Δ = 2 ft; filtered data with Δ = 2 ft and a = 1.5; filtered data with
Δ = 2 ft and a = 2.5; and filtered data with Δ = 6 ft and a = 2.0.

Analysis of these figures and other results not shown here indicates that:

(1) The mean values of q_c in different sublayers are not significantly affected by Δ (between 2 and 6 ft) and a (between 1.5 and 2.5). In fact, filtering has little effect on the mean values of q_c (within 15%) but results in a smoother profile of q_c especially in regions where the variation in q_c is large, e.g., between the depths of 80 to 95 ft in EABPL clay.

(2) Filtering decreases the changes in the standard deviation σ with depth. Furthermore, σ is more sensitive to the parameters Δ and a than the mean, and tends to increase with increasing values of Δ and a. The fact that σ increases with Δ, even in a relatively uniform region, indicates that q_c is not really stationary within 2 to 6 ft sublayers. When Δ = 2 ft, varying a between 1.5 and 2.5 causes σ to change by less than 20%.

In addition to the mean and the standard deviation of the data, new design methods based on probabilistic concepts require the probability distribution function to be determined. Each sublayer of thickness, Δ, generally contains 10 to 25 data points (depending on the total number of tests and the discretization frequency), which are insufficient for a reliable assessment of data distribution. To overcome this problem we study the distribution of a normalized random variable x defined as:

$$x = \frac{q_c - \text{mean } q_c}{\sigma_{q_c}} \quad , \quad (6.3)$$

where mean q_c and σ_{q_c} are computed for each sublayer of thickness Δ. If the computed distribution of x is approximately the same for all sections of the profile (each containing several sublayers of thickness Δ), then the distribution x can be assumed to be independent of depth and the probabilistic function of q_c at any depth, d, can be written as:

$$q_c(d) = \text{mean}_{q_c}(d) + \sigma_{q_c}(d) \cdot x \qquad (6.4)$$

Figures 6.8a and 6.8b show the cumulative probability distribution function of x (curve '1'), computed from 3 standard cone tests for two 46 ft layers of Boston Blue Clay: a heavily to moderately overconsolidated layer (depth = 26 to 72 ft); and a slightly over-consolidated layer (depth = 72 to 118 ft). Also shown for comparison are the theoretical normal probability distribution function (curve '2') and the Kolmogorov-Smirnov 95% confidence band (curves '3' and '4') around the sample probability distribution function (Kendall and Stuart, 1961; IMSL, 1975, subroutine USPC). These figures indicate that x has approximately the same distribution in both layers, that the distribution is close to a normal distribution (with zero mean and $\sigma = 1$), and hence that Eq. 6.4 is valid.

In summary, the analysis of cone resistance variability indicates that q_c at any depth, d, can be obtained from Eq. 6.4. The random variable x has zero mean, a standard deviation $\sigma = 1$, and is approximately normally distributed. The mean and standard deviation of q_c (appearing in Eq. 6.4) depend on depth as shown in Figs. 6.4c, 6.5c and 6.6c for the three clay deposits tested.

6.4   Soil Variability

The scatter in cone penetration resistance can be due to soil variability and/or equipment errors. In order to determine the relative importance of these two factors, an analysis of the variability of q_c measurements was conducted and the results compared to an identical analysis of field vane measurements. Similarities in the results of these two tests, which involve totally different equipment and obtained by different personnel, provide a good indication of soil variability.

In studying variability we consider the coefficient of variation, V, defined as:

$$V = \frac{\text{standard deviation}}{\text{mean}} \tag{6.5}$$

According to the theory presented in Chapter 4, the difference between cone resistance, q_c, and the horizontal total stress, σ_{ho}, represents a good measure of the undrained shear strength of clays. Therefore, the variability of cone penetration results is indicated by[*]

$$V(q_v - \sigma_{ho}) \tag{6.6}$$

Figures 6.9a, b and c show $V(q_c - \sigma_{ho})$ for the three clay deposits, computed with two filters from 3 standard cone tests in the case of Boston Blue Clay and EABPL Clay, and 2 standard cone tests in the case of Connecticut Valley Varved Clay (Figs. 6.4, 6.5 and 6.6). For Boston Blue Clay and EABPL Clay, $V(s_u$ field vane), computed with the same filtering procedure from 4 tests located within the same 200 ft radius of the cone tests (Figs. 5.4 and 5.9), is also shown for comparison. We note from these figures that:

(1) A filter with large sublayer thickness, Δ, produces a smoother V profile than a filter with a small Δ, and tends to increase V, especially when V is small (this can be attributed to the increased sample size and/or the errors due to the stationary assumption).

(2) In Boston Blue Clay, V(cone) decreases with depth, from about 0.20 to about 0.05. In EABPL Clay, two layers can be distinguished: one between

---

[*]An analysis of $V(q_c - \sigma_{vo})$, where σ_{vo} represents the total vertical stress, shows identical patterns as $V(q_c - \sigma_{ho})$ but about 5 to 15% higher.

depths of 45 and 75 ft, and one below 75 ft depth. In both layers, V(cone) decreases with depth, from more than 0.30 to about 0.12 and 0.10, respectively. In Connecticut Valley Varved Clay, V(cone) is relatively uniform and varies between 0.03 to 0.08, except at the top of the layer where it increases significantly.

(3) V(field vane) has approximately the same magnitude and shows the same pattern as V(cone). This is somewhat surprising and suggests that variabilities in measurements indeed reflect soil variabilities.

(4) In Boston Blue Clay and EABPL Clay, V(cone) and V(field vane) show a good correlation with the overconsolidation ratio, OCR, of the soils (Figs. 5.16). Low values of V occur in clays with low OCR (V $\approx$ 0.05 in Boston Blue Clay, and V $\approx$ 0.100 in EABPL Clay), while in the more heavily overconsolidated regions, V increases by 2 to 4 times. This significant variation of V with stress history provides another indication that equipment errors are not the main source of measurement variability. In Connecticut Valley Varved Clay where OCR varies almost as much as in Boston Blue Clay, V(cone) is, however, very small throughout the deposit (less than 0.08). This suggests that high OCR is not a direct cause of soil variability. Geology (Chapter 5) indicates that the highly overconsolidated Boston Blue Clay and the overconsolidated EABPL Clay have both been strongly affected by desiccation, whereas overconsolidation in Connecticut Valley Varved Clay is primarily due to removal of overburden. Since the effects of desiccation is likely to be non-uniform, desiccated clays can be expected to show high variability.[*]

---

[*] Ladd et al. (1971b) present variability in the "apparent" OCR of Bangkok Clay which can also be caused by different degrees of desiccation.

Therefore, the variation in the V profiles of Fig. 6.9, apparently indicates different degrees of desiccation throughout the deposits.

(5) The EABPL clay is less uniform than the Boston Blue Clay and has a variability in the estimated undrained shear strength, s_u, which is roughly twice as high.

(6) The most uniform clay tested is the Connecticut Valley Varved Clay which has a typical value of $V = 0.05$. Assuming a normal distribution of s_u (as indicated previously), this means that one measurement of s_u obtained by means of a perfect laboratory test has a 95% chance to be within a band of $\pm 2V = \pm 10\%$ about the mean. Higher values of $V = 0.15$ obtained in the overconsolidated Boston Blue Clay indicate that perfect laboratory testing can only be expected to determine the value of s_u within a band of $\pm 30\%$ due to soil variability. Such a large uncertainty in s_u is surprising in a deposit such as BBC which is considered by the profession to be quite uniform. However, it is important to note that engineering designs are usually performed for sufficiently large structures (compared to Δ used in our variability analyses) such that strength uncertainty (about the mean) is much less than indicated by the point variability in Fig . 6.9. In order to relate point variability to foundation reliability, an additional variability parameter, the auto correlation distance, is required.

(7) Results shown in Figs. 6.9 can probably be used to evaluate the effect of sample disturbance on s_u determined from laboratory tests after a similar variability analysis is conducted on the results of these tests.

6.5 Summary

The continuous measurements of cone resistance, q_c, and pore pressure, u, during cone penetration allow a better estimate of soil stratigraphy and variability than discrete measurements, e.g., field vane tests or laboratory tests on selected samples. In a marine illitic clay, a plastic deltaic clay and a glacial lake varved clay, q_c is repeatable within a reasonable margin of uncertainty ($\pm$ 5 to 15%). Typical q_c profiles include small scale anomalies, probably due to soil inhomogeneity, which must be discarded when the variability of the clay mass is investigated. A computerized filtering procedure to eliminate these anomalies is developed and applied to records of q_c at the three test sites. The filtered data are approximately normally distributed about the mean and have a standard deviation which varies with depth. An analysis of soil variability based on the coefficient of variation (= standard deviation/mean) shows that both the cone resistance and the field vane data detect the same soil variability which depends on the soil type and shows a significant increase in desiccated regions.
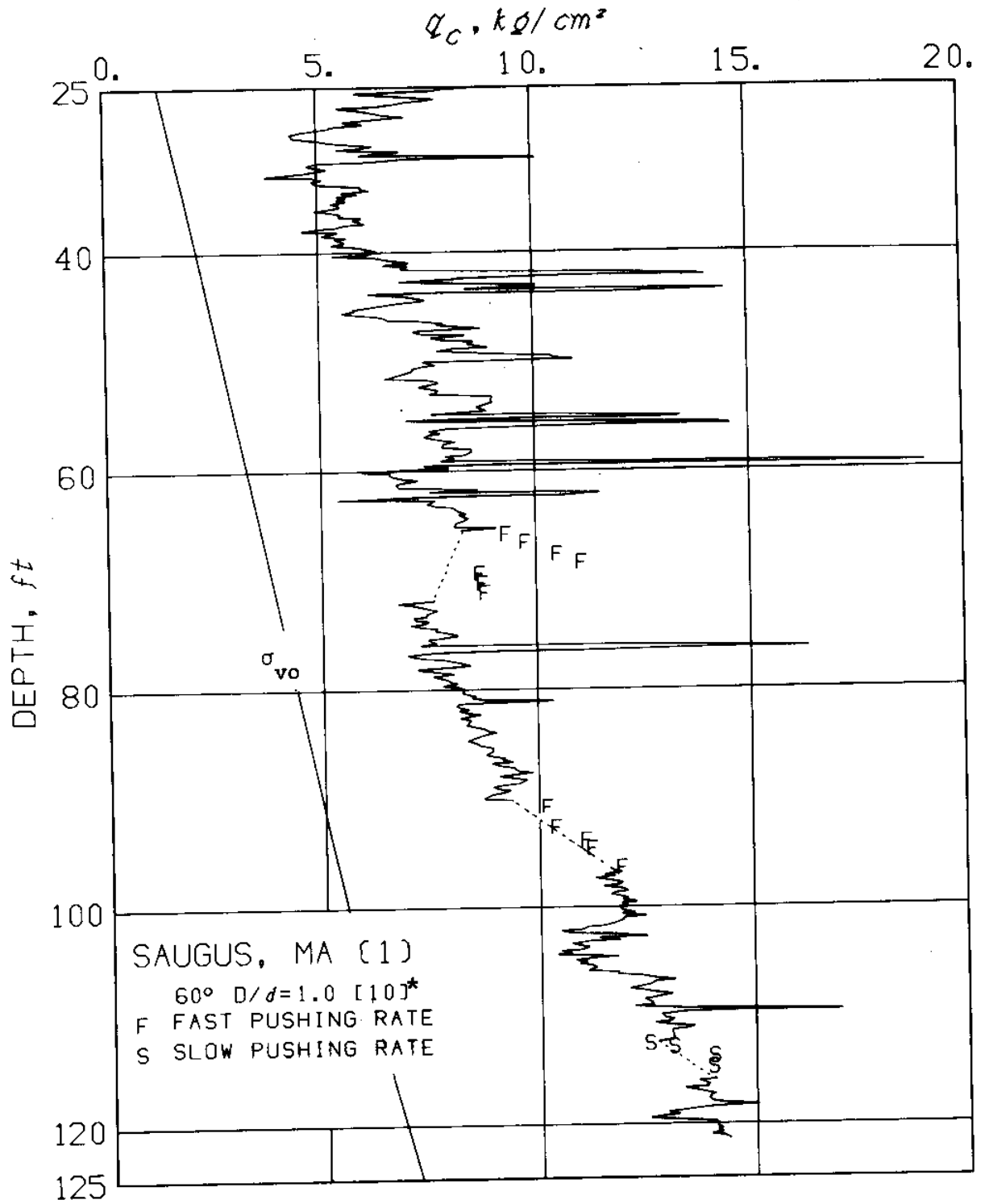
Fig. 6.1a Typical cone resistance profile in Boston Blue Clay.
(* test number)
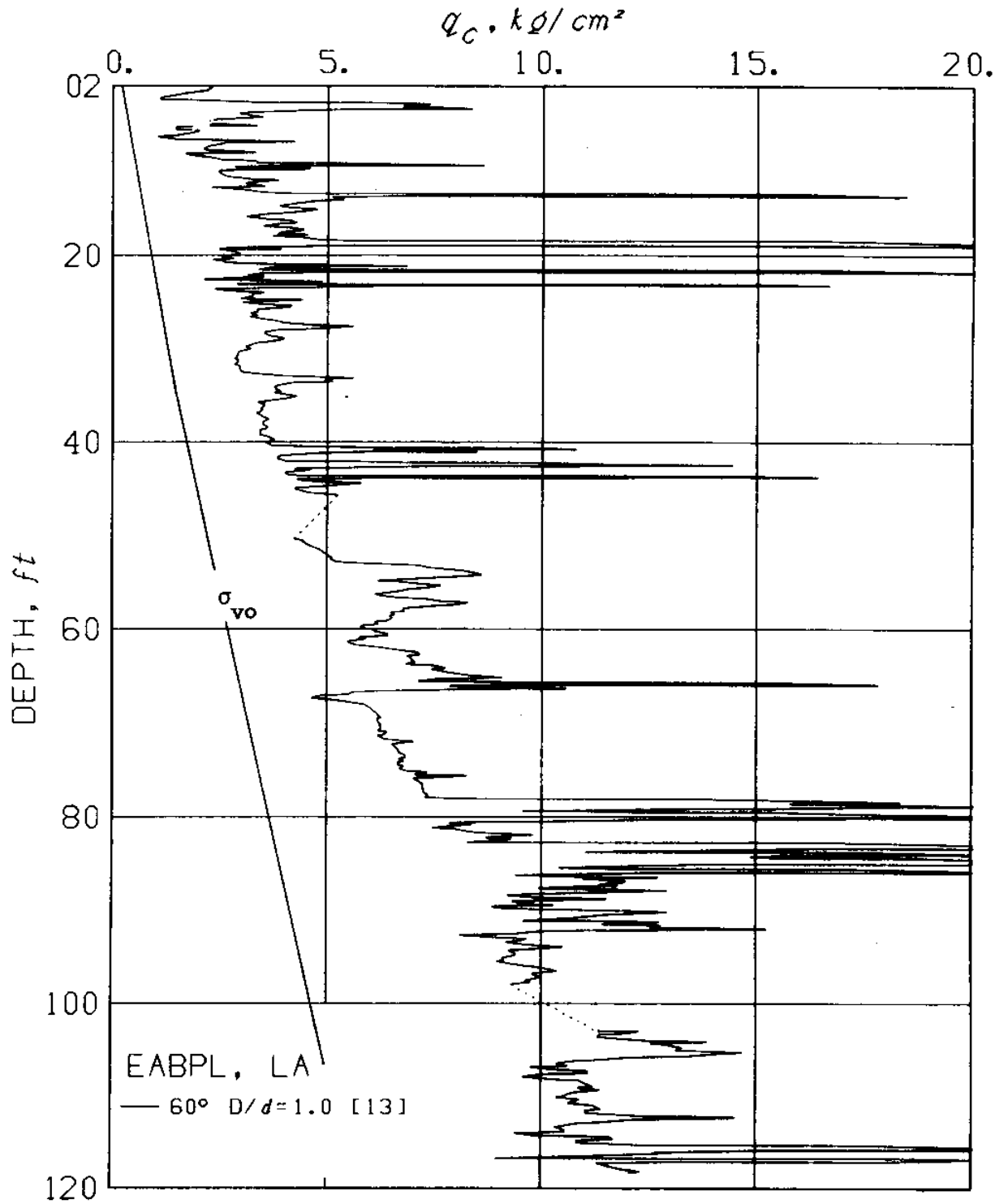
Fig. 6.1b   Typical cone resistance profile in EABPL Clay.
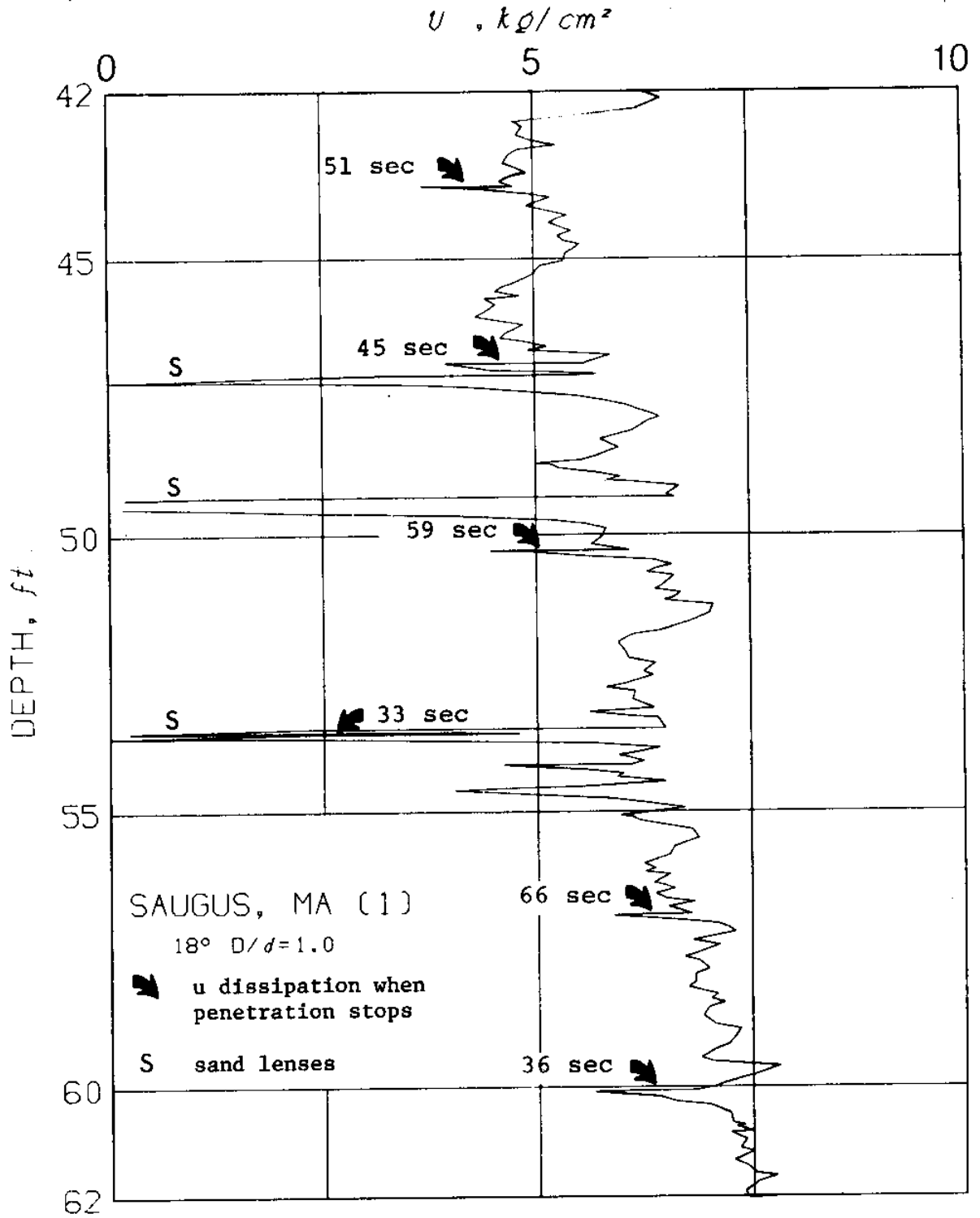
Fig. 6.2 Details of pore pressure measurements for an 18°,
D/d = 1, conical probe with porous stone at tip.
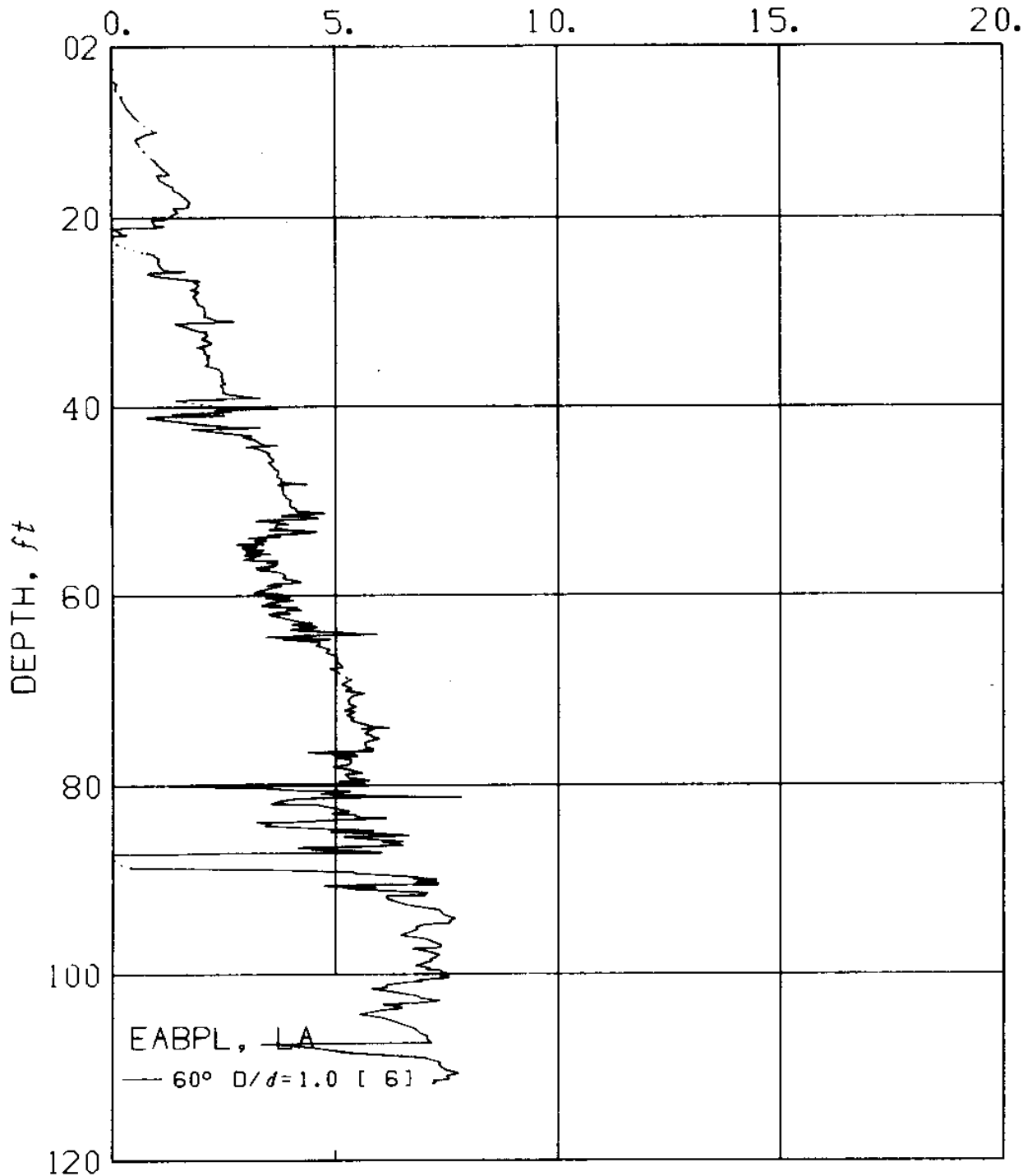
Fig. 6.3 A profile of steady penetration pore pressure in
EABPL Clay (60°, D/d = 1, conical probe with porous
stone at tip).
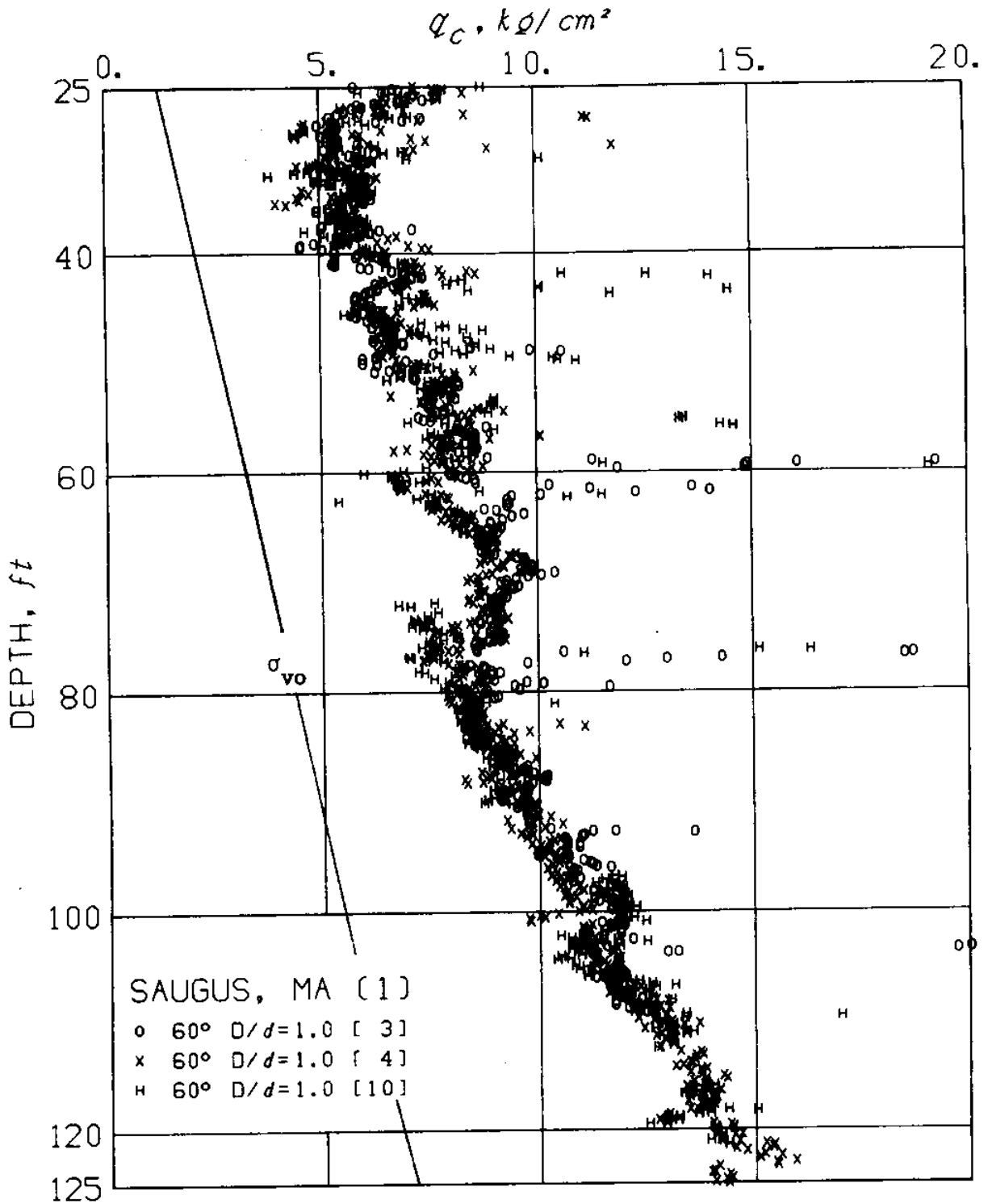
Fig. 6.4 Variability of q_c in Boston Blue Clay.

(a) Measurements from 3 standard cone tests.
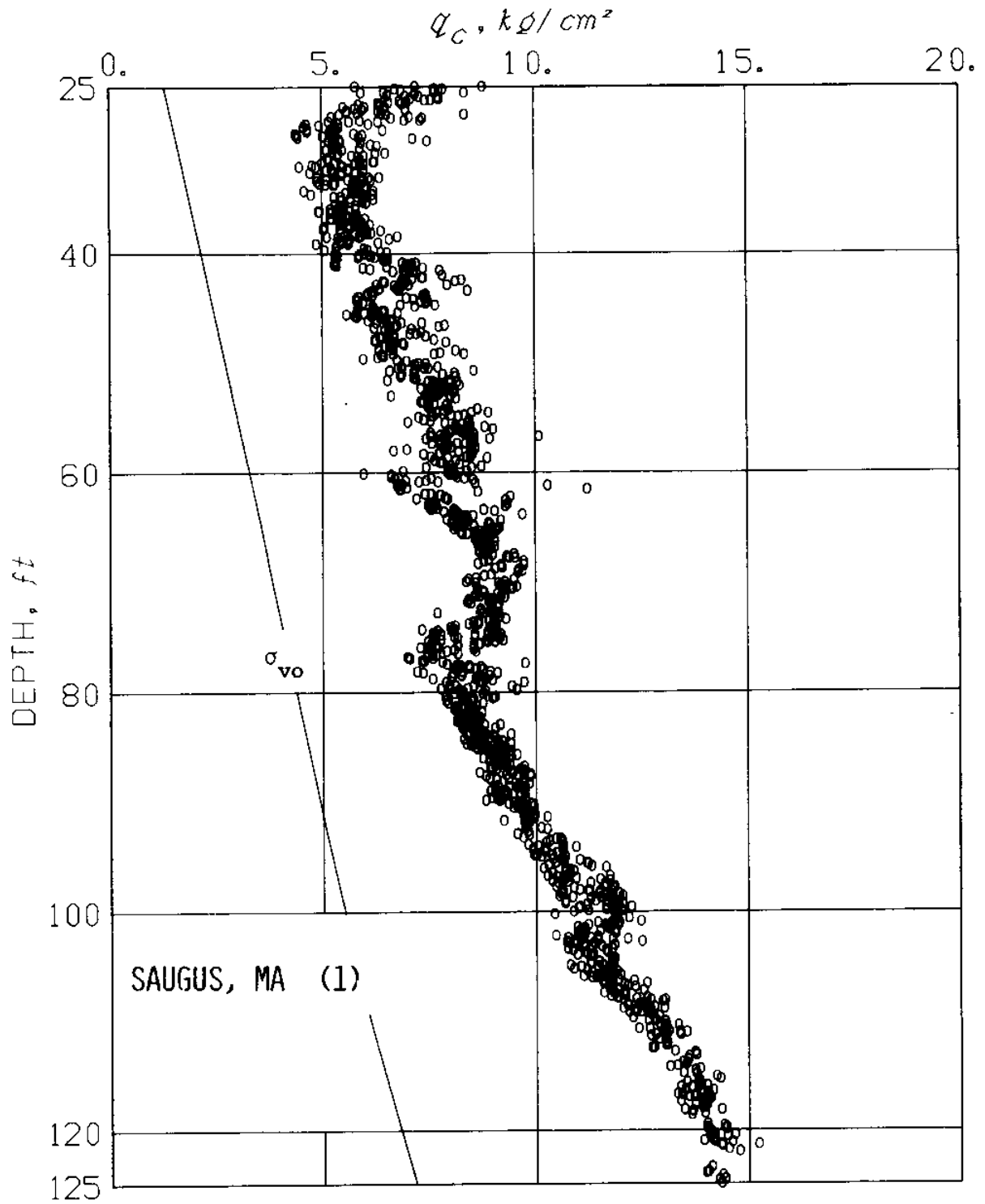
Fig. 6.4 Variability of q_c in Boston Blue Clay.

(b) Filtered q_c data (Δ = 2ft, a = 2.0).
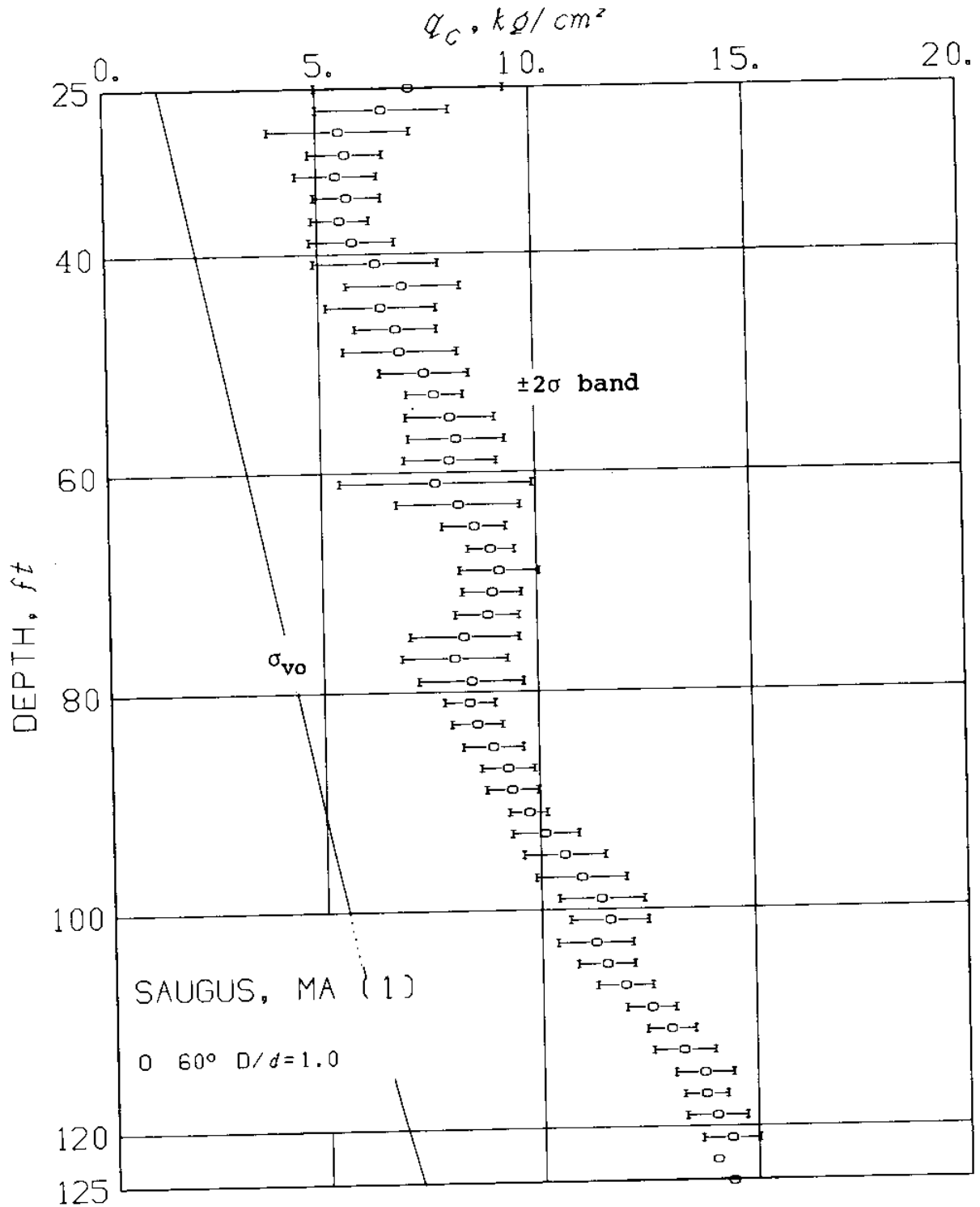
Fig. 6.4 Variability of q_c in Boston Blue Clay.
(c) Statistics of filtered q_c data (Δ = 2ft, a = 2.0).
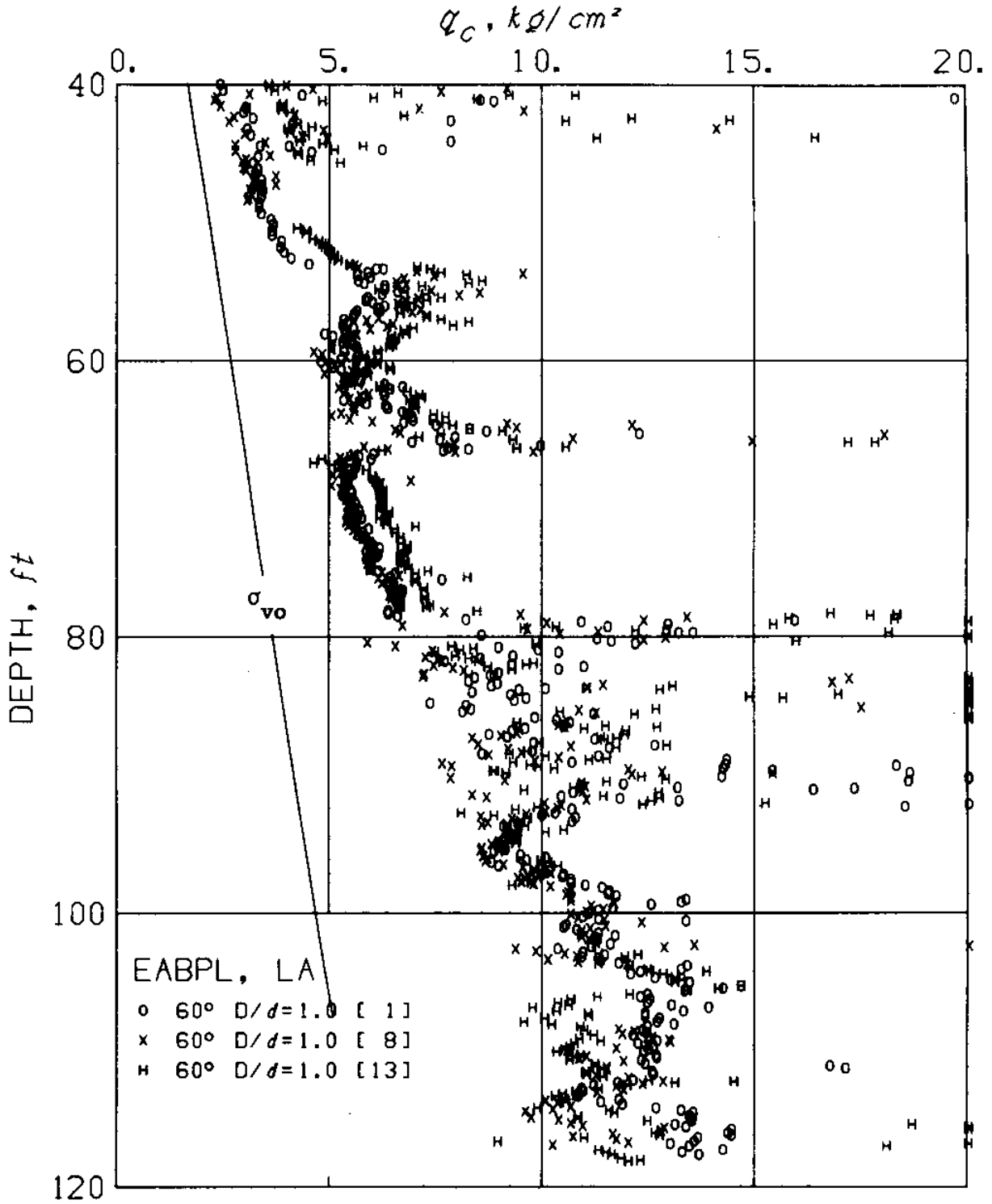
Fig. 6.5 Variability of q_c in EABPL Clays.

(a) Measurements from 3 standard cone tests.
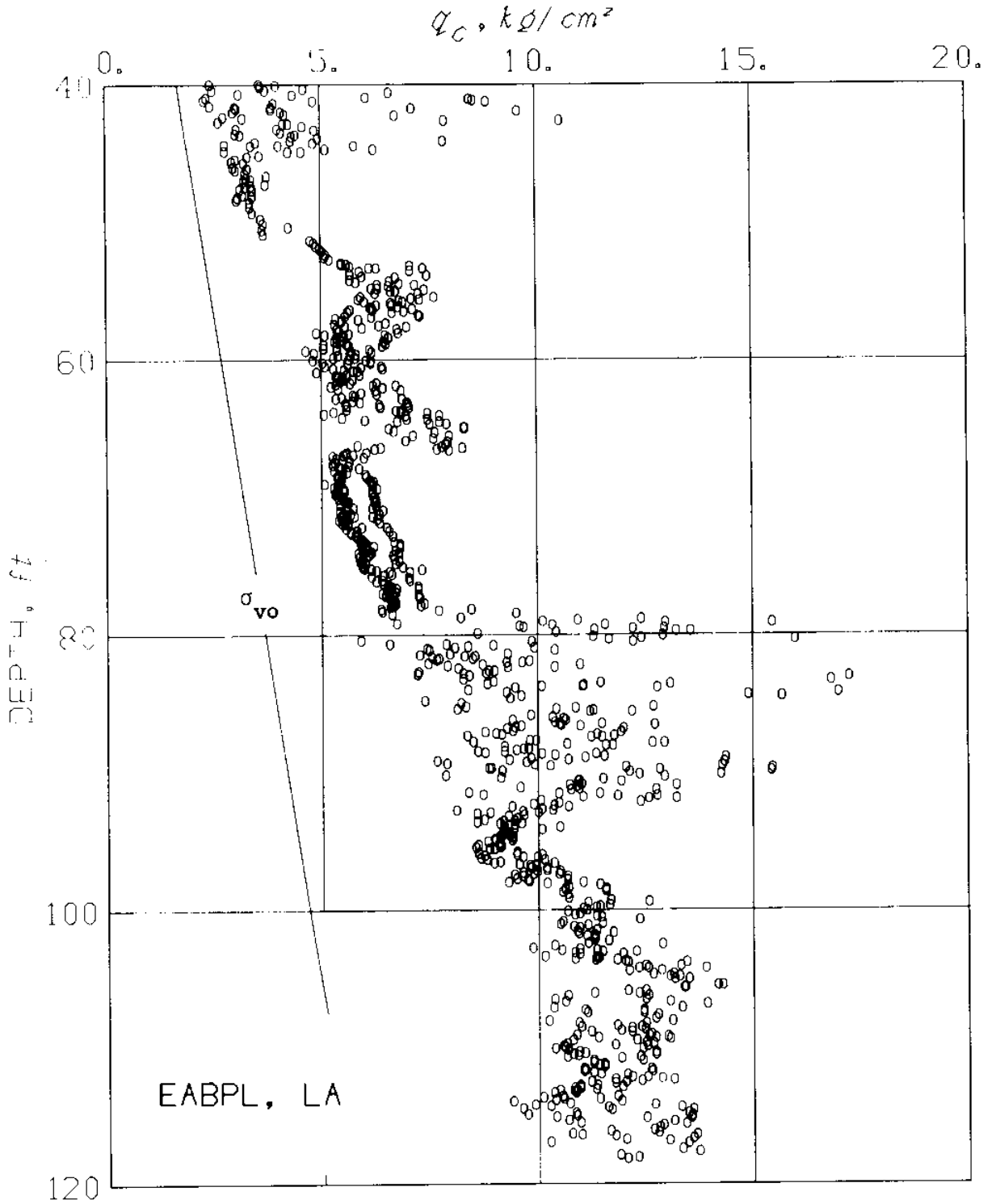
Fig. 6.5 Variability of q_c in EABPL Clays.

(b) Filtered q_c data (Δ = 2 ft, a = 2)
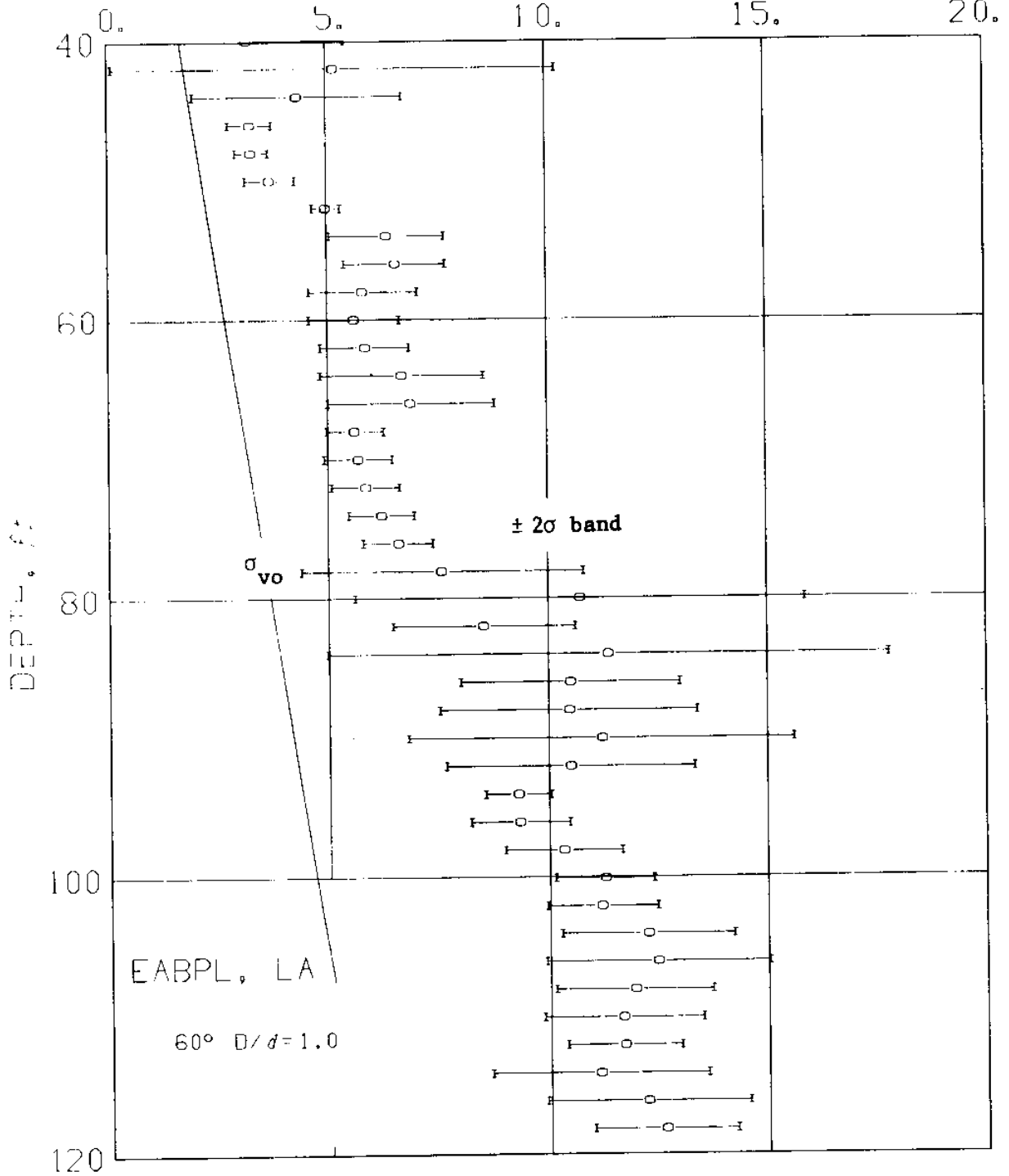
Fig. 6.5 Variability of q_c in EABPL Clays.

(c) Statistics of filtered q_c data (Δ = 2ft, a = 2.0).
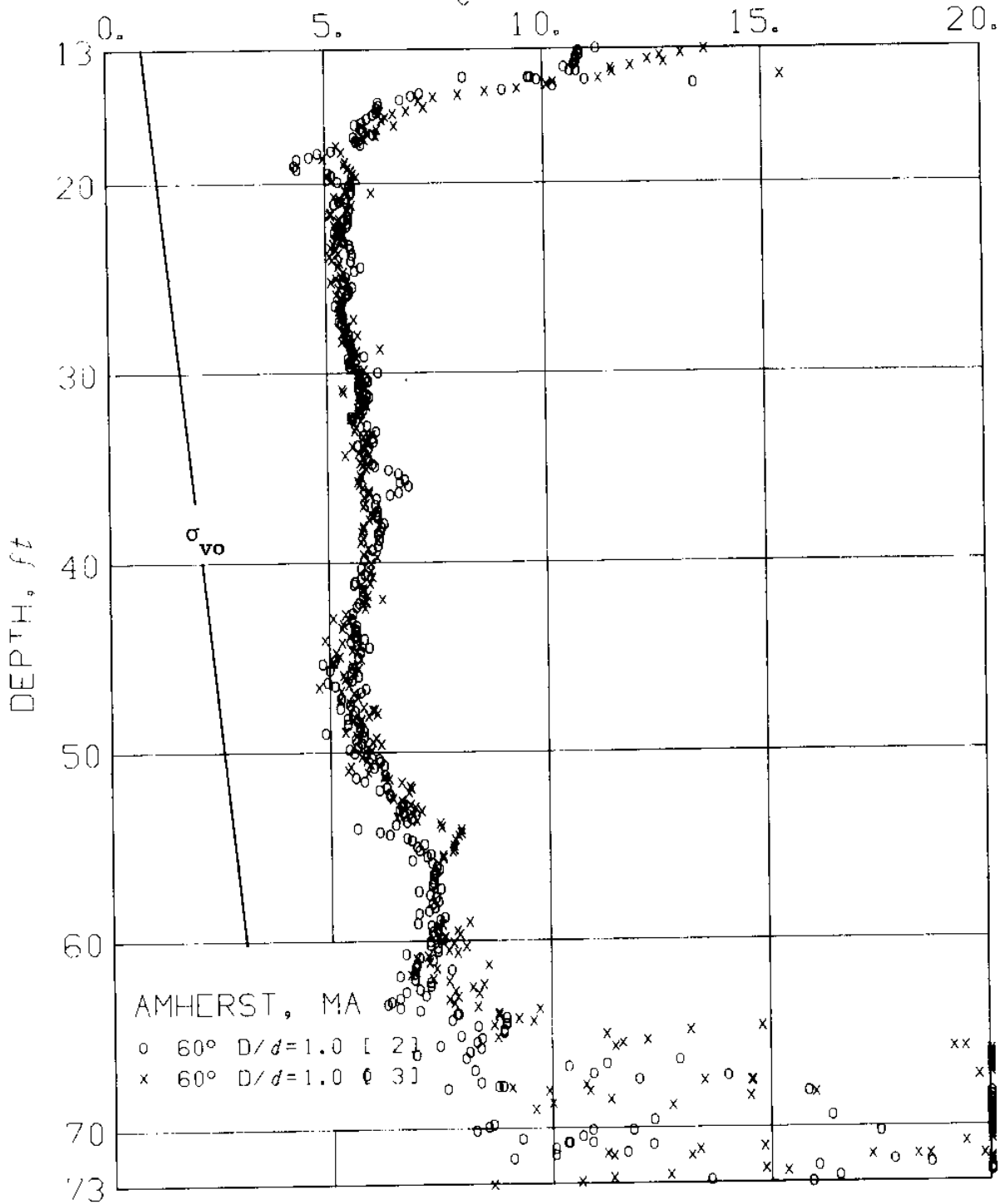
Fig. 6.6   Variability of q_c in Connecticut Valley Varved Clays.
(a) Measurements from 2 standard cone tests.
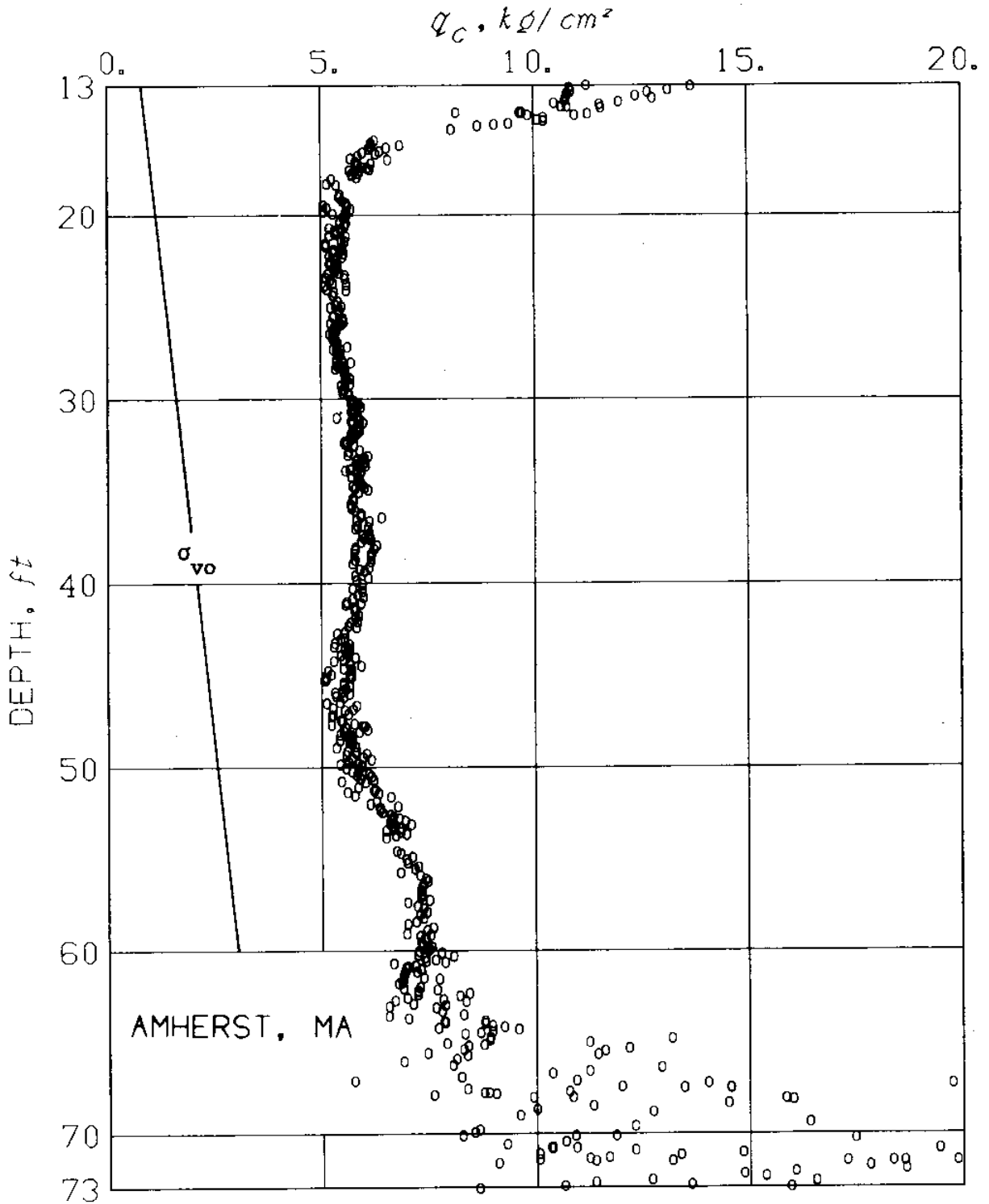
Fig. 6.6 Variability of q_c in Connecticut Valley Varved Clays.
(b) Filtered q_c data (Δ = 2ft, a = 2.0).
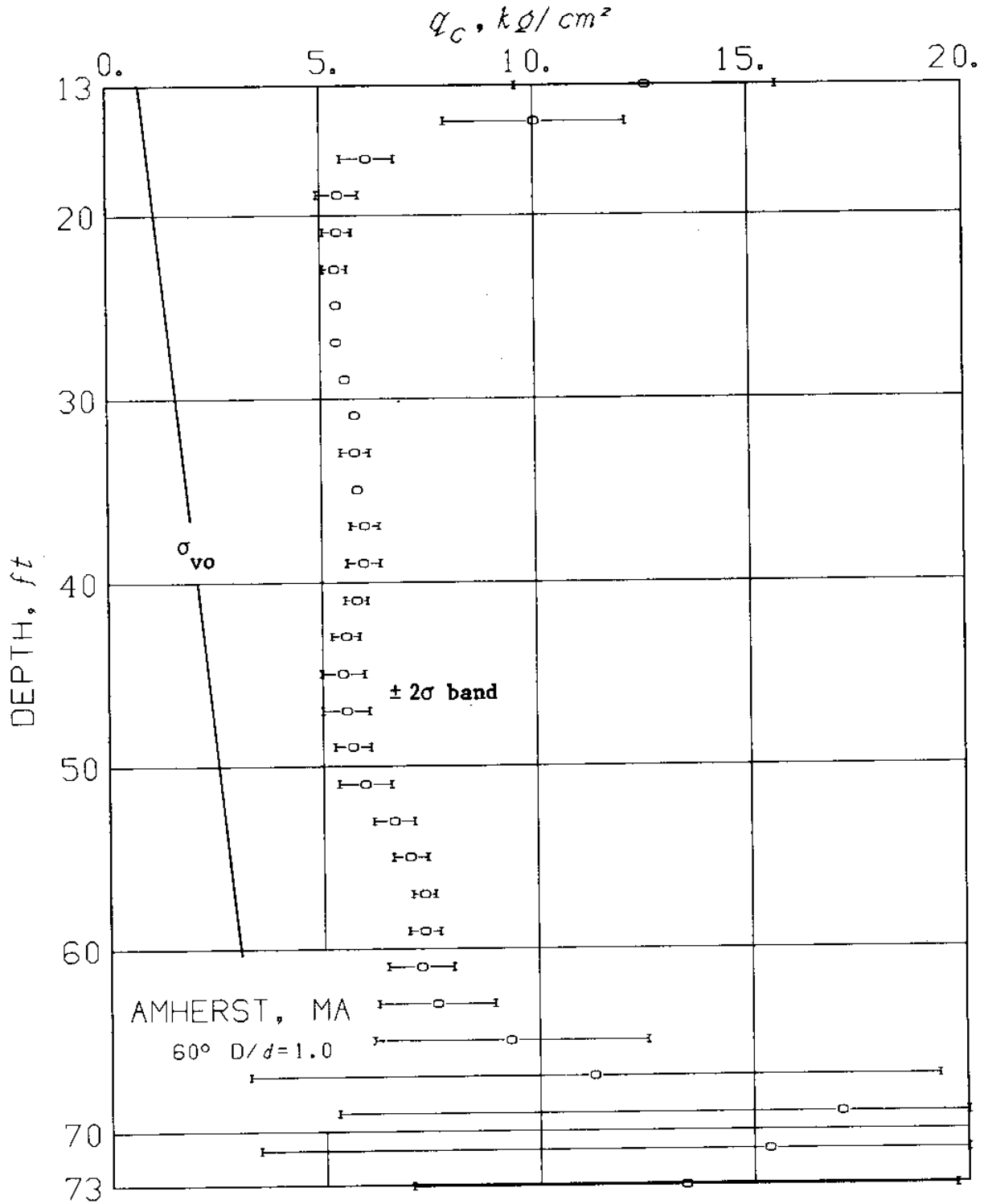
Fig. 6.6 Variability of q_c in Connecticut Valley Varved Clays.
(c) Statistics of filtered q_c data (Δ = 2ft, a = 2.0)
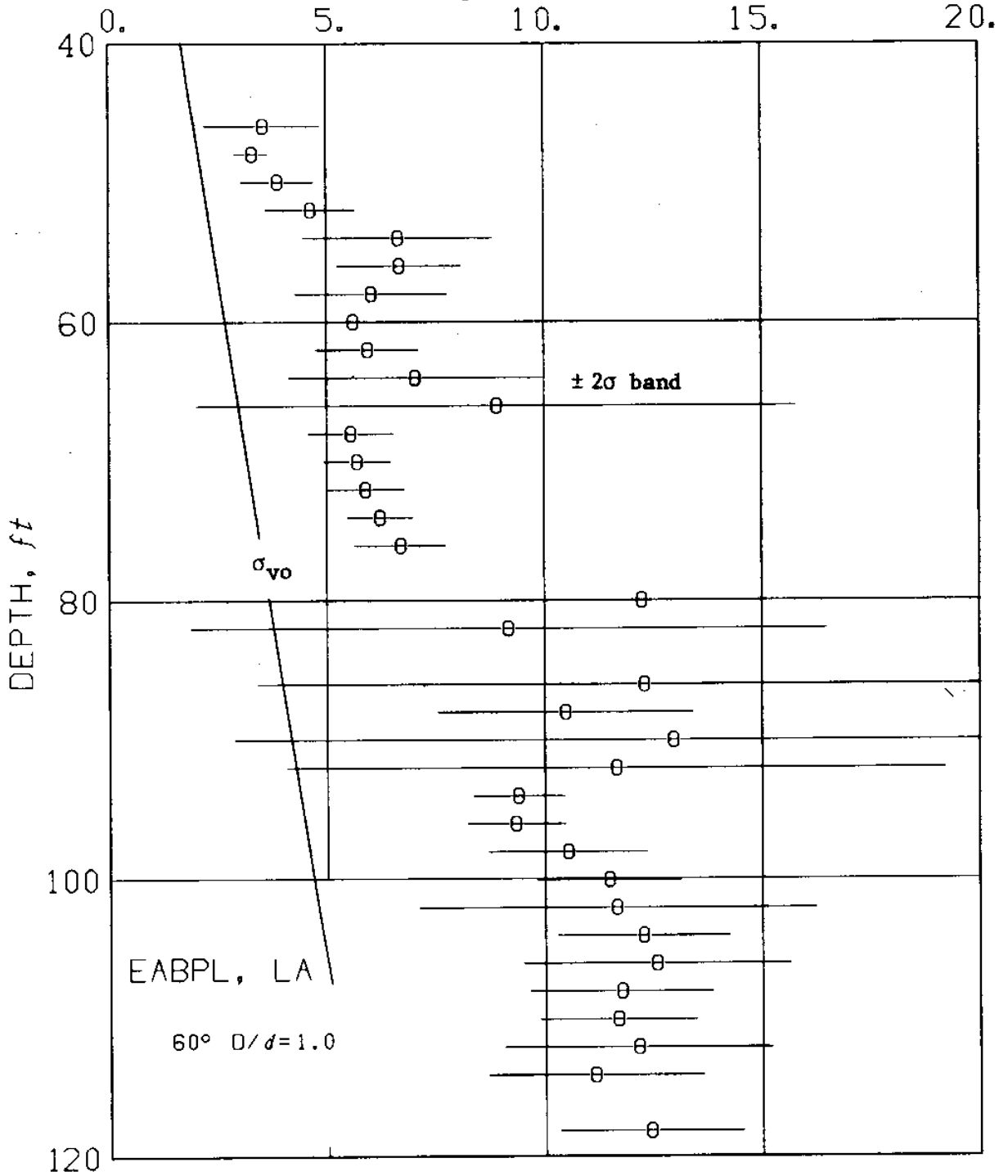
Fig. 6.7 Effects of filtering on the mean and standard deviation of q_c.
(a) No filtering.
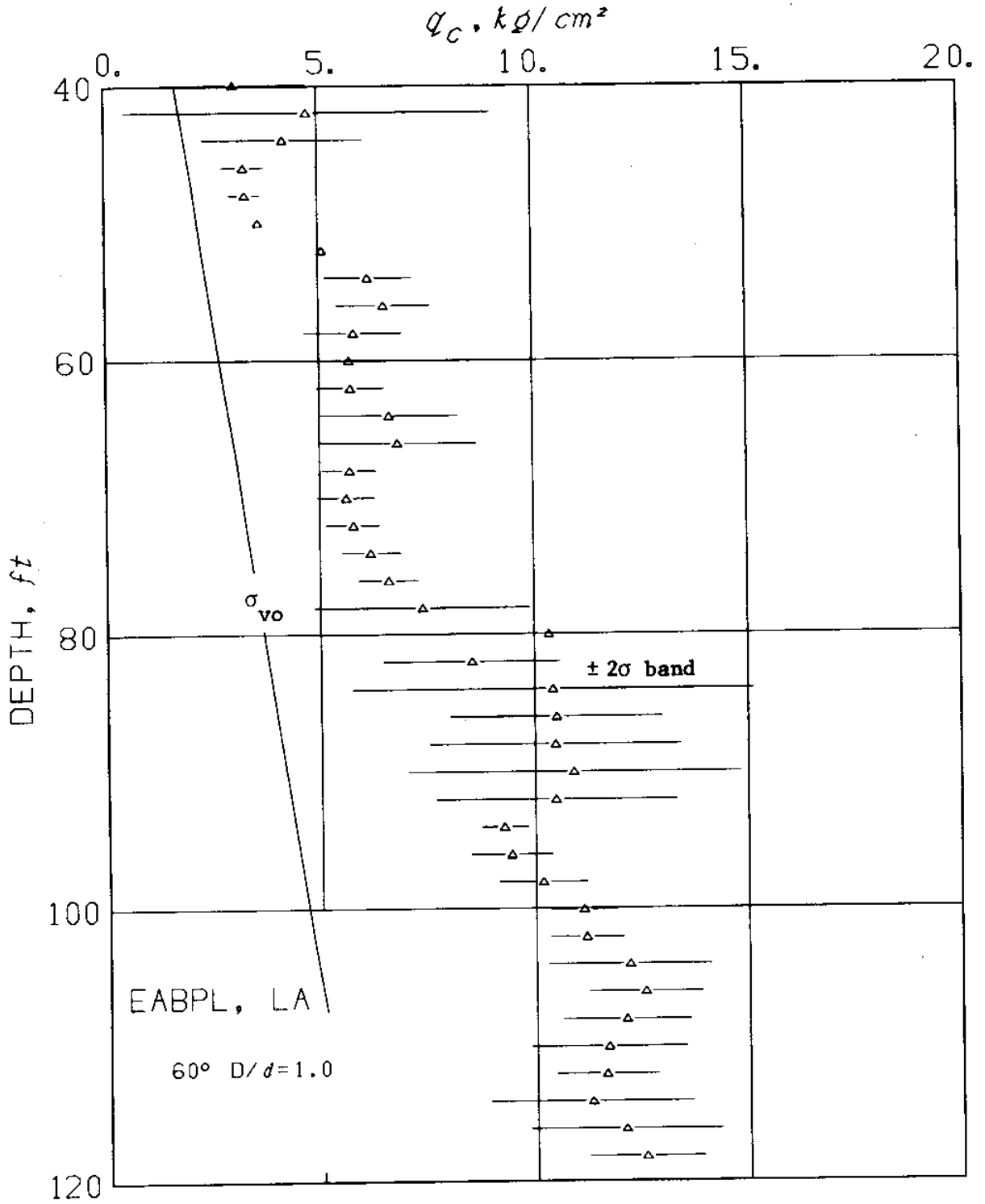
Fig. 6.7 Effects of filtering on the mean and standard deviation of q_c. (b) Filtered data with Δ = 2ft, a = 1.5.
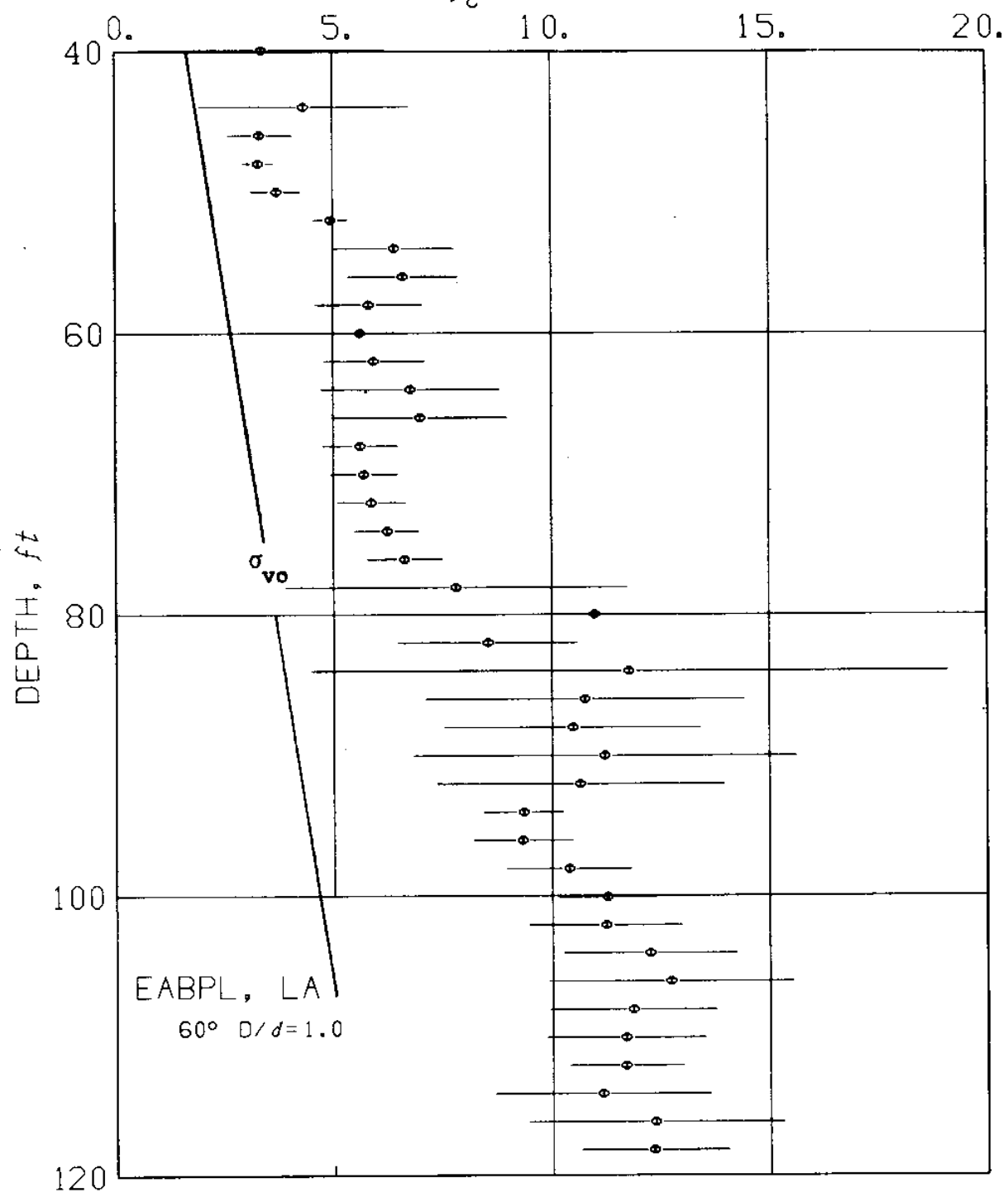
Fig. 6.7 Effects of filtering on the mean and standard deviation of q_c. (c) Filtered data with Δ = 2ft, a = 2.5.
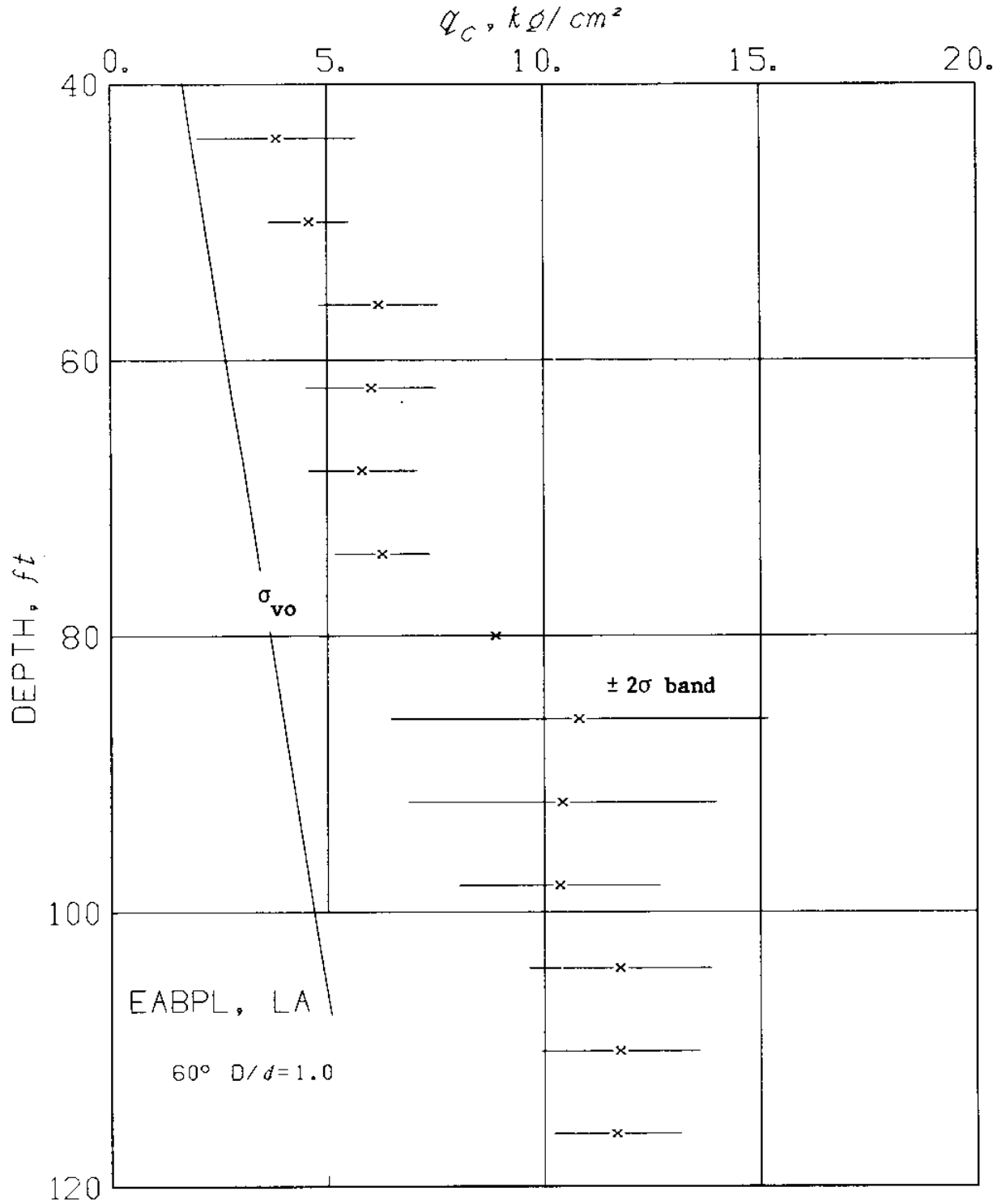
Fig. 6.7 Effects of filtering on the mean and standard deviation of q_c,
(d) Filtered data with Δ = 6ft, a = 2.0.

CUMULATIVE SAMPLE AND THEORETICAL PDFS

```
0.1000E+01  .................................................................
            .                              I                44     1HH HH 2           .
            .                              I               444   HHHH                 .
            .                              I               44  HH        33 11      3  3
0.9000E+00  .                              I               44 HH1   3333              .
            .                              I              44426I  3333                .
            .                              I               44 211  33                 .
            .                              I              44 2H1  33                   .
            .                              I              4 211  3                      .
0.8000E+00  .                              I             44H11 333                     .
            .                              I             44H1  33                       .
            .                              I             44H1 J33                       .
            .                              I            H221 J3                          .
            .                              I            HH21 3                           .
0.7000E+00  .                              I            44H11JJ                         .
            .                              I            44 H1 33                         .
            .                              I            44 H1 33                         .
            .                              I           44 H1 33                          .
            .                              I 44 HH 33                                    .
0.6000E+00  .                              I44 1H 33                                    .
            .                              44 1HJ33                                      .
            .                              44 1HJJ                                       .
            .                              4I12J11                                       .
            .                              4 11231                                       .
0.5000E+00  .                              HH11H33                                      .
            .                              44112H                                        .
            .                              441124                                        .
            .                              411 HJ                                         .
            .                              H41 H31                                        .
0.4000E+00  .                              H11H  1                                       .
            .                              401H  I                                        .
            .                              44110  I                                       .
            .                              4410  I                                        .
            .                              44 123  I                                      .
0.3000E+00  .                              4 1HH3  I                                      .
            .                              4418H3  I                                      .
            .                              441HH3  I                                      .
            .                              441HH3  I                                      .
            .                              44 HH3  I                                      .
0.2000E+00  .                              4 HH3  I                                       .
            .                              41HH33  I                                      .
            .                              44H2 J  I                                      .
            .                              44HH33  I                                      .
            .                              442H133  I    1 = SAMPLE PROBABILITY DENSITY FUNCTION  .
0.1000E+00  .                              444221 3  I    2 = NORMAL PROBABILITY DENSITY FUNCTION  .
            .         4      44   444444 22211  33  I    H = 1 AND 2                               .
            .                   444422H11 33  I                                                    .
            .                    2222 11 333  I    3,4 = 95% CONFIDENCE BANDS                      .
0.0         H**********H****HH**HH3333333333****......................................
        -0.3221E+01      -0.1889E+01      -0.5565E+00      0.7756E+00      0.2108E+01      0.3440E+01
```

SAMPLE VALUES

(a) BOSTON BLUE CLAY

Depth: 26 to 72 ft

3 standard cone tests

636 data points

Fig. 6.8 Cumulative probability density function of x, its Kolmogorov-Smirnov band, and the cumulative normal probability density function (mean = 0, σ = 1). Circles denote where normal pdf falls on the confidence limit.

CUMULATIVE SAMPLE AND THEORETICAL PDFS

Fig. 6.8 (cont'd.).
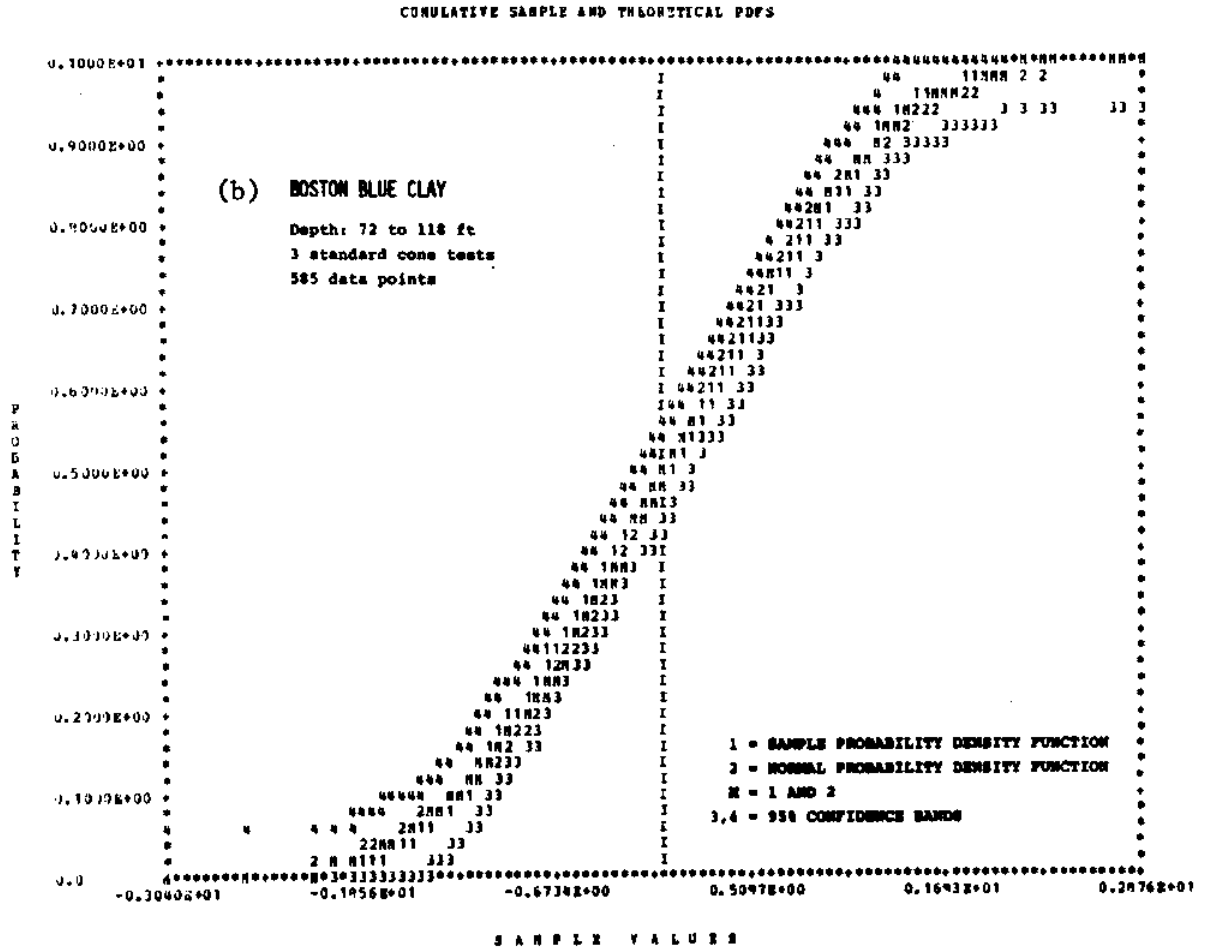
COEFFICIENT OF VARIATION, V
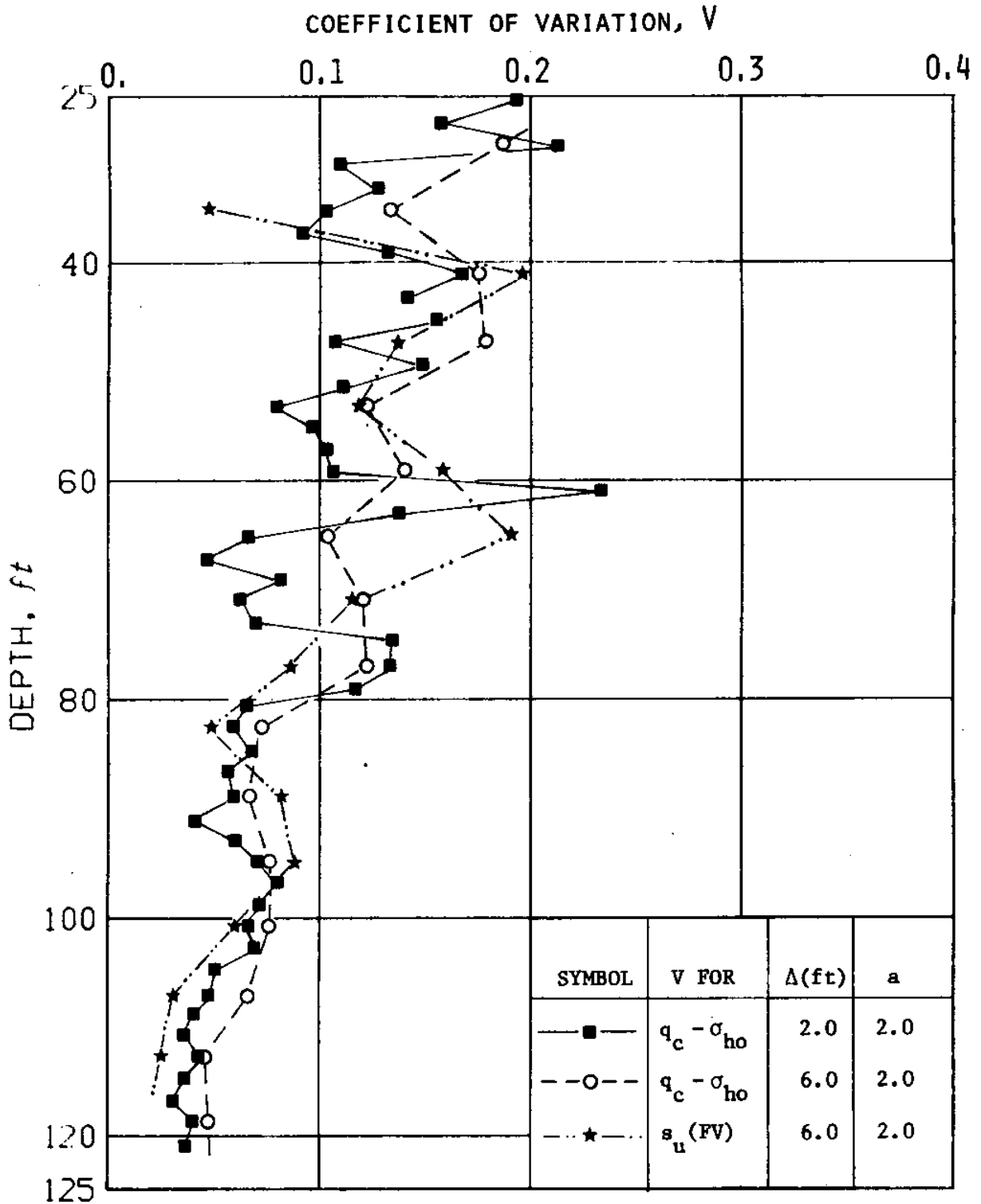
Fig. 6.9a Coefficients of variation of cone resistance and the
field vane strength, Boston Blue Clay.
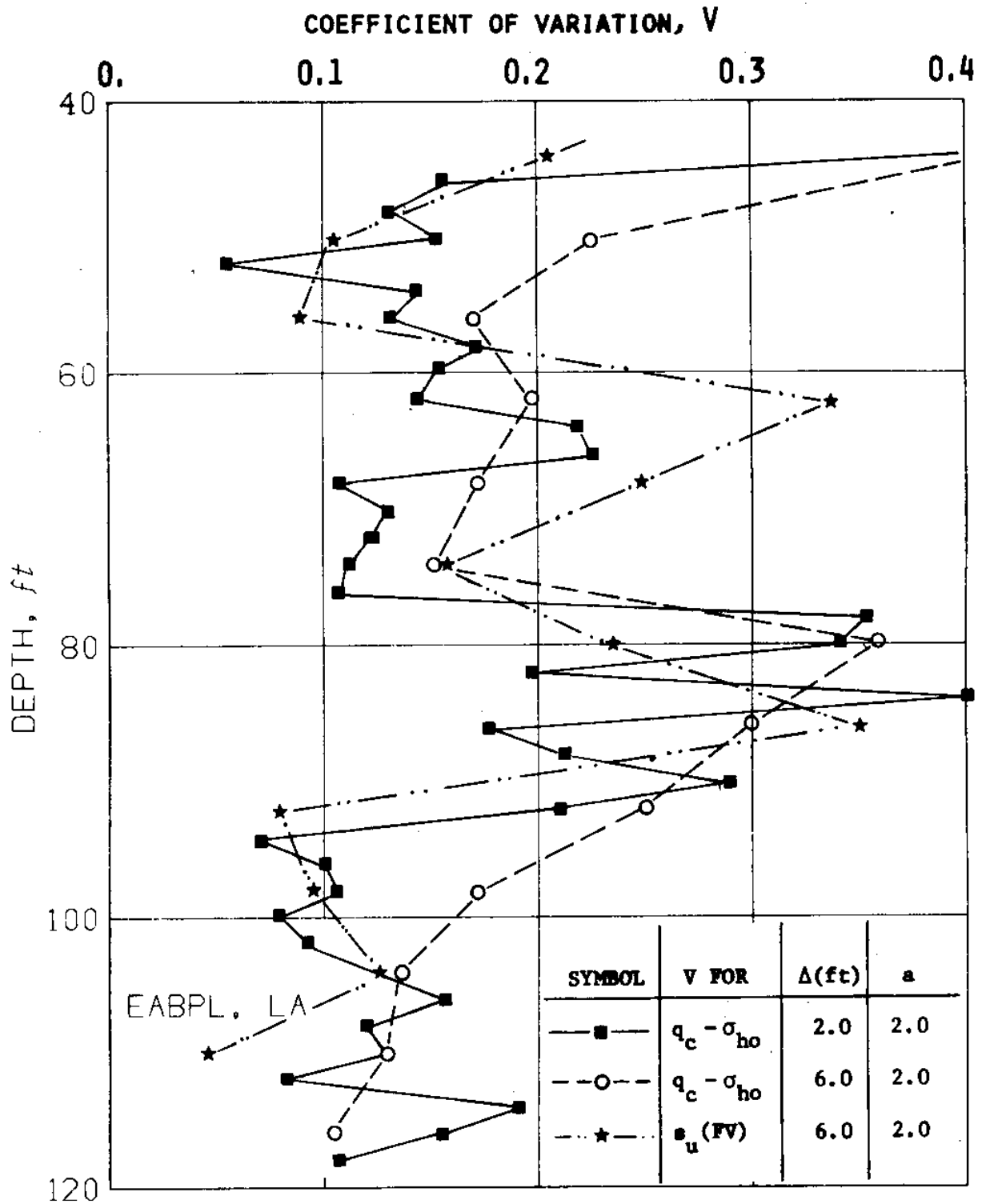
Fig. 6.9b Coefficients of variation of cone resistance and field
vane measurements in EABPL Clay.
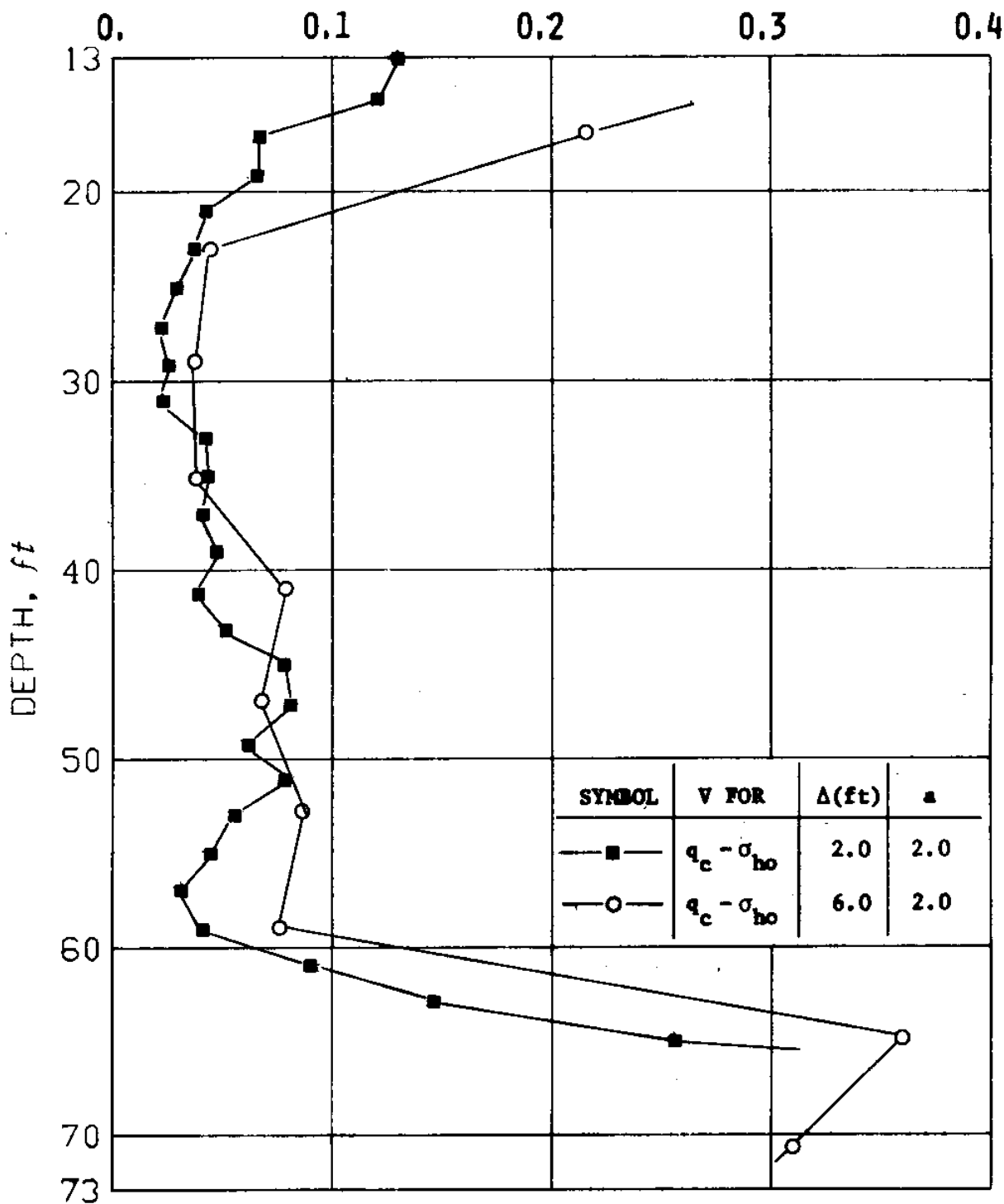
Fig. 6.9c Coefficients of variation of cone resistance in
Connecticut Valley Varved Clay.

CHAPTER 7

TEST RESULTS

7.1 Introduction

This chapter presents field measurements obtained from more than 6,000 ft

of cone penetration in three clay deposits. Results of cone resistance, q_c,

and pore pressures, u, during steady state penetration are compared to deter-

mine the effect of cone angle, 2δ, tip enlargement, D/d, penetration velocity,

and clay type. In addition, pore pressures at different locations on the cone

and the pushing rods behind it are presented and the cone resistance of elec-

trical cones is compared to that of the mechanical cones.

Chapter 4 presents theoretical concepts that strongly affected the selec-

tion of the field testing program outlined in Chapter 5 (equipment, clay depo-

sits, measurements.., etc.). Chapter 6 describes the filtering and averaging

methods used in order to simplify the comparison of the extensive data avail-

able. Filtering and averaging was generally performed with Δ = 2 ft and a = 2

(see Chapter 6) unless otherwise stated. Available equipment allows one type

of measurement per test, i.e., q_c or u. When more than one test of the same

characteristics (same 2δ and D/d) is performed, the _average_ of these tests is

presented. This is important in evaluating the following comparisons since

possible soil variability in different tests must always be kept in mind.

7.2 Cone Penetration Resistance

(1) _Effect of cone angle._ Figures 7.1 show q_c profiles in Boston Blue

Clay and EABPL Clay from "enlarged" cones (D/d = 2) with three different apex

angles (2δ): 60°, 30° and 18°. As predicted by the theory in Chapter 4,

q_c in both deposits increases as δ decreases. In Boston Blue Clay, Fig. 7.1a,

$q_c(2\delta = 18°)$ is about 30% greater than $q_c(2\delta = 60°)$ throughout the profile

as predicted for the idealized enlarged cones with very large D/d (Eq. 4.2).

For EABPL Clay, Fig. 7.1b, the difference between $q_c(2\delta = 18°)$ and $q_c(2\delta = 60°)$ is only 10 to 20% between depths of 40 and 80 ft, but increases to about 30% below depths of 90 ft. Measurements of enlarged cone resistance in Connecticut Valley Varved Clay (CVVC) were not conducted.

Figures 7.2 show the effect of cone angle on q_c for unenlarged or "regular" cones (D/d = 1). As for enlarged cones, q_c increases as 2δ decreases. In Boston Blue Clay, the difference between $q_c(2\delta = 18°)$ and $q_c(2\delta = 60°)$ is generally more pronounced than for enlarged cones, whereas in EABPL and Connecticut Valley Varved Clays, it is generally less pronounced (less than 20%).

Muromachi (1974) reports similar effects of cone angles on q_c in a resedimented clay. The cone used is a hand penetrometer of the type shown in Fig. 7.3a, with a D/d = 3.2 and a projected tip base area of 6.45 cm^2. He finds that q_c remains relatively constant for $2\delta \geq 30°$, and that $q_c(2\delta = 15°)$ is about 25% higher than $q_c(2\delta = 60°)$.

(2) <u>Effect of cone shape</u>. Figures 7.3 show various cone types and shapes in common use. The force required to push the mechanical cones in Figs. 7.3a, b and c is measured at the surface by means of oil pressure gage, proving ring, etc., whereas electro-mechanical transducers are used for the electric cones in Figs. 7.3d and e. In order to study the effect of tip shape on cone resistance, tests were conducted by means of the Fugro equipment using cones with different tip enlargement ratios (D/d), and the results were then compared with the mechanical cone (Fig. 7.3c).

The effect of tip enlargment in the more uniform Boston Blue Clay is illustrated by Fig. 7.4a for the three cone angles $2\delta = 60°$, 30° and 18°. Noting that each test is performed in a separate hole, an allowance must be made for soil variability when comparing results of regular cones (D/d = 1) to enlarged cones (D/d = 2). An estimate of this effect is given

by Fig. 6.5 which shows that soil variability can account for 2 to 3 kg/cm^2 difference in cone resistance between one test to another. Bearing this in mind, we can see in Fig. 7.4a that:

1.   In the soft (slightly overconsolidated) clay below a depth of 70 ft, the resistance of regular cones (D/d = 1) exceeds the cone resistance of enlarged cones (D/d = 2) for all three cone angles. This difference in q_c tends to increase with depth and is about 50 to 80% of the initial vertical total stress.[*]

2.   In the overconsolidated clay above a depth of 70 ft, no consistent trend between regular and enlarged cones can be detected for the three cone angles tested. In fact, the differences in q_c between regular and enlarged cones in the upper clay can be due to the scatter resulting from possible soil variability between different holes.

3.   The above effects of tip enlargement are in general agreement with the theory presented in Chapter 4 which can only predict that q_c of enlarged cones is "less" than regular cones. A rigorous justification of the inconsistent difference in q_c (between regular and enlarged cones) throughout the profile is difficult to achieve. However, a possible exploration of this phenomenon can be provided by a simplified model based on the soil tendency to squeeze in behind enlarged cones. When the soil is "strong" enough, it can conceivably withstand a cylindrical hole behind a penetrating enlarged cone with little (or no) squeezing-in. In such a case, the (normal) pressure on the rigid pushing rods (or sleeve) behind a regular (unenlarged) cone should not be significantly different from an enlarged cone. On the other hand, "weak" soils with a tendency to

---

[*]or about 20% of q_c (D/d = 1).

squeeze-in behind enlarged cones require a larger pressure on the pushing

rods behind regular cones to maintain the soil cylinder with the same

diameter as the cone. Since an increased pressure behind the cone causes

an increase in cone resistance, this argument leads to the conclusion that:

the difference in q_c between regular and enlarged cones increases in

"weak" soils which tend to squeeze-in behind enlarged cones. In this con-

text, a possible distinction between "weak" and "strong" soils can prob-

ably be provided by the ratio of the total stress (as expressed by σ_{vo},

say,) and the undrained shear strength of the soil, s_u. High values of

σ_{vo}/s_u indicate the presence of a weak soil where a difference between

q_c (regular) and q_c (enlarged) is expected. Figure 5.16a shows the profile

of σ_{vo}/s_u in Boston Blue Clay where s_u is determined by the field vane

test. High values of $\sigma_{vo}/s_u = 12$ to 13 occur below a depth of 80 ft in

the zone where the effect of tip enlargement is clear, Fig. 7.4a. Figure

5.16a also shows that the overconsolidation ratio, OCR, of the deposit is

an equally good measure of soil weakness since it is (generally) correlated

to σ_{vo}/s_u.

The effect of tip enlargement in EABPL clay is shown in Fig.

7.4b for cone angles $2\delta = 60°$ and $18°$. After excluding results in the

highly variable layer between depths 77 and 95 ft (see Fig. 6.5), Fig.

7.4b indicates that:

1) For a cone angle $2\delta = 60°$, the effect of tip enlargement in

EABPL clay is similar to BBC: above a depth of 70 ft, the difference

between q_c (regular) and q_c (enlarged) is difficult to detect in view of

soil variability. On the other hand, below 70 ft, q_c (regular) is con-

sistently larger than q_c (enlarged).

2) Results for $2\delta = 18°$ show no clear effect of tip enlargement throughout the profile of EABPL clay, probably because of the very variable nature of this deposit.

Thomas (1965) determines the effect of tip enlargement on q_c in London Clay by means of the mantle cones shown in Fig. 7.3b. The base area of his "regular" cone tip equals 10 cm^2 and his "enlarged" tip is 20 cm^2 . He finds that the effect of tip enlargement is not noticeable at a depth less than 15 to 20 ft, but becomes pronounced at a greater depth where q_c (regular tip) exceeds q_c (enlarged tip) by about 15 to 25%. At his test site, however, the clay is much stiffer below a depth of 25 ft than the clay above. This suggests that OCR alone is not sufficient to explain the variation in the effect of tip enlargement on q_c.

Joustra (1974) compares q_c measurements from Fugro and Delft electrical cones (Figs. 7.3d and c). The Fugro cone has an unenlarged tip, whereas the Delft is slightly enlarged (D/d = 1.3). The soil at the test site consists basically of 25 ft of soft clay overlying dense sand. Results indicate that q_c (Fugro) equals or only slightly exceeds q_c (Delft) in the clay, but exceeds q_c (Delft) by 30%, on the average, in the deeper sand. This provides another indication that a tip enlargement tends to reduce q_c when the overburden stress is high (compared with the strength of the soil). At shallow depth, enlargement of the tip has little or no effect on q_c, probably because the hole left behind the cone tip has little tendency to close.

(3) Electrical cone vs. Begemann cone. The Begemann mechanical cone shown in Fig. 7.3c has a large mantle area behind the tip, on which some friction acts and hence can overestimate the actual cone resistance, q_c.

Figure 7.5 compares q_c for Fugro cones with 60° enlarged and unenlarged tip

with q_c for a Begemann mechanical cone in Boston Blue Clay. q_c (Begemann

cone) exceeds q_c (electrical cones) by about 20% above a depth of 70 ft,

where q_c (D/d = 1) $\approx q_c$ (D/d = 2), but is approximately equal to q_c (D/d = 2)

below that depth. However, the profile for q_c (Begemann) differs sub-

stantially from that of q_c (D/d = 1) or q_c (D/d = 2). This difference is

most likely due to friction on the mantle behind the tip and the weight of

the pushing rods* in the Begemann cone. The dashed line in Fig. 7.5 shows

q_c (Begemann) "corrected" for the weight of the rods. The "corrected"

q_c (Begemann) profile agrees reasonably well with q_c (D/d = 2) but consis-

tently exceeds it by 40 to 75%. This is probably due to the friction on

the mantle behind the tip.

Other investigators report similar effects of friction on the

mantle behind the tip. De Beer et al. (1974) observe that, in stiff clay,

q_c (mantle cones) exceeds q_c (mechanical cone without mantle, Fig. 7.3a) by

about 40%. Brand (1974) reports that, in soft clay, q_c (mantle cones)

exceeds q_c from a hand penetrometer (similar in shape but about 2/3 the

size of the cone in Fig. 7.3a) by about 25%.

(4) Effects of penetration rate. Penetration rate (velocity)

affects the cone penetration process by influencing the rate of straining

in the soil around the cone. Figures 7.6a and b show changes in q_c due to

changes in penetration rate (from a standard rate of 2 cm/sec) in Boston

---

*The steel inner pushing rods have a diameter of 1.3 cm and a cross-
sectional area of 1.7 cm^2. The contribution of their weight to q_c (Begemann)
is approximately equal to 70% of σ_{vo} and should be added to the cone
resistance measured by a load cell at the surface (Schmertmann, 1975).

Blue Clay and EABPL Clay. These results are obtained by increasing or decreasing the penetration rate by 5 to 10 times during selected depth intervals of 0.5 to 2 m. Clearly, q_c tends to increase when the penetration rate increases for both regular and enlarged cones. The magnitude of this increase is difficult to determine accurately because of the scatter in q_c (at constant penetration rate) caused by soil variability, especially that the increase in q_c is small (about 10%) due to a large (tenfold) increase in penetration rate, Figs. 7.6a and b. This is approximately the same effect of strain rate determined by laboratory undrained shear strength tests (Ladd et al., 1977). Similar effects of penetration velocity on q_c are reported by Thomas (1965) and Muromachi (1974).

(5) Access to water. The theory in Chapter 4, predicts that a cavity forms behind enlarged cones (D/d = 2) and that the pressure in this cavity affects cone resistance. One possible method of checking this theory consists of comparing q_c when this cavity is filled with water to q_c when the cavity is not (necessarily) filled with water by changing the access to water behind the cone. Penetration tests using enlarged cones where the cone is pushed through a predrilled hole (about 2 ft deep) filled with water are therefore compared with penetration tests conducted from the surface. Figures 7.7 compare q_c (wet), where water is available behind the cone, with q_c (dry), where the cone is pushed from the surface. For a cone angle $2\delta = 60°$, Fig. 7.7a indicates that q_c from "wet" and "dry" tests are essentially identical, except at a depth of 85 ft, where the q_c (dry) is very high, probably due to the presence of a sand lense. For a cone angle $2\delta = 18°$, Fig. 7.7b shows that q_c (wet) is 10% to

20% higher than q_c (dry) along most of the deposit.[*] Since this difference can be due to soil variability (see Fig. 6.5a), no clear effect of access to water can be reached from the limited tests performed.

(6) <u>Scale effects</u>. For cones with the same geometry, a change in cone size affects cone resistance in two ways. First, it influences strain-rate in the soil around the cone because, for the same penetration velocity, the strain-rate is inversely proportional to the diameter of the cone. However, results of strain-rate effects presented earlier indicate that this factor is relatively unimportant. The second scale effect results from soil inhomogeneities. Larger cones cause deformations, strains and stresses in a larger volume of soil. Inhomogeneities in the soil due to the presence of varves, fissures or other impurities having sizes of the same order as the cone are expected to affect q_c.

The present testing program did not investigate scale effects. Muromachi (1974) varies the base area of the cone from less than 2 cm^2 to 20 cm^2 while keeping the shape[**] constant. He finds that q_c in remolded clay decreases about 15% due to a tenfold increase in diameter. This is in general agreement with predictions based on strain rate effects. De Beer et al. (1974) vary the cone diameter from 3.6 cm to 25 cm, using the cone shape shown in Fig. 7.3a. Penetration tests in stiff clay indicate

---

[*] If the cavity in the "dry" test is not filled with water, the theory predicts the q_c difference to be 25% of the pore pressure measured behind the cone tip. This pore pressure is approximately the same as the left-most curve in Fig. 7.11a. Therefore, the theory predicts that the difference between q_c (wet) and q_c (dry) to be 0.5 to 1 kg/cm^2 (assuming zero pressure in the cavity behind the "dry" cone).

[**] 60° cone. Geometry unclear from his paper.

that the increase in cone diameter generally causes a 0 to 30% reduction in q_c.

In conclusion, scale effects can affect q_c. Their importance is probably on the same order as scale effects on laboratory testing of soil samples. However, in uniform clays, no significant scale effects are expected due to doubling the diameter of the cone (as in our tests on enlarged cones).

(7) <u>Friction sleeve measurements</u>. Because of the analogy between cone penetrometers and piles, many investigators have devised methods to measure the frictional resistance of soil during cone penetration in addition to cone resistance q_c. The ratio between the shearing force per unit area, f_s, exerted on the friction sleeve behind the cone and q_c is often used for soil identification. For mechanical cones, typical correlations between f_s/q_c and soil type are given below:

<u>Begemann (1965)</u>

Soil Type	$f_s/q_c(\%)$
Coarse to fine sand	1-1.5
Silty sand	1.5-2.5
Clayey sand	2.5-3.5
Loam	3.5-4
Clay	4-6

<u>Sanglerat (1972)</u>

Soil Type	$f_s/q_c(\%)$
Sands	1-2
Clays, silts, sands	1-4
Clays	4-8
Clays and peat	3-10

Measurements of f_s made with the Fugro electrical cone at the Saugus and Amherst, Massachusetts, test sites did not yield reasonable results (f_s is often negative at large depth). This is probably due to the small

value of f_s compared to equipment uncertainties. In the Atchafalaya

Basin Clay, the f_s/q_c ratio varies generally between 2 and 7%,[*] with

f_s tending to increase with q_c.[**]

7.3 Pore Pressures During Steady Cone Penetration

Pore pressures developed during steady state cone penetration are

essential in the understanding of the cone penetration process. This

section presents measurements of pore pressures at different locations on

four cones with different geometries. The data in this section are from

the Saugus, Massachusetts, test site, where extensive pore pressure mea-

surements were obtained[***] and where the clay deposit is relatively uni-

form, thus allowing an easy comparison of test results.

Figures 7.8 show the measured pore pressures, u, during the steady

penetration of 18° enlarged and unenlarged cones. Different curves repre-

sent the results obtained in adjacent holes. For the unenlarged cone,

Fig. 7.8a indicates that, above a depth of 40 ft, the u profiles are not

consistent, probably because of significant soil variability. Below 40 ft,

all u profiles are approximately parallel and show the same pattern

with depth. The largest pore pressure u is measured at mid-height of the

cone (curve "2") and decreases behind the tip. Torstensson (1975)

---

[*] Data including cone tests at Bayou Sorrel, LA, performed by Fugro
Gulf, Inc., for Ardaman and Assoc., Inc., in 1977, courtesy of Ardaman and
Assoc.

[**] Test loading of some cones indicates that readouts of f_s and q_c are
not perfectly uncoupled.

[***] In addition to steady penetration, pore pressures during driving,
after penetration stops, during and after monotonic or cyclic axial or
rotational motion, were measured and will be reported elsewhere.

observes similar trends in pore pressures measured at the tip and behind a 60° cone during steady penetration in a normally consolidated clay, using a different probe design.

Pore pressures measured at the tip of the cone (curve"1") are about 1 kg/cm^2 lower than at the middle of the cone (curve"2").[*] On the cylindrical shaft behind the conical tip, u decreases for a distance of 4d to 5d (d is the shaft diameter = 3.8 cm for the pore pressure probes), and then appears to remain constant, at least to a distance of 11d behind the tip.

Pore pressure variation along the cone and the shaft behind it can result from one of two reasons:

1.   a change in the total stress along the cone and shaft;

2.   pore pressure dissipation, i.e., soil consolidation.

In order to assess the effect of consolidation on the pore pressure difference between points 3 and 6 on the shaft behind the cone, we first estimate the time required for a soil particle to travel the distance 11d between the two points. For a penetration velocity of 1 to 2 cm/sec used in the tests, this time is about 20 to 40 sec. During such a time period, records of pore pressure decay after penetration is stopped (for a u measurement behind the tip) indicate that little consolidation takes place. This, in addition to the very close values of u at points 5 and 6, suggest that the measured pore pressures in Fig. 7.8a reflect the variation in the total stresses along the cone and shaft. The magnitude and variation of these total stresses, in turn, affect cone resistance.

---

[*] Pore pressure at the tip is measured with probes similar in design to Fig. 5.2a. The porous stone in these probes protrudes slightly in front of the conical tip of the instrument. Figure 5.2c shows a photograph of the 18° conical probe.

Figure 7.8b shows the steady state pore pressures u along an 18° en-
larged cone (D/d = 1.9). As in the case of an unenlarged cone, we note
that u at the cone tip (curve "1") is greater than u behind the cone (curves
"2" and "3"). The pore pressure at the tip is essentially the same as
u (tip) for an unenlarged cone, Fig. 7.8a. Furthermore, u behind the
enlarged cone is uniform along the shaft at least up to a distance 11d.
This supports the theoretical prediction of a cavity behind enlarged
cones. Comparing this cavity pressure to the pore pressures far behind an
18° unenlarged cone (curves "5" and "6" in Fig. 7.8a), we note that they
are essentially identical below a 70-ft depth, but at shallower depths u
behind the enlarged cone is about 0.5 to 1 kg/cm^2 smaller than u far
behind the unenlarged cone.

Figures 7.9 show the steady penetration pore pressures around enlarged
and unenlarged 60° cones. As in the case of 18° cones, Fig. 7.9a
indicates that u at the tip of an unenlarged cone is higher than u on the
shaft behind that tip. Figure 7.9b shows that u is uniform behind an
enlarged cone. u at a distance of 3.2d behind the tip of the unenlarged
60° cone is consistently about 1 kg/cm^2 larger than u behind the enlarged
60° cone, and is essentially identical to u at the same distance behind an
18° unenlarged cone (curve "4" in Fig. 7.8a). Since u is not measured
very far behind the 60° unenlarged cone, no conclusion can be drawn
regarding the effect of cone angle on this pore pressure. For the enlarged
cones, however, u behind the 60° cone is consistently about 0.5 to 1.0 kg/cm^2
larger than u behind the 18° cone.

The pore pressures behind cones are of practical interest in the under-
standing and prediction of shaft behavior during and after pile installa-
tion. From the data presented above, we note that these pore pressures

are generally large (> σ_{vo}) and therefore are expected to be important

in affecting pile behavior. Koizumi and Ito (1967) present measurements of

normal stresses and pore pressures on and around a jacked pile in silty clay

which show that the total stresses and the pore pressures on the pile

shaft are essentially equal, and that their magnitude is as much as 2 to

3 times σ_{vo}.

7.4 Comparison Between Steady State Pore Pressures and Cone Resistance

This section compares the pore pressures, u, measured during steady

penetration to the cone resistance, q_c, in three clay deposits using 60°

and 18° cones.

(1) <u>Boston Blue Clay</u>. Figure 7.10a shows q_c, u (tip) and u (far

behind) for an 18° unenlarged cone (2δ = 18°, D/d = 1). Clearly q_c exceeds

u throughout the profile. Above a depth of 60 ft (OCR > 2), both u (tip)

and u (far behind) are small compared to q_c. Below a 60-ft depth

(OCR = 1.2 to 2), u (tip) is about 70% of q_c, whereas u (far behind) is

about 55% of q_c.

Figure 7.10b shows q_c and u (tip) for a 60° unenlarged (2δ = 60°,

D/d = 1) cone which exhibits trends similar to the 18° cone in Fig.

7.10a. However, below a depth of 60 ft, u (tip) exceeds q_c by about 10%.

This is contrary to theoretical predictions in Chapter 4 and is believed

to reflect inaccuracies in q_c measurements.[*]

Figure 7.10c shows the smoothed profiles of the u/q_c ratio

---

[*] q_c measurements for unenlarged cones can underestimate the actual
cone resistance by as much as 15% due to pore pressures u acting behind the
tip (location 3 in Fig. 7.8a). This error is, however, reduced when u
at this location is small compared to q_c.

obtained from filtered u and q_c data where anomalies due to small scale inhomogeneities in the soil (e.g., sand or silt lenses) have been eliminated. All three u/q_c profiles in Fig. 7.10c increase with depth to about 70 ft and thereafter remain constant. Curve 1, corresponding to a 60° cone where u is measured at the tip, shows the highest value of u/q_c. Values of $u/q_c > 1$ attained by this curve below a depth of 60 ft are believed to be caused by inaccuracies in q_c measurements as discussed earlier.

(2) <u>Atchafalaya Basin Clay</u>. Figure 7.11a shows the cone resistance, q_c, the steady state pore pressure at mid-height of the cone, u (mid-cone), and u far behind an unenlarged 18° cone.[*] Generally, steady penetration pore pressures, u, are smaller in this plastic (high PI) clay deposit than in the lean (low PI) Boston Blue Clay. u (far behind) is less than σ_{vo} except beween depths of 40 to 53 ft, 70 to 82 ft, and below 95 ft, where it is approximately equal to σ_{vo}. These locations correspond to regions of normally consolidated clay (Fig. 5.16b). u (tip) shows a variation with depth identical to that of u (far behind), and the difference in their magnitudes is almost uniform in the normally consolidated regions, as was observed in the Boston Blue Clay below the desiccated crust. Both pore pressures tend to decrease when q_c increases. This important feature will be discussed subsequently when the ratio u/q_c is treated.

Figure 7.11b shows q_c and u (tip) for a 60° unenlarged cone. In

---

[*]Measurements of u (tip) are not available at the main test site; for u (mid-cone) see location 2 in Fig. 7.8.

this case, u (tip) exceeds q_c at a depth of about 50 ft, and is almost equal to q_c at a depth of 70 ft. Again, these locations of high pore pressure correspond to normally consolidated regions in the deposit.

Figure 7.11c shows the smoothed u/q_c profiles which clearly show three "soft" strata where u/q_c is "large". It is perhaps worth mentioning that the three curves in Fig. 7.11c showing identical patterns of u/q_c are obtained from five different instruments and seven soundings. This consistent feature of u/q_c indicates its great potential in soil profiling and soil identification. However, additional research is needed in order to use these results reliably in practice.

(3) <u>Connecticut Valley Varved Clay</u>. Figure 7.12a shows q_c and u (tip) for an 18° unenlarged cone. In this deposit, u (tip) is relatively close to q_c except in the desiccated crust near the surface and in the sandy material below a depth of 60 ft. Figure 7.12b shows q_c and u (tip) for a 60° unenlarged cone which shows the same pattern as the 18° cone, except that the difference between u and q_c becomes very small. Figure 7.12c shows that the smooth u/q_c profiles are relatively constant and equal to 0.8 to 0.9 between depths of 30 to 60 ft, where OCR varies between 1.3 and 2.

7.5 Summary

Extensive cone penetration measurements (q_c and u) in three clay deposits conducted to identify important parameters affecting cone penetration show that:

(1) The cone resistance q_c increases as the cone angle 2δ decreases (i.e., for sharper cones). The effect of 2δ on q_c is in general agreement with theoretical predictions presented in Chapter 4.

(2) The effect of enlarging the cone diameter with respect to the pushing rods tends to reduce q_c. However, the importance of this effect depends on the soil type. In "soft" clays (OCR $\approx$ 1), doubling the cone diameter reduces q_c by 0.5 to 1 times σ_{vo} (relative to "unenlarged" cone). In a "stiff" desiccated region, the effect of tip enlargement becomes very small or nonexistent.

(3) The mantle cone can significantly overestimate q_c, especially in "stiff" desiccated clay, where the friction acting on the sleeve is probably more pronounced. However, it may underestimate q_c in deep "soft" clay (OCR $\approx$ 1), due to the weight of the pushing rods.

(4) Moderate variations of cone penetration velocity (say, by a factor 2), from the standard rate of 1 to 2 cm/sec, is unlikely to cause any noticeable change in q_c. However, extensions of these results to the very slow shearing rates associated with actual field failures (which often require days or weeks to take place) require additional data.

(5) Pore pressure measurements, u, during steady cone penetration in clays at the "standard" velocity of 1 to 2 cm/sec show that u is not uniform at different locations on the cone and the pushing rods behind it. u at mid-height of the cone is larger than the u at the tip. Furthermore, u decreases behind unenlarged (regular) cones for a distance of 4 to 5 times the shaft diameter, d, and is more or less constant up to (at least) a distance of 11d. For enlarged cones, u is uniform behind the cone. These measurements indicate the existence of a non-uniform total stress field around the cone because no significant pore pressure dissipation is believed to take plase during steady cone penetration in the clays tested.

(6) Measurements obtained by means of 18° cones indicate that u (tip) is not significantly affected by tip enlargement. In "soft" clays, u at

a distance greater than 4d to 5d behind the cone is essentially identical

to u behind an enlarged cone. In Boston Blue Clay where extensive pore

pressure measurements are available, u at the tip of unenlarged cones and

u behind enlarged cones increases with increasing the cone angle, 2δ.

(7) In the soil deposits tested, u tends to decrease when q_c

increases. In "soft" clays (OCR $\approx$ 1) u (tip) varies between 0.6 and 1.1

times q_c. Values of u > q_c are believed to indicate inaccuracies in q_c

measurements. The ratio u/q_c, using u at the tip, mid-cone, or behind the

cone, is strongly correlated to the stress history of the soil and

might prove very valuable in detecting the overconsolidation ratio (OCR)

or clays. However, tests are required in a wider variety of clays because

u/q_c appears to depend on the clay type.
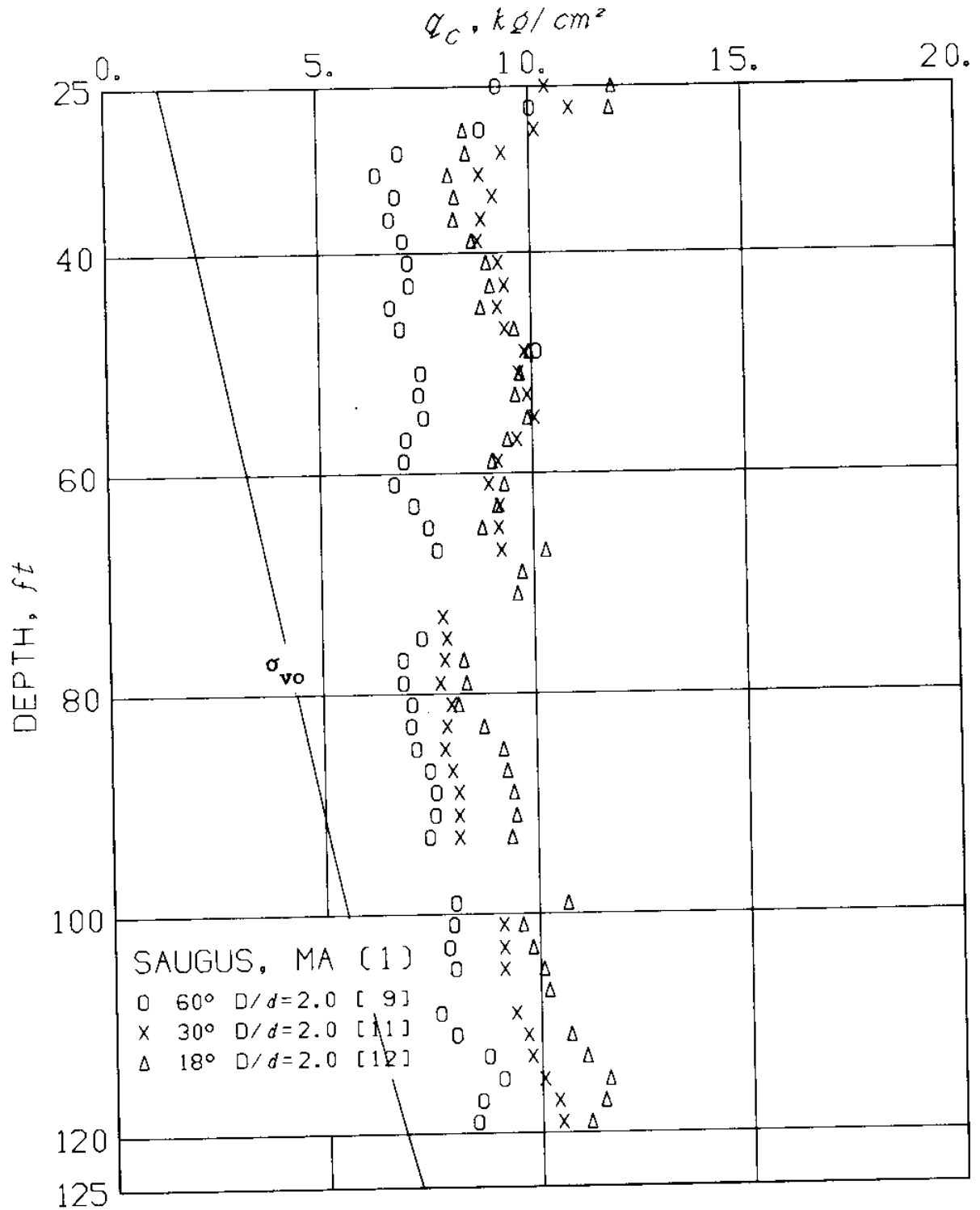
Fig. 7.1a Effect of cone angle on q_c from "enlarged" cones,
Boston Blue Clay.
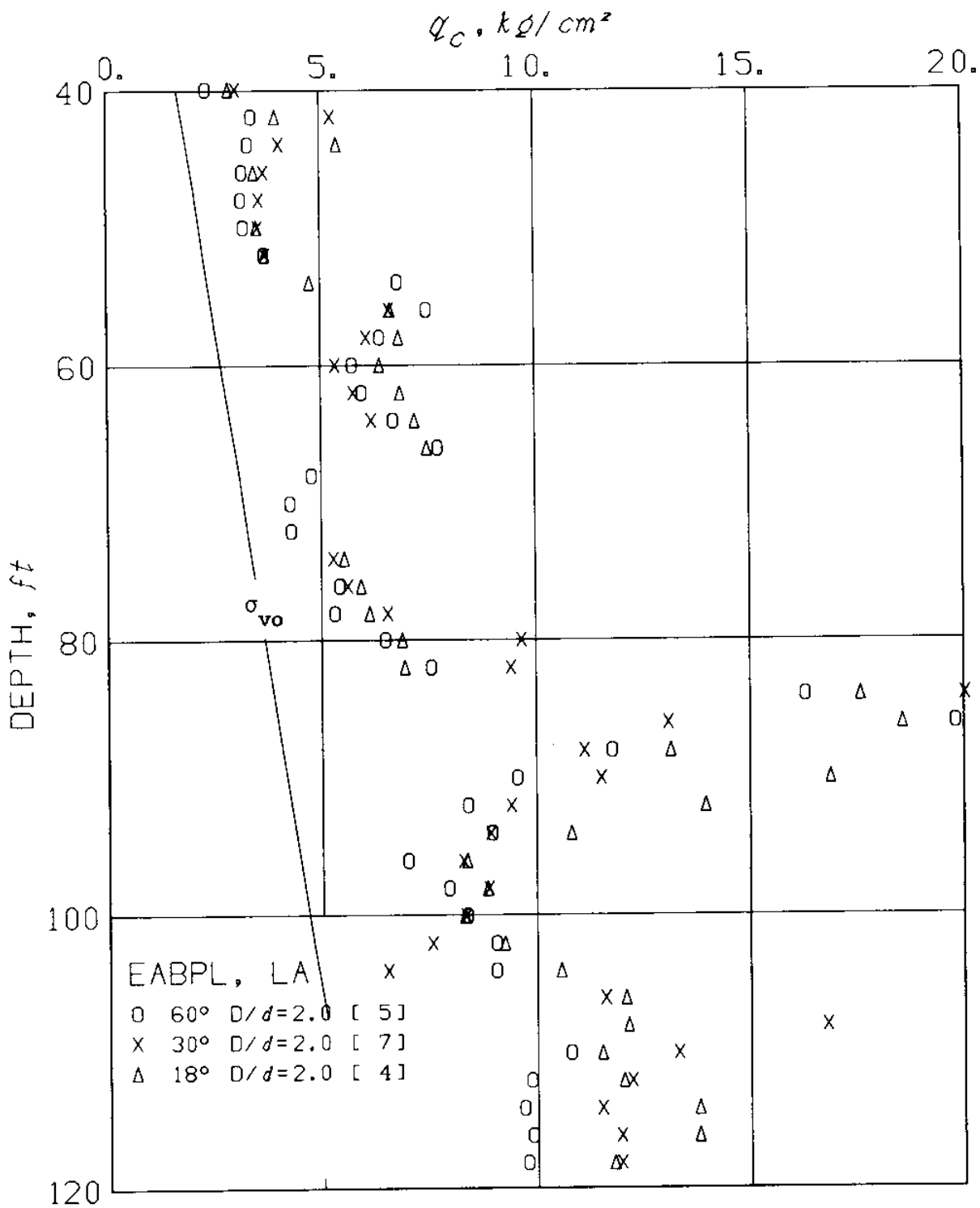
Fig. 7.1b Effect of cone angle on cone resistance from "enlarged" cones, EABPL Clay.
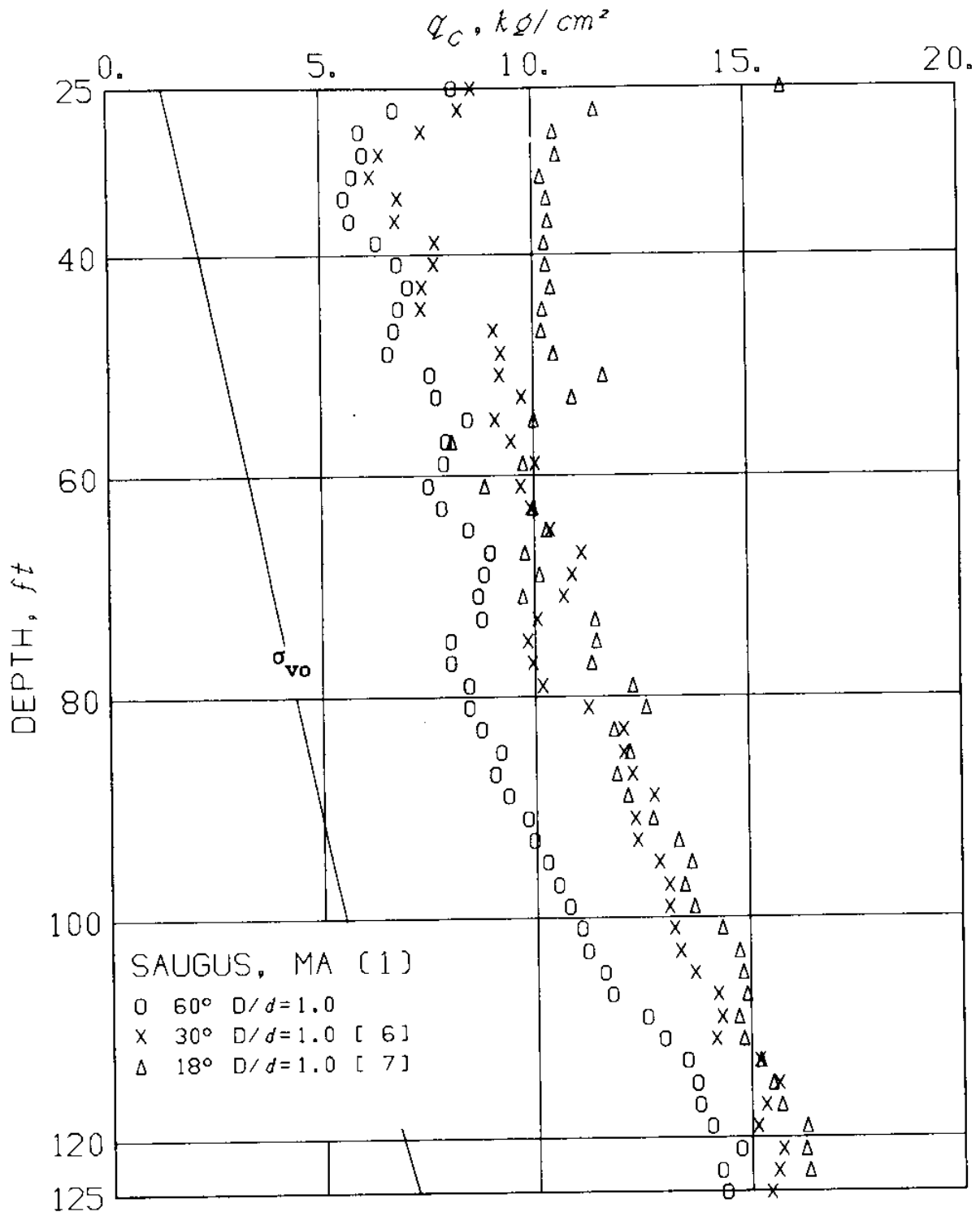
Fig. 7.2a Effect of cone angle on cone resistance of "regular" cones, Boston Blue Clay.
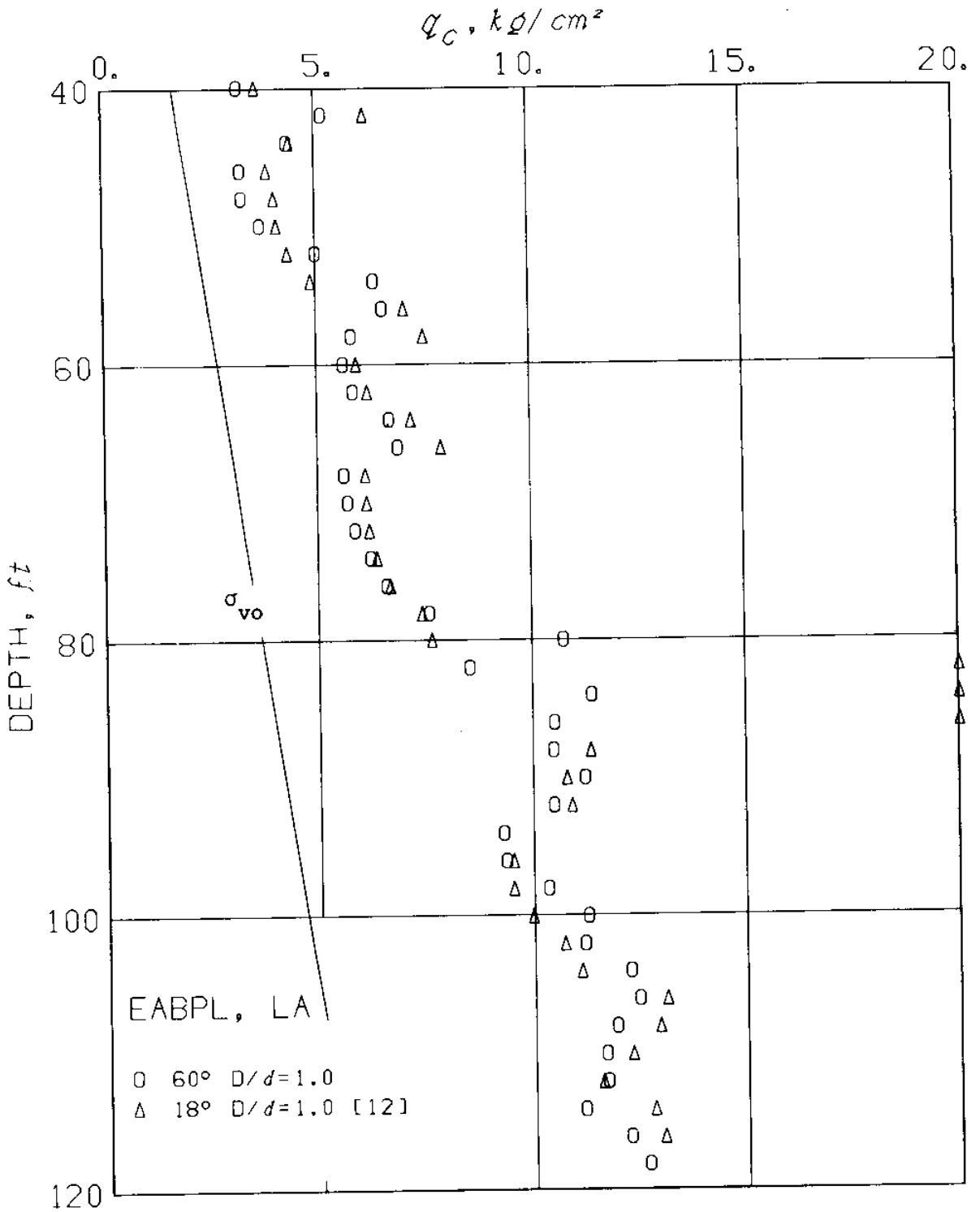
Fig. 7.2b Effect of cone angle on cone resistance of "regular"
cones, EABPL Clay.

q_C , $k\emptyset/cm^2$
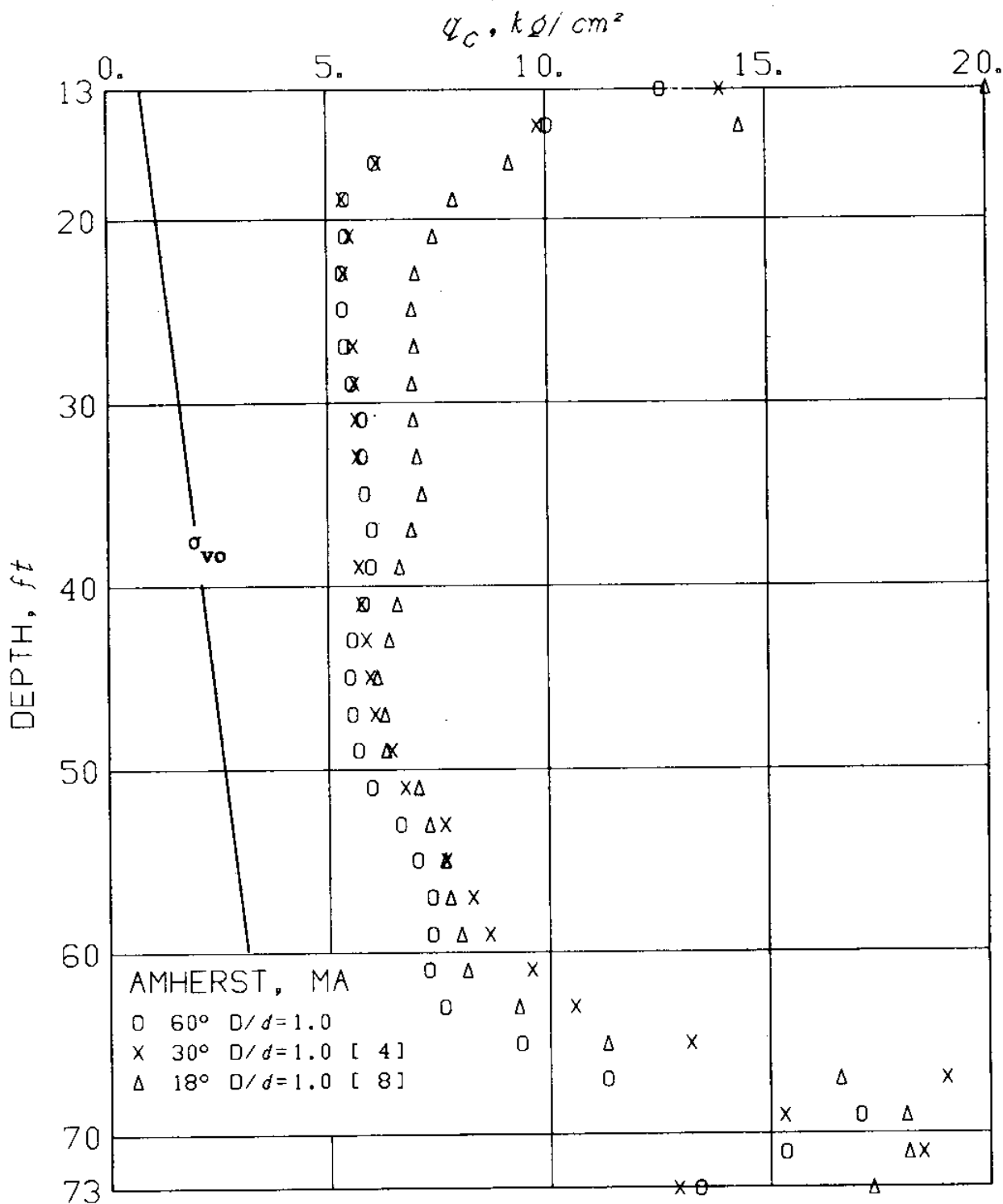
Fig. 7.2c Effect of cone angle on cone resistance from "regular"
cones, Connectidut Valley Varved Clay.
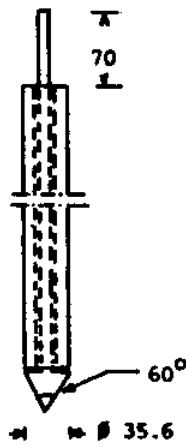
Fig. 7.3a
Original Dutch Cone
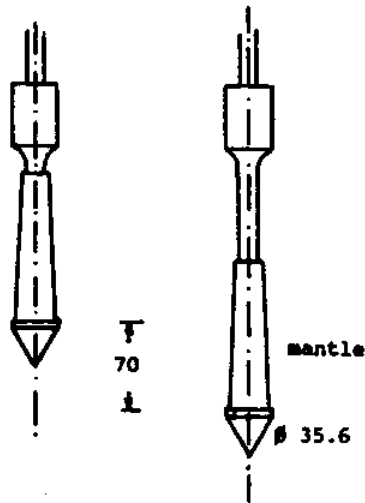
Fig. 7.3b
Mantle Cone
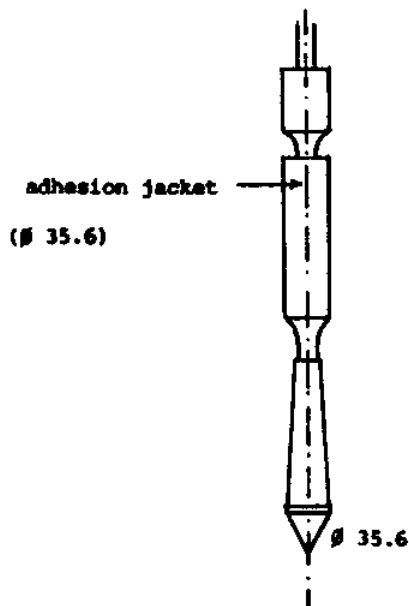
Fig. 7.3c
Adhesion Jacket Cone (Begemann)

Fig. 7.3d
Fugro Electric Cone

friction mantle (∅ 35.6)

∅ 35.6

friction mantle

Fig. 7.3e
Delft Electric Cone

300

200
∅ 28

∅ 35.6
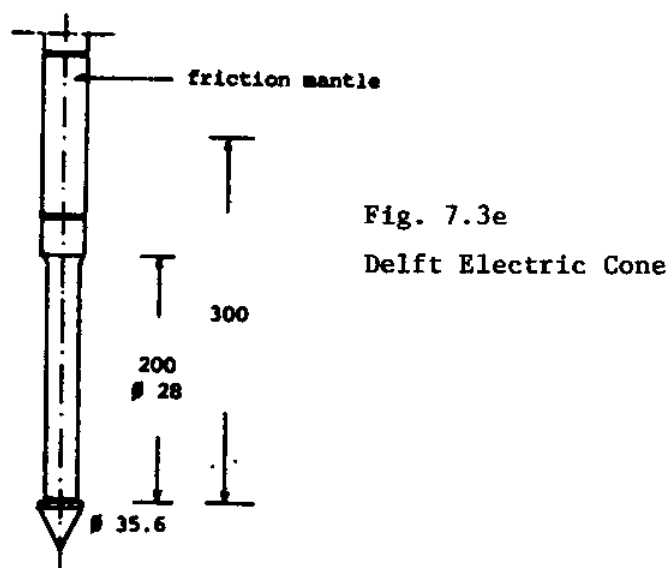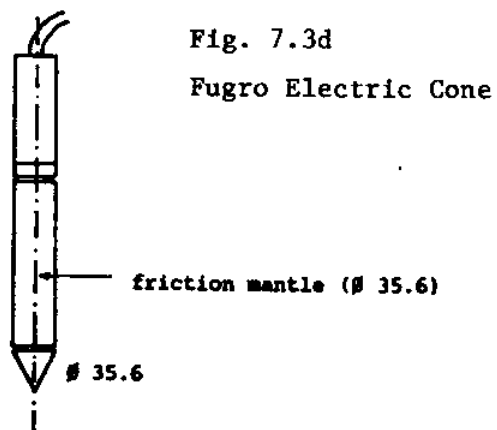
(Drawings adapted from Heijnen, 1974.)

Dimensions in millimeters
1 in = 25.4 mm.
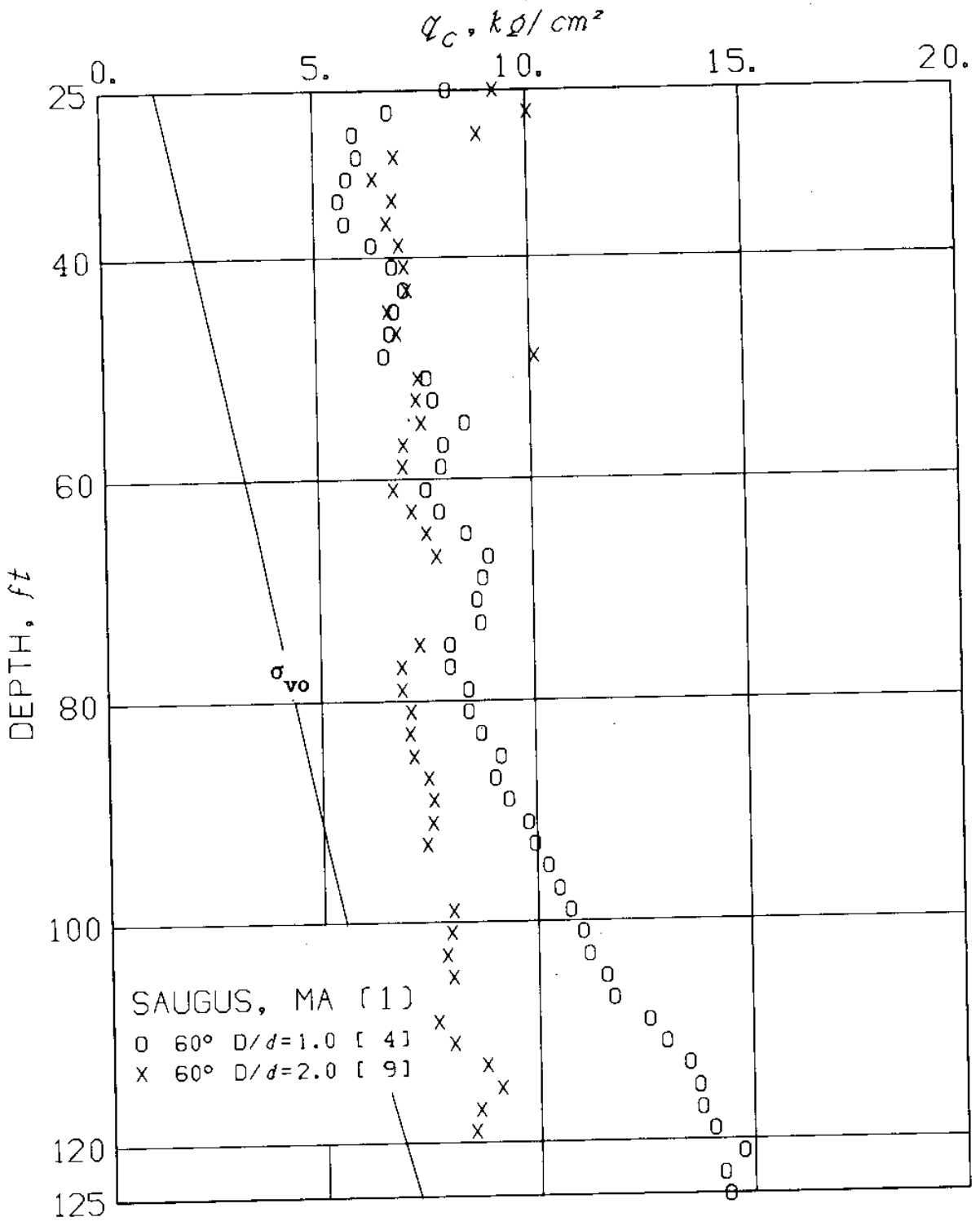
Fig. 7.4a Effects of tip enlargement on resistance, Boston Blue Clay.
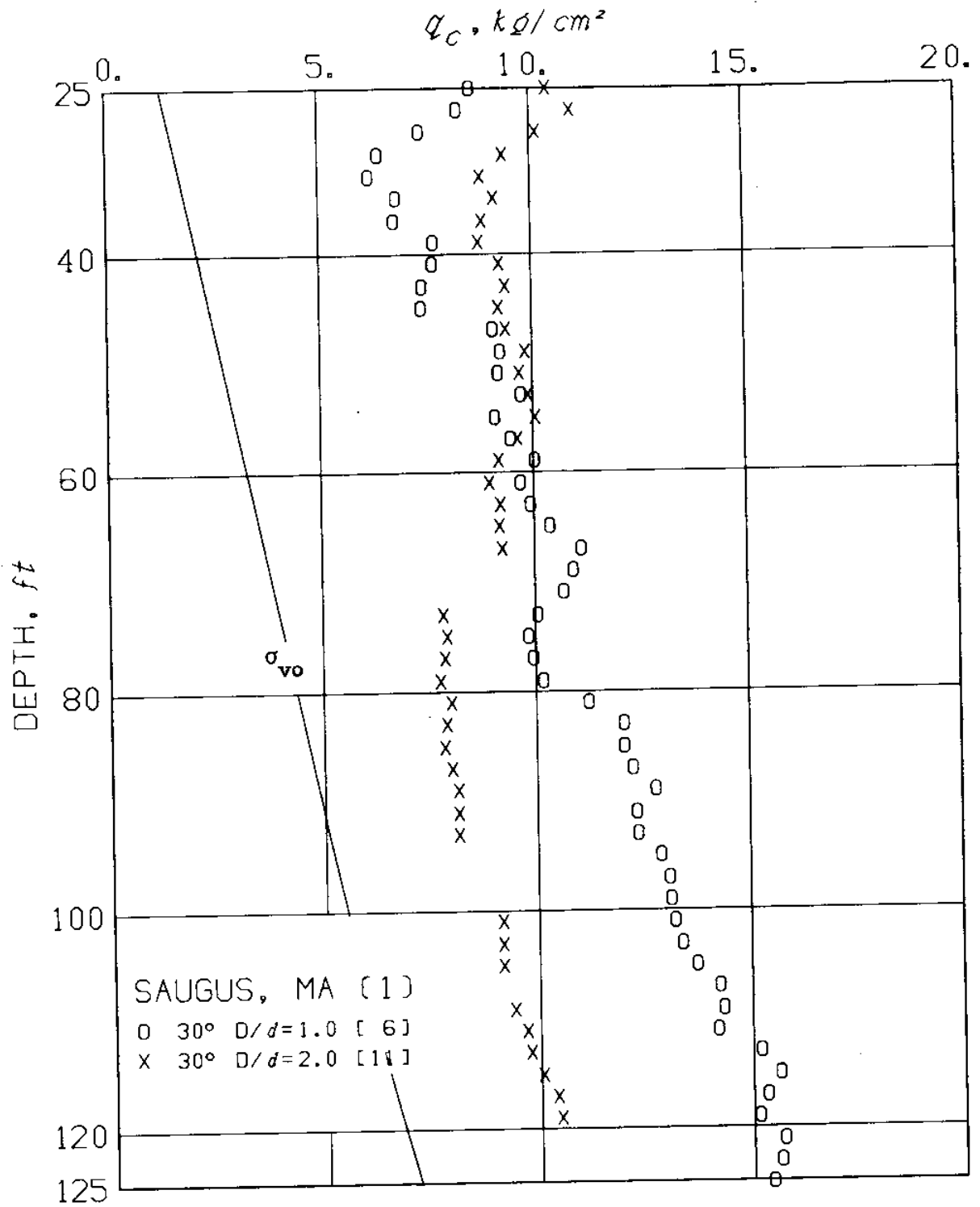
Fig. 7.4a (cont'd.).
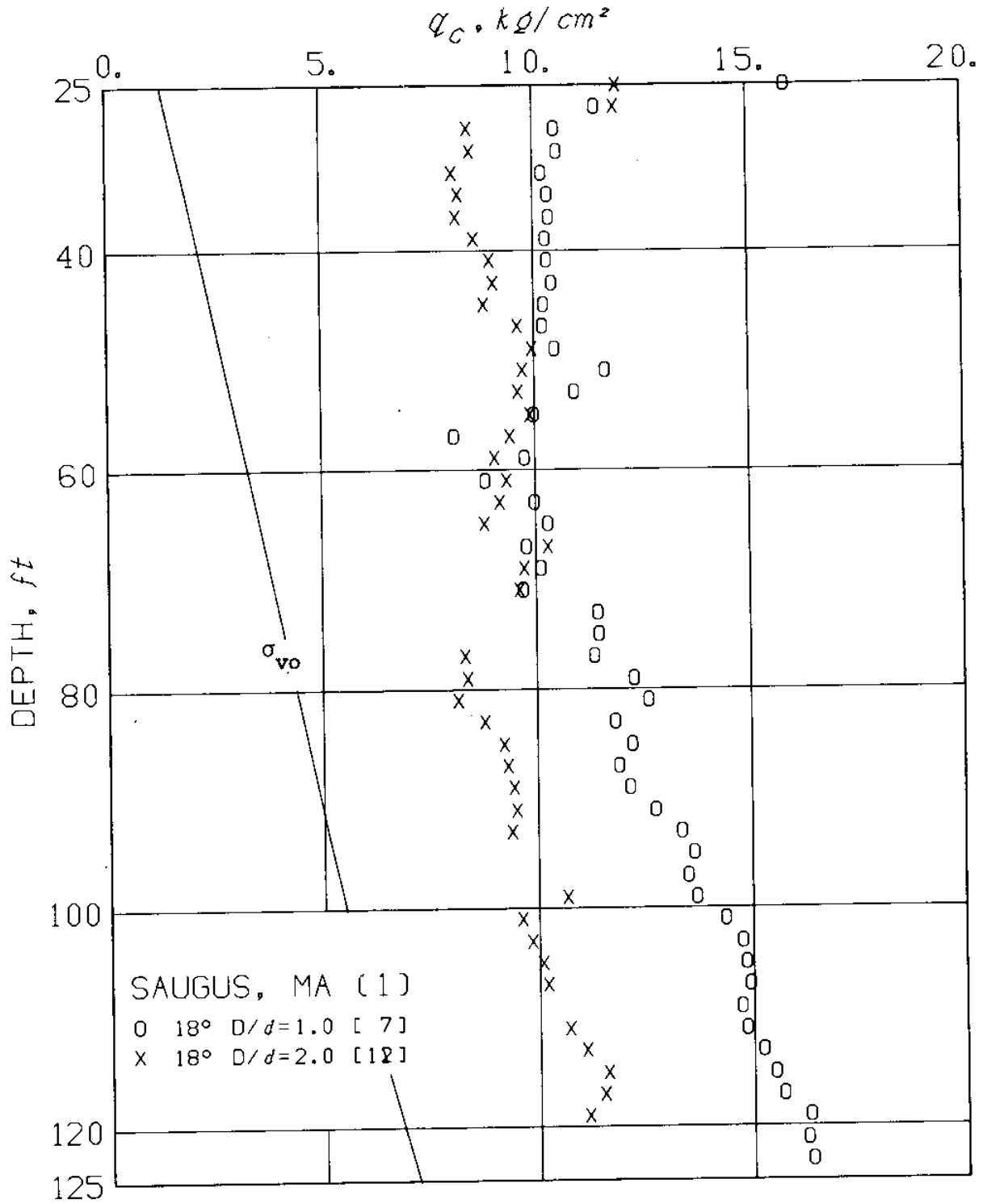
Fig. 7.4a (cont'd.).
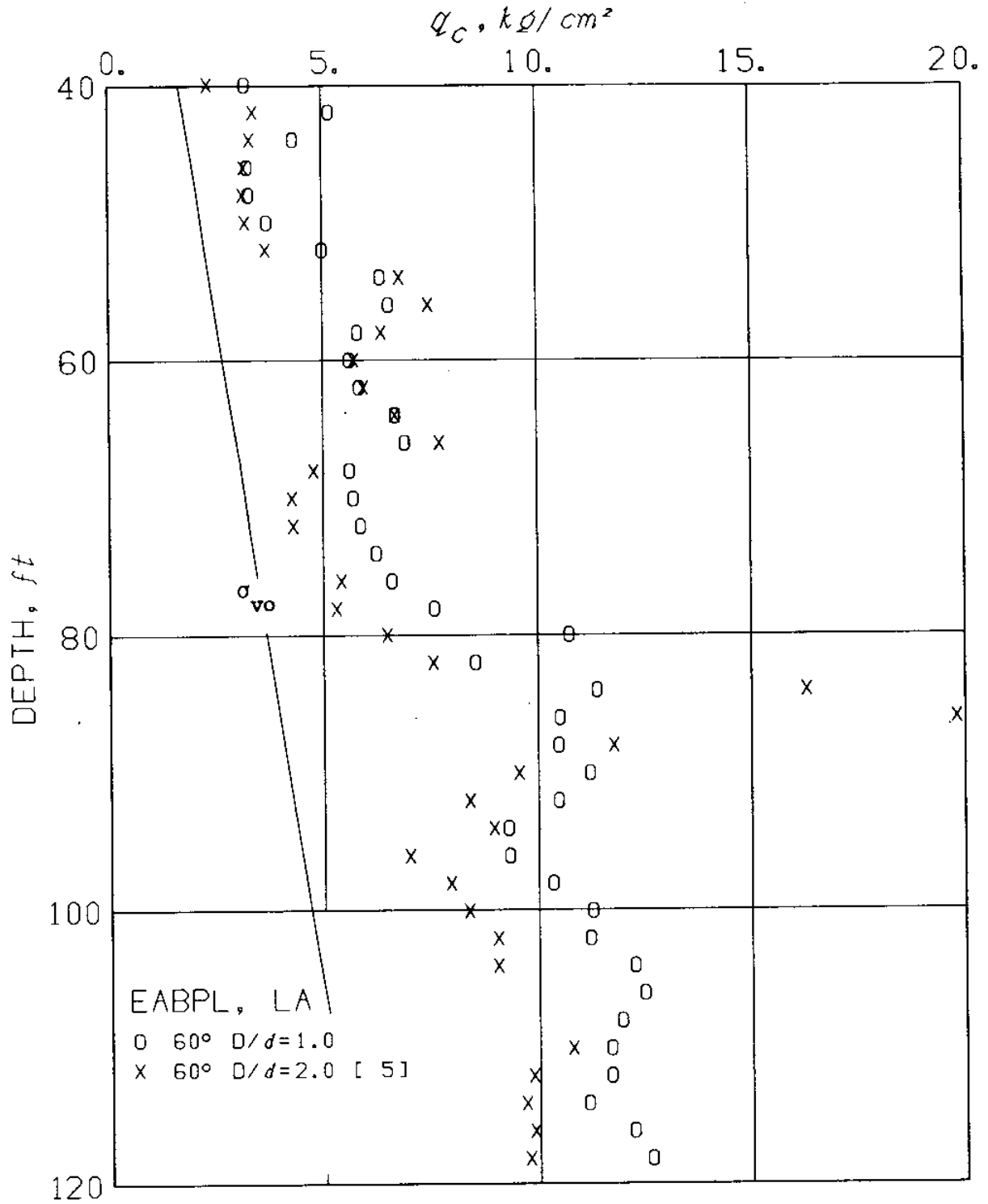
Fig. 7.4b   Effects of tip enlargement on cone resistance, EABPL Clay.
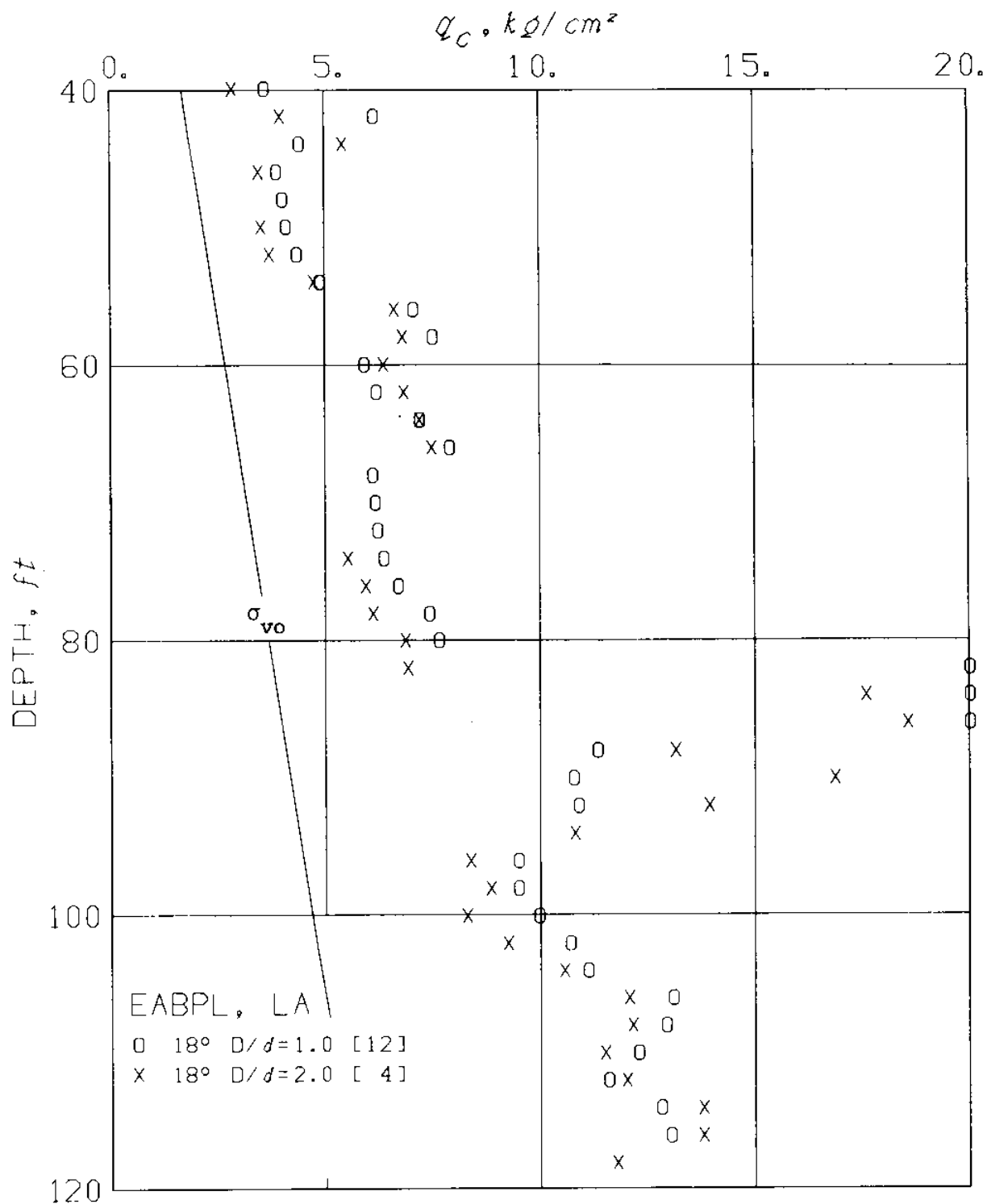
Fig. 7.4b (cont'd.).
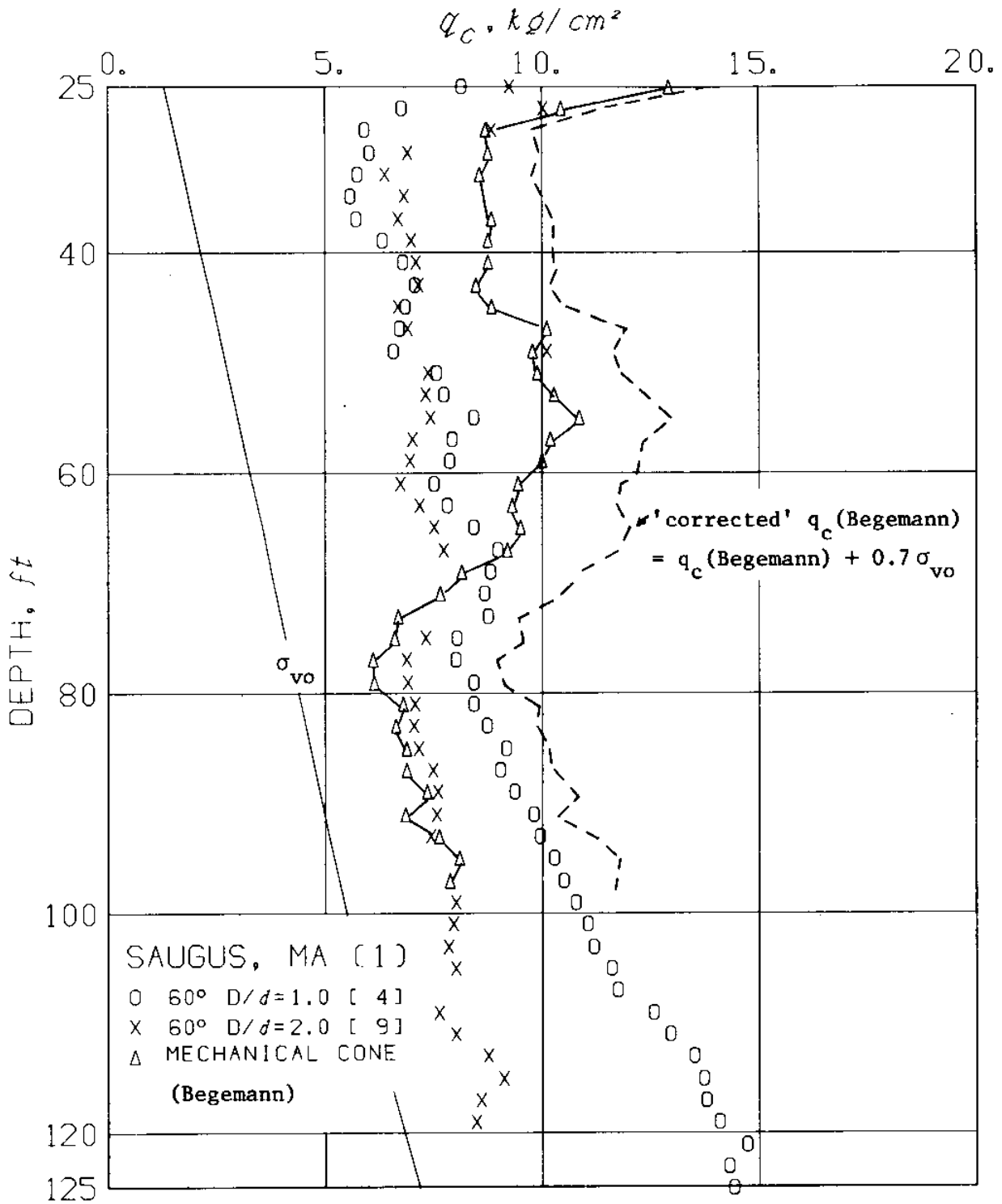
Fig. 7.5 Cone resistance of Fugro electric cones vs. Begemann
mechanical cone, Boston Blue Clay.
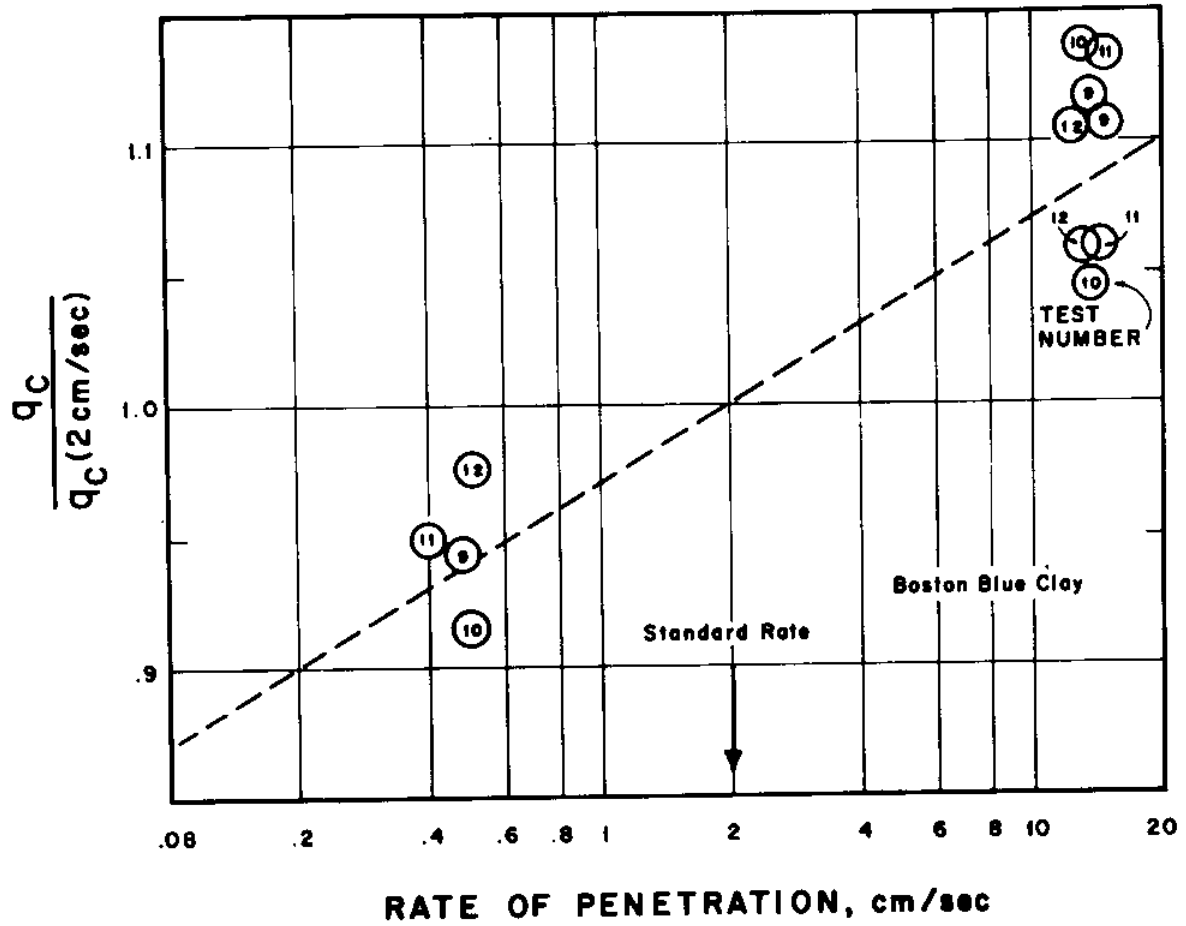
Fig. 7.6a   Effect of penetration rate on cone resistance, Boston Blue Clay.
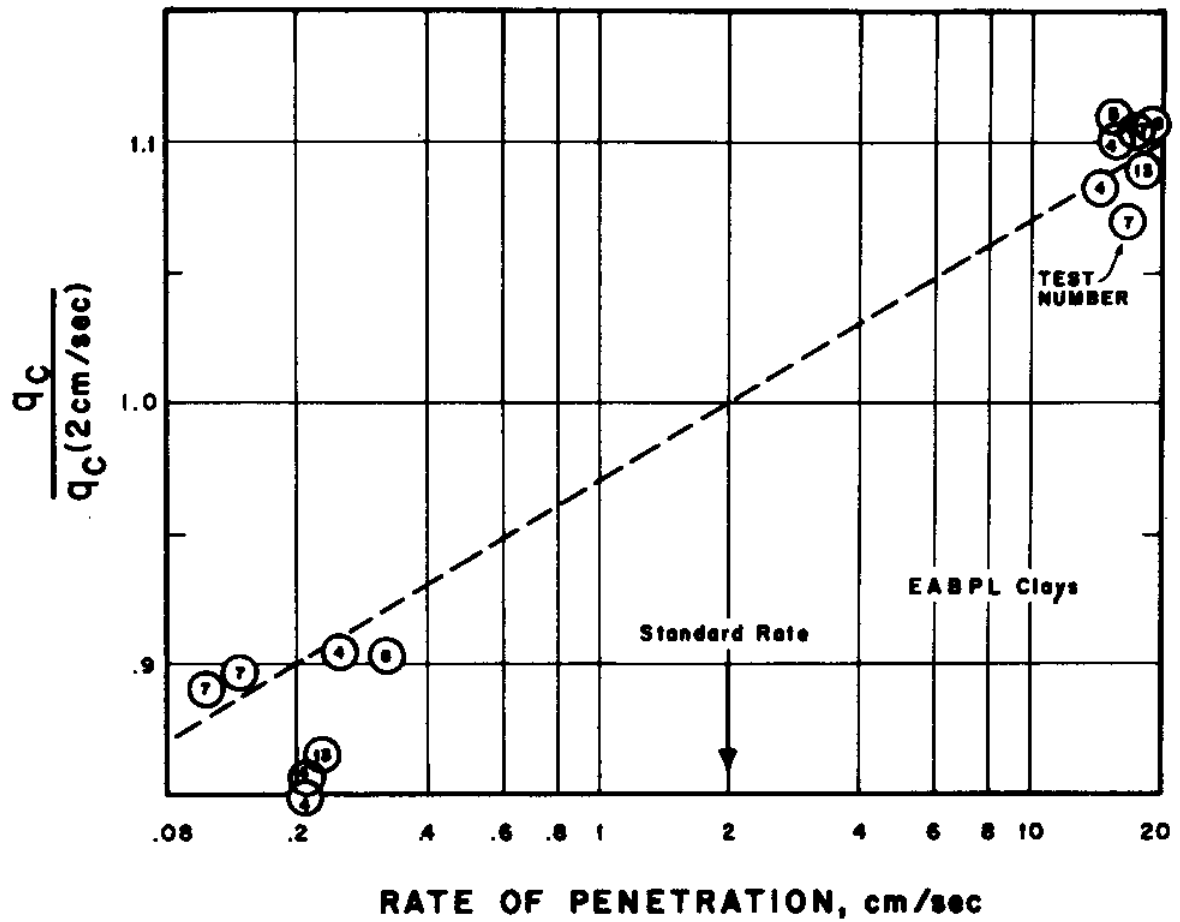
Fig. 7.6b   Effect of penetration rate on cone resistance, EABPL Clays.
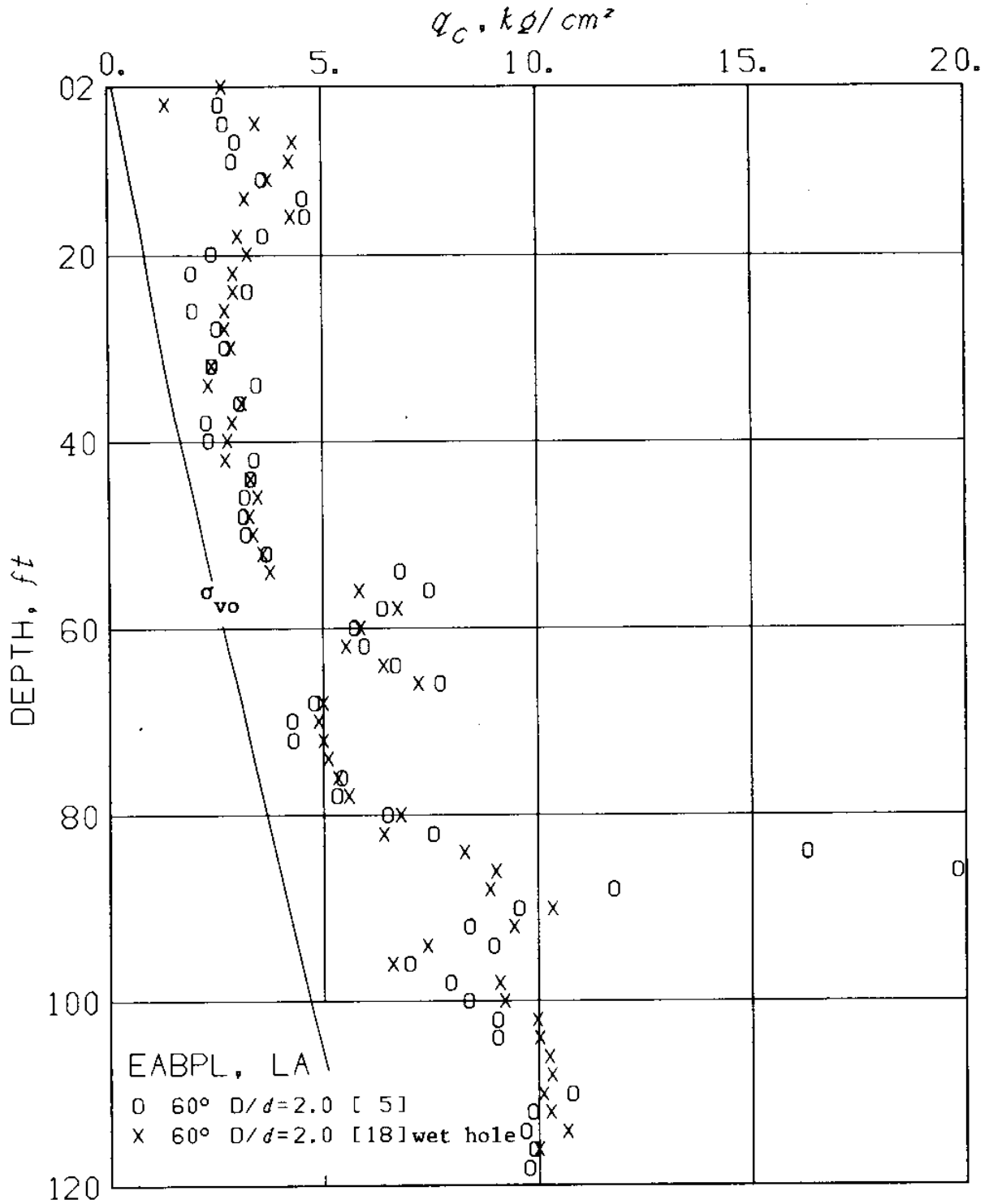
Fig. 7.7 Effect of access to water on q_c.

(a) 60° enlarged cones.
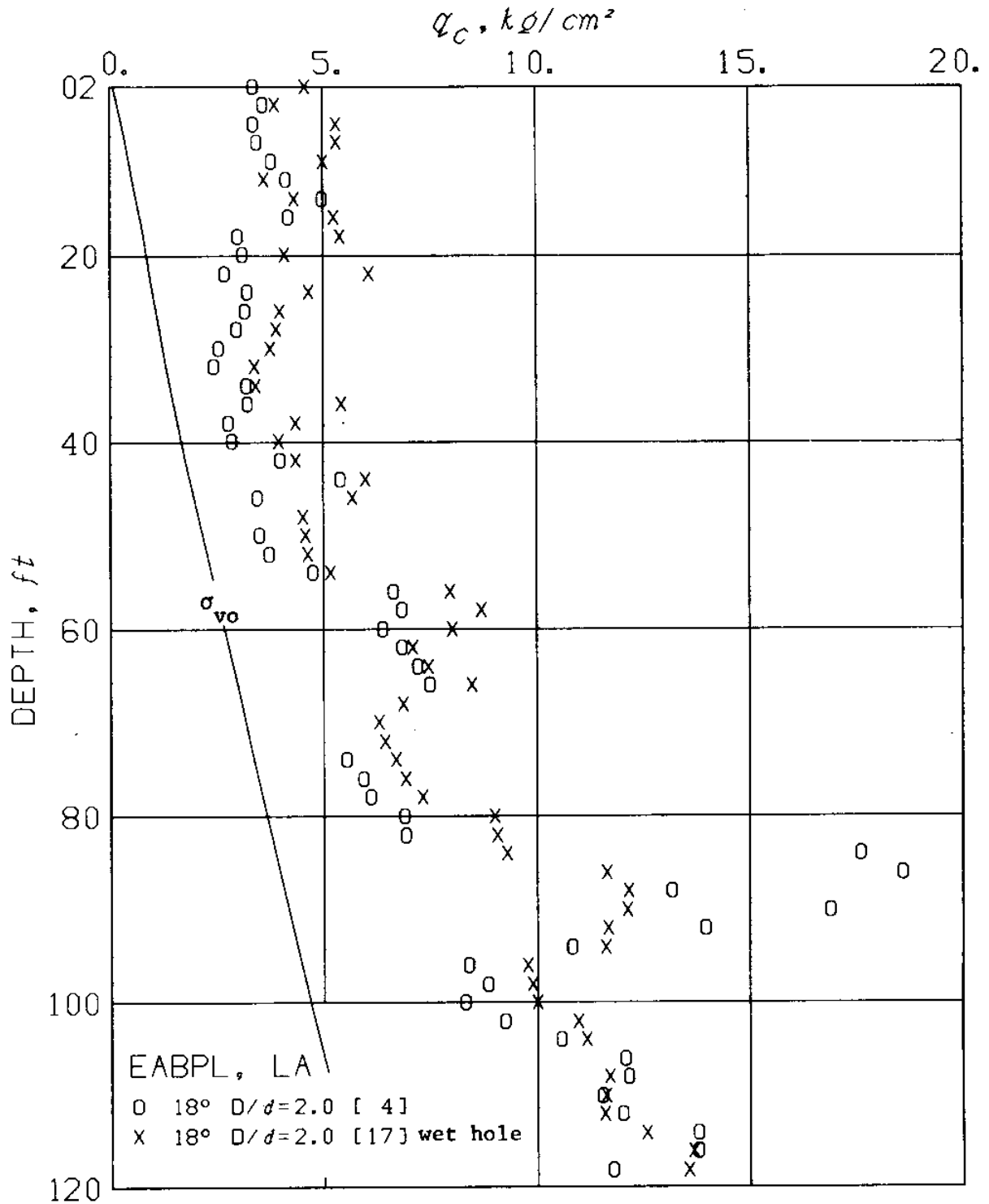
Fig. 7.7 Effect of access to water on q_c.

(b) 18° enlarged cones.
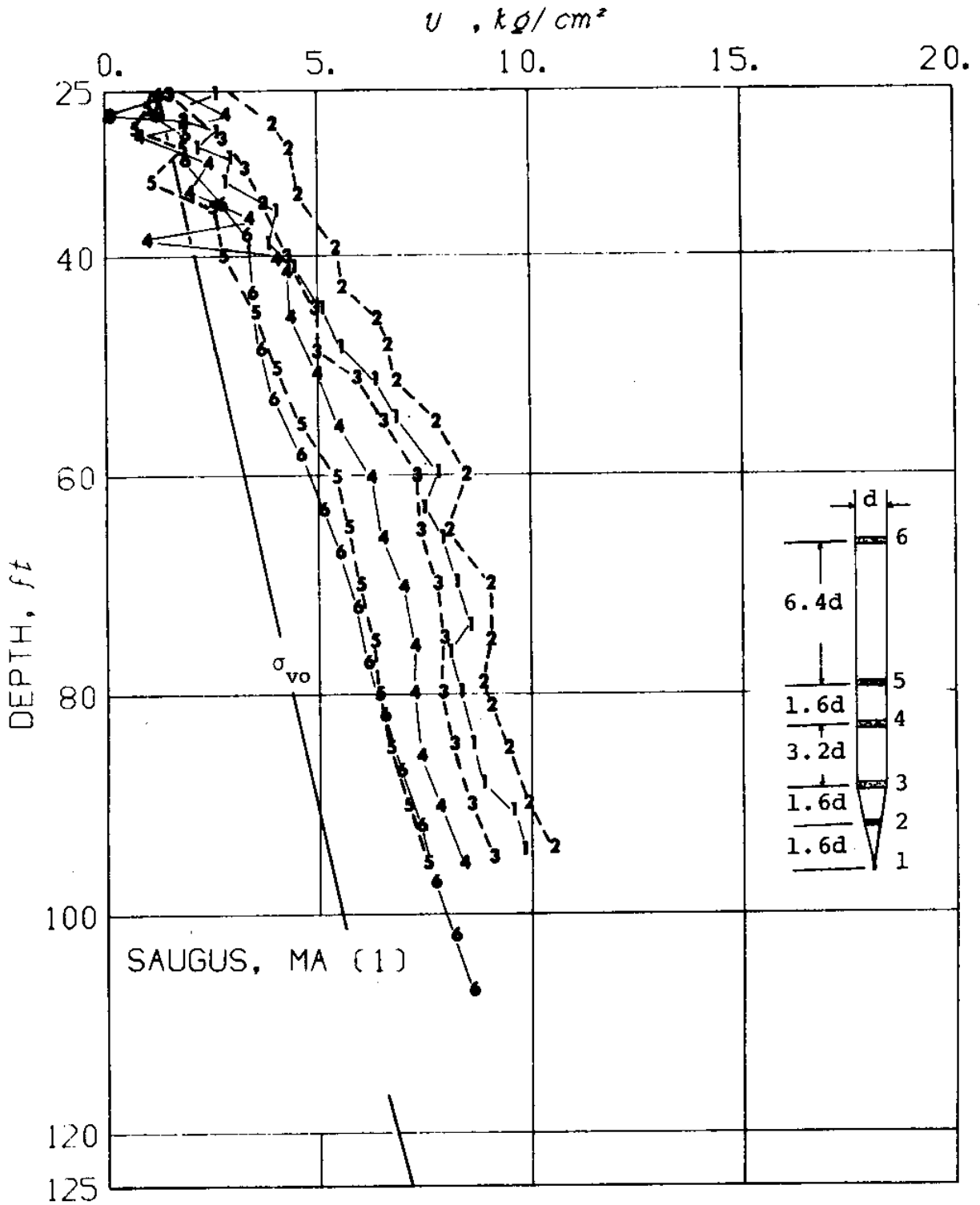
Fig. 7.8a Pore pressures measured along an 18° unenlarged cone during steady penetration.
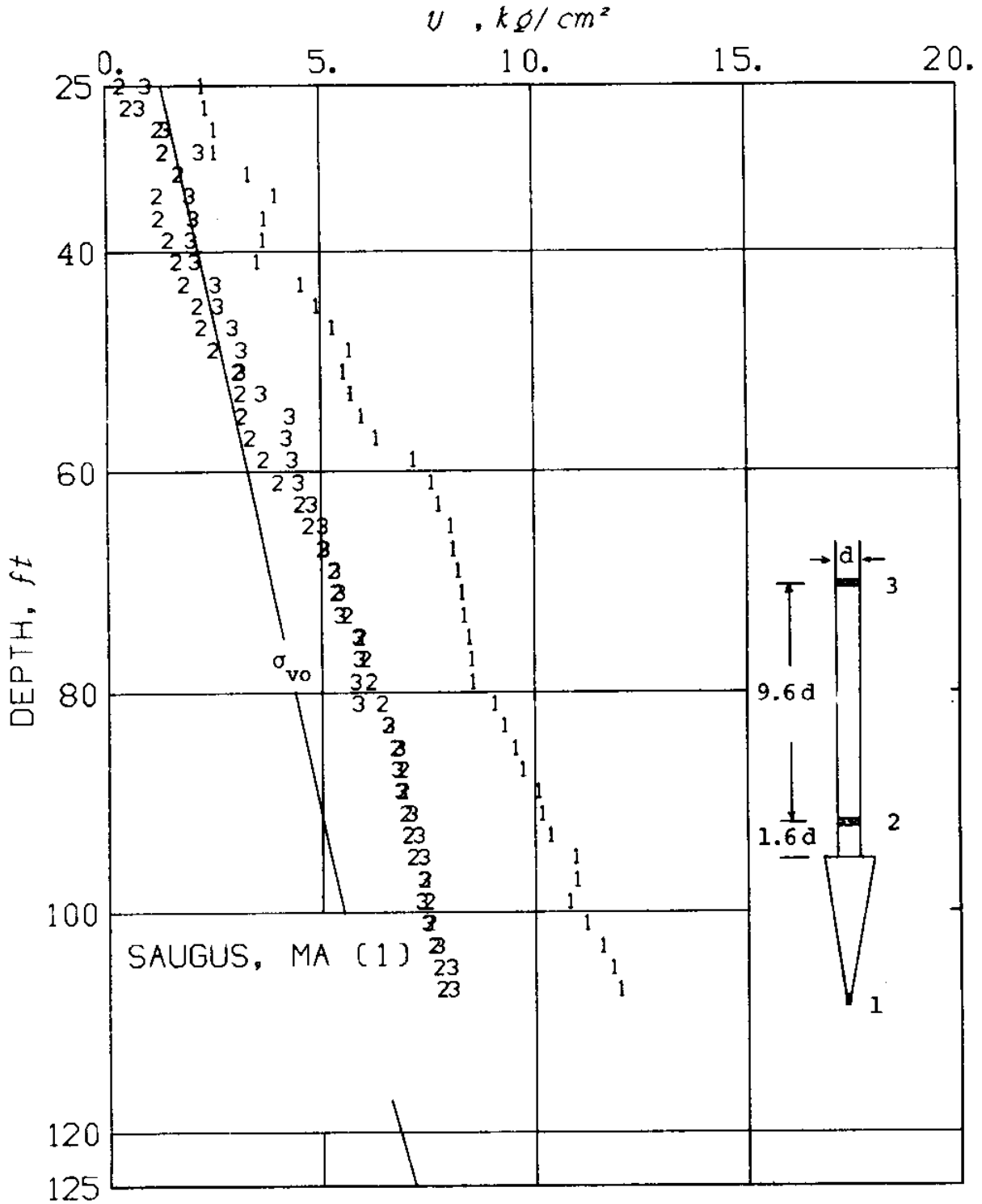
Fig. 7.8b Pore pressures measured along an 18° enlarged cone
during steady penetration.

U or Q_C , kg/cm^2
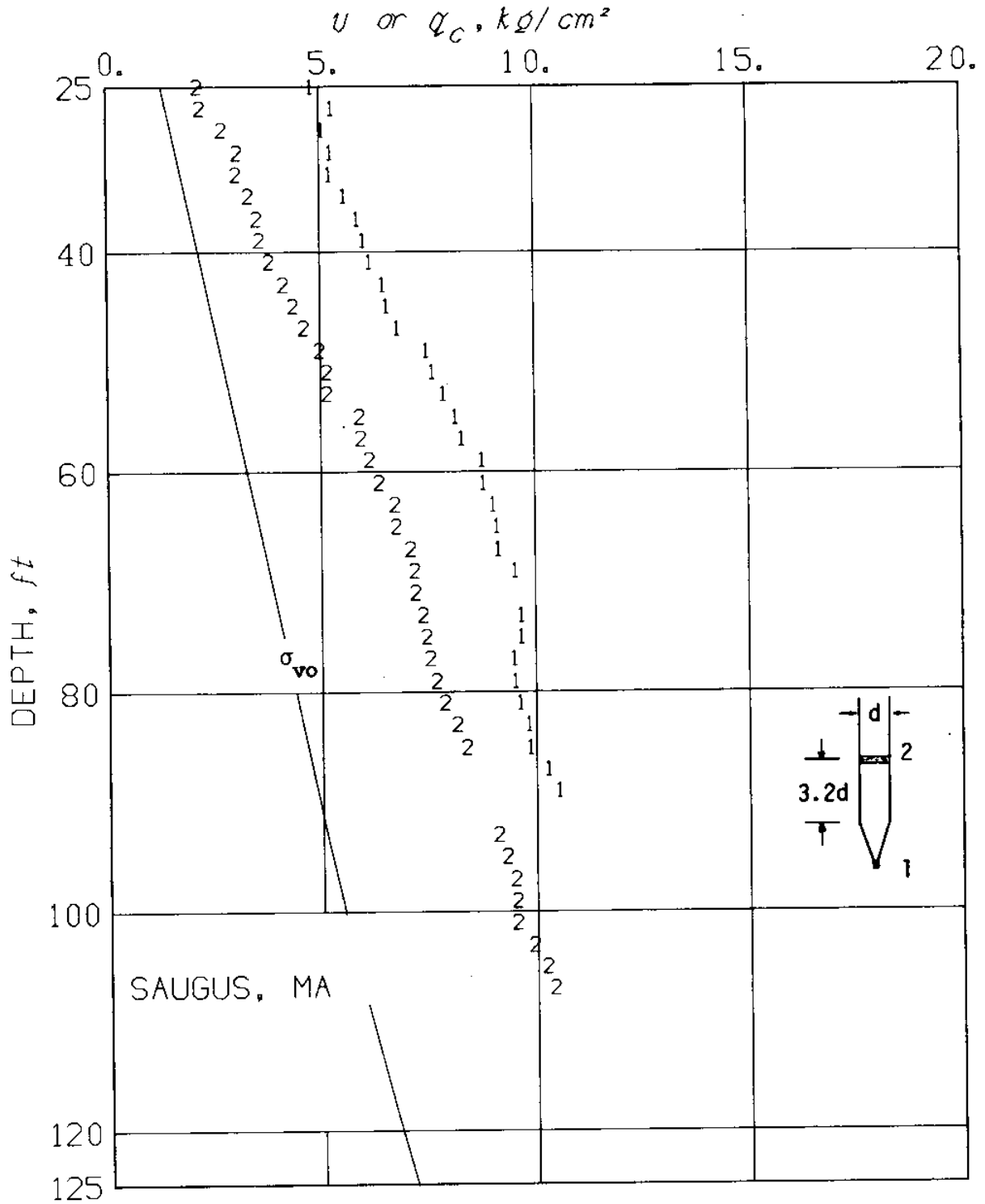
Fig. 7.9a Pore pressures measured along a 60° unenlarged
cone during steady penetration
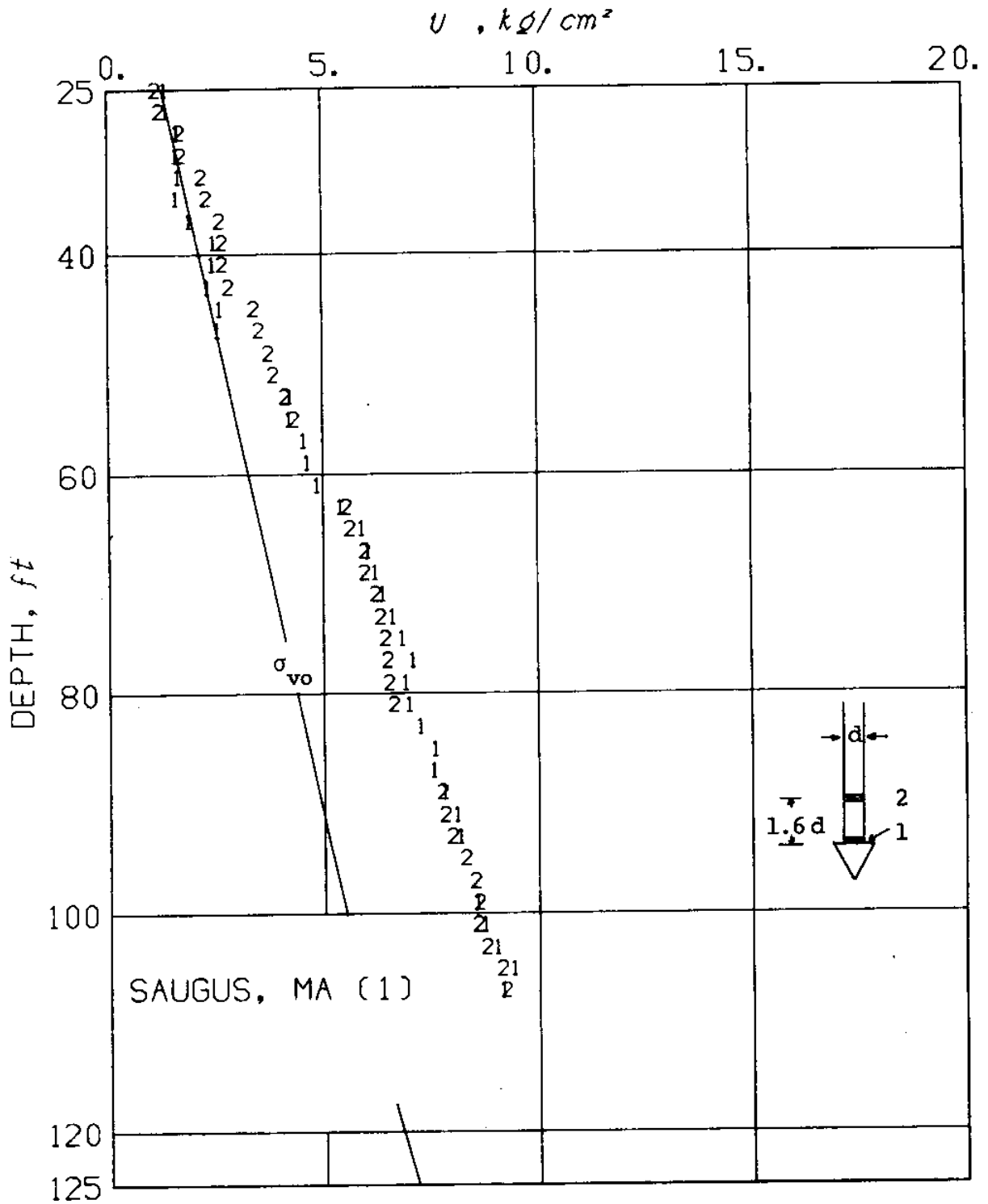
Fig. 7.9b Pore pressures measured along a 60° enlarged cone
during steady penetration.
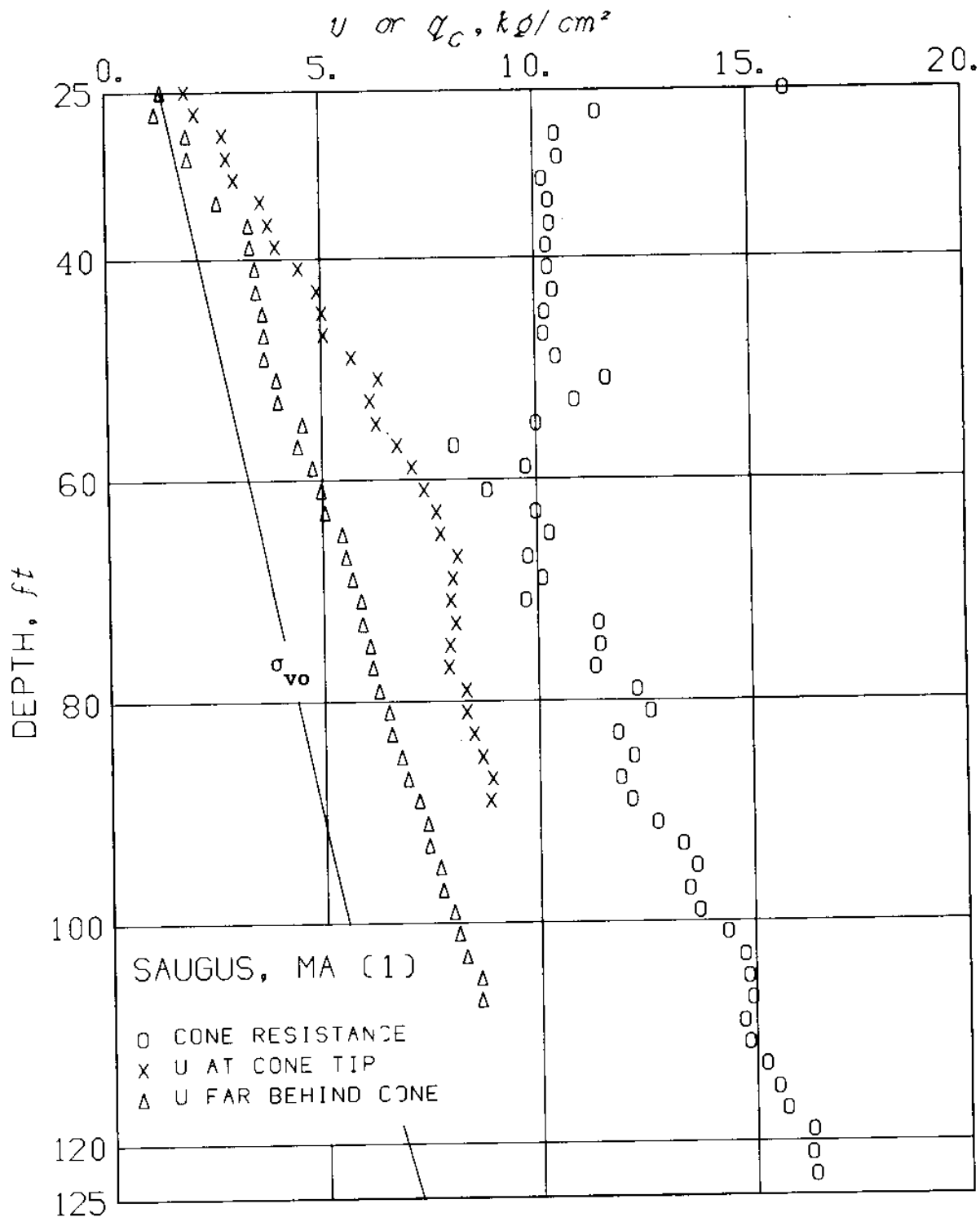
Fig. 7.10a Cone resistance and pore pressures for an 18° unenlarged cone (2δ = 18°, D/d = 1) in Boston Blue Clay
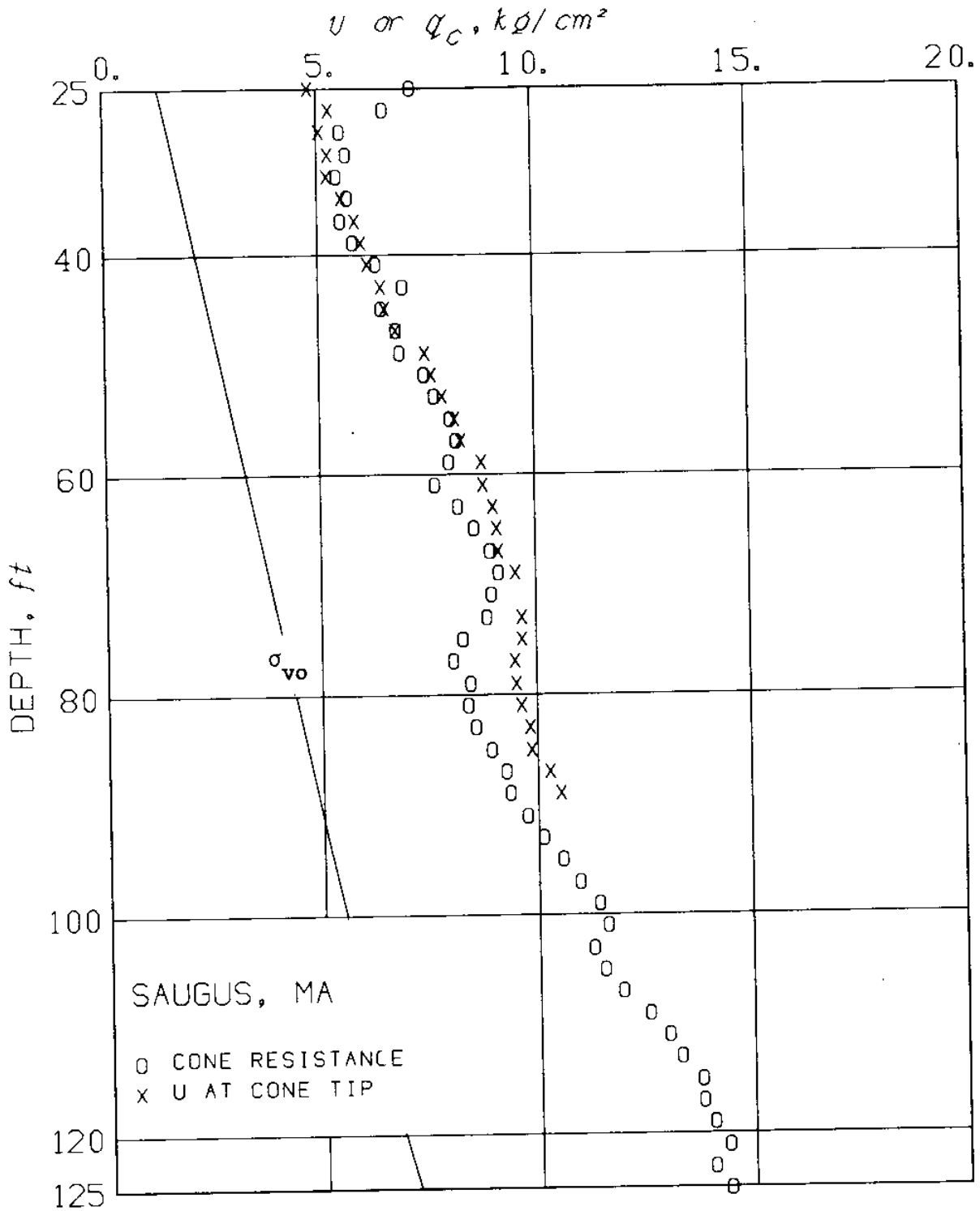
Fig. 7.10b Cone resistance and pore pressures for a 60° unen-
larged cone (2δ = 60°, D/d = 1) in Boston Blue Clay
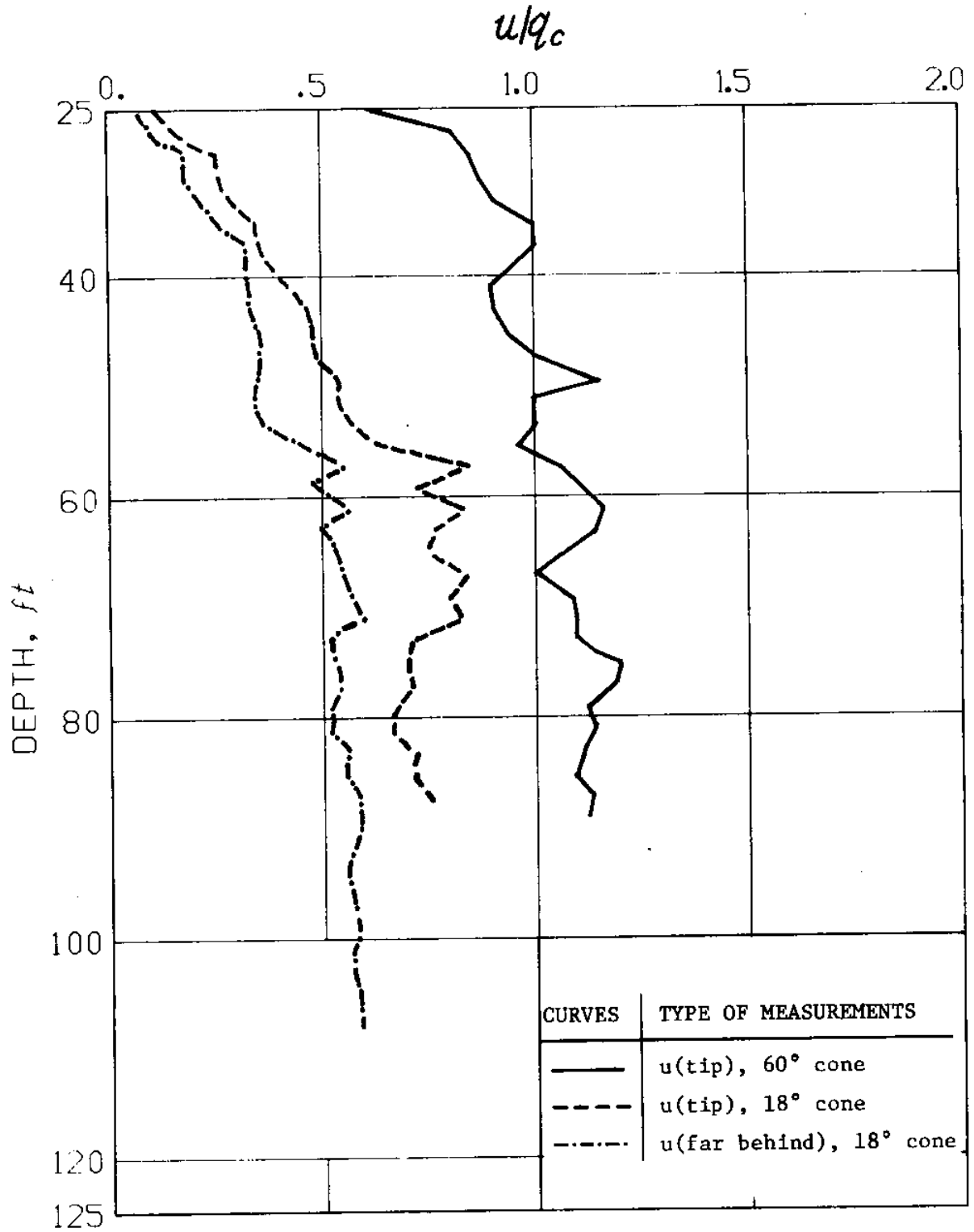
Fig. 7.10 c   Pore pressure to cone resistance ratios in Boston Blue Clay.
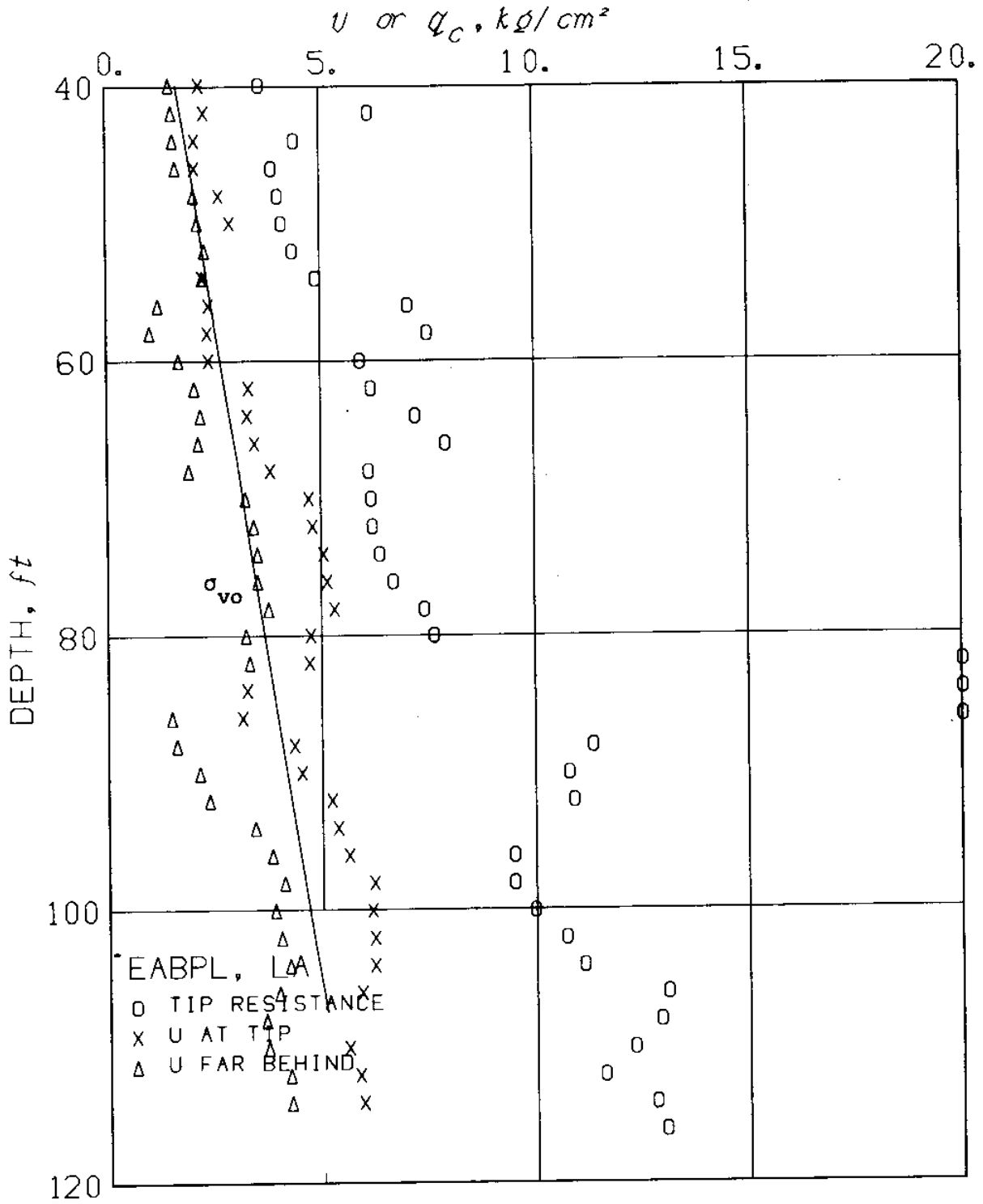
Fig. 7.11a Cone resistance and pore pressure for an 18° unenlarged
cone (2δ = 18°, D/d = 1) in EABPL Clay
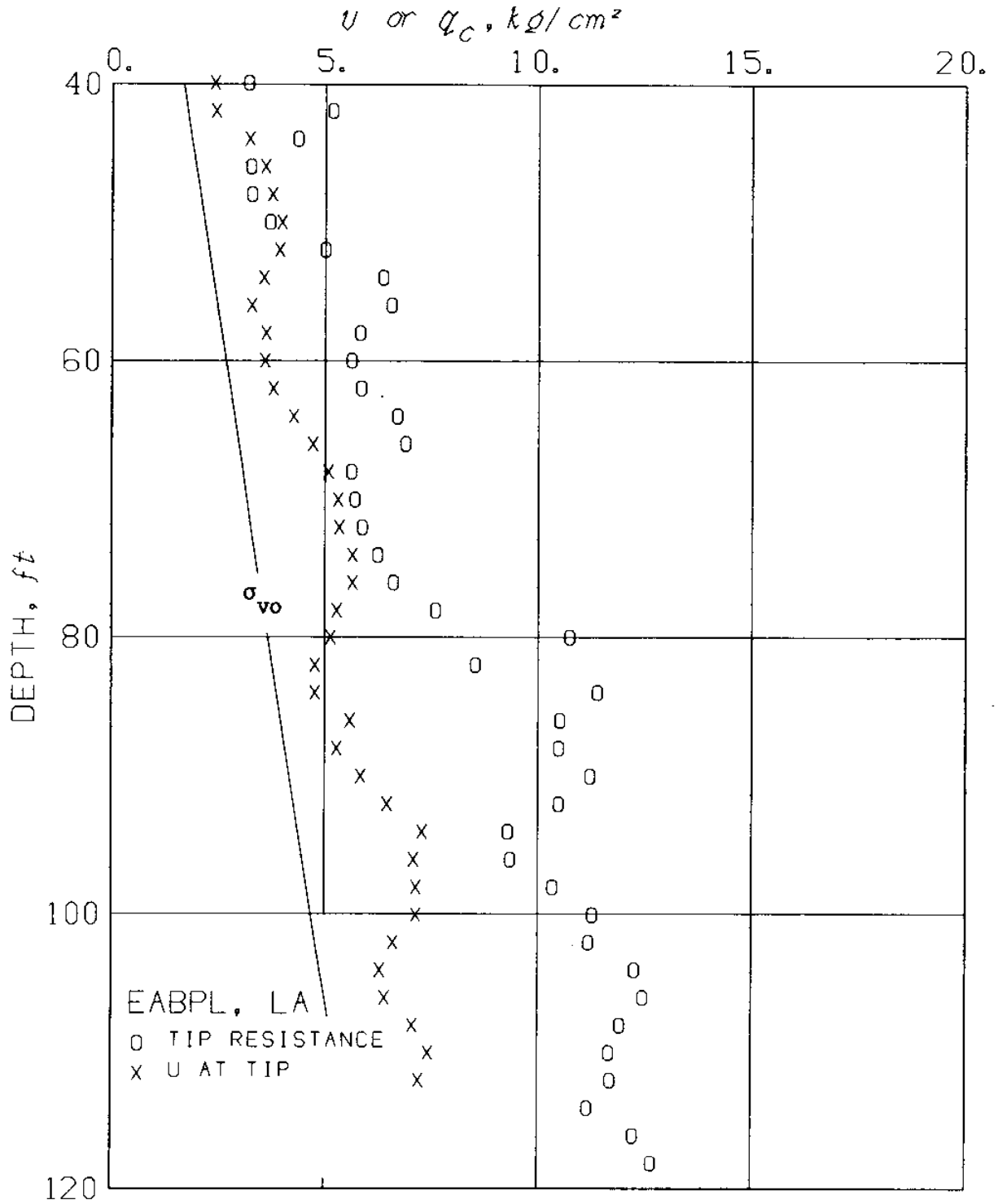
Fig. 7.11b   Cone resistance and pore pressure for a 60° unenlarged
cone (2δ = 60°, D/d = 1) in EABPL Clay
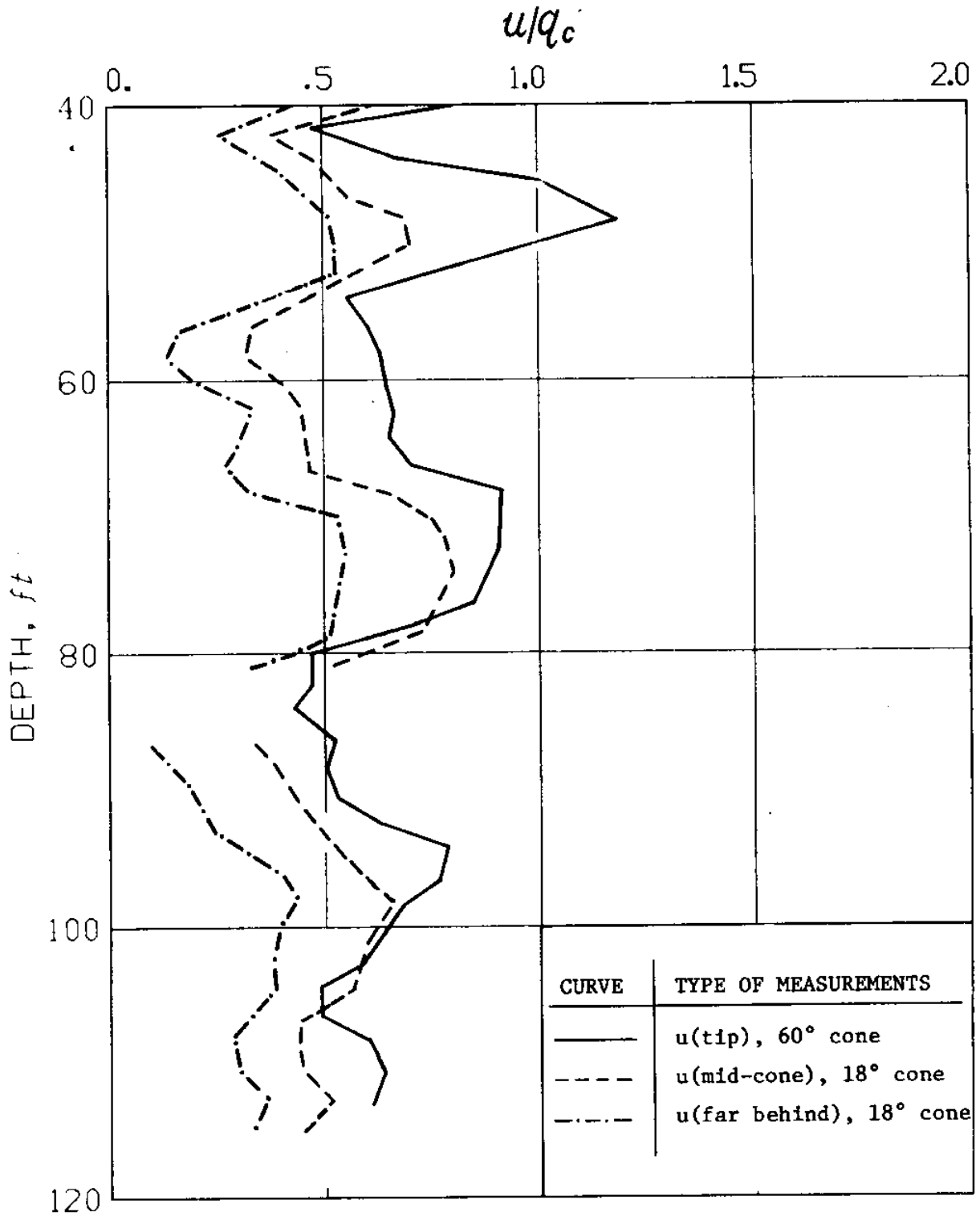
Fig. 7.11c   Pore pressure to cone resistance ratios in EABPL clay
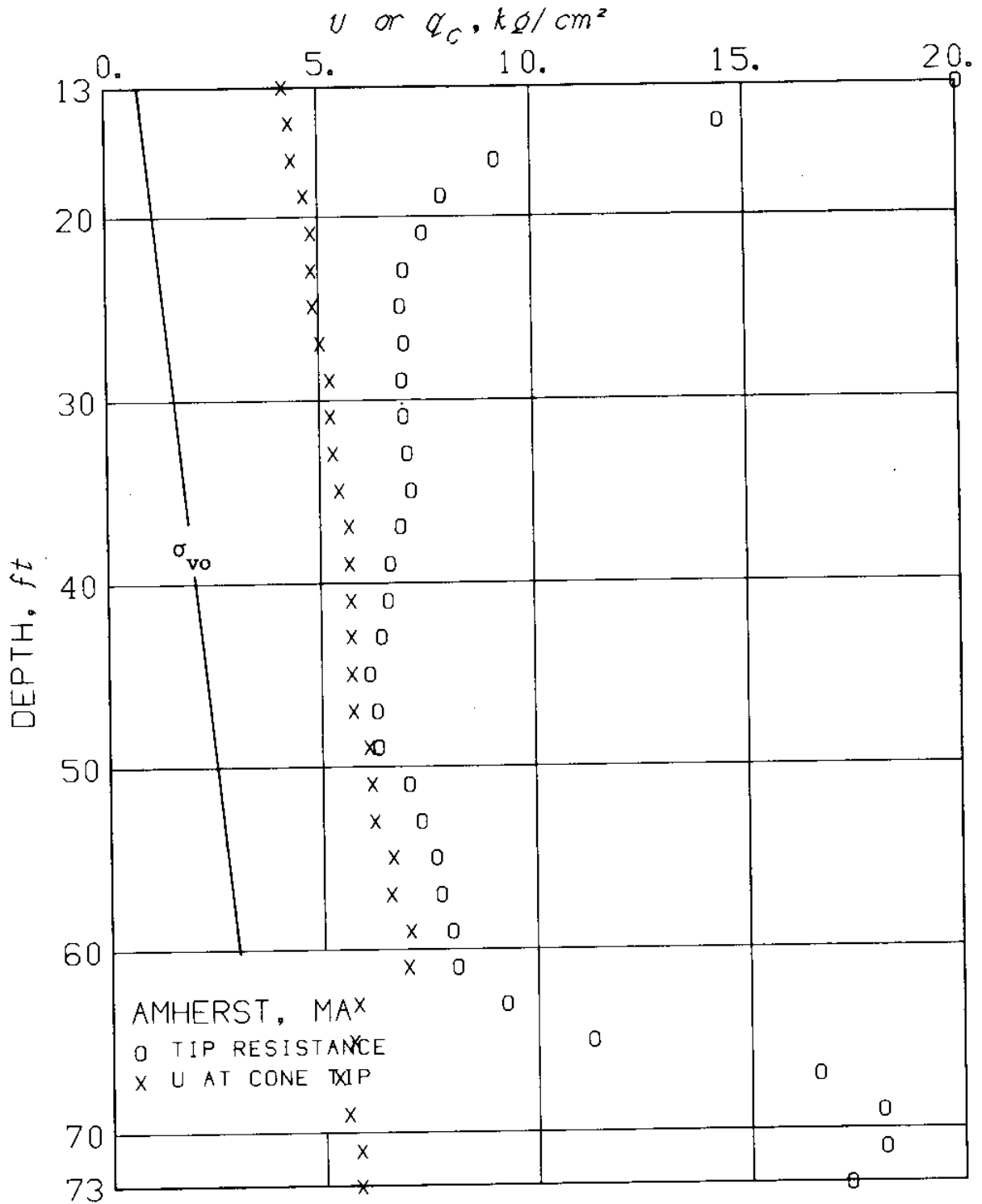
Fig. 7.12a Cone resistance and pore pressure for an 18° unenlarged
cone (2δ = 18°, D/d = 1) in Connecticut Valley Varved Clay
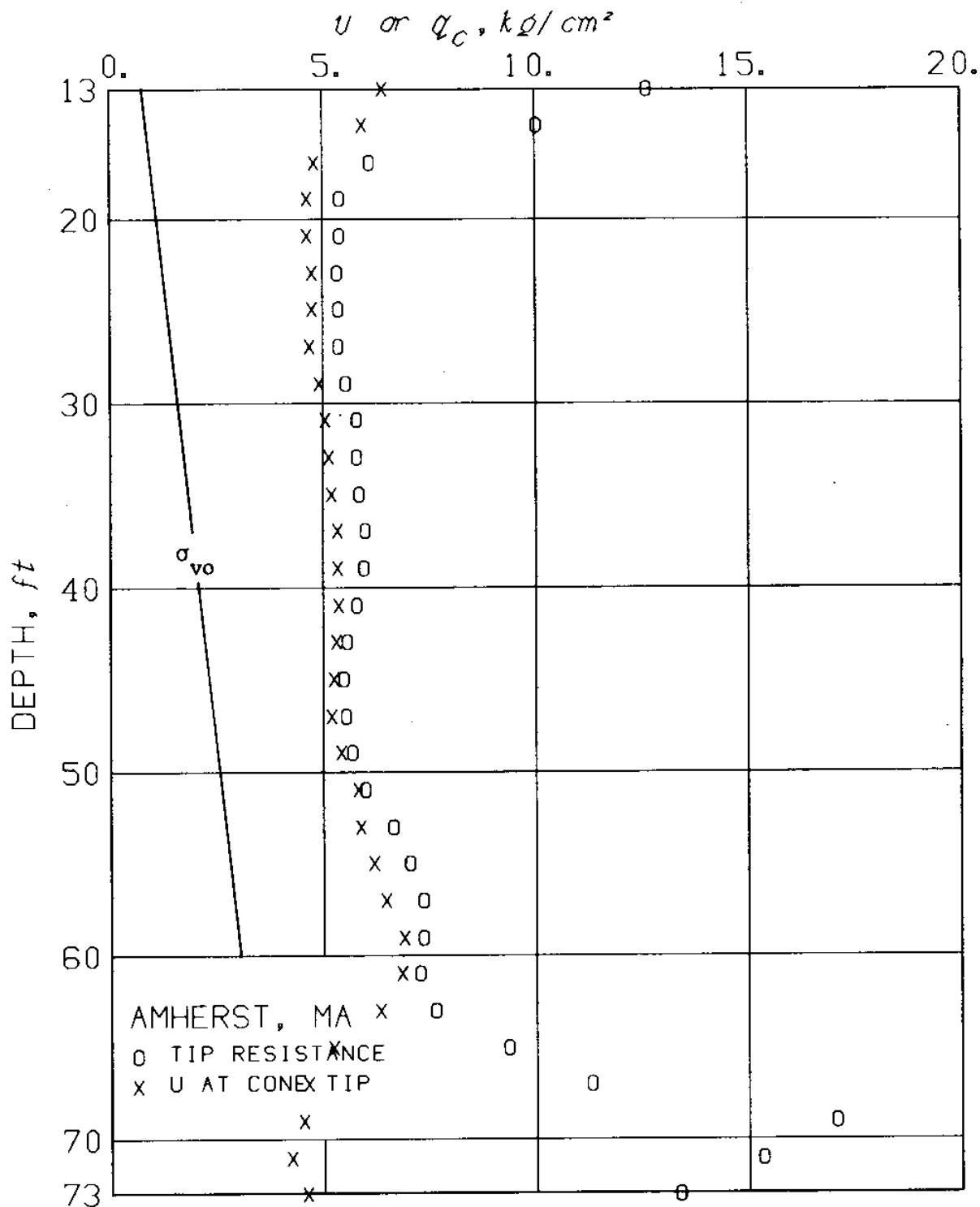
Fig. 7.12b   Cone resistance and pore pressure for a 60° unenlarged
cone (2δ = 60°, D/d = 1) in Connecticut Valley Varved clay
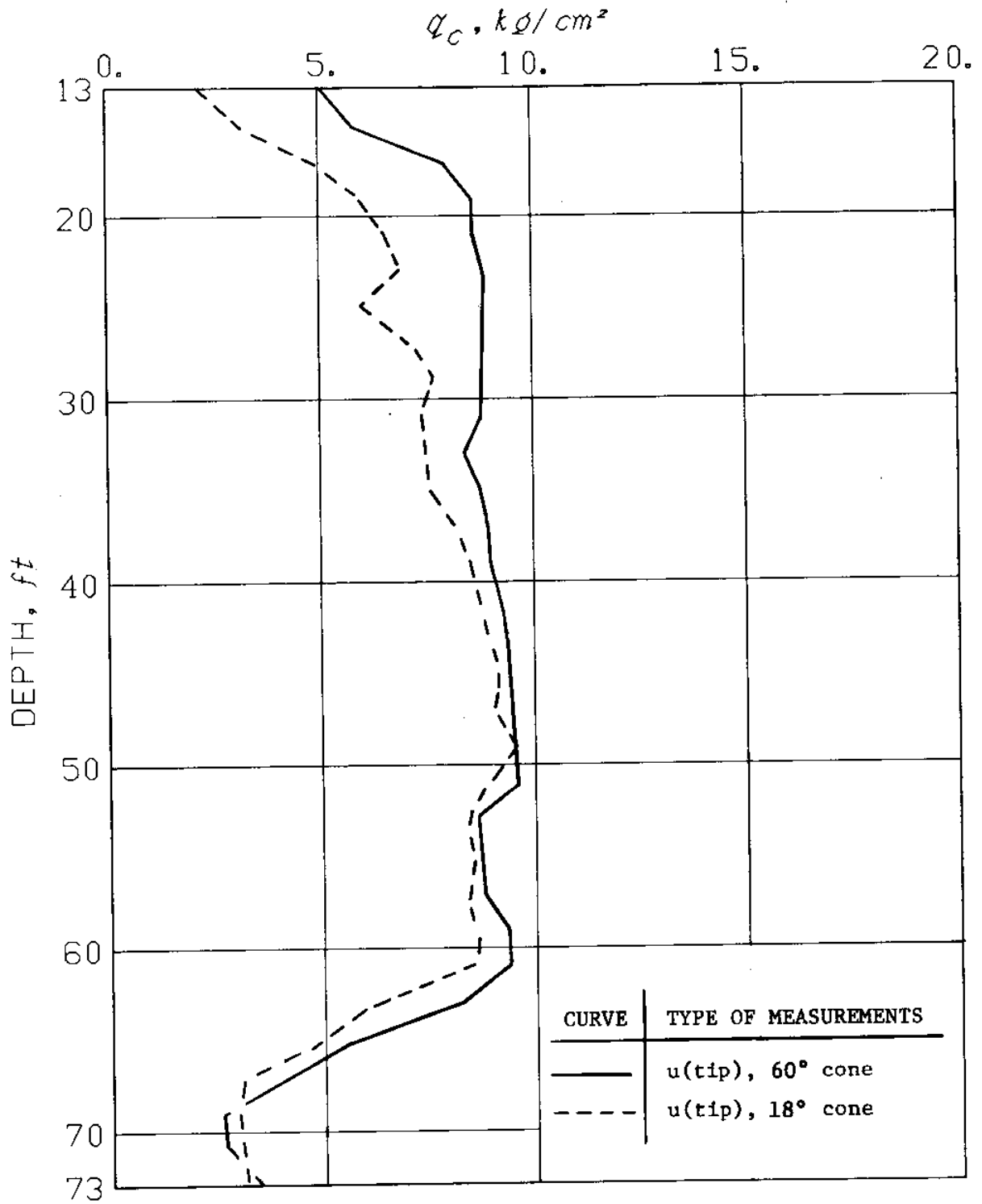
Fig. 7.12c   Pore pressure to cone resistance ratios in
Connecticut Valley Varved Clay.

CHAPTER 8

EVALUATION OF THEORETICAL PREDICTIONS

8.1 Predictions

(1) Theoretical predictions. The theory of cone penetration presented in Chapter 4 provides a rational basis for predicting the undrained shear strength of clays, s_u(cone), based on the cone resistance, q_c.

For enlarged cones (D/d > 1), the theory predicts that:

$$s_u(\text{cone}) = \frac{q_c - (d/D)^2 p_b}{N_c} \tag{8.1}$$

where

p_b = pore pressure in the gap behind the enlarged cone

N_c = cone factor

$$= 1.2(5.71 + 3.33\delta + \frac{1}{\tan \delta}) \tag{8.2}$$

= 11, 12.4, 15.1 for the cone angles (2 δ) 60°, 30° and 18°, respectively, used in this research.

For regular (unenlarged) cones, D/d = 1, the theory can only predict upper and lower bounds for s_u(cone):

$$\frac{q_c - \sigma_{ho}}{N_c + 1 + \ln(G/s_u)} \leq s_u(\text{cone}) \leq \frac{q_c}{N_c} \tag{8.3}$$

σ_{ho} = initial horizontal total stress

G = undrained shear modulus

N_c = cone factor given by Eq. 8.2

(2) Empirical formulas. In addition to the theoretical predictions, results of regular (unenlarged) cones can be interpreted by means of the empirical formula:

$$s_u(\text{cone}) = \frac{q_c - \sigma_{ho}}{N_c} \tag{8.4}$$

which provides a reasonable "average" between the bounds in Eq. 8.3 . A second empirical formula to be evaluated is the widely used expression:

$$s_u(\text{cone}) = \frac{q_c - \sigma_{vo}}{N_c} \tag{8.5}$$

where σ_{vo} = initial total vertical stress

Table 8.1 summarizes the theoretical and empirical predictions of s_u(cone) to be evaluated subsequently.

8.2 Undrained Shear Strength of Clays

The evaluation of theoretical predictions is complicated by the extremely difficult task of defining the undrained shear strength of clays, s_u, and estimating the necessary profiles to be compared with the profiles of s_u(cone).

(1) Laboratory strength. The undrained shear strength, s_u, obtained by means of laboratory tests invariably suffers from the effects of sampling disturbances (Ladd and Lambe, 1963). Results of crude laboratory tests (e.g., unconfined compression and unconsolidated undrained) are seriously affected by sampling disturbance and hence are too scattered and unreliable to allow a meaningful evaluation of s_u(cone). Ladd and Foott (1974) propose a procedure to reduce the effect of disturbance on clay samples tested in the laboratory: the SHANSEP approach (Stress History And Normalized Soil Engineering Properties). This approach applies to

clays exhibiting <u>normalized</u> behavior and requires an accurate estimate of
the <u>stress history</u> of the clay. By using different laboratory equipment
and applying different stress paths, this approach predicts s_u for dif-
ferent stress histories and different modes of failure, e.g., plane-strain
compression, extension, simple shear, etc., and thus contributes signif-
icantly to the fundamental understanding of soil behavior. Chapter 5
presents SHANSEP strength profiles for the three clay deposits considered
in this research (see Figs. 5.5, 5.10 and 5.14).

Laboratory test results are relatively easy to interpret compared to
in situ tests results (e.g., field vane test). On the other hand, the
use of laboratory data to evaluate cone penetration theories (or the
performance of foundations) presents serious problems: 1) the uncertain-
ties regarding in situ soil conditions: stress history, soil variability,...
etc.; 2) the highly nonlinear, anisotropic and rate dependent stress-
strain-strength behavior of clays; 3) the limited capabilities of existing
laboratory equipment to duplicate the stress-paths (or strain-paths) of <u>all</u>
soil elements; and, 4) the limited theoretical capabilities to model
all aspects of soil behavior or to provide complete analyses. Factors
which were not rigorously considered or totally neglected by theoreti-
cal predictions (in Eqs. 8.1 through 8.3) include: anisotropy in shear
strength and initial stresses, soil deformation prior to yield, strain
softening, strain rate, and reduced friction at the soil-cone interface (see
Table 3.2).

(2) <u>The field vane strength, s_u(FV)</u>. The field vane consists of
four metal blades welded to a small circular shaft. The blades are rec-
tangular with a height h and a width (diameter) d = h/2. The "vane"
is pushed into the soil (usually from the bottom of a predrilled hole) and

rotated at a constant rate (0.1° per sec according to ASTM D-2573). Traditional interpretation of the test assumes that the maximum shear strength, s_u, is simultaneously mobilized along the surface of revolution described by the vane (a closed end right cylinder) when the maximum torque, T_{max} is measured, i.e.,

$$s_u(FV) = \frac{T_{max}}{(7\pi d^3/6)} \qquad \text{for } h/d = 2 \qquad (8.6)$$

Figures 5.4, 5.9 and 5.14 show $s_u(FV)$ for the three clay deposits considered in this research. Like other in situ tests, the field vane test avoids the effect of sampling disturbances on laboratory test results, but is very difficult to interpret rigorously (Ladd et al., 1977).

(3) __The field strength, s_u(field)__. The field strength s_u(field) is the shear strength profile required for design. In general, s_u(field) depends on the problem at hand, e.g., embankment stability, footing bearing capacity, pile resistance,...etc. and the method of analysis (see Appendix A).

Full scale tests are the best means of estimating s_u(field). However, full scale tests can only provide average values of s_u(field) within a limited depth of soil, i.e., they cannot establish the necessary profiles of s_u(field) to evaluate cone penetration theories. Therefore, profiles of s_u(field) in the three clay deposits considered herein were not only established on the basis of embankment performance (evaluated in the course of several earlier research programs at M.I.T,), but also from profiles of field vane or SHANSEP strengths. Table 8.2 presents our best estimates of s_u(field) to be used in stability analyses of embankments at the three test sites. In two of the sites, s_u(field) equals a correction factor μ

times s_u(FV) whereas in the Atchafalaya clay, s_u(field) equals the SHANSEP

strength obtained from the Direct Simple Shear Test. Appendix A describes

the difficulties encountered in selecting s_u(field) at the Boston Blue

Clay site.

The correction factor, μ , required to obtain s_u(field) from

s_u(FV) was introduced by Bjerrum (1972). He reviewed 16 well-documented

embankment failures on cohesive foundations and plotted the factors of

safety computed from circular arc analysis ($\phi = 0$) using the field vane

strength, s_u(FV), versus the plasticity index (PI) of the soil. From the

best fit line through these data points, he proposed the use of a correc-

tion factor, μ , Fig. 8.1a, to get s_u(field) $= \mu\ s_u$(FV) for the design of

embankments. Subsequently, Bjerrum (1973) evaluated failures of footings

and unsupported excavations and concluded that the same correction factor is

also applicable for these problems.

Table 8.3 presents a comparison between the back figured values

of s_u(field) based on actual embankment performance (Table 8.2) and the field

vane (FV) data at the three sites considered. We note that the s_u(field)/

s_u(FV) ratio varies between 0.6 and 1.1 and is generally within 15% of the

empirical correction factor μ proposed by Bjerrum.

(4) The reference strength, s_u(REF). In evaluating theoretical cone

predictions, s_u(cone) is compared to the reference strength s_u(REF) which

basically represents the field strength s_u(field) corrected for strain rate

effects by a factor μ_R^*. Bjerrum (1973) proposes values of the empirical

correction factor μ_R "to be applied to the result of a shear test with a

duration of a few minutes in order to obtain the strength which can be

mobilized over a period of some weeks or several months;" Fig. 8.1b.

---

*Laboratory triaxial compression tests indicate that s_u often decreases
by 10 $\pm$ 5% for a 10-fold decrease in strain-rate (Bjerrum, 1971; Berre and
Bjerrum, 1973).

Cone penetration causes very rapid straining of the soil and μ_R values proposed by Bjerrum are not carefully documented, however, μ_R in Fig. 8.1b provides a reasonable basis for estimating s_u(REF) from s_u(field), i.e.,

$$s_u(REF) = s_u(field)/\mu_R; \qquad (8.7)$$

$$= \text{strength to be compared with } s_u(cone),$$

and $\qquad s_u(cone) = $ strength predicted from cone resistance q_c with the theoretical expressions in Table 8.1.

Table 8.2 presents values of s_u(REF) for the three clay deposits studied.

8.3 Evaluation of Predictions

Table 8.4 summarizes the cone penetration tests used in predicting s_u(cone) using the formulas in Table 8.1. Detailed measurements obtained in these tests are presented in Chapter 7 and their variability studied in Chapter 6.

(1) Enlarged cones. Figure 8.2 shows s_u(cone) predicted for 18° and 60° enlarged cones (D/d = 2) using Eq. 8.1. The results indicate that the two cone shapes give essentially identical strengths and hence that the theory (Chapter 4) accounts for the effect of the cone angle appropriately. Furthermore, the predicted strength, s_u(cone), is almost identical to the reference strength, s_u(REF), in the upper overconsolidated deposit (above 65 to 75 ft), but is closer to s_u(field) below 80 ft. In this lean-clay deposit, strain rate effects expressed by μ_R, are not very significant and hence the difference between s_u(REF) and s_u(field) is relatively small. Therefore, predictions of s_u(cone), according to Eq. 8.1, is considered satisfactory in Boston Blue Clay.

Figure 8.3 shows s_u(cone) predicted for 18°, 30°, and 60° enlarged cones (D/d = 2) in the Atchafalaya clay using Eq. 8.1.[*] The three cone shapes give almost identical values of s_u(cone) which shows a pattern similar to both the (uncorrected) field vane strength, s_u(FV), and the reference strength, s_u(REF), based on SHANSEP s_u(DSS) from direct simple shear tests.

In summary, results of enlarged cone resistance and pore pressure measurements behind the cone tip in two clay deposits[**] indicate that s_u(cone) determined by means of Eq. 8.1 can be used to estimate s_u(REF). The field strength, s_u(field), for stability analyses can then be safely determined by reducing s_u(REF) by the factor μ_R in Fig. 8.1b for strain rate effects.

(2)   Regular (unenlarged) cones.

(2.a) Upper and lower bounds for the FUGRO cone. Figures 8.4 show the ratio q_c/s_u(REF) as obtained from cone tests and strength data from Table 8.2 for regular (unenlarged, D/d = 1) 60° FUGRO cones in the three clay deposits studied herein (Figs. a, b, and c). The figures also show predictions based on the assumption that s_u(cone) = s_u(REF).

---

[*]Measurements of pore pressures u behind 60° and 18° enlarged cones were conducted at a location 400 ft from the main test site. The results indicate no noticeable effects of cone angle and show a pattern and value very similar to u measured far behind an 18° unenlarged cone (test conducted at the main test site). In view of the soil variability at this site, the average of these three tests was used to compute p_b in Eq. 8.1 for the strength prediction.

[**]No enlarged cone tests were conducted in the third deposit of Connecticut Valley Varved clay.

The upper bound on q_c (Eq. 8.3) depends on the three parameters N_c, σ_{ho}, and G/s_u. For the FUGRO cone with an angle $2\delta = 60°$, the theory predicts the cone factor $N_c = 11$. The initial horizontal stress, σ_{ho}, is computed from the expression $\overline{\sigma}_{ho} + u_o$ where $\overline{\sigma}_{ho} = K_o \overline{\sigma}_{vo}$. Values of K_o are estimated from the OCR profiles (Figs. 5.3, 5.8, 5.13) and the relationship between K_o and OCR (Figs. 5.6, 5.11, 5.15). In view of the large uncertainties in estimating the rigidity index G/S_u, upper bounds for q_c are plotted for 3 values of G/s_u (=50, 150 and 400). Fortunately, the effects of uncertainties. in σ_{ho} and G/s_u have a minor effect on the upper bounds for q_c. Furthermore, the lower bound on q_c is clearly determined by Eq. 8.3.

Comparing the measured values of q_c and the predicted upper and lower bounds in Fig. 8.4, we note that most of the test results at the 3 sites are within the predicted bands. This indicates that Eq. 8.3 reliably predicts a range for s_u(REF). "Safe" values of s_u(REF) are obtained using the expressions for the upper bound on q_c (representing the lower bound for s_u).

Noting that theoretical upper and lower bounds differ by approximately a factor of 2, practical applications may often require better estimates of s_u. Therefore, q_c was also computed from Eqs. 8.4 and 8.5 and plotted in Fig. 8.4. In view of the many uncertainties in these predictions and the scatter in q_c, the difference between the two expressions is not very significant. However, Eq. 8.4 where σ_{ho} is subtracted from q_c (instead of σ_{vo} in Eq. 8.5) appears to give a slightly better agreement with measurements.

In summary, results obtained at the three sites show that reasonable estimates of s_u(REF) can be obtained from the resistance of FUGRO

60° cones by means of Eq. 8.4 with $N_c = 11$. Since σ_{vo} is easier to estimate than σ_{ho}, Eq. 8.5 can also be used without seriously affecting the predicted values of $s_u(REF)$. The field strength, $s_u(field)$, to be used in stability analyses can then be determined from $s_u(REF)$ by applying the strain rate correction factor μ_R in Fig. 8.1b according to Eq. 8.7.

(2.b) <u>Effect of cone angle.</u> An evaluation of the effect of cone angle, 2δ, as predicted by the theory, is presented in Fig. 8.5 for the three sites (Figs. a, b and c). $s_u(cone)$ is determined from Eq. 8.4 which, according to the above discussion, gives a good estimate of $s_u(REF)$.

Figure 8.5 shows that the predicted values of $s_u(cone)$ exhibit no consistent trend with the cone angle 2δ at any of the three sites.[*] Noting that the theoretical cone factor N_c is significantly different for the cone angles used (see Table 8.1), this indicates that the effect of cone angle is adequately predicted by the theory. However, the scatter of $s_u(cone)$ for regular cones in Fig. 8.5 is higher than for enlarged cones, Figs. 8.2 and 8.3. Finally, predicted values of $s_u(cone)$ based on Eq. 8.4 are reasonably close to $s_u(REF)$ although in the highly overconsolidated Boston Blue Clay (above 60 ft depth, Fig. 8.5a) and in the Atchfalaya clay (Fig. 8.5b) $s_u(cone)$ might be considered closer to $s_u(field)$.

8.4   Summary

The semi-empirical cone penetration theory presented in Chapter 4 provides a rational basis for the interpretation of cone penetration measurements to estimate the undrained shear strength of clays, $s_u(cone)$.

The evaluation of $s_u(cone)$ is complicated by the very difficult task

---

[*] e.g., $s_u(cone)$ for $2\delta = 30°$ is not consistently between values predicted for $2\delta = 60°$ and $2\delta = 18°$.

of estimating a reference shear strength, $s_u(REF)$, to compare with theoret-

icle predictions. Motivated by the need to relate $s_u(cone)$ to field per-

formance, $s_u(REF)$ is estimated from the "field" strength,[*] $s_u(field)$, through

an empirical correction factor, μ_R, to account for strain rate effects,

Fig. 8.1b.

Theoretical predictions of $s_u(cone)$ based on enlarged cone resistances

(see diagram in Table 8.1), supplemented by pore pressure measurements

behind the tip, provide very acceptable profiles compared to $s_u(REF)$ for all

cone angles tested in a marine illitic clay (Boston Blue Clay, low PI,

medium sensitivity) and a plastic deltaic clay (Atchafalaya clay, high PI,

low sensitivity). For unenlarged (regular) cones (see diagram in Table 8.1),

the theory can only predict upper and lower bounds for $s_u(cone)$, Eq. 8.3.

Results at three sites (Fig. 8.4) indicate that the predicted bands are

reasonably reliable assuming $s_u(cone) = s_u(REF)$.

Figure 8.6 summarizes the recommended procedures for interpreting

regular and enlarged cone resistance data.

---

[*]Average values of $s_u(field)$ are based on full-scale embankment failures,
and profiles of $s_u(field)$ are estimated from field vane data or SHANSEP labora-
tory test results.
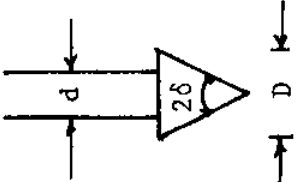
Type of Measurements	s_u(cone) given by	Special Requirements
q_c from enlarged cones (D/d > 1)	Theoretically, $[q_c - (d/D)^2 \, p_b]/N_c$ (8.1)	Measurement of pore pressure behind the cone, p_b.
q_c from unenlarged cones (D/d = 1)	Theoretical lower and upper bounds $\dfrac{q_c - \sigma_{ho}}{N_c + 1 + \ell n\,(G/s_u)} \le s_u \le q_c/N_c$ (8.3) Empirical formulas $s_u = (q_c - \sigma_{ho})/N_c$ (8.4) $s_u = (q_c - \sigma_{vo})/N_c$ (8.5)	Evaluation of the initial horizontal total stress, σ_{ho}. For most soft clays, $\sigma_{ho} = (0.80 \pm 0.08)\,\sigma_{vo}$

N_c = cone factor;

$= 1.2 \,(5.71 + 3.33\delta + 1/\tan \delta)$;

$= 11.0,\ 12.4,\ 15.1$ for $2\delta = 60°,\ 30°,\ 18°$ respectively;

σ_{ho} = initial horizontal total stress

σ_{vo} = initial vertical stress

G = undrained shear modulus

Table 8.1 Predictions of undrained shear strength from cone penetration measurements.

(1) Deposit	(2) s_u(field)	(3) Correction Factor for Rate Effect[†] μ_R (Fig. 8.1b)	(4) Reference Strength s_u(REF) = (2)/(3)	(5) Relevant Figures	(6) References
Boston Blue Clay 25 to 65 ft depth	$0.9\ s_u$(FV)*	0.82	$1.1\ s_u$(FV)	Fig. 5.4,	Azzouz and Baligh (1978), Appendix A
65 to 125 ft depth	$1.1\ s_u$(FV)	0.82	$1.35\ s_u$(FV)	Fig. 5.5	
Atchafalaya Basin Clay	s_u(DSS)* SHANSEP	0.65	$1.5\ s_u$(DSS)	Fig. 5.9, Fig. 5.10	Fuleihan and Ladd (1976)
Connecticut Valley Varved Clay	$0.85\ s_u$(FV)*	0.80	$\approx s_u$(FV)	Fig. 5.14	Ladd (1975)

* Based on evaluation of embankment performance

[†] Recommended by Bjerrum (1973) for clays as a function of plasticity index.

Table 8.2 Back figured strength based on embankment performance and correction for the effects of strain-rate (FV = field vane test; DSS = direct simple shear test).

(1) Deposit	(2) Depth (ft)	(3) $\dfrac{s_u(\text{field})^{**}}{s_u(\text{FV})}$	(4) Bjerrum's μ (Fig. 8.1a)
Boston Blue Clay (PI = 20 - 24%)	25 - 65 65 - 125	0.9* 1.1*	1.0 1.0
Atchafalaya Basin Clay (PI = 60 - 80%)	40 - 120	0.6 - 0.7	0.7
Connecticut Valley Varved Clay (PI ≈ 30%, bulk)	15 - 50	0.85	0.9

*See appendix A, Section A.2, for prediction methods.

**s_u(field based on embankment performance)

Table 8.3   Comparision between the back figured field strength, s_u(field), and the strength obtained from field vane data at the three sites considered.

Type of Measurements	Cone Type		Number of Tests Used in s_u(cone) Prediction		
	2 δ	D/d	Boston Blue Clay	Atchafalaya Basin Clay	Connecticut Valley Varved Clay
q_c	18°	2	1	2	--
q_c	30°	2	--	1	--
q_c	60°	2	1	2	--
q_c	18°	1	1	1	1
q_c	30°	1	1	--	1
q_c	60°	1	3	3	2
u (tip)	18°	2	1	--	--
u (behind cone)	18°	2	2	--	--
u (behind cone)	60°	2	2	--	--

Table 8.4 - Summary of tests used in strength prediction
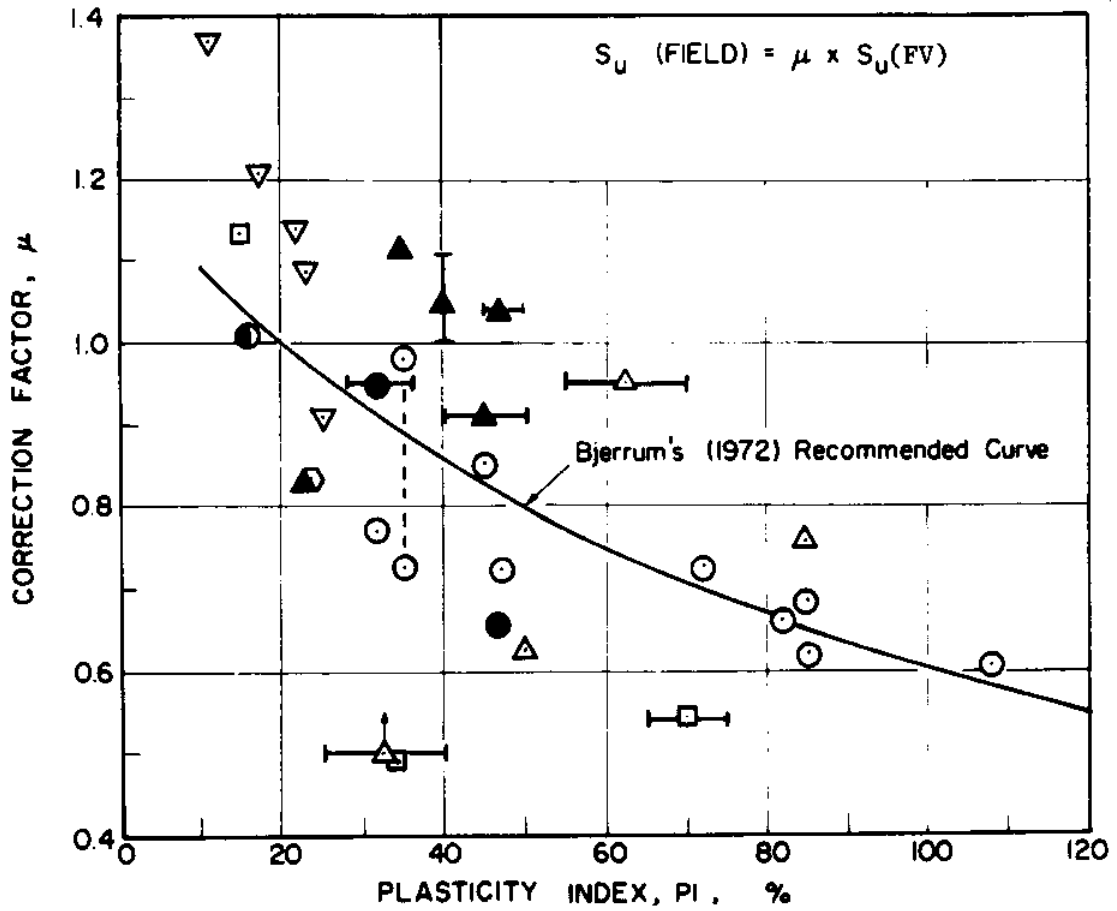
Fig. 8.1a Empirical correction factor derived from embankment
failures for the field vane test (from Ladd, 1975).
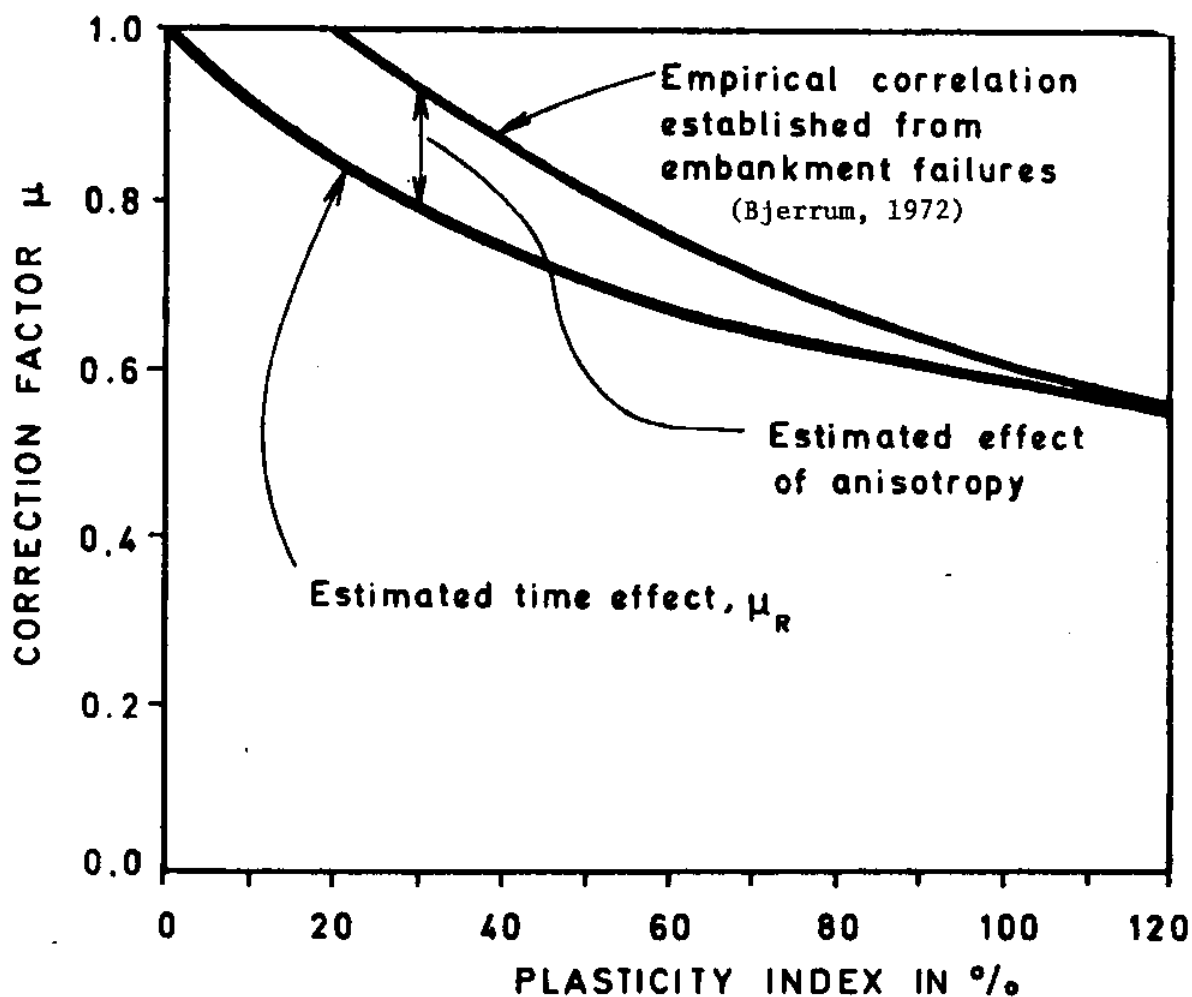
Fig. 8.1b   Components of the field vane correction factor according
to Bjerrum (1973).
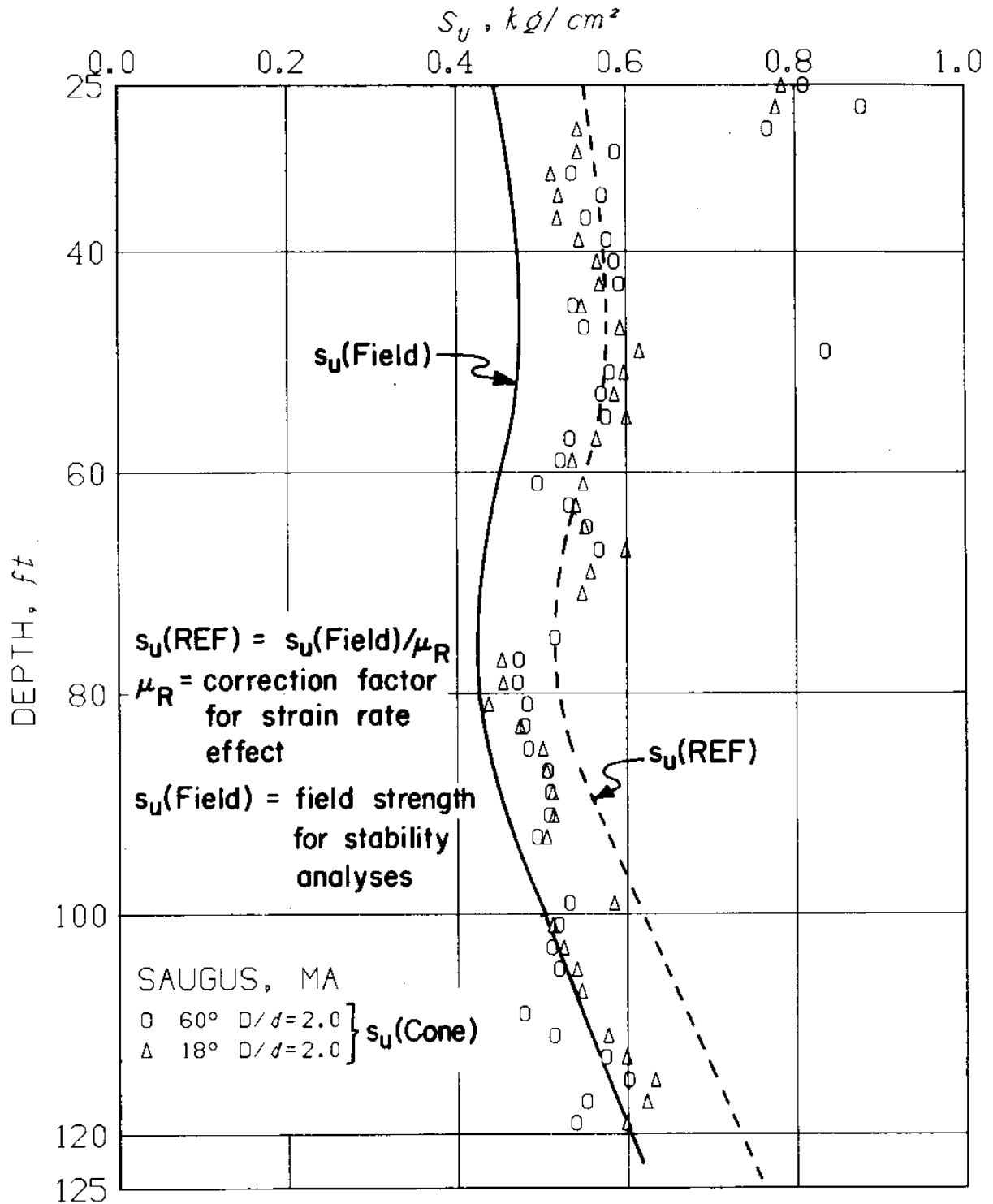
Fig. 8.2 Predicted strength from enlarged cone resistance in Boston Blue Clay
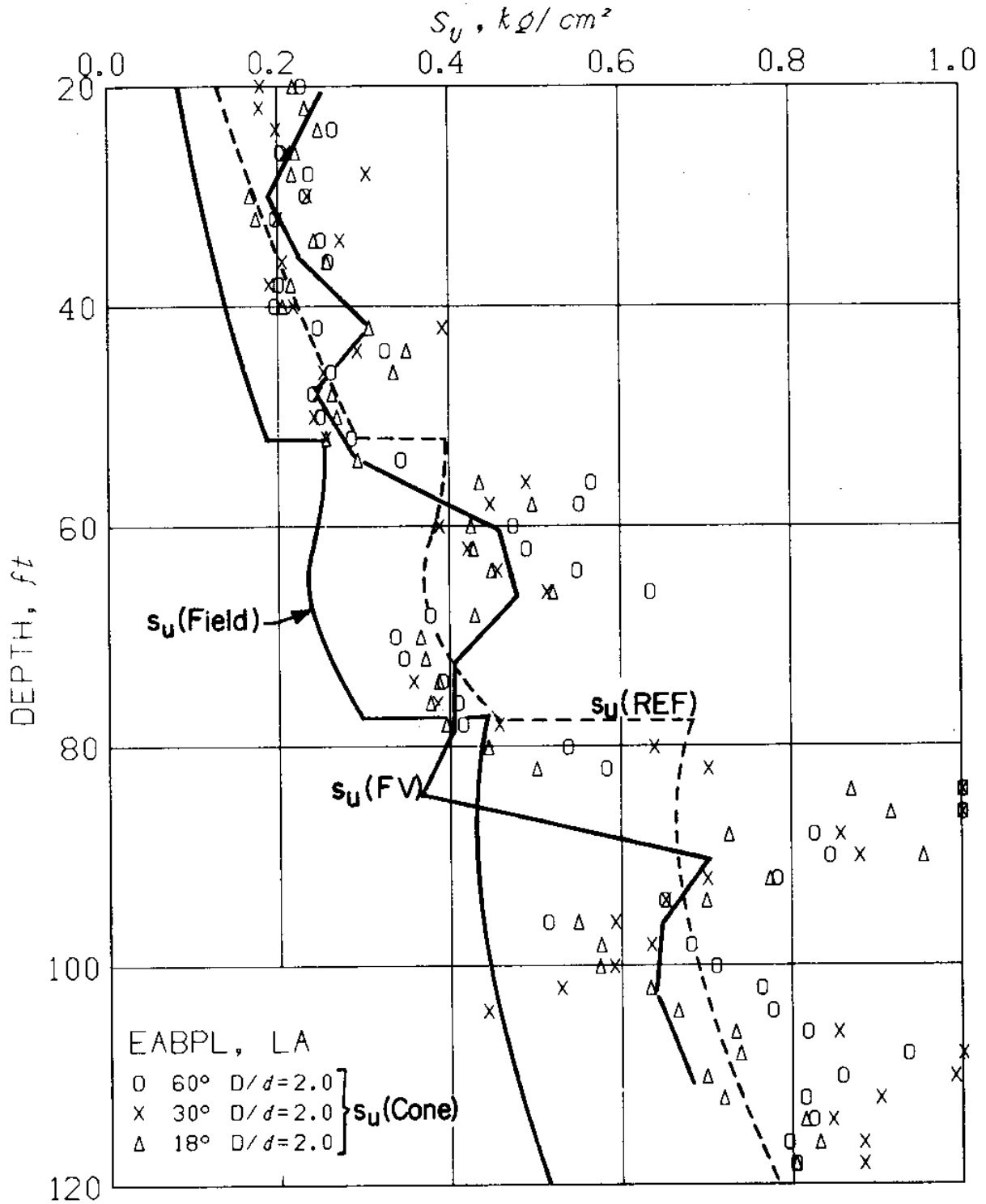
Fig. 8.3 Predicted strength from enlarged cone resistance in Atchafalaya Basin Clay.

$$\frac{q_c}{s_u}(REF)$$

Approximate Curve ①

$$\frac{q_c}{s_u} = N_c + \frac{\sigma_{ho}}{s_u}$$

± 2σ band

Approximate Curve ②

$$\frac{q_c}{s_u} = N_c + \frac{\sigma_{vo}}{s_u}$$

Theoretical
Lower Bound →

$$\frac{q_c}{s_u} = N_c$$

Theoretical Upper
Bound

$$\frac{q_c}{s_u} = N_c + 1 + \ln\left(\frac{G}{s_u}\right) + \frac{\sigma_{ho}}{s_u}$$

$G/s_u = 50$ 150 400

SAUGUS, MA

O 60° D/d = 1.0

For 60° cone,
theory predicts
$N_c = 11$

DEPTH, ft
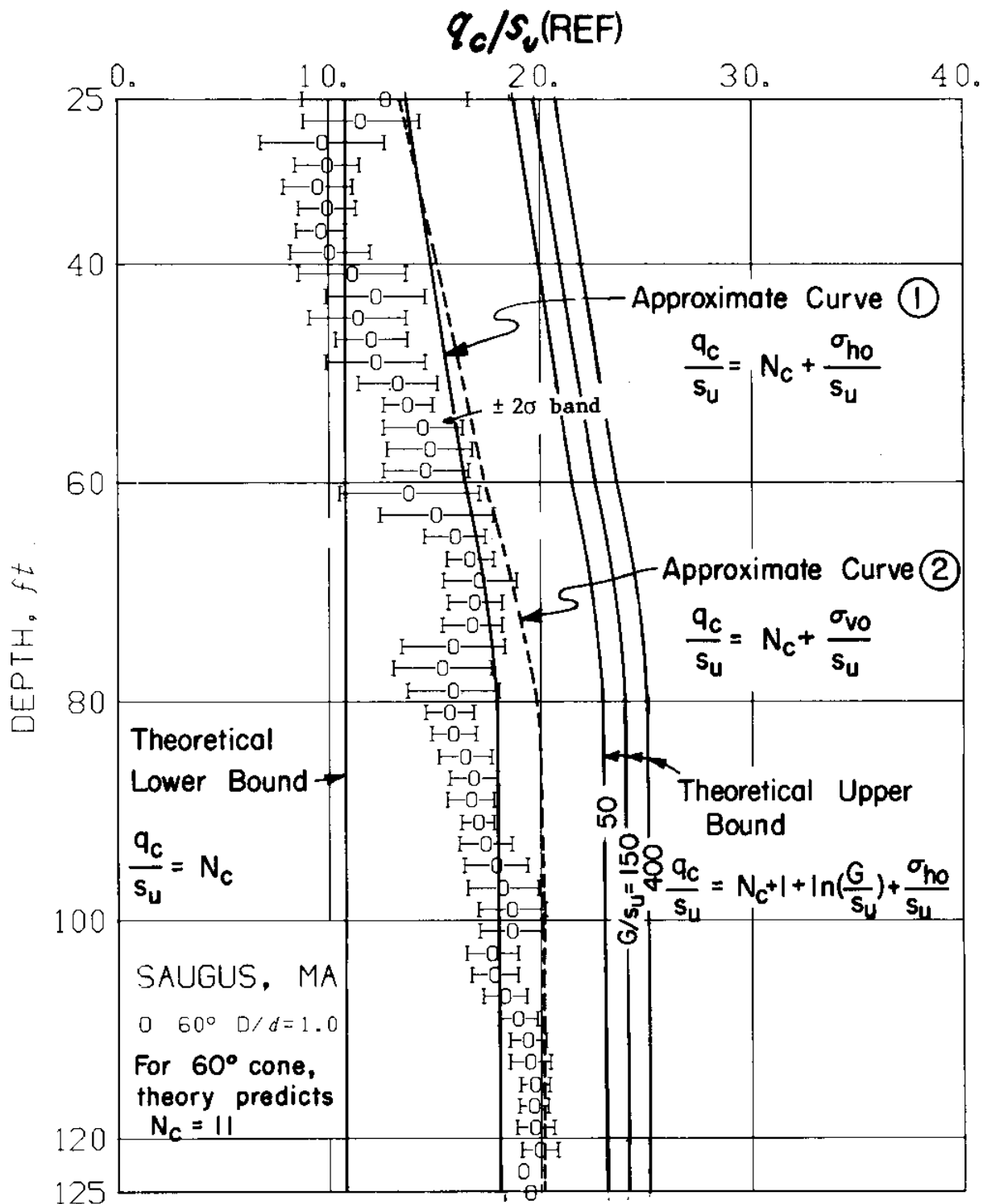
Fig. 8.4a   The cone resistance-reference strength ratio at the
Saugus, MA, test site (Fugro cone).
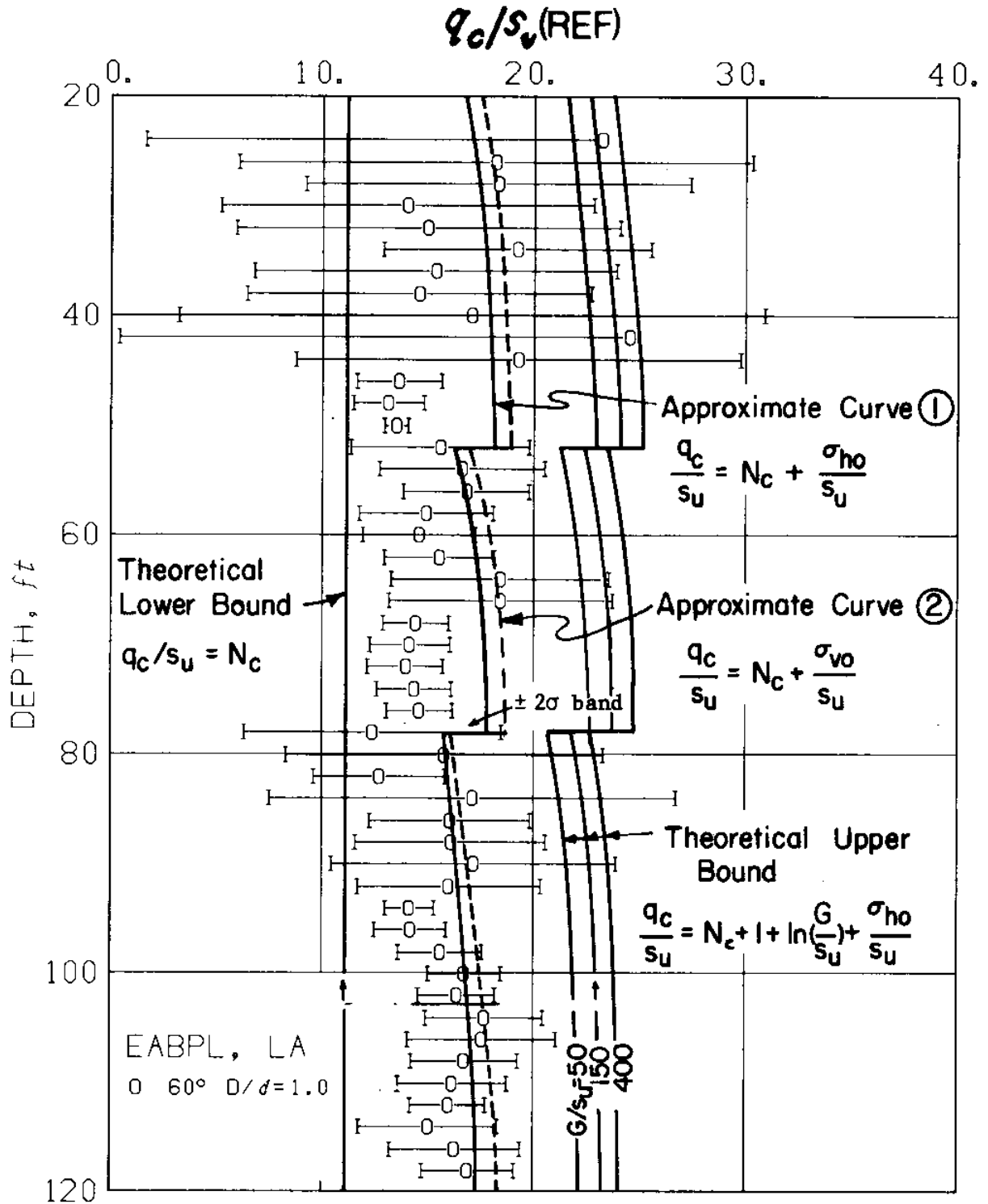
Fig. 8.4b The cone resistance-reference strength ratio at the
EABPL, LA, test site (Fugro cone).
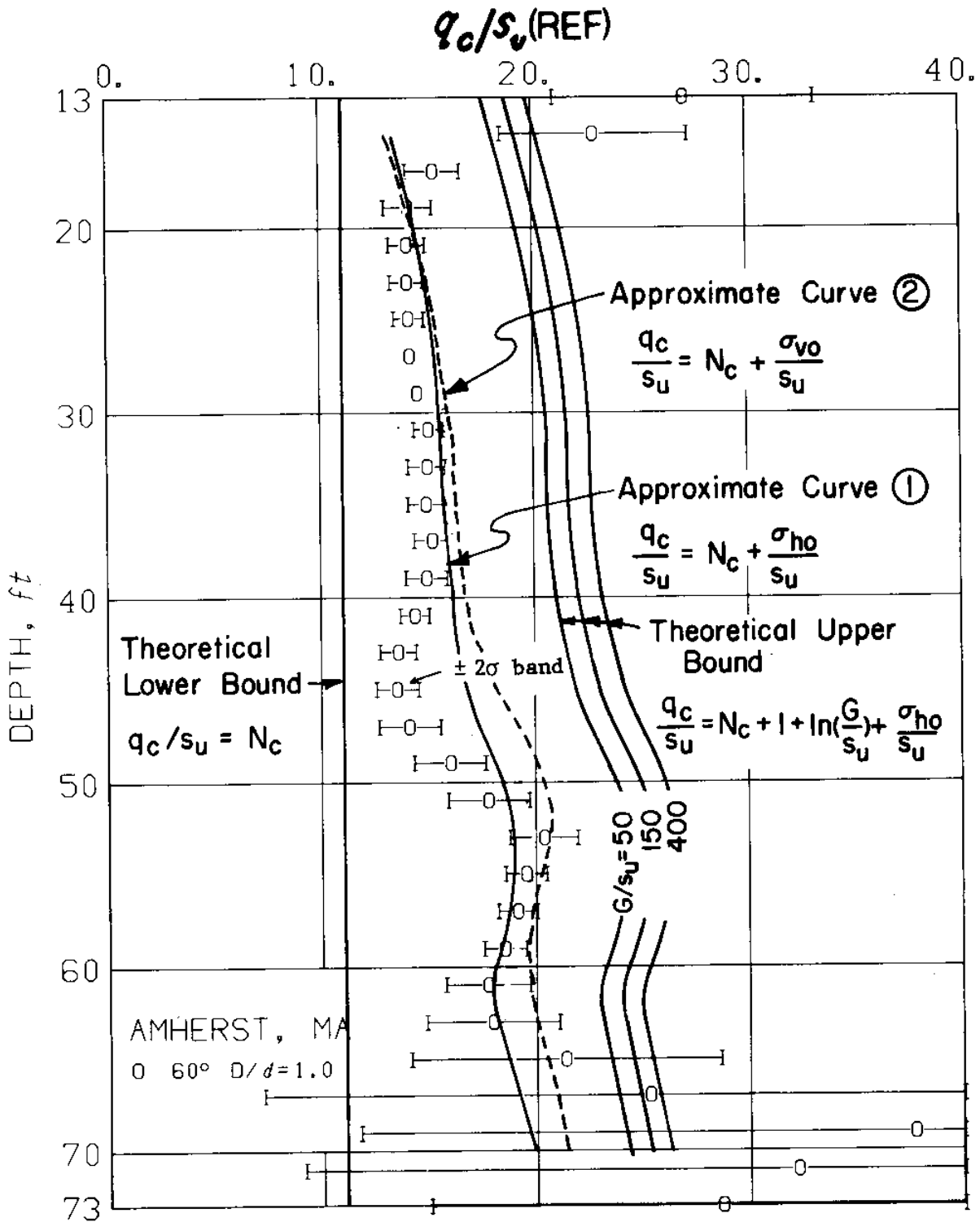
Fig. 8.4c The cone resistance-reference strength ratio at the Amherst, MA, test site (Fugro cone).
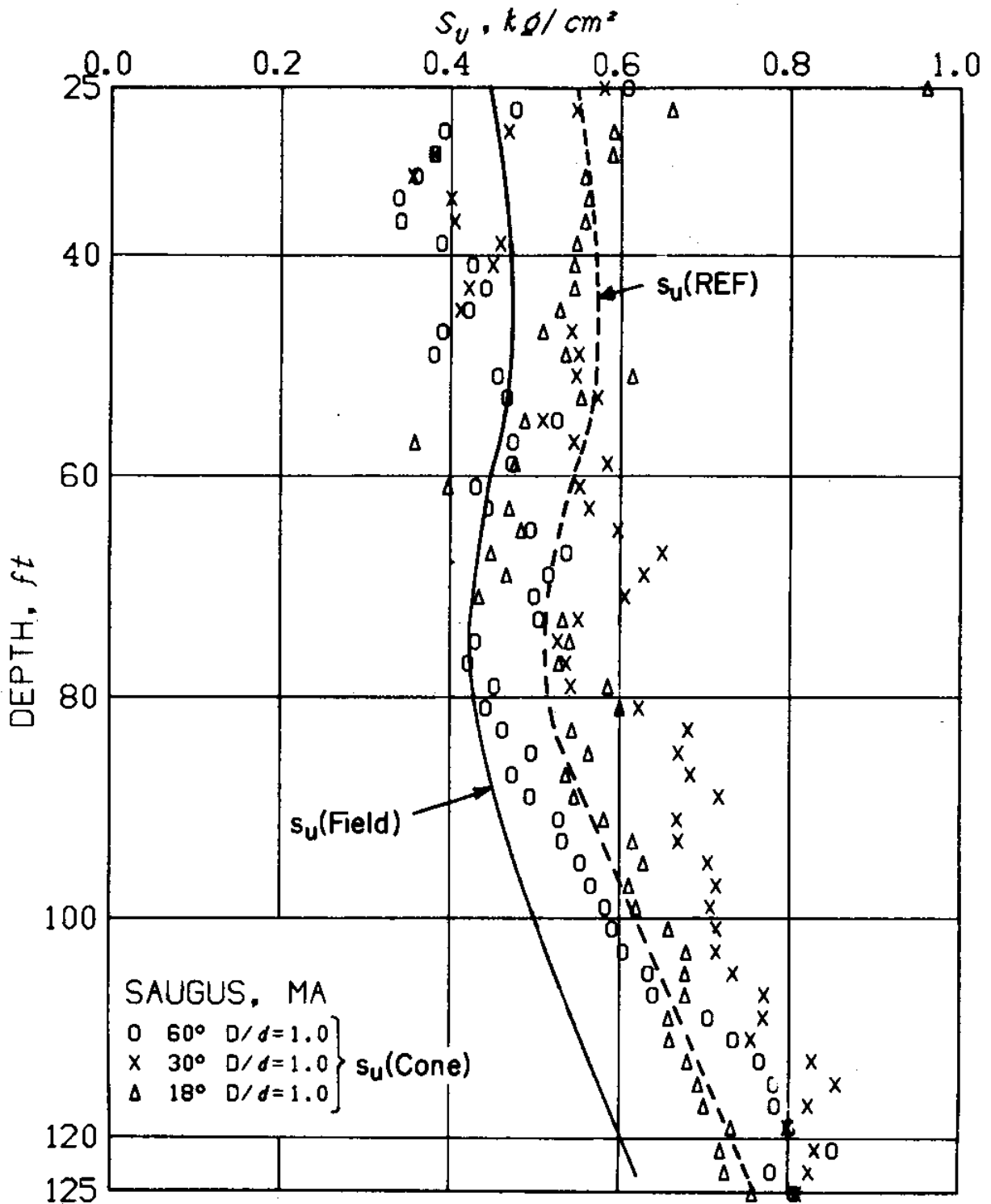
Fig. 8.5a **Prediction of undrained shear strength from unenlarged cones with Eq. (8.4), Boston Blue Clay.** (REF = reference strength)
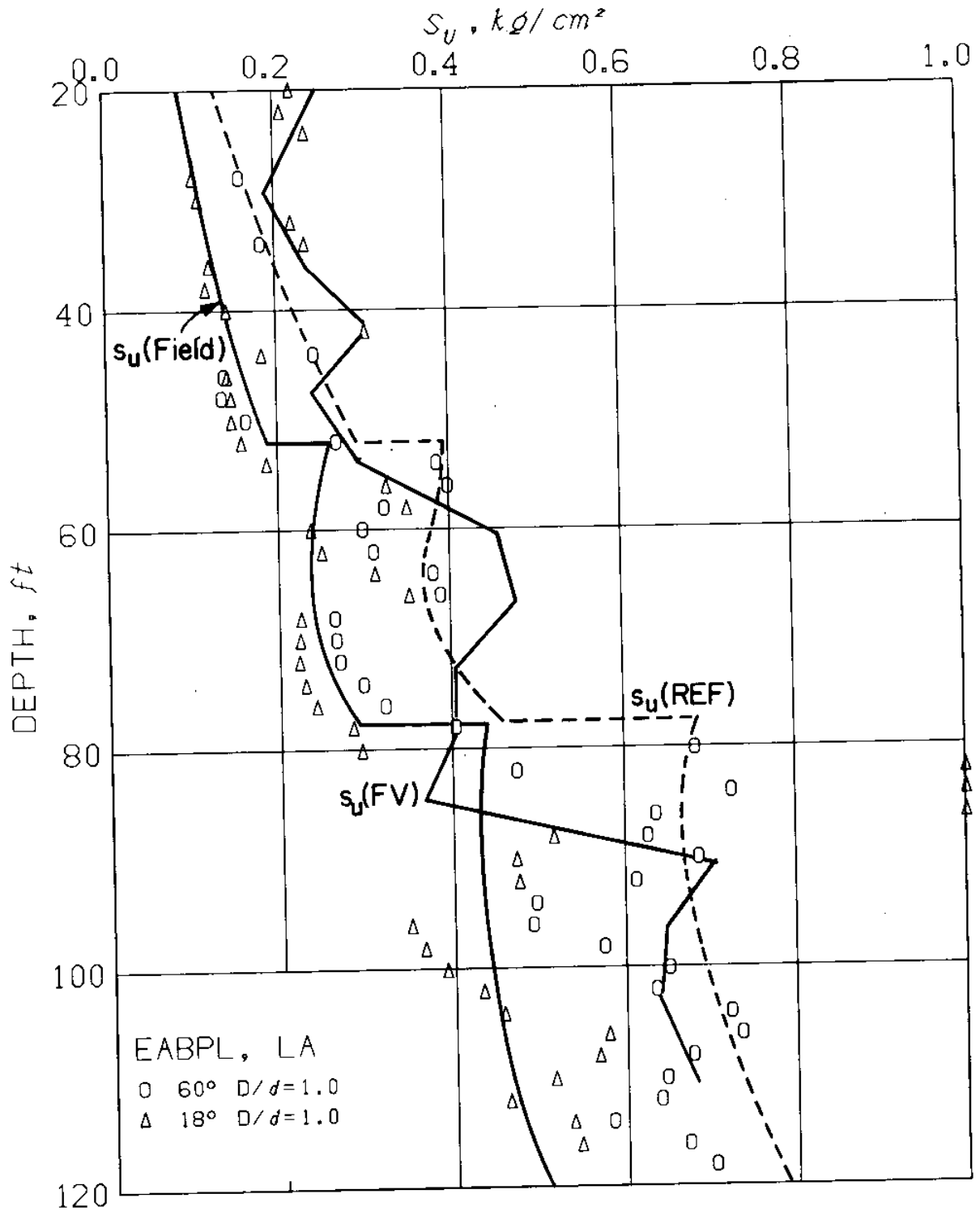
Fig. 8.5b   Prediction of undrained shear strength from unenlarged cones with Eq. (8.4), Atchafalaya Basin Clay. (REF = reference strength, FV = field vane strength.)
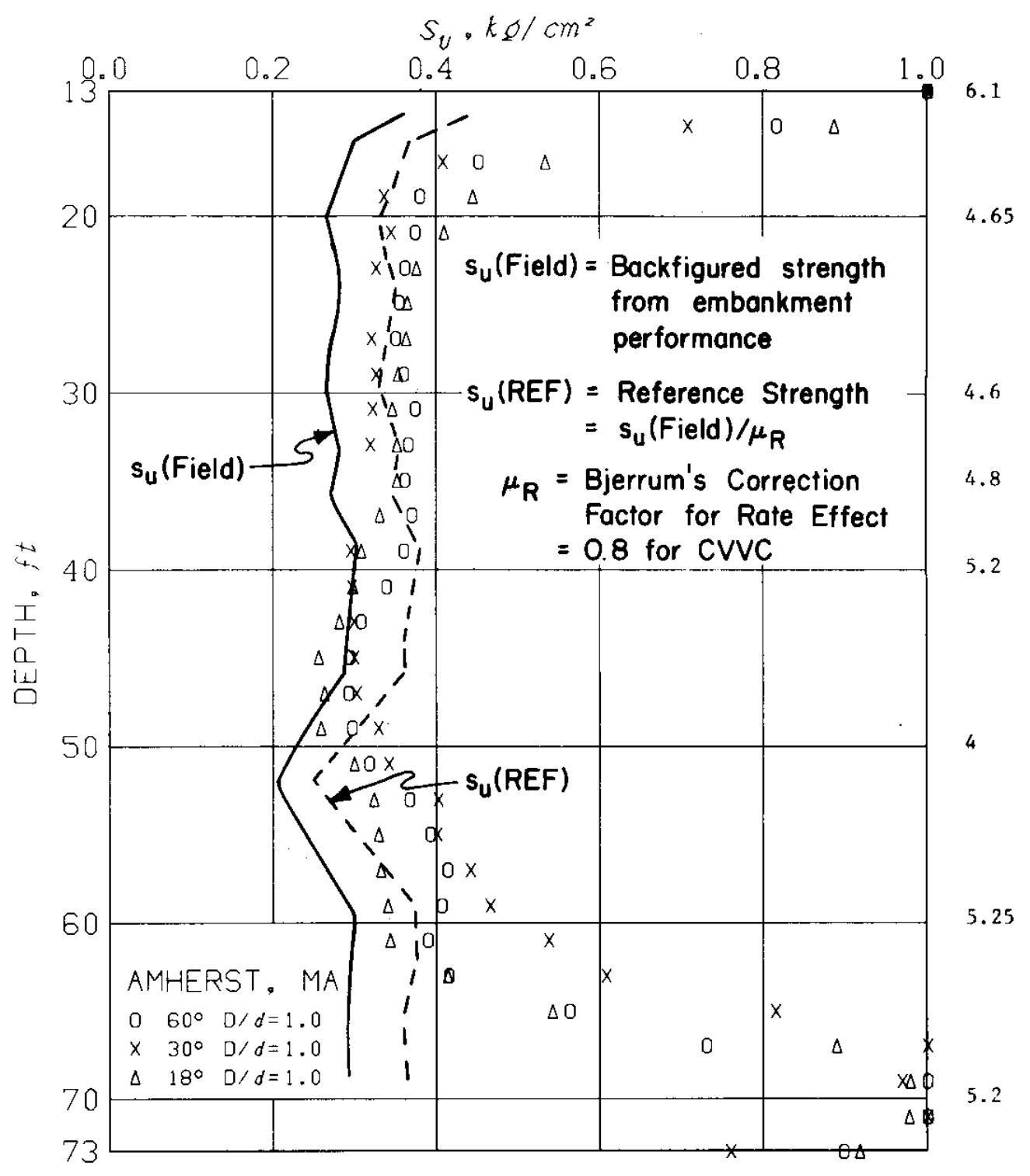
Fig. 8.5c Prediction of undrained shear strength from unenlarged cones
with Eq. (8.4), Connecticut Valley Varved Clay (REF =
reference strength).

PROCEDURES AND REQUIREMENTS FOR STRENGTH PREDICTION

ENLARGED CONES

1. Measure the cone resistance q_c and the pore pressure p_b behind the cone.

2. Compute s_u(cone) from the theoretical expression in Eq. 8.1 (Table 8.1)

3. Estimate the strain-rate factor μ_R, from Fig. 8.1b depending on the plasticity index of the soil.

4. Compute s_u(field) = $\mu_R\, s_u$(cone) for bearing capacity and stability analyses.

UNENLARGED CONES (REGULAR)

1. Measure the cone resistance q_c.

2. Estimate the maximum and minimum values of the q_c/s_u ratio using Eq. 8.3. Figures 4.2 and 4.3b might prove useful. The dependence of the rigidity index G/s_u on OCR is given in Fig. 5.17; and on the applied shear stress level in Fig. 19 (Ladd et al., 1977).

3. Estimate the strain-rate factor μ_R, from Fig. 8.1b.

4. Compute s_u(field) = $\mu_R\, s_u$(cone) for bearing capacity and stability analyses.

Fig. 8.6 Prediction of undrained shear strength using the proposed theory

CHAPTER 9

DESIGN CORRELATIONS FOR THE FUGRO CONE

9.1   Introduction

A semi-empirical theory of cone penetration is presented in Chapter 4

and evaluated in Chapter 8. For the FUGRO cone geometry (Chapter 5), the

theory predicts reasonable upper and lower bounds for the undrained shear

strength of clays. This chapter provides empirical correlations between

cone resistance, q_c, and the undrained shear strength obtained by the field

vane test, s_u(FV). These correlations, together with the evaluated experience

of s_u(FV), (Bjerrum, 1972 and 1973; Ladd et al., 1977) provide a good frame-

work for the practical use of q_c in design until q_c is directly correlated to

foundation performance.

9.2   Correlations with the Field Vane Test

Following the traditional bearing capacity equation in soil mechanics,

an empirical cone factor N_c(FV) can be defined as:

$$q_c = N_c(FV) \cdot s_u(FV) + \sigma_{vo},$$ (9.1)

or

$$N_c(FV) = \frac{q_c - \sigma_{vo}}{s_u(FV)} = (q_c - \sigma_{vo})(\frac{T_{max}}{7\pi d^3/6}) ,$$ (9.2)

where q_c = cone resistance;

               σ_{vo} = initial vertical total stress,

and where s_u(FV) and T_{max} are the "strength" and the maximum torque measured

in the field vane test respectively (see Chapter 8;   or Ladd et al., 1977).

Eqs. 9.1 and 9.2 essentially relate the force (per unit area) required

for continuous penetration of electric cone penetrometers to the maximum

torque measured during vane rotation, and the initial vertical total stress in the soil.

Figures 9.1a, 9.1b and 9.1c show the mean and the $\pm 2\sigma$ band of $N_c(FV)$ (σ = standard deviation) computed from Eq. 9.1 for tests in Boston Blue Clay, Atchafalaya Basin Clay, and Connecticut Valley Varved Clay, respectively. The geology and soil conditions at these sites are presented in Chapter 5. In computing the factor $N_c(FV)$, q_c data is obtained from two to three FUGRO cone tests (see Table 8.4) performed within a close proximity (40-ft radius). On the other hand, $s_u(FV)$ are the _average_ of existing field vane measurements conducted within a 200-ft radius of the cone tests[*] (data were presented in Chapter 5). The computed $N_c(FV)$ data are filtered by the procedure presented in Chapter 6 to reduce the influence of clear local soil inhomogeneities (e.g. sand lenses). The variability of $N_c(FV)$ shown in Fig. 9.1 thus reflects the variability of the cone tests, but not the scatter of the field vane data. (Chapter 6 studies the variability of both tests individually.) The three case studies and some results reported by others are discussed below.

(1) _Boston Blue Clay_. (q_c and $s_u(FV)$ profiles are shown in Figs. 6.4 and 5.5, respectively). Figure 9.1a shows that the average value of $N_c(FV)$ decreases from 12 (or higher) in the stiff crust to about 7.5 at a depth of 35 ft. Below this depth, the average N_c (FV) increases almost linearly to 14 at a depth of 120 ft. Furthermore, the point variability of $N_c(FV)$, i.e., its standard deviation σ, tends to decrease slightly with depth. The $\pm 2\delta$ band which includes approximately 95% of the (filtered) data points

---

[*]The field vane tests in the Boston Blue Clay and Connecticut Valley Varved Clay were performed by M.I.T., using the ASTM Standard with the Geonor equipment; in the Atchafalaya Basin Clay, they were performed by the U.S. Corps of Engineers.

(Chapter 6, Section 6.3) corresponds to an uncertainty of $N_c(FV)$ of ± 2 in the top 40 ft (heavily overconsolidated) and ± 1.5 in the bottom 60 ft (slightly overconsolidated). Finally, we notice in Fig. 9.1a that below a depth of 60 ft where OCR ≤ 2, the average value of $N_c(FV)$ is approximately given by 12 ± 2.

(2) <u>EABPL Clay.</u> The soil profile at this site is very variable (see q_c in Fig. 6.5) and the estimated profile of the average $s_u(FV)$ (Fig. 5.10) involves significant local uncertainty. The variability of q_c is illustrated by the large scatter in $N_c(FV)$ shown in Fig. 9.1b; especially in the 3 layers: above a depth of 44 ft (where the soil is highly organic), between 54 to 66 ft and between 78 to 92 ft (because of numerous silt lenses; USCE, 1968). In the remaining layers, the point variability of $N_c(FV)$ is small, i.e., $2\delta \leq \pm 2.5$. Finally, the average value of $N_c(FV)$ throughout this deposit (with OCR ≤ 1.5) is mostly within the range 9 ± 4.

(3) <u>Connecticut Valley Varved Clay</u>. (q_c and $s_u(FV)$ profiles are shown in Figs. 6.6 and 5.14, respectively). In this deposit, $N_c(FV)$ decreases from more than 15 in the crust to a very uniform value of 10 to 12 up to a depth of 40 ft. A dip in $N_c(FV)$ near depth $= 45$ ft is probably caused by soil variability between the locations where cone and field vane tests were conducted. (The cone tests detect slightly weaker soil at depths of about 46 ft, whereas the field vane test, conducted 200 ft away, detects it at about 52 ft depth.) The point variability of $N_c(FV)$ is relatively small, i.e., $2\delta = \pm(1 \text{ to } 1.5)$. The average values of $N_c(FV)$ is within the range of 11 ± 2 (excluding the region between 42 and 52 ft). Thus the variation of $N_c(FV)$ with depth in this case is of the same order as its point variability.

(4) <u>Comparison of $N_c(FV)$ in different clay deposits.</u> Figure 9.2 shows the average field vane strength, $s_u(FV)$, at the three M.I.T. test sites

(curves B, C, L), and also at six Scandinavian sites (curves 1 to 6) where

cone resistance data were obtained by NGI-FUGRO (Lunne et al., 1976).

Table 9.1 provides soil information on Scandinavian sites. More details are

given by Lunne et al. (1976).

Figure 9.3a presents the average N_c(FV) profiles obtained from

these nine sites. We note that:

1.   Excluding site No. 3, where s_u(FV) below a depth of 15 m is

unusually low (probably because of the high sensitivity of the

clay, Table 9.1 and Fig. 9.2), the values of N_c(FV) are between

5 and 21 for the remaining eight sites.

2. N_c(FV) profiles obtained by M.I.T. are either constant with

depth or tend to increase with depth, whereas N_c(FV) profiles

obtained by NGI-FUGRO tend to decrease with depth.

3.   Comparing the average value of N_c(FV) in each deposit, we note

that the values obtained by M.I.T. are generally lower than

those obtained by NGI-FUGRO.

The different trends and values in N_c(FV) shown in Fig. 9.3a

can be attributed to one or more of the following reasons:

1.   Errors or distortions in s_u(FV), q_c, or both.

2.   The inability of Eq. 9.1 to account for the dependence

of q_c on depth.

3.   Differences in the clay properties among these sites, e.g.,

plasticity index and/or sensitivity as well as the stress his-

tory and/or strength. For example, curves 1 and 4 showing

N_c(FV) decreasing with depth correspond to deposits where sensi-

tivity decreases with depth. Curve L with the lowest value of

N_c(FV) corresponds to the highest value of plasticity index.

Curve 3 below 12 m with very high value of N_c(FV) corresponds to a very sensitive clay.

Lunne et al (1976) do not consider the dependence of N_c(FV) on depth, but indicate a relationship between N_c(FV) and PI for "medium" to "very soft" clays. Their data are shown in Table 9.1 and are replotted in Fig. 9.4a with the uncertainty bands indicated by Lunne et al. (1976). Also shown for comparison in Fig. 9.4a are the results from the M.I.T. test sites, excluding the "stiff" or heavily overconsolidated clays and the more variable regions in the profiles, Table 9.2 and Figs. 9.1. The data in Fig. 9.4a indicate a decreasing trend in N_c(FV) with increasing PI. At any value of PI, the scatter in N_c(FV) is approximately $\pm$ 5

(5) <u>Application of Bjerrum's Correction Factor</u>. Case studies of embankment and footing failures indicate that s_u(FV) is not always the appropriate strength to use in bearing capacity or stability analyses.[*] A better estimate of the field strength is obtained if s_u(FV) is corrected by the empirical factor, μ, Fig.8.1a, based on actual failures (Bjerrum, 1972 and 1973, Ladd et al., 1977). Lunne et al. (1976) use Bjerrum's empirical correction factor, μ, to compute another empirical cone factor, N_c'(FV) defined by:

$$N_c'(\text{FV}) = \frac{q_c - \sigma_{vo}}{\mu \, s_u(\text{FV})} \qquad (9.3)$$

Therefore, the factor N'_c provides an empirical means of estimating the field strength s_u(FV) (to be used in the design of embankments and in problems involving bearing capacity of clays[*]) from q_c measurements.

---

[*] Appendix A discusses the validity of using the same strength for these two types of analyses.

Figure 9.3b shows profiles of the average values of $N_c'(FV)$ for the deposits described in Fig. 9.3a (data tabulated in Tables 9.1 and 9.2). Comparing Fig. 9.3b and Fig. 9.3a, we note that the correction factor slightly reduces the scatter in the empirical cone factor at any given depth. However, each $N_c'(FV)$ curve shows almost as much dependence on depth as $N_c(FV)$. Furthermore, we note in Fig. 9.3b that:

1. Values of N_c' obtained from all 9 sites are mostly within a band described by the expression:

$$N_c' = 14 \pm \alpha \qquad\qquad (9.4)$$

where $\alpha = 8 - 0.15z$

z = depth in meters (1 m = 3.28 ft)

≤ 40 m

2. The only exceptions to the above bands are some results obtained by NGI-FUGRO at site 3 (Børresen where PI is very low, the sensitivity very high and $s_u(FV)$ is suspiciously low (Fig. 9.2); and, the EABPL site (tested by M.I.T., Table 9.2) where the soil is too variable to give reliable values of N_c' (see for example, Fig. 9.1b).

3. Low values of N_c' (near the $N_c' = 14 - \alpha$ band) are obtained by M.I.T. (at the three sites denoted by B, L and C) whereas high values of N_c' (near the $N_c' = 14 + \alpha$ band) were determined at the Scandinavian sites. Noting that the clays tested by M.I.T. are generally stiffer than the Scandinavian sites, (see Fig. 9.2) this indicates that N_c' is probably related to OCR.

Figure 9.4b shows a plot of $N_c'(FV)$ vs. PI for "medium" to "very soft" clays at the 9 sites under consideration. Comparing this figure to

Fig. 9.4a, we note that N'_c(FV) does not vary with the plasticity index, PI, as much as N_c(FV). The range of N'_c(FV) for these "medium" to "very soft" clays is 8 to 20 for PI greater than 10%. At any PI, the uncertainty in N'_c(FV) is the same as in N_c(FV), and is about ± 5. For a mean value of N'_c(FV) of 14 to 15, this uncertainty range is about ± 33 %, which is larger than the scatter of the data associated with Bjerrum's correction factor for the field vane test (± 25%, Fig. 8.1). However, the greater uncertainty involved in interpreting cone resistance compared to field vane data based on this purely empirical approach should be expected since s_u(FV) (or corrections thereof) is assumed to represent the field strength. Direct correlations between q_c and actual performance of foundations should provide more reliable empirical interpretation methods.

9.3   Summary and Discussion

Empirical correlations between cone resistance, q_c, and corrected and uncorrected s_u(FV) are presented for a marine illitic clay (low PI, medium sensitivity), a plastic deltaic clay (high PI, low sensitivity), and a glacial lake varved clay (medium PI and sensitivity). The empirical cone factor N_c(FV) = $[q_c - \sigma_{vo}]/s_u$(FV) varies between 5 and 15 depending on stress history, sensitivity, depth, and possibly other factors. This range of N_c(FV) is lower than that presented by Lunne et al. (1976) for "medium" to "very soft" Scandinavian clays. Bjerrum's (1972) empirical correction factor, μ, for s_u(FV) slightly reduces the variation of N_c(FV) with soil type (PI) but cannot account for the dependence of N_c(FV) on depth, stress history, or sensitivity. The range of N'_c(FV) = $[q_c - \sigma_{vo}]/\mu s_u$(FV) for the three deposits tested by M.I.T and the six sites tested by Lunne et al., (1976) is 9 to 20 for medium to very soft clays with PI greater than 10. This large range of uncertainty in N'_c(FV) poses a serious limitation on the use of cone resistance for design purposes.

The complications associated with the empirical interpretation of q_c through the "corrected" $s_u(FV)$ arise due to the highly approximate nature of Eqs. 9.1 and 9.2 , the uncertainty in the interpretation of the field vane test, and the complicated and different behavior of various soils. The uncertainty in this empirical correlation can be significantly reduced by using local experience and noting the dependence of $N_c'(FV)$ on depth, see Eq. 9.4 and Fig. 9.3b. It can perhaps be further reduced if measurements of pore pressure during penetration are also available. Chapters 7 and 8 show that this pore pressure depends on the soil type and stress history and can influence the penetration resistance. Additional study on correlation between $N_c'(FV)$ and pore pressure is, however, required for this approach.

For unfamiliar clay deposits, Chapter 8 provides a method for estimating the upper and lower bounds of the undrained shear strength based on the cone penetration theory presented in Chapter 4.

SITE	DEPTH m	PLASTICITY INDEX P.I.,%	SENSITIVITY S_t	N_c(FV)	N_c(FV)* corrected
1. Sundland (Drammen Clay)	4-9	23-30	6-14	17-18	17-19
	9-14	7-10	1-2	18-20.5	16.5-18
	16-22	9-12	2-3	15.5-16.5	14-15
2. Dansviks Gate (Drammen)	3-10	20-35	6-9	13.5-17	15-16
	11-20	10-14	2-4	14-18	13-18
	20-35	10	3-4	13-16	12-14.5
3. Børresen Gate (Drammen)	6-12	15-20	13-22	17-20	16-19
	12-15.5	8	5-14	25-26	22.5-23.5
	15.5-30	4-5	40-130	20-26	18-23
4. Onsøy	2-9	25-30	5-10	17-19	18-19
	9-27	36	4-7	12-17	14-18
5. Gøteborg	2-10	45-60	11-24	12-15	17-20
	10-20	50-60	15-19	13	
	20-31	40	13-17	12-14	14-16
6. Ska-Edeby	2-4	40	6-9	8-9	10
	4-12	35-50	10-12	10.5-12.5	12.5-14.5

* corrected in each 1 - m section using applicable PI, exclude extreme values

Table 9.1   Tabulation of correlations between cone resistance and the field vane strengths at NGI-FUGRO sites (data from Lunne et al. 1976).

Test Site	Depth (ft)	PI (%)	$s_t^{(1)}$	$N_c(FV)$ $= \dfrac{q_c - \sigma_{vo}}{s_u(FV)}$	$N_c'(FV)^{(2)}$ $= \dfrac{q_c - \sigma_{vo}}{\mu\, s_u(FV)}$
Saugus, MA (Boston Blue Clay)	65 - 125	≈ 24	6	9 - 15	9 - 15
EABPL, LA (Atchafalaya Basin Clay)	50 - 120	60 - 80	1 ?	5.5 - 12.5	9 - 17
Amherst, MA (Connecticut Valley Varved Clay)	15 - 65 (excluding) 42 - 52	≈ 30 (bulk)	4 - 7	9 - 13	10 - 14

(1) from field vane data

(2) computed from the range of $N_c(FV)$

Table 9.2 Tabulation of correlations between cone resistance and the field vane strengths at M.I.T test sites
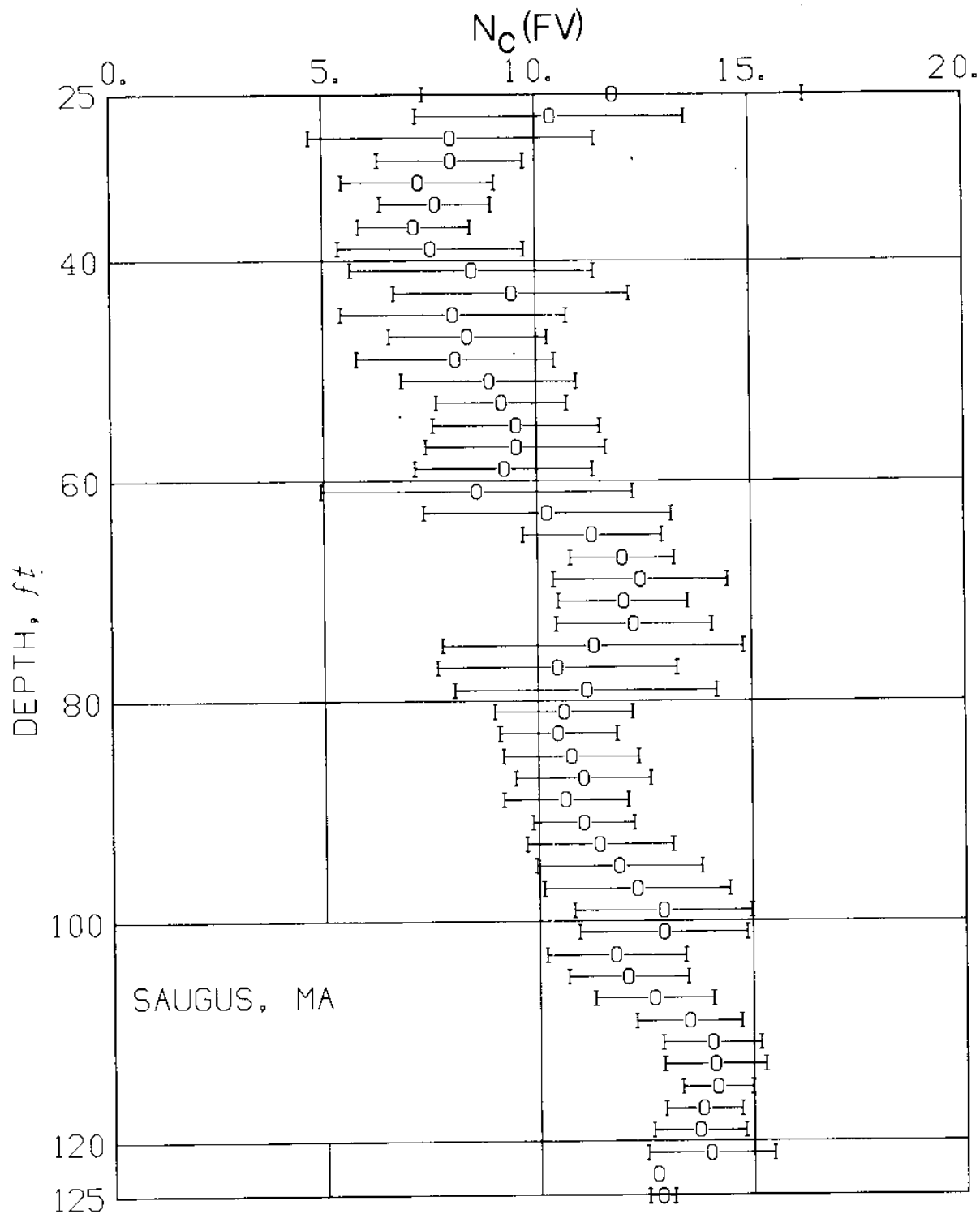
Fig. 9.1a Empirical Cone Factor, $N_c(FV) = [q_c - \sigma_{vo}]/s_u(FV)$,

at the Saugus, MA, test site
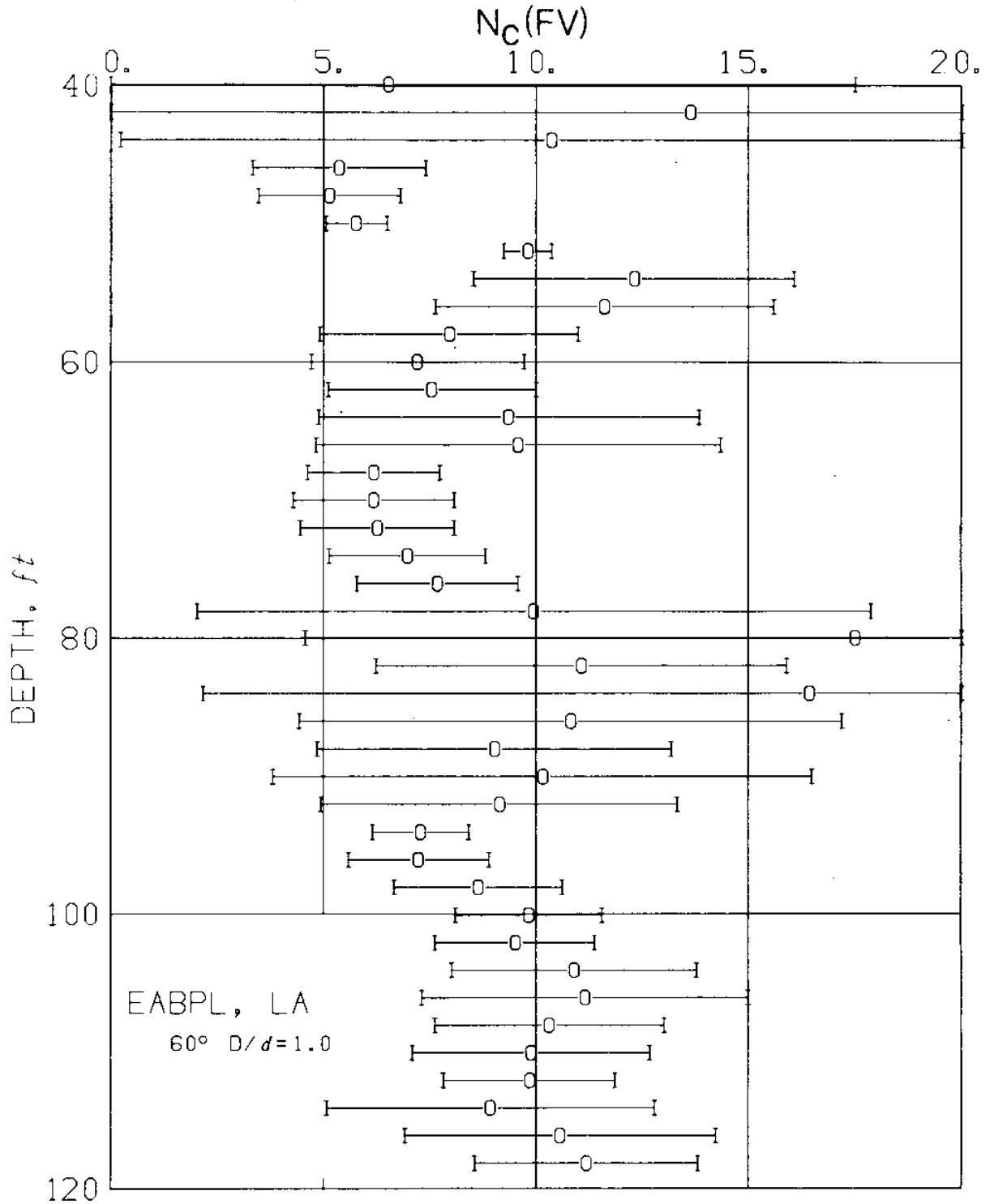
Fig. 9.1b Empirical Cone Factor, N_c(FV) = [q_c − σ_{vo}]/s_u(FV), at EABPL, LA
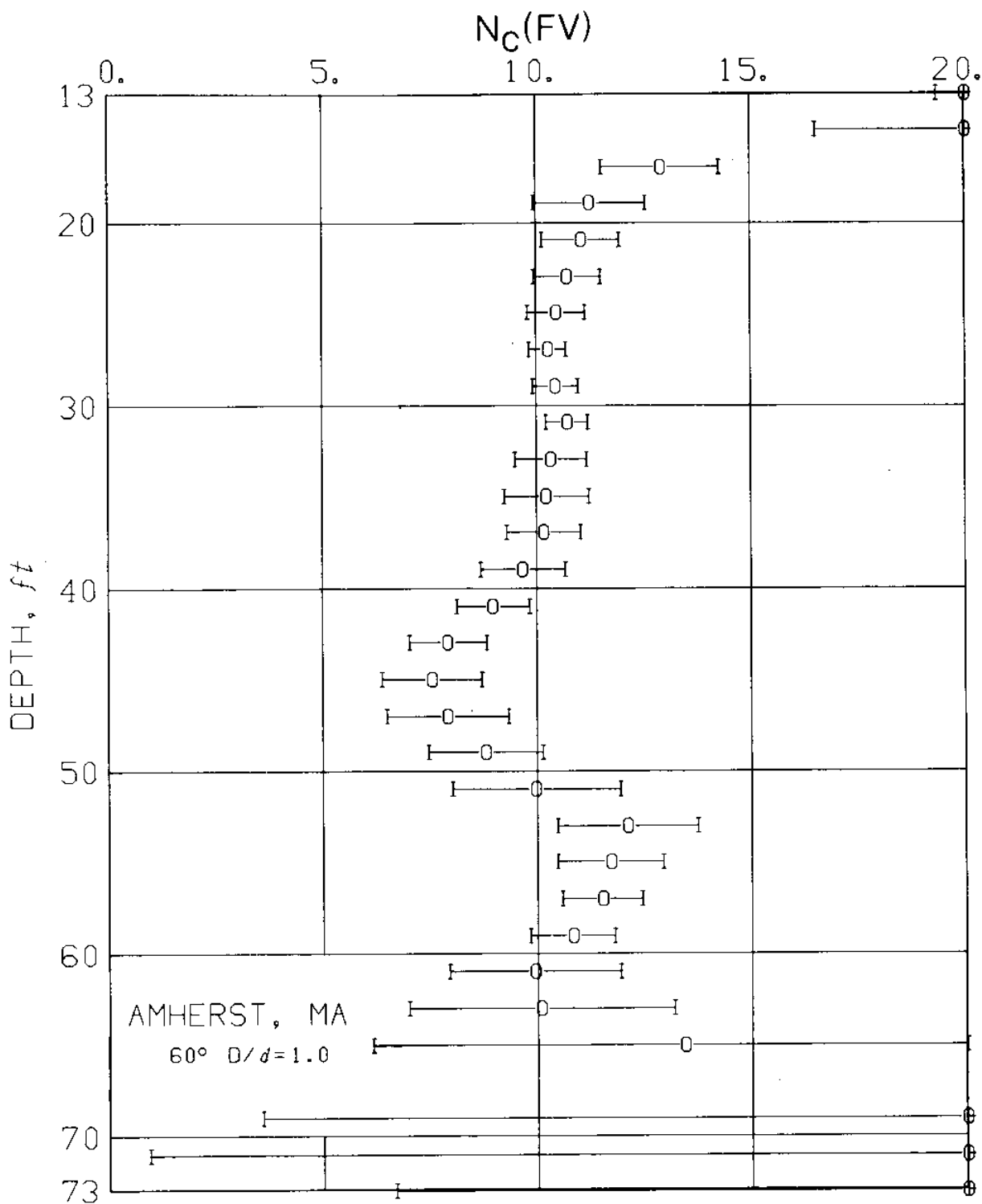
Fig. 9.1c Empirical Cone Factor, $N_c(FV) = [q_c - \sigma_{vo}]/s_u(FV)$,
at Amherst, MA
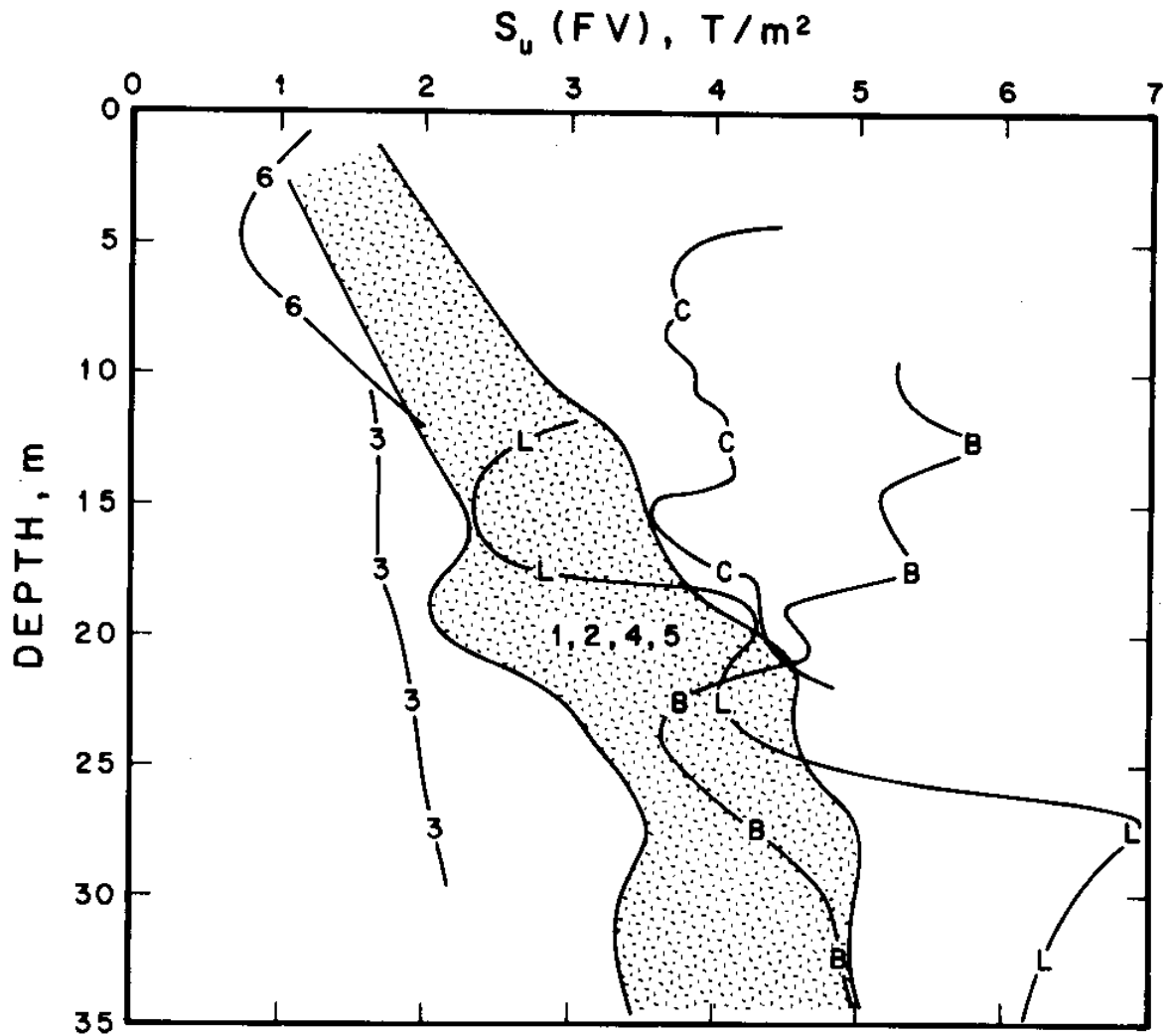
Fig. 9.2 Average field vane strength profiles at M.I.T. and NGI-FUGRO
test sites (see Tables 9.1 and 9.2 for site identification).

$$N_c \, (FV) = (q_c - \sigma_{vo}) \, / \, S_u \, (FV)$$
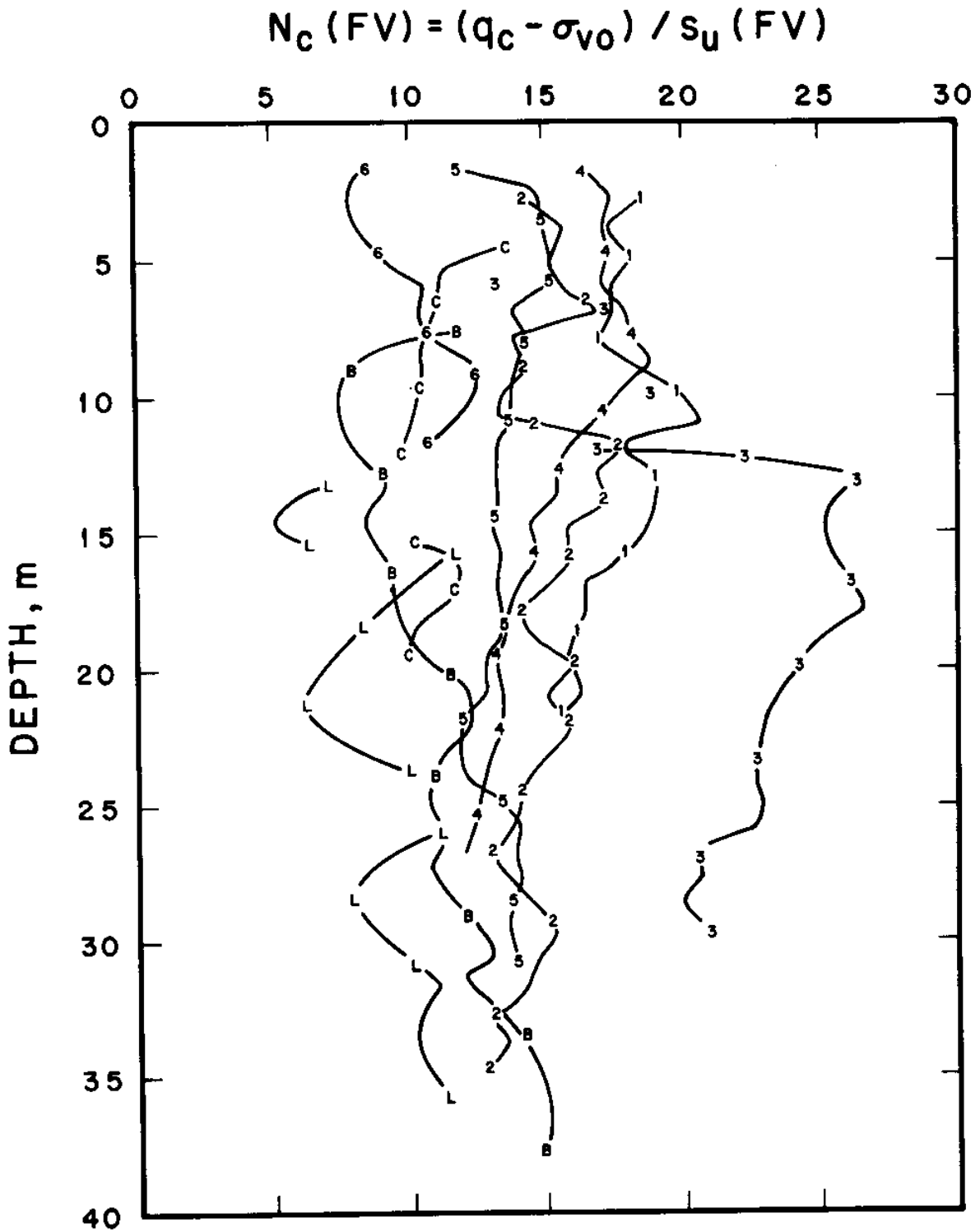
Fig. 9.3a Empirical cone factor N_c(FV) vs. depth for nine clay deposits

$$N_c' \, (FV) = (q_c - \sigma_{vo})/\mu \, s_u \, (FV)$$
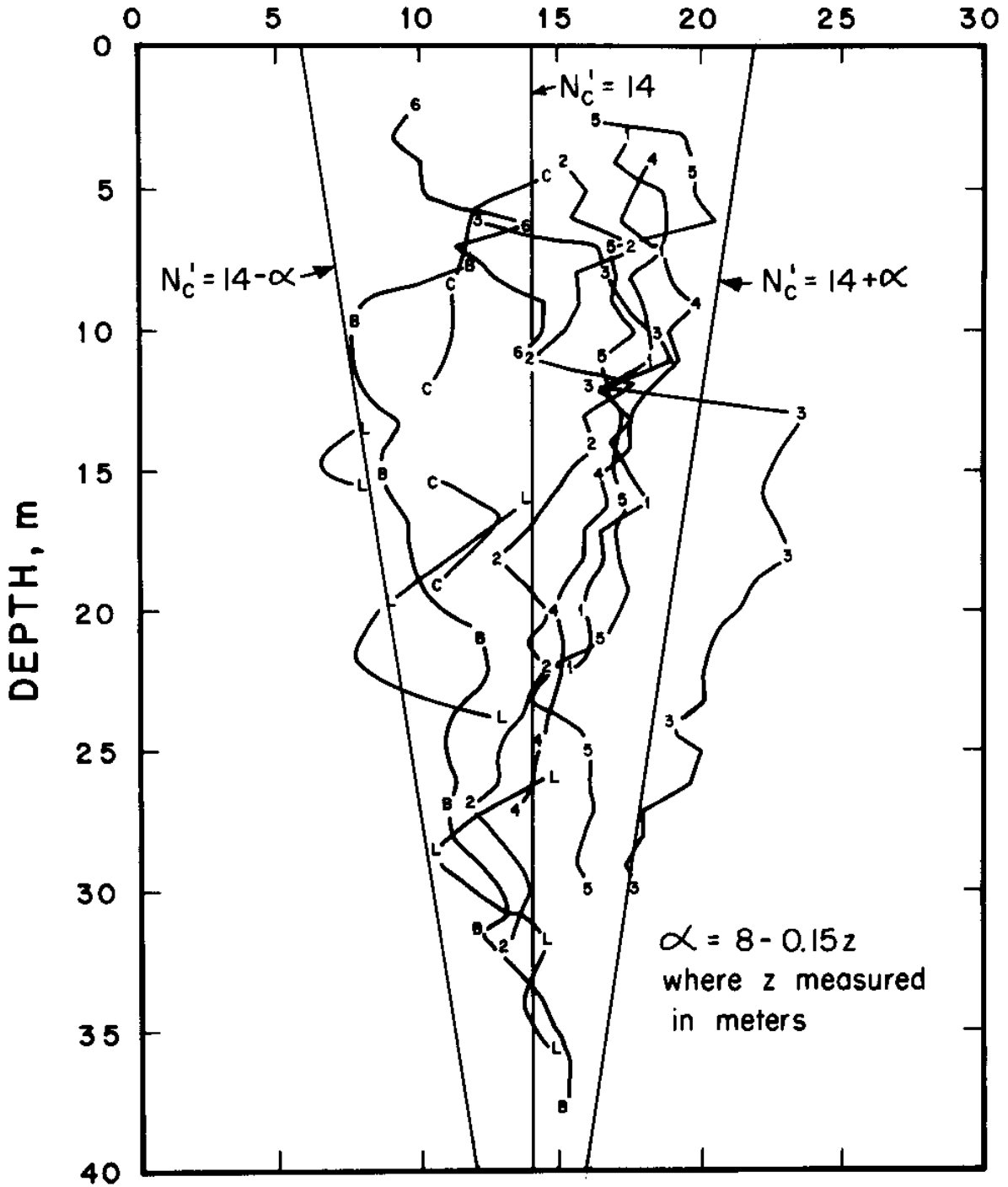
Fig. 9.3b   Empirical cone factor N_c'(FV) vs. depth for nine clay deposits

$$N_c = \frac{q_c - \sigma_{vo}}{s_u(FV)}$$

NGI TEST SITES

○ Sunland
□ Danviks
▽ E. Borresens
△ Onsoy
✕ Sko-Edeby
+ Goteborg

MIT TEST SITES

Ⓑ Saugus, Ma.
Ⓒ Amherst, Ma.
Ⓛ EABPL, La.

(a)

PLASTICITY INDEX, PI, %

a – cone factor N_c(FV)

$$N_c' = \frac{q_c - \sigma_{vo}}{\mu s_u(FV)}$$

NGI TEST SITES

○ Sunland
□ Danviks
▽ E. Borresens
△ Onsoy
✕ Sko-Edeby
+ Goteborg

MIT TEST SITES

Ⓑ Saugus, Ma.
Ⓒ Amherst, Ma.
Ⓛ EABPL, La.

(b)

PLASTICITY INDEX, PI, %
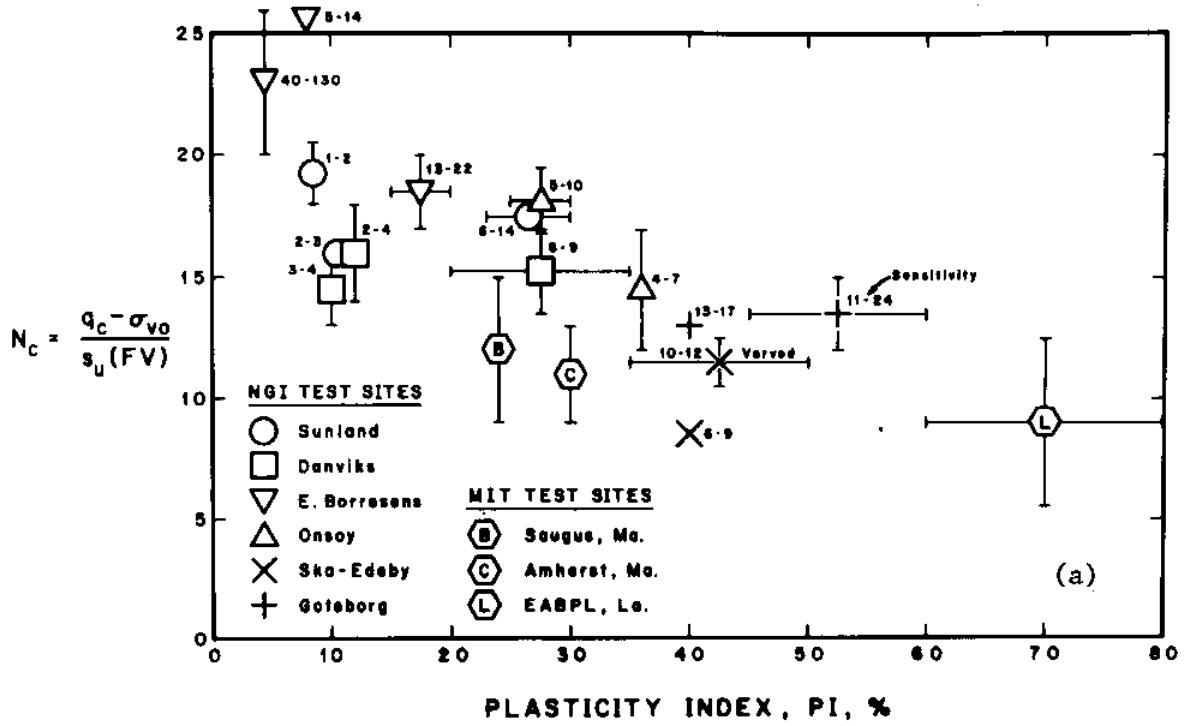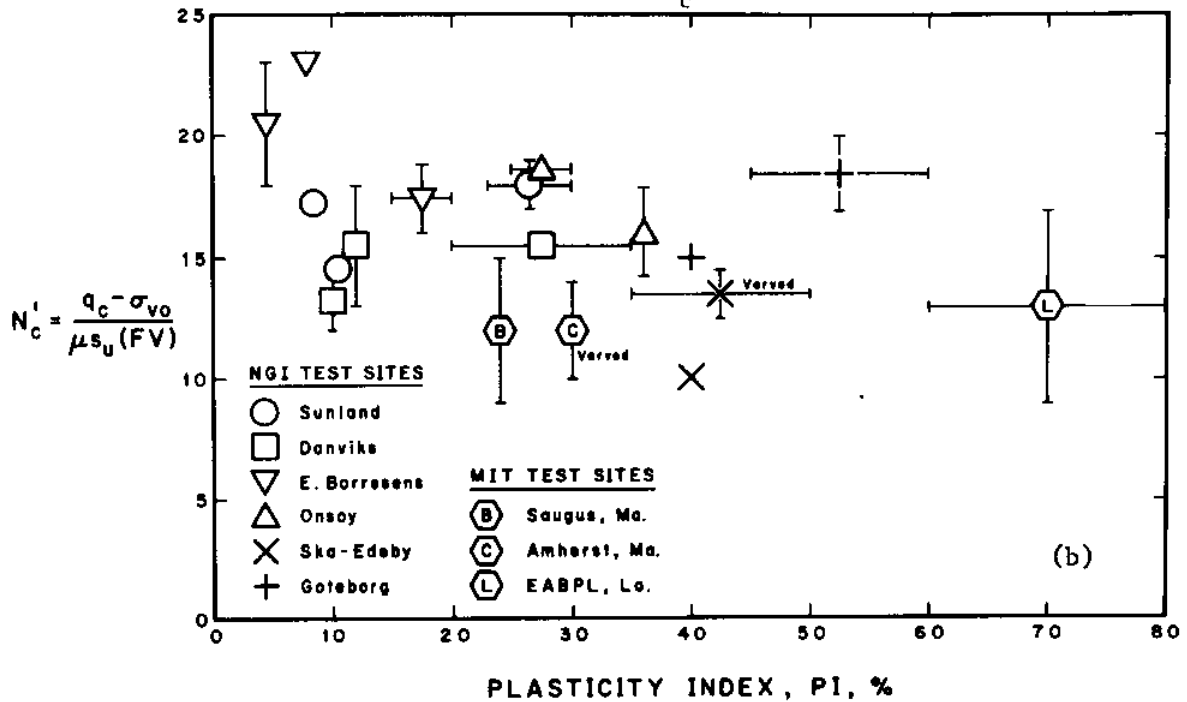
b – cone factor N_c'(FV)

Fig. 9.4 Empirical cone factors N_c(FV) and N_c'(FV) for very soft to medium clays

CHAPTER 10

SUMMARY AND CONCLUSIONS

(1) In situ soil testing is gaining importance in site investigation
and in the determination of the necessary soil properties for foundation
engineering design. This results from: (a) a growing concern over the es-
calating cost and the reliability of traditional exploration techniques
based on boring, sampling and laboratory testing; (b) the increasingly dif-
ficult and unfamiliar environments in which engineering structures are
founded; and (c) the necessity to assess soil conditions, in situ proper-
ties, and their variability in more detail to complement the development in
analytical capability of the geotechnical profession.

(2) The electric cone penetrometer and the pore pressure probe repre-
sent a new generation of in situ testing devices combining wide applicabil-
ity with simplicity, consistency and economy. Both have no mechanically
moving parts and are readily amenable to remote control and automated data
recording and processing, and are thus ideal instruments for difficult loca-
tions with no easy access, e.g., in deep water. They provide continuous
measurements, allowing better identification of soil stratigraphy and vari-
ability than discrete field measurements, e.g., the field vane test, or
laboratory tests on selected samples. For application in medium to soft
clays, however, they lack a solid evaluated experience by the profession
and a well-defined common basis for analysis, especially in the U.S. This
report attempts to establish a better understanding of the cone penetra-
tion mechanism through analytical and experimental means in order to pro-

vide a more rational interpretation method of cone penetration test
results.

Analytic Work

(3) Continuous penetration of a rigid indentor such as a cone
or a wedge in deep soil strata represents a steady state problem where
deformation and strains should be given primary consideration. During
penetration of blunt cones (or piles), the deformations and strains can
be estimated, with some limitations, using a relatively simple velocity
field. The analysis indicates that significant shearing occurs in the
soil ahead of the cone tip, and that the maximum shear strain,
$1/2(\epsilon_1 - \epsilon_3)$, in a soil element occurs in a circumferential direction.
The maximum shear strain on vertical (meridian) planes, $1/2(\epsilon_1 - \epsilon_2)$,
is as large as $1/2(\epsilon_1 - \epsilon_3)$ ahead of the cone.

(4) Rigorous solutions for steady state cone penetration in clay
are difficult to obtain because the problem is axisymmetric, involves
very large deformations and strains, and because soil behavior is very
complicated. All existing theories of cone penetration rely either on
rigorous solutions to simplified problems or on simple incomplete
solutions. Most of the existing theories are based on incipient plane-
strain deformation modes or on expansion of cavities; neither of these
approaches yields meaningful deformations nor strains. Chapter 2 offers
a more rational approach based on steady penetration of a wedge (Baligh,
1975).

(5) Chapter 2 discusses different approaches to the cone pene-
tration problem and concludes that the strain-path approach is the most
promising. The strain path approach relies on the fact that the deforma-

tion pattern (velocity field) for penetration problems can be predicted
with far less uncertainty than the stress pattern (Baligh, 1975). In
this approach, strain history is estimated for selected soil elements,
and the resulting stresses determined from laboratory tests or appro-
priate constitutive laws. The procedure for obtaining an associated
self-equilibrated stress field is, however, quite complicated, and requires
considerable additional effort. Research is currently underway at M.I.T.
to extend this approach to its logical conclusion and determine the pene-
tration resistance.

(6) Baligh (1972) and Baligh and Scott (1976) present a complete
ideal plasticity solution of steady state wedge penetration in isotropic
clays under undrained conditions. The theory predicts the wedge resis-
tance, the stress-increment, deformation and strain fields around the
wedge. The wedge resistance is relatively constant for apex angles, 2δ,
between 40° and 90° and approximately equal to 9.5 ± 0.3 times the iso-
tropic undrained shear strength of the clay, but increases rapidly for
sharper wedges. The deformation around a penetrating wedge is intense,
especially for wedges with apex angles, 2δ, greater than 40°. The maximum
shear strain in a soil element increases as it is approached by the wedge,
and, depending on its location, may remain constant or decrease after-
wards.

(7) Factors which were not rigorously considered or totally
neglected by the above mentioned theory include: anisotropy in shear
strength and initial stresses, soil deformation prior to yielding, strain
softening, strain rate, and reduced friction at the soil-cone interface
(see Table 3.2). Vivatrat (1978) presented a slip-line solution to steady
wedge penetration in anisotropic clays having elliptic yield contours. His

theory indicated that, within an error of $\pm$ 15%, the isotropic theory developed by Baligh (1972) and Baligh and Scott (1976) will yield a weighted "average" strength, $s_u(AVE)$, reflecting the shearing resistance of the clay in a combination of failure modes. Vivatrat (1978) also shows that values of the wedge-soil interface shear stresses smaller than the shear strength of the clay will cause a reduction in penetration resistance.

(8) Based on a comparison of plane strain and axisymetric deformation problems and the empirical shape factors often used in soil mechanics, the wedge penetration theory was used to estimate penetration resistance, stress and deformation fields during cone penetration in clays.

(9) For enlarged cones, $D/d \geq 1$ (D = tip diameter, d = shaft diameter) the cone resistance, q_c, is given by:

$$q_c = s_u N_c + (d/D)^2 \, p_b$$

where

p_b = pore pressure in the gap behind the enlarged cone;

N_c = cone factor = 11.0, 12.4 and 15.1 for apex angles

2δ = 60°, 30° and 18°, respectively; and

s_u = undrained shear strength of the clay.

(10) For regular (unenlarged) cones, $D/d = 1$, the theory can only predict upper and lower bounds for q_c:

$$s_u N_c \leq q_c \leq (N_c + 1 + \ln \frac{G}{s_u}) \, s_u + \sigma_{ho}$$

where:

σ_{ho} = initial horizontal total stress

G = undrained shear modulus

N_c = cone factor (same as for enlarged cones)

Experimental Work

(11) Extensive penetration testing was conducted in three clay deposits representing a wide spectrum of cohesive soils. The testing program identifies important parameters controlling cone penetration and evaluates the validity of the proposed cone penetration theories. The clay deposits studied are: Boston Blue Clay (marine illitic clay, low plasticity index and medium sensitivity), Atchafalaya Basin Clay (backswamp clay, high plasticity index and low sensitivity), and Connecticut Valley Varved clay (glacial lake varved clay, medium plasticity index and sensitivity). In the last decade, M.I.T. had extensively studied both the engineering properties of these clays by laboratory and field tests, and the performance of embankments constructed on these clays.

(12) In the three clay deposits studied, the cone resistance, q_c, measured with standard FUGRO equipment, is repeatable within a reasonable margin of uncertainty. Typical q_c profiles include small-scale anomalies, probably due to soil inhomogeneity, which must be discarded when the variability of the clay mass is investigated. A computerized filtering procedure to eliminate these anomalies in a consistent manner is developed and applied to records of q_c at the three test sites. The procedure emphasizes the importance of the median (rather than the mean) because of its insensitivity to anomalies in the data. Though it is not based on a rigorous statistical analysis, this procedure provides reasonable results which can be exactly duplicated.

The filtered data are approximately normally distributed about the mean and have a standard deviation which varies with depth. An analysis of soil variability based on the coefficient of variation (= standard deviation/mean) shows that both the cone resistance and the field vane detect approximately the same soil variability which depends on the soil type and shows a significant increase in desiccated regions.

(13) Factors investigated that influence cone resistance q_c (measured with electrical cones) are:

        a.   <u>Apex Angle</u>. q_c increases as the apex angle 2δ decreases (sharper cone). The effect of 2δ on q_c agrees with theoretical preditions (Chapter 4).

        b.   <u>Tip Shape</u>. As predicted by the theory, tip enlargement reduces q_c. This reduction, however, depends on the soil type. In "soft" clays (OCR $\approx$ 1), doubling the cone tip diameter reduces q_c by 0.5 to 1 times σ_{vo} (relative to "unenlarged" cones). In a "stiff" desiccated region, the effect of tip enlargement becomes negligible.

        c.   <u>Penetration Velocity.</u> Moderate variation (say, by a factor of 2) from the standard penetration velocity of 1 to 2 cm/sec causes no noticeable change in q_c. The limited data obtained in this research on penetration rate do not allow extrapolation to very slow shearing rates encountered in field failures developing over days or weeks.

(14) Pore pressures, u, measured during cone penetration by means of special pore pressure probes varies with the location on the cone (i.e., location of the porous elements). Maximum measured values of u were

obtained at the middle of the cone and decrease along the shaft behind the cone. Furthermore, u at the tip is slightly smaller than u at the middle of the cone. For unenlarged cones (tip diameter D = shaft diameter d), u decreases behind the cone for a distance of 4d to 5d and then remains constant at least to a distance of 11d. For enlarged cones (D > d), u is uniform behind the cone.

(15) Measurements from 18° cones indicate that u (tip) is not significantly affected by tip enlargement. In "soft" clays, u at a distance greater than 4d to 5d behind the cone is very close to u behind an enlarged cone. In Boston Blue Clay, where extensive pore pressure measurements are available, u at the tip of unenlarged cones and u behind enlarged cones increases with increasing apex angle.

(16) In all three clay deposits tested, steady penetration pore pressure u tends to decrease when cone resistance q_c increases. In "soft" clay (OCR $\approx$ 1) regions, u (tip) varies between 0.6 and 1.1 times q_c. Values of u > q_c are believed to indicate inaccuracies in q_c measurements. The ratio u/q_c, using u at tip, mid-cone or behind the cone, provides an excellent indication of the variation in stress history and soil type.

Thus a new instrument capable of measuring both q_c and u simultaneously will have great potential in soil exploration. This new instrument will be very sensitive to inhomogeneities or variation in soil properties and will be more valuable for soil identification than the existing friction ratio method (see Sanglerat, 1972, or Begemann, 1965). In addition, this new instrument will be capable of providing information on the in situ static pore pressure and permeability or consolidation properties of one soil.

Prediction of Undrained Shear Strength

(17) The semi-empirical cone penetration theory presented in Chapter 4 provides a rational basis for the interpretation of cone penetration measurements to estimate the undrained shear strength of clays, s_u(cone).

The evaluation of s_u(cone) is complicated by the very difficult task of estimating a reference shear strength, s_u(REF), to compare with theoretical predictions. Motivated by the need to relate s_u(cone) to field performance, s_u(REF) is estimated from the "field" strength, s_u(field), through an empirical correction factor, μ_R, to account for the difference in strain rate between cone penetration and actual failures developing over days or weeks. Average values of s_u(field) are based on full-scale embankment failures, and profiles of s_u(field) are estimated from field vane data or SHANSEP laboratory test results.

(18) Theoretical predictions of s_u(cone) based on enlarged cone resistances, supplemented by pore pressure measurements behind the tip, provide very acceptable profiles compared to s_u(REF) for all cone angles tested in a marine illitic clay (Boston Blue Clay, low PI, medium sensitivity) and a plastic deltaic clay (Atchafalaya clay, high PI, low snesitivity).

(19) For unenlarged cones (no diameter reduction) including the "standard" cone (60° tip), theoretical upper and lower bounds are confirmed by q_c measurements at the three sites. An average estimate of q_c (or inversely, s_u) lying approximately in the middle of the bounds predicts a shear strength with a significantly larger scatter than in predictions based on enlarged cones.

For unenlarged cones, the rigid shaft behind the tip constrains the soil deformation and complicates the interpretation of cone resistance.

A more accurate interpretation technique for this cone geometry requires additional measurements of pore pressures and/or more sophisticated methods of analyses. For immediate practical application of cone resistance in design, empirical correlations based on local experiences are necessary.

(20) Empirical correlations between cone resistance, q_c, and uncorrected and corrected field vane strengths [s_u(FV) and μs_u(FV)] are presented for a marine illitic clay (low PI, medium sensitivity), a plastic deltaic clay (high PI, low sensitivity), and a glacial lake varved clay (medium PI and sensitivity). The empirical cone factor N_c(FV) = [$q_c - \sigma_{vo}$]/s_u(FV) varies between 5 and 15 depending on stress history, sensitivity, depth, and possibly other factors. This range of N_c(FV) is lower than that presented by Lunne et al. (1976) for "medium" to "very soft" Scandinavian clays.

Bjerrum's empirical correction factor, μ, slightly reduces the variation of N_c(FV) with soil type (PI) but cannot account for the dependence of N_c(FV) on depth, stress history, or sensitivity. The range of another empirical cone factor, N_c'(FV) = [$q_c - \sigma_{vo}$]/μs_u(FV) for the three sites tested by M.I.T. and the six sites tested by Lunne et al (1976) is 9 to 20 for medium to very soft clays with PI greater than 10. The uncertainty in this empirical correlation can be significantly reduced by using local experience and noting the dependence of N_c'(FV) on depth. It can perhaps be further reduced if measurements of pore pressure during penetration are also available. Field experiments indicate that this pore pressure depends on the soil type and stress history and can perhaps influence the penetration resistance. Additional correlations between

N'_c(FV) and pore pressure is, however, required for practical application

of this approach.

REFERENCES

Al-Awkati, Z. (1975), "On Problems of Soil Bearing Capacity at Depth," Ph.D. Dissertation to the Dept. of Civil Engineeirng, Duke University, 204 p.

Aldrich, H.P. Jr. (1970) "Back Bay Boston, Part I," Journal of BSCE/ ASCE, Vol. 57, No. 1, pp. 1-33.

Azzouz, A.S. and Baligh, M.M. (1978), "Three-Dimensional Stability of Slopes," Research Report R78-8, Order No. 595, M.I.T. Dept. of Civil Engineering, 249 p.

Baguelin, F., Jezequel, J.F., Le Mee, H. and Le Mehaute, A. (1972),"Expansion of Cylindrical Probes in Cohesive Soils," Journal of the Soil Mechanics and Foundations Division, ASCE, Vol. 98, No. SM11, pp. 1129-1142.

Baligh, M.M. (1972), "Application of Plasticity Theory to Selected Problems in Soil Mechanics," Soil Mechanics Lab. Report, California Institute of Technology, 228 p.

Baligh, M.M. (1975), "Theory of Deep Site Static Cone Penetration Resistance," Research Report R75-56, No. 517, M.I.T. Dept. of Civil Engineering, 133 p.

Baligh, M.M. and Scott, R.F. (1976), "Wedge Penetration in Clays," Geotechnique, Vol. 26, No. 1, pp. 185-208.

Baligh, M.M., Vivatrat, V., and Ladd, C.C. (1977), "Exploration and Evaluation of Engineering Properties of Marine Soils for Foundation Design of Offshore Structures, Interim Report No. 1," Report No. MITSG 77-18, M.I.T. Sea Grant Program, 88 p.

Begemann, H.K.S. (1965), "The Friction Jacket Cone as an Aid in Determining the Soil Profile," Proceedings, 6th International Conference on Soil Mechanics and Foundation Engineering, Montreal, Vol. I, pp. 17-20.

Berre, T. and Bjerrum, L. (1973), "Shear Strength of Normally Consolidated Clays," Proceedings, 8th International Conference on Soil Mechanics and Foundation Engineering, Moscow, Vol. 1.1, pp. 39-49.

Bishop, R.F., Hill, R. and Mott, N.F. (1945), "Theory of Indentation and Hardness Tests," Proceedings, Physical Society of London, Vol. 57, Part 3, No. 321, pp. 147-159.

Bjerrum, L. (1971), "Recent Research on the Consolidation and Shear Behavior of Normally Consolidated Clay," Internal Report No. 50302, Norwegian Geotechnical Institute, Oslo.

Bjerrum, L. (1972), "Embankments on Soft Ground," State-of-the-Art Report, Proceedings, ASCE Specialty Conference on Performance of Earth and Earth-Supported Structures, Lafayette, Vol. 2, pp. 1-54.

Bjerrum, L. (1973), "Problems of Soil Mechanics and Construction on Soft Clays," State-of-the-Art Report, Session 4, Proceedings, 8th International Conference on Soil Mechanics and Foundation Engineering, Moscow, Vol. 3,pp. 109-159.

Brand, E.W. (1974), "Comparison of Hand Cone and Dutch Cone Resistance," Discussions, Proceedings, European Symposium on Penetration Testing, Stockholm, Vol. 2:1, pp. 117-119.

Brinch-Hansen, J. (1961), "A General Formula for Bearing Capacity," Bulletin No. 11, Danish Geotechnical Institute, Copenhagen, pp. 8-13.

Brinch-Hansen, J. (1970), "A Revised and Extended Formula for Bearing Capacity," Bulletin No. 28, Danish Geotechnical Institute, Copenhagen, Denmark,pp. 5-11.

Buisman, A.S.K. (1935), "De Weerstand van Paalpunten in Zand," De Ingenieur 50, pp. Bt. 25-28, 31-35.

Caquot, A. (1934), "Equilibre des Massifs a Frottement Interne,"Paris, (Gauthier-Villars).

Chadwick, P., Cox, A.D. and Hopkins, H.G. (1963), "Mechanics of Deep Underground Explosions," Philosophical Trans., Royal Society of London, Series A, Vol. 256, pp. 235-300.

Chung, T.J. and Lee, J.K. (1974), "Recent Developments in Soil Yield Criteria and Numerical Applications," Journal of Terramechanics, Pergamon Press, Vol. 11, No. 384, pp. 79-91.

Connell, D.H., Garlanger, J.E. and Ladd, C.C. (1973), "Performance of an Embankment Constructed on Varved Clay," Research Report R73-26, Soils Publication No. 321, M.I.T. Dept. of Civil Engineering.

D'Appolonia, D.J., Lambe, T.W. and Poulos, H.G. (1971a), "Evaluation of Pore Pressures Beneath an Embankment," Journal of the Soil Mechanics and Foundations Division, ASCE, Vol. 97, No. SM6, pp. 881-898.

D'Appolonia, D.J., Poulos, H.G., and Ladd, C.C. (1971b), "Initial Settlement of Structures on Clay," Journal of the Soil Mechanics and Foundations Division, ASCE, Vol. 97, No. SM10, October, pp. 1359-1377.

Davis, E.H. and Christian J.T. (1971), "Bearing Capacity of Anisotropic Cohesive Soil," Journal of the Soil Mechanics and Foundations Division, ASCE, Vol. 97, No. SM5, pp. 753-769.

De Beer, E.E., et al. (1974), "Scale Effects in Results of Penetration Tests Performed in Stiff Clays," Proceedings, European Symposium on Penetration Testing, Stockholm, Vol. 2:2, pp. 105-114.

de Ruiter, J. (1971), "Electric Penetrometer for Site Investigation," Journal of the Soil Mechanics and Foundations Division, ASCE, Vol. 97, No. SM2, pp. 457-472.

Fisk, H.N., Kolb, C.R. and Wilbert, L. J. (1952), "Geological Investigation of the Atchafalaya Basin and the Problem of Mississippi River Diversion," U.S. Army Engineer Waterway Experimental Station, Vicksburg, Miss.

Foott, R. and Ladd, C.C. (1973), "The Behavior of Atchafalaya Test Embankments during Construction," Research Report R73-27, Order No. 322, M.I.T.Dept. of Civil Engineering, 364 p.

Fuleihan, N.F. and Ladd, C.C. (1976), "Design and Performance of Atchafalaya Flood Control Levees," Research Report R76-26, No. 543, M.I.T. Dept. of Civil Engineering, 753p. (2 Vol.).

Gibson, R.E. (1950), Discussion of G. Wilson, "The Bearing Capacity of Screw Piles and Screwcrete Cylinders," Journal of the Institution of Civil Engineers, Vol. 34, No. 4, pp. 382.

Harr, A. and von Karman, Th., (1909), "Zur Theorie der Spannungszustände in plastischen und sandartigen Medien," Nachr. Gesellsch. Wiss. Göttingen, Math.-phys.Kl., H. 2, 204-218.

Heijnen, W. J. (1974), "Penetration Testing in Netherlands," Proceedings, European Symposium on Penetration Testing, Stockholm, Vol. 1., pp. 79-83.

Hill, R. (1950), The Mathematical Theory of Plasticity, Oxford University Press.

Hill, R. (1963), "A General Method of Analyses for Metal-Working Process," Journal of the Mechanics and Physics of Solids, London, Vol. 11, pp. 305-326.

Hirst, W. and Howse, M.G. (1969), "The Indentation of Materials by Wedges," Proceedings, Royal Society of London, Series A, Vol. 311, pp. 429-444.

IMSL (1975), Reference Manual for IMSL Library 1, Edition 5, International Mathematical & Statistical Libraries, Inc., Houston, Texas, (3 vols.).

Joustra, K. (1974), "Comparative Measurements on the Influence of the Cone Shape on Results of Soundings," Proceedings, European Symposium on Penetration Testing, Stockholm, Vol. 2:2, pp. 199-204.

Kaufman, R.I. and Weaver, F.J. (1967), "Stability of Atchafalaya Levees," Journal of the Soil Mechanics and Foundations Division, ASCE, Vol. 93, No. SM4, pp. 157-176.

Kendall, M.G. and Stuart, A. (1961), The Advanced Theory of Statistics, Vol. 2, Hafner Publishing Co., New York, 457 p.

Kenney, T.S. (1964), "Sea Level Movements and the Geologic Histories of the Post Glacial Marine Soils at Boston, Nicolet, Ottawa and Oslo," Geotechnique, Vol. 14, No. 3, pp. 203-230.

Kinner, E.B. and Ladd, C.C. (1970), "Load-Deformation Behavior of Saturated Clays During Undrained Shear," Research Report R-70-27, Soil Publication No. 259, M.I.T. Dept. of Civil Enginering, 306 p.

Kinner, E.B. and Ladd, C.C. (1973), "Undrained Bearing Capacity of Footing on Clay", Proceedings, 8th International Conference on Soil Mechanics and Foundation Engineering, Moscow, Vol. 1.1, pp. 209-215.

Koizumi, Y. and Ito, K. (1967), "Field Tests with Regard to Pile Driving and Bearing Capacity of Piled Foundations," Soils and Foundations, Japan, Vol. 7, No. 3, pp. 30-53.

Kolb, C.R. and Shockley, W.G. (1959), "Engineering Geology of the Mississippi Valley," ASCE Transactions, Vol. 124, pp. 633-645.

Krinitzsky, E.L. and Smith, F.L. (1969), "Geology of Backswamp Deposits in the Atchafalaya Basin, Louisiana," Technical Report S-69-8, U.S. Army Engineer Waterways Experiment Station, Vicksburg, Miss.

Lacasse, S.M., Connell, D.H. and Ladd, C.C. (1972), "Interim Report on the Shear Strength of Connecticut Valley Varved Clays," Research Report R72-16, Soils Publication No. 299, M.I.T. Dept. of Civil Engineering, 121 p.

Lacasse, S.M., Ladd, C.C. and Baligh, M.M. (1978), "Evaluation of Field Vane, Dutch Cone Penetrometer and Piezometer Probe Testing Devices," Research Report, R-78-26, No. 608, M.I.T. Dept. of Civil Engineeirng.

Ladanyi B. (1967), "Deep Punching of Sensitive Clays," Proceedings, 3rd Panamerican Conference on Soil Mechanics and Foundation Engineering, Caracas, Vol. 1, pp. 533-546.

Ladanyi, B. (1972), "In Situ Determination of Undrained Stress-Strain Behavior of Sensitive Clays with the Pressuremeter," Canadian Geotechnical Journal, Vol. 9, No. 3, pp. 313-319.

Ladd, C.C. (1971), "Strength Parameters and Stress-Strain Behavior of Saturated Clays," Research Report R71-23, No. 278, M.I.T. Department of Civil Engineering.

Ladd, C.C. (1975), "Foundation Design of Embankments Constructed on Connecticut Valley Varved Clays," Research Report R75-7, No. 343, M.I.T. Dept. of Civil Engineering, 439 p.

Ladd, C.C. and Edgers, L. (1972), "Consolidated-Undrained Direct- Simple Shear Test on Saturated Clays," Research Report R72-82, No. 284, M.I.T. Department of Civil Engineering.

Ladd, C.C. and Foott, R. (1974), "New Design Procedure for Stability of Soft Clays," Journal of the Geotechnical Engineering Division, ASCE, Vol. 100, No. GT7, pp. 763-786.

Ladd, C.C. and Foott, R. (1977), "Foundation Design of Embankments on Varved Clays," U.S. Department of Transportation, FHWA, Washington, D.C., 234 p.

Ladd, C.C. and Lambe, T.W. (1963), "The Strength of 'Undisturbed' Clay Determined from Undrained Tests," ASTM, STP No. 361, pp. 342-371.

Ladd, C.C. and Varallyay, J. (1965), "Influence of Stress System on the Behavior of Saturated Clays During Undrained Shear," Research Report R65-11, M.I.T. Dept. of Civil Engineering.

Ladd, C.C. and Wissa, A.E.Z. (1970), "Geology and Engineering Properties of Connecticut Valley Varved Clays with Special Reference to Embankment Construction," Research Report R70-56, Soils Publication No. 264, M.I.T. Dept. of Civil Engineering.

Ladd, C.C., et al., (1971a), "Consolidated-Undrained Plane-Strain Shear Tests on Boston Blue Clay," Research Report R71-13, No. 272, M.I.T. Dept. of Civil Engineering.

Ladd, C.C., Moh, Z.C. and Gifford, D. (1971b), "Undrained Strength of Soft Bangkok Clay," Proceedings, 4th Asian Regional Conference on Soil Mechanics and Foundation Engineering, Bangkok, Thailand, Vol. I, pp. 135-140.

Ladd, C.C. et al. (1972), "Engineering Properties of Soft Foundation Clays at Two South Louisiana Levee Sites," Research Report R72-26, No. 304, M.I.T. Department of Civil Engineering.

Ladd, C.C. et al. (1977), "Stress-Deformation and Strength Characteristics," State-of-the-Art Report for Session I, Proceedings 9th International Conference on Soil Mechanics and Foundation Engineering, Tokyo, Vol. 2, pp. 421-494.

Ladd, C.C. et al. (1979), "Evaluation of Self-Boring Pressuremeter Tests in Boston Blue Clay," Research Report No. R79-4, M.I.T. Dept. of Civil Engineering (in preparation).

Lambe, T.W. (1967), "Stress Path Method," Journal of the Soil Mechanics and Foundation Division, ASCE, Vol. 93, No. SM6, pp. 309-331.

Lambe, T.W. (1973), "Predictions in Soil Engineering: 13th Rankine Lecture," Geotechnique, Vol. 23, No. 2, pp. 149-202.

Lambe, T.W. and Whitman, R.V. (1969), Soil Mechanics, John Wiley & Sons, New York, 553 p.

Lambe, T.W., et al (1972), "The Performance of the Foundation under a High Embankment," Journal of the BSCES/ASCE, April, pp. 71-94.

Lo, K.Y. (1965), "Stability of Slopes in Anisotropic Soils, "Journal of the Soil Mechanics and Foundations Division, ASCE, Vol. 91, No. SM4, pp. 85-106.

Lockett, F.J., et al. (1963), "Indentation of a Rigid/Plastic Material by a Conical Indenter," Journal of the Mechanics and Physics of Solids, Vol. 11, pp. 345-355.

Lunne, T., Eide, O. and de Ruiter, J. (1976), "Correlations between Cone Resistance and Vane Shear Strength in Some Scandinavian Soft to Medium Stiff Clays," Canadian Geotechnical Journal, Vol. 13, pp. 430-441.

Marr, W.A. (1974), "In Situ Measurements of Stresses in Soil," Thesis presented to M.I.T., Cambridge, Massachusetts, in partial fulfillment of the requirements for the degree of Doctor of Philosophy, 241 p.

Marsh, D.M. (1964), "Plastic Flow in Glass," Proceedings, Royal Society of London, Series A., Vol. 279, pp. 420-435.

M.I.T. (1975), "Proceedings of the Foundation Deformation Prediction Symposium," Research Report R-75-32, No. 512, Vol. 1, Dept. of Civil Engineering, 157 p.

Meyerhof, G.G. (1951), "The Ultimate Bearing Capacity of Foundations," Geotechnique, Vol. II, No. 4, pp. 301-332.

Meyerhof, G.G. (1961), "The Ultimate Bearing Capacity of Wedge-Shaped Foundations," Proceedings, 5th International Conference on Soil Mechanics and Foundations Engineering, Vol. 2, pp. 103-109.

Mitchell, J.K. and Durgunoglu, H.T. (1973), "In Situ Strength by Static Cone Penetration Test," Proceedings, 8th International Conference on Soil Mechanics and Foundations Engineering, Moscow, Vol. 1, pp. 279-286.

Mitchell, J.K. and Gardner, W.S. (1975),"In Situ Measurement of Volume Change Characteristics." State-of-the-Art Paper, Proceedings ASCE Specialty Conf. on In Situ Measurement of Soil Properties,Raleigh, Vol. II, pp. 279-345.

Mulhern, T.O. (1959), "The Deformation of Metals by Vickers-type Pyramidal Indenters," Journal of the Mechanics and Physics of Solids, London, Vol. 7, pp. 85-96.

Muromachi, T. (1974), "Experimental Study on Application of Static Cone Penetrometer to Subsurface Investigation of Weak Cohesive Soils," Proceedings, European Symposium on Penetration Testing, Stockholm, Vol. 2:2, pp. 285-292.

Palmer, A.C. (1972), "Undrained Plane Strain Expansion of a Cylindrical Cavity in Clay: A Simple Interpretation of the Pressuremeter Test," Geotechnique, Vol. 22, No. 3, pp. 451-457.

Prandtl, L. (1920), "Uber die Harte Plastischer Korper" (Concerning the Hardness of Plastic Bodies), Nachr. Kgl, Ges. Wiss. Göttingen, Math. phys. Klasse.

Prevost, J.H. and Hoeg, K. (1975a), "Soil Mechanics and Plasticity Analysis of Strain-Softening," Geotechnique, Vol. 25, No. 2, pp. 279-297.

Prevost, J.H. and Hoeg, K. (1975b), "Analysis of Pressuremeter in Strain-Softening Soil," Journal of the Geotechnical Engineering Division, ASCE, Vol. 101, No. GT8, pp. 717-732.

Reissner, H. (1924), "Zum Erddruckproblem," Proceedings, First International Congress of Applied Mechanics, Delft, pp. 295-311.

Robinsky, E.I. and Morrison, C.F. (1964), "Sand Displacement and Compaction Around Model Friction Piles," Canadian Geotechnical Journal, Vol. 1, pp. 81-93.

Roscoe, K.H. (1970), "The Influence of Strains in Soil Mechanics," 10th Rankine Lecture, Geotechnique, Vol. 20, No. 2, pp. 129-170.

Rourk, T.L. (1961), "Model Studies of a Pile Failure Surface in a Cohesive Soil," M.S. Thesis, Civil Engineering Dept., Georgia Institute of Technology, Atlanta, 56 p.

Sambhandharaksa, Surachat (1977), "Stress-Strain-Strength Anisotropy of Varved Clays," Thesis presented to M.I.T., at Cambridge, Massachusetts, in partial fulfillment of the requirements for the degree of Doctor of Science.

Sanglerat, G. (1972), The Penetrometer and Soil Exploration, Elsevier Publishing Co., Amsterdam.

Schmertmann, J.H. (1975), "Measurement of In Situ Shear Strength," State-of-the-Art Report, Proceedings, ASCE Specialty Conference on In Situ Measurement of Soil Properties, Raleigh, N.C., Vol. II, pp. 57-138.

Shield, R.T. (1955), "On the Plastic Flow of Metals under Conditions of Axial Symmetry," Proceedings, Royal Society of London, Series A, Vol. 233, pp. 267-287.

Skempton, A.W. (1948), "The $\phi = 0$ Analysis of Stability and Theoretical Basis," Proceedings, 2nd International Conference on Soil Mechanics and Foundation Engineering, Rotterdam, Vol. 1, pp. 72-78.

Skempton, A.W. (1951), "The Bearing Capacity of Clays," Building Research Congress, London, The Institute of Civil Engineering, Division I, London, pp. 180-189.

Szechy, K. (1968), "Deformations Around and Below Driven and Vibrated Test Tubes," Acta Technica Acad. Sci., Hungary, Vol. 62, pp. 97-113.

Terzaghi, K. (1943), Theoretical Soil Mechanics, John Wiley and Sons, New York, 1943.

Thomas, D. (1965), "Static Penetration Tests in London Clay," Geotechnique, Vol. 15, No. 2, pp. 174-179.

Torstensson, B.A. (1975), "Pore Pressure Sounding Instrument," Discussion, Session 1, Proceedings ASCE Specialty Conference on In Situ Meaurement of Soil Properties, Raleigh, N.C., Vol. 2, pp. 48-54.

USCE (1968), "Interim Report on Field Tests on Levee Construction, Test Sections I, II and III, EABPL, Atchafalaya Basin Floodway, La., " U.S.A.E., New Orleans District, New Orleans, Louisiana.

Vesic, A.S. (1963), "Bearing Capacity of Deep Foundations in Sands," Stresses in Soils and Layered Systems, Highway Research Board Record No. 39, pp. 112-153.

Vesic, A.S. (1967), "Ultimate Loads and Settlements of Deep Foundations in Sand," Proceedings Symposium on Bearing Capacity and Settlement of Foundations, Duke University, Durham, N.C., 53 p.

Vesic, A.S. (1973), "Analysis of Ultimate Loads of Shallow Foundations," Journal of the Soil Mechanics and Foundations Division, ASCE, Vol. 99, No. SM1, pp. 45-73.

Vesic, A.S. (1975), "Principles of Pile Design," Lecture Series on Deep Foundations Sponsored by the Geotechnical Group, BSCES/ASCE.

Vesic, A.S. (1977), "Design of Pile Foundation," Synthesis of Highway Practice 42, Transportation Research Board, National Research Council, Washington, D.C. 68 p.

Vivatrat, V. (1978), "Cone Penetration in Clays." Thesis presented to M.I.T. in partial fulfillment of the requirements for the degree of Doctor of Science, 427 p.

Wissa, A.E.Z., Martin, R.T. and Garlanger, J.E. (1975), "The Piezometer Probe," Proceedings, ASCE Specialty Conference on In Situ Measurement of Soil Properties, Raleigh, N.C., Vol. I, pp. 536-545.

APPENDIX A

SPECIAL DESIGN CONSIDERATIONS

A.1 Strengths for Undrained Bearing Capacity and Stability Analyses

As discussed in Chapter 3 (Section 3.3), Ladd (1971) recommends the use of $s_u = q_f$ in undrained bearing capacity analyses, but $s_u = \tau_{ff}$ in "total stress" circular arc stability analyses.

A.2 Design Strength for the Saugus, Massachusetts, Test Site

The Saugus, Massachusetts, test site and the adjoining section of an unfinished highway embankment is one of the most extensively instrumented and studied clay sites. In addition, the foundation clay, the Boston Blue Clay, has been the subject of extensive research at M.I.T. for decades. However, this massive volume of information available (see Table 5.2 for example) does not easily or simply lead to the appropriate strength to use in embankment stability and/or bearing capacity analyses. This results from the immensely complicated soil behavior coupled with the highly simplified methods of analysis available at present.

The following paragraphs illustrate four different approaches for predicting the "field" strength, s_u(field):

1. Kinner and Ladd (1970, 1973) studied the load deformation behavior of model footings on resedimented Boston Blue Clay under carefully controlled laboratory conditions at OCR values of 1, 2 and 4. The results are summarized below:

OCR	$\dfrac{s_u(\text{AVE})}{\bar{\sigma}_{vc}}$	$\dfrac{s_u(\text{MFT})}{\bar{\sigma}_{vc}}$	$\dfrac{s_u(\text{AVE})}{s_u(\text{MFT})}$
1	0.25	0.26	0.96
2	0.44	0.47	0.94
4	0.76	0.81	0.94

where $s_u(\text{AVE})$ is the "average" strength defined in Eq. 3.5 and Fig. 3.7 based on results of laboratory K_o consolidated-undrained plane strain shear tests and $s_u(\text{MFT})$ is the s_u back calculated from the model strip footing tests interpreted using the Davis and Christian (1971) anisotropic bearing capacity equation. These data suggest excellent agreement between SHANSEP predicted s_u values and measured bearing capacity results. However, the agreement is considered fortuitious since two aspects of soil behavior, now considered to be potentially important, were ignored. These are the effects of strain compatibility and strain rate. Thus the above data will be interpreted considering these two factors.

Analysis of laboratory CK_oU plane strain data on Boston Blue Clay indicates that the $s_u(\text{AVE})$ should be decreased by about 10% to account for strain compatibility (Ladd, 1975; Azzouz and Baligh, 1978). That is, the s_u that can be mobilized along an actual failure surface, assuming uniform strain along this surface, is 10% less than the average of the peak strengths due to the strain-softening behavior shown in Figs. 3.5a and b. Thus, $s_u(\text{AVE})$ should be multiplied by 0.9 to account for strain compatibility. The model footing tests were carried to failure in about 15 seconds, in order to minimize consolidation and creep effects during

loading, whereas the laboratory CK_oU tests had typical times to failure
on the order of 1 to 2 hours. If one assumes a 5 to 10% reduction in
s_u per log cycle of time to failure, the measured bearing capacities
would then be decreased by:

$$(5 \text{ to } 10\%) \; [\log \; (1.5 \times 3600)/(15)] = 13 \text{ to } 26\%$$

Thus, multiplication of $s_u(MFT)$ by 0.8 to 0.9 should account for strain
rate effects.

The results presented by Kinner and Ladd (1970, 1973) are now
adjusted in accordance with the above estimated effects of strain com-
patibility and strain rate:

OCR	$\dfrac{s_u(AVE) \times (0.90)}{\overline{\sigma}_{vc}}$	$\dfrac{s_u(MFT) \times (0.8\text{-}0.9)}{\overline{\sigma}_{vc}}$	Adjusted $\dfrac{s_u(AVE)}{s_u(MFT)}$
1	0.225	0.21 – 0.235	0.96 – 1.07
2	0.395	0.375 – 0.425	0.93 – 1.05
4	0.685	0.65 – 0.73	0.94 – 1.05

Hence after adjusting the laboratory shear tests for strain compatibility
and the model footing tests for strain rate, the resulting values of
undrained strength agree within about ± 5%. This suggests that use of
$s_u(field) = 0.9 \; s_u(AVE)$ would be appropriate for bearing capacity problems
at the Saugus, Massachusetts. test site assuming:

(1) In situ Boston Blue Clay behaves similarly to resedimented
samples of the same soil (CK_oU triaxial compression and extension
test data obtained at M.I.T. on both types of samples show
good agreement in $s_u/\overline{\sigma}_{vc}$ values).

(2) Negligible strain rate effects between CK_oU laboratory
tests and the in situ condition (note that decreases in the field s_u

due to longer times to failure may be partly compensated by partial consolidation).

(3) That the in situ history is sufficiently well defined to provide a reliable estimate of the OCR profile required to compute s_u(AVE) from previously established $s_u/\bar{\sigma}_{vc}$ vs. OCR relationships (e.g. Figs. 5.3 and 5.16a).

2. Extensive field vane test data exist at the test site and since the PI of Boston Blue Clay is about 20%, Bjerrum's (1972) empirical correlation would suggest that the measured FV strengths are appropriate for evaluating the stability of embankments via circular arc analyses. Bjerrum (1973) later concluded that the same empirical correlation also applies to bearing capacity analyses using plasticity theory. The FV s_u values have been normalized with respect to $\bar{\sigma}_{vo}$ and correlated versus the stress history shown in Fig. 5.3 (Lacasse et al., 1978). These data are compared below to s_u(field) = 0.9 s_u(AVE) established from Method 1 as appropriate for bearing capacity analyses.

OCR	$\dfrac{s_u(FV)}{\bar{\sigma}_{vo}}$	$\dfrac{0.9\ s_u(AVE)}{\bar{\sigma}_{vc}}$	$\dfrac{0.9\ s_u(AVE)}{s_u(FV)}$
1	0.165	0.225	1.36
2	0.32	0.395	1.23
4	0.625	0.685	1.10

The above comparison shows that Method 1 yields strengths 23 ± 13% larger than those recommended by Bjerrum. This apparent discrepancy will be discussed shortly.

3. According to Ladd (1971, 1975), s_u(field) for circular arc

stability analyses should be based on $\tau_{ff} = q_f \cos \bar{\phi}$ rather than q_f.

For Boston Blue Clay, $\cos \bar{\phi} = 0.83$ and hence s_u(field) for circular arc

analysis based on SHANSEP becomes equal to $0.9\ s_u(AVE) \times 0.83 = 0.745\ s_u(AVE)$.

Comparing this to $s_u(FV)$, as shown below:

OCR	$\dfrac{s_u(FV)}{\bar{\sigma}_{vo}}$	$\dfrac{s_u(SHANSEP)}{\bar{\sigma}_{vc}}$	$\dfrac{s_u(SHANSEP)}{s_u(FV)}$
1	0.165	0.185	1.12
2	0.32	0.33	1.03
4	0.625	0.57	0.91

We note that: Method 3 gives field strengths about 10% larger than $s_u(FV)$

for normally consolidated Boston Blue Clay and that the implied FV cor-

rection factor decreases with increasing OCR of the clay. Note also that

Ladd would use $s_u = \tau_{ff}$ for circular arc analyses and $s_u = q_f$ for bearing

capacity analyses whereas Bjerrum (1973) implies that the same strength

applies to both types of analyses.

4. Azzouz and Baligh (1978) analyzed the planned embankment failure

close to the test site (M.I.T.,1975) with $s_u(FV)$ and $s_u(SHANSEP)$ using

both 2 and 3-D methods of analysis. It should be noted that the critical

failure surface extended down to about El. 70 ft and thus primarily in-

volved the upper "stiff" clay which had an average OCR of about 3 to 4.

First looking at the result of the 2-D analyses, shown below:

Method	F.S.	Implied Correction Factor
No. 2 $s_u(FV)$	0.91 ± 0.02	1.10 ± 0.02
No. 3 $s_u(SHANSEP)$	0.82	1.22

we see that Methods 2 and 3 both underpredicted the in situ strength. However, the failure involved substantial end effects compared to most embankment failures (Azzouz and Baligh, 1978); thus the results of the 3-D analyses should give a better indication of the actual in situ s_u. This analyses showed:

Method	F.S.	Implied Correction Factor
No. 2 s_u(FV)	1.13 ± 0.04	0.885 ± 0.03
No. 3 s_u(SHANSEP)	1.03 ± 0.03	0.97 ± 0.03

which would lead to the following conclusions regarding s_u(field) for circular arc stability analysis in "stiff" Boston Blue Clay

$$s_u(\text{field}) \approx 0.9 \ s_u(\text{FV}) \approx 1.0 \ s_u(\text{SHANSEP})$$

Note that the ratio of the implied correction factors of 0.885/0.97 = 0.91 is also equal to s_u(SHANSEP)/s_u(FV) = 0.91 at an OCR = 4. Further, the results of the model footing tests suggest that laboratory CK_oU test data give a good indication of the changes in s_u with OCR. Thus one might logically conclude that the in situ s_u of Boston Blue Clay appropriate for circular arc stability analyses should also vary with stress testing as predicted by s_u(SHANSEP)/$\overline{\sigma}_{vc}$ vs. OCR. This conclusion, if correct, has two important implications:

(1) That the FV correction factor for Boston Blue Clay varies significantly with OCR, e.g., from about 1.1 for normally consolidated clay to about 0.9 for heavily overconsolidated clay.

(2) That the correct s_u to use in ϕ = 0 bearing capacity analyses is different from that for circular arc stability analyses,

i.e., $s_u = q_f$ vs. $s_u = \tau_{ff} = q_f \cos \bar{\phi}$. (Note that both values should be reduced by about 10% for strain compatibility.)

Figure A.1 presents in summary the normalized strength data thought to apply to Boston Blue Clay at the Saugus test site based on the above discussion. It assumes that:

$$s_u(\text{field-bearing capacity analyses}) = 0.9\, s_u(\text{AVE})$$

where
$$s_u(\text{AVE}) = 0.47\,[q_f(\text{PSC}) + q_f(\text{PSE})]$$

and
$$s_u(\text{field - circular arc analyses}) = s_u(\text{SHANSEP})$$

where
$$s_u(\text{SHANSEP}) = (0.47)(0.9)\,[\tau_{ff}(\text{PSC}) + \tau_{ff}(\text{PSE})]$$

Also shown are $s_u(\text{FV})/\bar{\sigma}_{vo}$ and the corresponding correction factor for circular arc stability analyses.

Fig. A.1 Recommended undrained strength parameters for Boston Blue Clay and the corresponding field vane correction factor, μ.